

TECHNISCHE UNIVERSITÄT MÜNCHEN

Institut für Luft- und Raumfahrt

# **Advanced Methods for Propulsion System Integration in Aircraft Conceptual Design**

Arne Seitz

Vollständiger Abdruck der von der Fakultät für Maschinenwesen der Technischen  
Universität München zur Erlangung des akademischen Grades eines

**Doktor-Ingenieurs (Dr.-Ing.)**

genehmigten Dissertation

Vorsitzender: Univ.-Prof. Dr.-Ing. Horst Baier

Prüfer der Dissertation: 1. Hon.-Prof. Dr.-Ing. Dr. h.c. Dieter Schmitt  
2. apl. Prof. Dr.-Ing. habil. Hans Rick (i. R.)  
3. Univ.-Prof. Dr.-Ing. Mirko Hornung

Die Dissertation wurde am 15.06.2011 bei der Technischen Universität München  
eingereicht und durch die Fakultät für Maschinenwesen am 20.01.2012 angenommen.







Für meine Eltern



# Vorwort

Die vorliegende Arbeit entstand während meiner Arbeit als wissenschaftlicher Mitarbeiter am Bauhaus Luftfahrt. Die hervorragenden Rahmenbedingungen im Arbeitsumfeld trugen wesentlich zum Erfolg dieser Arbeit bei. Mein erster Dank gilt Herrn Prof. Dr.-Ing. Dr. h.c. Dieter Schmitt, der mir als Doktorvater und zentraler Unterstützer meiner wissenschaftlichen Arbeit viel Zeit in wertvollen Gesprächen gewidmet hat. Des Weiteren danke ich Herrn Prof. Dr.-Ing. Hans Rick und Herrn Prof. Dr.-Ing. Mirko Hornung für die freundliche Übernahme der zweiten und dritten Begutachtung dieser Arbeit. Frau Dr. Anita Linseisen danke ich für ihre Unterstützung in allen organisatorischen Angelegenheiten am Bauhaus Luftfahrt. Ferner gilt mein Dank Herrn Prof. Dr.-Ing. Klaus Broichhausen als früher Förderer meiner wissenschaftlichen Tätigkeit am Bauhaus Luftfahrt. Herrn Prof. Dr.-Ing. Horst Baier danke ich für die freundliche Übernahme des Prüfungsvorsitzes. Für die jahrelange wissenschaftliche Begleitung möchte ich Herrn Prof. Dr.-Ing. Hans-Peter Kau danken.

Mein ausgesprochener Dank gilt Herrn Dr.-Ing. Stefan Donnerhack, der mir über Jahre hinweg als ständiger Ansprechpartner in inhaltlichen Fragen geholfen und als Koautor an wichtigen Veröffentlichungen im Rahmen meiner wissenschaftlichen Tätigkeit mitgewirkt hat. Ich danke Herrn Dr.-Ing. Reinhold Schaber für die intensive inhaltliche Zusammenarbeit und die zahlreichen fruchtbaren Diskussionen zur Modellbildung im Bereich Antriebssystem. Herrn Dr.-Ing. Klaus-Peter Rüd danke ich für wichtige inhaltliche Impulse während der Definition des wissenschaftlichen Kerns meiner Arbeit. Besonders danken möchte ich auch Herrn Dr.-Ing. Joachim Kurzke für die enge Zusammenarbeit in Fragen der Triebwerksleistungsrechnung.

Ich bedanke mich bei den Mitarbeiterinnen und Mitarbeitern des Bauhaus Luftfahrt für das optimale Arbeitsklima und die vielen inspirierenden Gespräche, die wesentlich zur Findung kreativer Lösungen für die Problemstellungen dieser Arbeit beigetragen haben. Mein besonderer Dank gilt hierbei Herrn Dr.-Ing. Corin Gologan, Herrn Hans-Jörg Steiner, Herrn Oliver Schmitz sowie Herrn Dr.-Ing. Kay Plötner, deren Ratschlag ich oft gesucht habe, und die mir stets als kompetente und kritische Gesprächspartner zur Verfügung standen. Speziell möchte ich Herrn Dr. Askin T. Isikveren danken, der mir in der finalen Phase der Fertigstellung der Arbeit viel wertvolle Zeit geschenkt hat und mich durch zahlreiche Hinweise and Ratschläge unterstützt hat. Ich danke auch Herrn Daniel Mayer für die exzellente Zusammenarbeit während seines Praktikums am Bauhaus Luftfahrt und den dabei geleisteten Beitrag zur Umsetzung der Methodik dieser Arbeit. Für wertvolle Ratschläge in der Umsetzung der Arbeit geht mein Dank außerdem an Herrn Dr. Roland Schneider sowie Herrn Dr. Andreas Sizmann.

Nicht zuletzt danke ich Herrn Matthias Aßmann für die fortwährende freundschaftliche Unterstützung und das stets offene Ohr für die Dinge abseits der wissenschaftlichen Arbeit. Mein größter Dank aber gilt meinen Eltern, die mich seit Anbeginn durch ihren bedingungslosen Rückhalt gestärkt haben und somit auch den Grundstein für den erfolgreichen Abschluss der vorliegenden Arbeit gelegt haben.

München, im Juni 2011

Arne Seitz



# Abstract

The development of future air transport systems is highly challenged by the rigorous demands for the enhancement of fuel efficiency, transport capacity, system safety, affordability and environmentally friendliness. The advancement of propulsion system technology represents a major element in meeting the drastic demand for reduced fuel consumption, exhaust and noise emissions. Radical propulsion technologies featuring extremely high propulsive efficiencies due to reduced specific thrust levels are considered potential candidates for future aircraft. The corresponding large propulsor dimensions pose significant challenges to propulsion system / airframe integration. The reliable evaluation of new propulsion concepts at early stages of technological development requires an integrated design and performance analysis on aircraft system.

In this thesis, a comprehensive approach to incorporating the design of advanced propulsion system concepts in the aircraft conceptual process is presented. The challenges connected to this multidisciplinary design problem are tackled by a rigorous discipline-oriented aircraft conceptual design procedure. Engine conceptual design and performance mapping is based on the software GasTurb 11, and subsequently integrated in the aircraft disciplinary analysis tasks via neural network based surrogate models. For the data sampling required during surrogate model creation and validation, a new approach is introduced using GasTurb 11 computer engine decks. For the conceptual mapping of future propulsion system technology, including the corresponding system installation implications and operational requirements, a consistent set of aircraft and engine conceptual design methods is formulated. The mapping of propulsion system design aspects involves the prediction of turbo component efficiencies, duct losses, propeller aerodynamics, as well as engine operational behaviour, dimensions and weight. The implications of propulsion system design and installation on aircraft design and sizing are discussed in detail. Classic conceptual design methodology is extended to adequately account for the integration of ducted and unducted (“open rotor”) propulsion concepts. The developed methods for system design and analysis are implemented in the proposed discipline-oriented aircraft synthesis process. The discipline-oriented conceptual design procedure is verified, validated and demonstrated based on selected design and analysis applications.

The presented studies include the comparative design investigation of advanced direct-drive turbofan and open rotor powered medium range aircraft. For advanced technology settings, design block fuel reductions of approximately 26% were computed for the turbofan engine concept, at typical cruise conditions. For the technologically equivalent open rotor concept additional fuel savings of approximately 9% were identified, while the advantage in thrust specific fuel consumption was more than 16%. The fuel burn benefit for the open rotor concept, however, were clearly reduced relative to the fuel savings predicted in the past. The gained results underline the importance of considering the system-level impact of new propulsion system concepts, in order to assess the true efficiency potentials relative to advanced conventional technology.



# Contents

<b>Vorwort</b>	<b>vii</b>
<b>Abstract</b>	<b>ix</b>
<b>List of Figures</b>	<b>xiv</b>
<b>List of Tables</b>	<b>xvii</b>
<b>Nomenclature</b>	<b>xix</b>
<b>Abbreviations and Acronyms</b>	<b>xxi</b>
<b>1. Introduction</b>	<b>1</b>
1.1. Challenges in Advanced Propulsion Integration . . . . .	2
1.2. Research Objectives and Methodological Approach . . . . .	3
1.3. Organisation of Thesis . . . . .	4
<b>2. State-of-the-Art in Aircraft Conceptual Design</b>	<b>5</b>
2.1. Current Practice in Transport Aircraft Development . . . . .	5
2.2. Significant Approaches to Sizing and Optimisation . . . . .	6
2.2.1. Multidisciplinary Design Optimisation . . . . .	8
2.2.2. Application of Surrogate Modelling Techniques . . . . .	10
2.2.3. Enhanced Design Assessment Capability . . . . .	10
2.3. Integration of Airframe and Engine Design . . . . .	11
2.3.1. Contemporary Methods . . . . .	11
2.3.2. Engine Design Representation in Existing Aircraft Conceptual Design Software . . . . .	13
2.3.3. Published Case Studies . . . . .	14
2.4. Reflection and Motivation of Presented Research . . . . .	15
<b>3. Proposed Aircraft Conceptual Design Methodology</b>	<b>17</b>
3.1. Aircraft Conceptual Design Logic . . . . .	17
3.1.1. Problem Formulation . . . . .	18
3.1.2. Impact of Engine Conceptual Design at Aircraft Level . . . . .	18
3.1.3. Discipline-Oriented Propulsion System Integration . . . . .	20
3.2. Design Process Implementation . . . . .	21
3.2.1. Information Flow Scheme . . . . .	22
3.2.1.1. System-Level Information Flow . . . . .	22
3.2.1.2. Outline of Disciplinary Subtasks . . . . .	23
3.2.1.3. The “Weights” Module - A Typical Example for Subtask Decomposition . . . . .	25

3.2.2.	Integration of Propulsion System Aspects . . . . .	26
3.2.3.	Iteration Strategy for Aircraft Scaling . . . . .	28
3.2.4.	Design Analysis Capabilities . . . . .	30
3.3.	Surrogate-Based Model Analysis . . . . .	32
3.3.1.	Problem-Tailored Data Sampling . . . . .	32
3.3.1.1.	On Sampling Plan Design Options . . . . .	33
3.3.1.2.	Latin Hypercube Sampling . . . . .	33
3.3.1.3.	Simulation of Sampling Plans . . . . .	35
3.3.2.	Surrogate Model Creation . . . . .	37
3.3.2.1.	Feedforward Neural Networks . . . . .	37
3.3.2.2.	Implemented Surrogate Model Creation Process . . . . .	39
3.3.3.	Validation and Quality Assurance . . . . .	41
3.3.3.1.	An Insightful Example . . . . .	41
3.3.3.2.	Detailed Exploration of Model Behaviour . . . . .	42
3.4.	Verification of Methodological Approach . . . . .	44
<b>4.</b>	<b>Integration of Propulsion System Simulation Software</b>	<b>47</b>
4.1.	The Software GasTurb 11 . . . . .	47
4.1.1.	Basic Characterisation . . . . .	47
4.1.2.	Analysis of Typical Work Flow . . . . .	48
4.1.3.	GasTurb Computer Decks . . . . .	49
4.1.3.1.	Basic Functionality . . . . .	49
4.1.3.2.	Dynamic Link Library Connection . . . . .	51
4.2.	Implemented Data Sampling Process . . . . .	51
4.2.1.	Engine Modelling and Process Setup . . . . .	52
4.2.2.	Experimental Design Preparation . . . . .	54
4.2.2.1.	Influence of Initial Values on Convergence . . . . .	54
4.2.2.2.	A Traveling Salesman Problem . . . . .	55
4.2.2.3.	Proposed Sorting Procedure . . . . .	56
4.2.3.	Sampling Plan Simulation . . . . .	58
4.2.3.1.	On Simulation Options . . . . .	59
4.2.3.2.	Solution Strategies for Convergence Problems . . . . .	59
4.2.3.3.	Integrated Handling of Design and Off-Design Modes . . . . .	59
4.2.4.	Validity of Results . . . . .	61
4.2.4.1.	Process Validation . . . . .	61
4.2.4.2.	Quality of Produced Results . . . . .	62
4.3.	Recapitulation . . . . .	62
<b>5.</b>	<b>Conceptual Design Methods for Aircraft and Propulsion System</b>	<b>63</b>
5.1.	Overview of Implemented Methods . . . . .	63
5.2.	Propulsion System Design Aspects . . . . .	65
5.2.1.	Overview of Propulsion System Modelling . . . . .	65
5.2.2.	Engine Design Strategy . . . . .	67
5.2.2.1.	Control Volume of Engine Modelling . . . . .	67
5.2.2.2.	Metrics for System Design and Performance Evaluation . . . . .	68
5.2.2.3.	Cycle Definition . . . . .	69
5.2.2.4.	Implemented Design Laws . . . . .	69
5.2.2.5.	Engine Thrust Sizing . . . . .	71

5.2.3.	Mapping of Turbo Component Design . . . . .	71
5.2.3.1.	Geometric Description . . . . .	72
5.2.3.2.	Aerodynamic and Mechanical Loadings . . . . .	74
5.2.3.3.	Component Efficiency . . . . .	76
5.2.3.4.	Turbine Cooling Air . . . . .	78
5.2.4.	Ducts and Associated Losses . . . . .	81
5.2.4.1.	Mapping of Pressure Losses . . . . .	81
5.2.4.2.	Air Intake . . . . .	82
5.2.4.3.	Nozzle Calculation . . . . .	82
5.2.5.	Propeller Aerodynamics and Design . . . . .	83
5.2.5.1.	Theoretical Basis . . . . .	84
5.2.5.2.	Implemented Propeller Design Code . . . . .	85
5.2.5.3.	Results and Discussion . . . . .	86
5.2.6.	Engine Operational Behaviour . . . . .	88
5.2.6.1.	Component Map Application . . . . .	88
5.2.6.2.	Compressor Handling Bleed Mapping . . . . .	89
5.2.6.3.	Engine Operational Envelope . . . . .	90
5.3.	Aircraft Geometric Description . . . . .	90
5.3.1.	Overview of Component Geometric Synthesis . . . . .	91
5.3.1.1.	Fuselage Shape . . . . .	91
5.3.1.2.	Wing Planform . . . . .	93
5.3.1.3.	Empennage . . . . .	93
5.3.1.4.	Landing Gear . . . . .	94
5.3.2.	Propulsion System Geometric Integration . . . . .	95
5.3.2.1.	Nacelle Dimensions . . . . .	96
5.3.2.2.	Turbofan Installation . . . . .	97
5.3.2.3.	Open Rotor Installation . . . . .	98
5.4.	Weights and Balance . . . . .	99
5.4.1.	Overview of Weight Estimation Methods . . . . .	99
5.4.2.	Propulsion System Components . . . . .	100
5.4.2.1.	Component Build-Up Method . . . . .	101
5.4.2.2.	Approach to Turbo Component Weight Mapping . . . . .	102
5.4.3.	Propulsion Installation Effects . . . . .	103
5.4.3.1.	Engine Pylon . . . . .	104
5.4.3.2.	Secondary Installation Weights . . . . .	106
5.4.4.	Aircraft Balancing . . . . .	109
5.5.	Aerodynamics . . . . .	110
5.5.1.	Overview of Methods . . . . .	110
5.5.2.	Propulsion Integration Aspects . . . . .	112
5.5.2.1.	Engine / Airframe Aerodynamic Interference . . . . .	112
5.5.2.2.	Propeller Slipstream Effects . . . . .	113
5.5.2.3.	Wind Milling Drag . . . . .	113
5.6.	System Performance and Sizing . . . . .	114
5.6.1.	Typical High-Speed Point Performances . . . . .	114
5.6.2.	Mission Simulation . . . . .	115
5.6.3.	Mapping of Aircraft Sizing Constraints . . . . .	116
5.6.4.	Aircraft Scaling Procedure . . . . .	118

<b>6. Demonstration of the Methodology</b>	<b>119</b>
6.1. Validation of Models . . . . .	119
6.1.1. Verification of System Iteration Strategy . . . . .	119
6.1.2. Propulsion System . . . . .	121
6.1.3. Overall Aircraft . . . . .	123
6.2. Parametric Design Studies . . . . .	127
6.2.1. Setup of Optimisation . . . . .	127
6.2.2. Performance Constraint Analysis . . . . .	129
6.2.3. Investigation of Turbofan Bypass Ratio . . . . .	131
6.2.3.1. System-Level Effects of Bypass Ratio . . . . .	131
6.2.3.2. Technology Impact on Optimum Bypass Ratio . . . . .	132
6.2.3.3. Engine Architectural Implications . . . . .	136
6.3. Comparison of Alternative System Concepts . . . . .	137
6.3.1. Considered System Configurations . . . . .	137
6.3.2. Setup of the Study . . . . .	138
6.3.3. Discussion of Simulation Results . . . . .	139
6.4. Critical Assessment of Methodology . . . . .	144
6.4.1. Assessment of the Discipline-Oriented Problem Decomposition . . . . .	144
6.4.2. On the Quality of Design Methods . . . . .	145
6.4.3. Extensibility of the Methodology . . . . .	146
<b>7. Conclusion and Future Work</b>	<b>147</b>
7.1. Important Results and Findings . . . . .	147
7.2. Reflection of Motivation and Research Goals . . . . .	148
7.3. Perspectives for Further Methodological Development . . . . .	149
<b>Bibliography</b>	<b>150</b>
<b>A. Additional Figures</b>	<b>167</b>
<b>B. Additional Tables</b>	<b>175</b>

# List of Figures

2.1. Aircraft conceptual and preliminary design process according to Torenbeek [221, Fig. 1-3] . . . . .	6
2.2. Current trends in multidisciplinary design modelling and optimisation (cf. also References [40] and [88]) . . . . .	7
3.1. Structural view of the aircraft conceptual design problem (the engine as a contributor to important aircraft design disciplines) . . . . .	19
3.2. Implemented discipline-oriented aircraft conceptual design scheme visualised in $N^2$ -matrix view . . . . .	22
3.3. Internal information flow scheme of weights module visualised in $N^2$ -matrix view . . . . .	26
3.4. Discipline-oriented integration of propulsion system aspects into the aircraft conceptual design process - a schematic overview . . . . .	27
3.5. Visualisation of iteration approach for aircraft conceptual design sizing (Example: Simplified nonlinear analysis structure for engine thrust sizing) . . . . .	29
3.6. Matrix of 2-dimensional projections of Latin hypercube sampling plans (Example: 4 dimensions, 10 sample points, 100 repetition cycles) . . . . .	35
3.7. Information flow scheme of implemented input data sampling process for surrogate model creation . . . . .	36
3.8. Typical structure of single-layer feedforward neural network . . . . .	38
3.9. Information flow scheme of implemented generic surrogate model creation process . . . . .	40
3.10. Matrix of partial dependencies for an interactive exploration of surrogate model behaviour (Shown example: Surrogate model-based turbofan engine deck including net thrust based on GasTurb 11 simulation) . . . . .	42
3.11. Visualisation of LHS-distributed validation points according to Table B.1: Sample showing SuMo relative errors $\epsilon_{val} > 0.8\%$ for the prediction of engine net thrust are highlighted. . . . .	43
3.12. Visualisation of LHS-distributed validation points according to Table B.1: Sample showing SuMo relative errors $\epsilon_{val} > 0.4\%$ for the prediction of specific fuel consumption are highlighted. . . . .	44
4.1. Basic visualisation of GasTurb general work flow . . . . .	48
4.2. Visualisation of engine design calculation process as used in GasTurb design mode . . . . .	50
4.3. Visualisation of implemented engine data sampling process using GasTurb dynamic link libraries . . . . .	53
4.4. Visualisation of implemented experimental design sorting procedure for reduced simulation time (Example: 40 sample points, 2 variables latin hypercube sampling) . . . . .	57

4.5.	Performance of implemented algorithm for sample plan sequence optimisation plotted against number of sample points (Example: latin hypercube designs for 2, 5 and 10 variables) . . . . .	58
4.6.	Solution strategy for convergence bottle necks in design space . . . . .	60
4.7.	Solution strategy for convergence problems due to temporary violation of design space boundaries . . . . .	60
4.8.	Comparison of design point calculation results: GasTurb 11 versus the presented data sampling process (Example: 200 points, 10 variables latin hypercube design) . . . . .	61
5.1.	Exemplary aircraft layouts considered for the demonstration of the proposed methodological approach . . . . .	64
5.2.	Visualisation of control volume considered for the mapping of propulsion system design aspects . . . . .	67
5.3.	Basic parameterisation of flow path geometry including thermodynamic station nomenclature (Example: 2-spool turbofan) . . . . .	73
5.4.	Basic parameterisation of turbo component geometry including the nomenclature used for stage description . . . . .	74
5.5.	Exemplary aerodynamic design charts for compressors (left) and turbines (right) as calculated based on the presented methodology . . . . .	78
5.6.	Turbine cooling air determination (Example case: 2-stage cooled high pressure turbine featuring $T_4 = 2000K$ , $T_3 = 900K$ at max. take-off conditions) . . . . .	80
5.7.	Fitted characteristics of important nozzle coefficients against nozzle pressure ratio according to Grieb [69, Figure 5.6.7] . . . . .	83
5.8.	Matrix of partial dependencies view for counter rotating propeller design model (Example: 6 + 6 bladed rotors, F7 / A7 blade shaping, NACA-16 series airfoil characteristics, propeller hub/tip ratio 0.3, blade sweep optimised for maximum propeller efficiency) . . . . .	87
5.9.	Geometric relations considered in the determination of main landing gear height	95
5.10.	Under-wing geometric integration of turbofan propulsion system . . . . .	97
5.11.	Aft-fuselage geometric integration of open rotor propulsion system . . . . .	98
5.12.	Visualisation of component build-up used for propulsion system weight estimation	101
5.13.	Matrix of partial dependencies for feedforward neural networks created from proposed engine weight model (Example: bare engine weight of 2-spool boosted turbofan) . . . . .	104
5.14.	Schematic of acting forces considered during pylon structural weight estimation	105
5.15.	Parametric study of aft-fuselage pylon weight for a wide range of potential load cases (Study parameters: pylon span and propulsion system weight) . . . . .	106
5.16.	Schematic of forces contributing to fuselage bending load in landing shock load scenario: under-wing engine installation (left), aft-fuselage engine installation (right) . . . . .	108
5.17.	Parametric study of fuselage structural weight penalty term due to propulsion installation . . . . .	109
5.18.	Component build-up of implemented models for aerodynamic drag estimation (clean configuration, landing gear retracted, all engines operative) . . . . .	112
6.1.	Analysis of iteration convergence behaviour for the aircraft configurations shown in Figure 6.2 . . . . .	121

6.2.	3-view drawings of the aircraft configurations calculated from the investigated design cases $S_{AD,k}$ . . . . .	122
6.3.	3-view drawing of the calculated Airbus A320 / IAE V2500 aircraft configuration	126
6.4.	Partial impact of exemplary system design parameters on design mission block fuel and aircraft $MTOW$ for a typical medium range application visualised using the matrix of partial dependencies view . . . . .	129
6.5.	Performance constraint chart gained from advanced medium range aircraft design study . . . . .	130
6.6.	Impact of varying turbofan bypass ratio on essential aircraft metrics . . . . .	132
6.7.	Comparison of technology scenarios according to Table 6.3 with respect to design block fuel and $MTOW$ as a function of turbofan bypass ratio and aircraft aerodynamic design Mach Number . . . . .	134
6.8.	Optimum turbofan bypass ratios against varying aircraft aerodynamic design Mach Number studies for different engine loss scaling factors based on technology scenario IV according to Table 6.3 . . . . .	136
6.9.	Schematic visualisations of the comparatively investigated engine architectures	138
6.10.	Results of comparative study of fuelburn optimised turbofan and open rotor powered aircraft designed for different Mach numbers . . . . .	140
6.11.	Visualisation of open rotor and turbofan powered aircraft designs according to Table 6.6 . . . . .	143
A.1.	Graphical user interface of the implemented software . . . . .	167
A.2.	Impact of conceptual engine design parameters on design point specific fuel consumption according to sensitivity analysis for generic 2-spool boosted turbofan engine performed in GasTurb11 . . . . .	168
A.3.	Validation of propeller design code: Ideal induced efficiency (Validation data taken from Reference [132, Figure 2]) . . . . .	168
A.4.	Parameterisation of Wing Planform . . . . .	169
A.5.	Validation of nacelle shape model for short duct separate flow turbofan engines	169
A.6.	Exemplary high-speed polar plot for a typical medium range aircraft configuration	170
A.7.	Visualisation of typical flight mission profile simulated . . . . .	170
A.8.	Characteristics of technology scenario I according to Table 6.3 with respect to design block fuel and $MTOW$ as a function of turbofan bypass ratio and aircraft aerodynamic design Mach Number . . . . .	171
A.9.	Characteristics of technology scenario II according to Table 6.3 with respect to design block fuel and $MTOW$ as a function of turbofan bypass ratio and aircraft aerodynamic design Mach Number . . . . .	171
A.10.	Characteristics of technology scenario III according to Table 6.3 with respect to design block fuel and $MTOW$ as a function of turbofan bypass ratio and aircraft aerodynamic design Mach Number . . . . .	172
A.11.	Characteristics of technology scenario IV according to Table 6.3 with respect to design block fuel and $MTOW$ as a function of turbofan bypass ratio and aircraft aerodynamic design Mach Number . . . . .	172
A.12.	Results of comparative study of fuelburn optimised turbofan and open rotor powered aircraft designed for different Mach numbers ( $M_{ADP}$ ): Study of propeller tip speed $V_{tip,prop}$ . . . . .	173



# List of Tables

5.1. Overview of propulsion system conceptual design methods . . . . .	66
5.2. Overview of aircraft geometry description . . . . .	92
5.3. Overview of weight prediction methods . . . . .	100
5.4. Overview of aerodynamic calculation methods . . . . .	111
5.5. Basic formulation of aircraft point performances . . . . .	114
5.6. Basic formulation of aircraft low-speed performance metrics . . . . .	117
5.7. Typical scheme of feedback information for aircraft scaling . . . . .	118
6.1. Model validation: Overview of engine synthesis results . . . . .	124
6.2. Summary of aircraft model validation . . . . .	126
6.3. Synopsis of technological scenarios . . . . .	133
6.4. Comparison of technology scenarios . . . . .	135
6.5. Findings from open rotor and turbofan powered aircraft comparison . . . . .	141
6.6. Comparison of open rotor and turbofan powered aircraft . . . . .	142
B.1. Demonstration of surrogate model creation and validation: An example . . . . .	175
B.2. Assignment of cooling air work potentials for cooled turbines . . . . .	176
B.3. Validation results for propeller design code . . . . .	176
B.4. Start value settings for verification of iteration strategy . . . . .	177
B.5. Outline of aircraft design cases used for solver verification . . . . .	178
B.6. Model validation: Aircraft geometry description . . . . .	179
B.7. Model validation: Aircraft weight prediction . . . . .	180
B.8. Investigated transport task scenario . . . . .	181



# Abbreviations and Acronyms

<b>AAA</b>	Advanced Aircraft Analysis
<b>AC</b>	Aerodynamic Center
<b>ACARE</b>	Council for Aeronautics Research in Europe
<b>ADM</b>	Aircraft Data Model
<b>ADP</b>	Aerodynamic Design Point
<b>AI</b>	Aircraft Integrators
<b>ANN</b>	Artificial Neural Networks
<b>APD</b>	Aircraft Preliminary Design
<b>APET</b>	Advanced Propfan Engine Technology
<b>ASDL</b>	Aerospace Systems Design Laboratory
<b>A-TF</b>	Advanced Turbofan
<b>ATM</b>	Air Traffic Management
<b>ATP</b>	Advanced Turboprop Project
<b>BFE</b>	Buyer Furnished Equipments
<b>BLISS</b>	Bi-Level Integrated System Synthesis
<b>BOD</b>	Beginning Of Descent
<b>BPR</b>	ByPass Ratio
<b>CAD</b>	Computer Aided Design
<b>CAS</b>	Calibrated Air Speed
<b>CDA</b>	Continuous Descent Approach
<b>CEA</b>	Chemical Equilibrium with Applications
<b>CEASIOM</b>	Computerised Environment for Aircraft Synthesis and Integrated Optimisation Methods
<b>CFD</b>	Computational Fluid Dynamics
<b>CO</b>	Collaborative Optimization
<b>CO<sub>2</sub></b>	Carbon Dioxide
<b>CR-TF</b>	Counter Rotating Turbofan
<b>CSSO</b>	Concurrent SubSpace Optimization
<b>DACE</b>	Design and Analysis of Computer Experiments
<b>DAR</b>	Design, Analysis and Research corporation
<b>DDM</b>	Disciplinary Data Model
<b>DD-TF</b>	Direct-Drive Turbofan
<b>DLL</b>	Dynamic Link Libraries
<b>DLR</b>	Deutsches Zentrum für Luft und Raumfahrt
<b>DOC</b>	Direct Operating Costs
<b>DOE</b>	Design Of Experiments
<b>DREAM</b>	valiDation of Radical Engine Architecture systeMs

## *Abbreviations and Acronyms*

<b>DSE</b>	Design Space Exploration
<b>DSP</b>	Data Sampling Process
<b>EBU</b>	Engine Build-up Unit
<b>EEE</b>	Energy Efficient Engine
<b>EMF</b>	Engine Model File
<b>ETOPS</b>	Extended-Range Twin-Engine Operations
<b>FEM</b>	Finite Element Analysis
<b>FFD</b>	Full Factorial Design
<b>FHV</b>	Fuel Heating Value
<b>FL</b>	Flight Level
<b>FLOPS</b>	FLight OPtimization System
<b>FNN</b>	Feedforward Neural Networks
<b>FP</b>	Framework Programme
<b>FPR</b>	Fan Pressure Ratio
<b>GE</b>	General Electric
<b>GSE</b>	Global Sensitivity Equations
<b>GSP</b>	Gas turbine Simulation Program
<b>G-TF</b>	Geared Turbofan
<b>H<sub>2</sub>O</b>	Water Vapour
<b>HPC</b>	High Pressure Compressor
<b>HPT</b>	High Pressure Turbine
<b>IAE</b>	International Aero Engines
<b>IDEA</b>	Integrated Design and Engineering Analysis
<b>IPAS</b>	Integrated Propulsion/Airframe Analysis System
<b>IPC</b>	Intermediate Pressure Compressor
<b>IPPD</b>	Integrated Product and Process Design
<b>IPT</b>	Intermediate Pressure Turbine
<b>IR-TF</b>	Intercooled Recuperated Turbofan
<b>L/R</b>	Long Range
<b>LCC</b>	Life Cycle Costs
<b>LDMF</b>	Long Duct Mixed Flow
<b>LFL</b>	Landing Field Length
<b>LHS</b>	Latin Hypercube Sampling
<b>LPC</b>	Low Pressure Compressor
<b>LPP</b>	Life Limiting Parts
<b>LPT</b>	Low Pressure Turbine
<b>LTH</b>	LuftfahrtTechnisches Handbuch
<b>LTO</b>	Landing and Take-Off
<b>M/R</b>	Medium Range
<b>MAC</b>	Mean Aerodynamic Chord
<b>MCL</b>	Maximum CLimb
<b>MDO</b>	Multidisciplinary Design Optimisation
<b>MLW</b>	Maximum Landing Weight
<b>MOPEDS</b>	MOdular Performance and Engine Design System

<b>MOPS</b>	MOdular Performance Synthesis program
<b>MPD</b>	Matrix of Partial Dependencies
<b>MTO</b>	Maximum Take-Off
<b>MTOW</b>	Maximum Take-Off Weight
<b>NACRE</b>	New Aircraft Concepts REsearch
<b>NASA</b>	National Aeronautics and Space Administration
<b>NEPP</b>	NASA Engine Performance Program
<b>NEWAC</b>	New Aero Engine Core Concepts
<b>NO<sub>x</sub></b>	Nitrogen Oxides
<b>NPSS</b>	Numerical Propulsion System Simulation
<b>NSI</b>	Numerical Status Indicator
<b>OEI</b>	One Engine Inoperative
<b>OPR</b>	Overall Pressure Ratio
<b>OR</b>	Open Rotor
<b>OWE</b>	Operating Weight Empty
<b>PASS</b>	Program for Aircraft Synthesis Studies
<b>PL</b>	Power Loading
<b>PLA</b>	Power Lever Angle
<b>PrADO</b>	Preliminary Aircraft Design and Optimisation
<b>PROOSIS</b>	PRopulsion Object Oriented SIMulation Software
<b>PSFC</b>	Power Specific Fuel Consumption
<b>PT</b>	Power Turbine
<b>RCEM</b>	Robust Concept Exploration Method
<b>RECAT</b>	Reduced Energy for Commercial Air Transportation
<b>RSM</b>	Response Surface Methodology
<b>S/R</b>	Short Range
<b>SAE</b>	System Analysis Equations / society of Automotive Engineers
<b>SAEPP</b>	Sophisticated Aero Engine Performance Program
<b>SAR</b>	Specific Air Range
<b>SBAO</b>	Surrogate-Based Analysis and Optimisation
<b>SDSF</b>	Short Duct Separate Flow
<b>SFC</b>	Specific Fuel Consumption
<b>SimSAC</b>	Simulating Aircraft Stability And Control Characteristics for Use in Conceptual Design
<b>SLS</b>	Sea Level Static
<b>SRA</b>	Strategic Research Agenda
<b>SRV</b>	Swirl Recovery Vanes
<b>TAS</b>	True Air Speed
<b>TERA</b>	Techno-economic and Environmental Risk Assessment
<b>TERTS</b>	Turbine Engine Real-Time Simulator
<b>TF</b>	Turbofan
<b>TIVA</b>	Technology Integration for the Virtual Aircraft
<b>TLAR</b>	Top Level Aircraft Requirements
<b>TLER</b>	Top Level Engine Requirements

## *Abbreviations and Acronyms*

<b>TOC</b>	Top Of Climb
<b>TOFL</b>	Take-Off Field Length
<b>TSFC</b>	Thrust Specific Fuel Consumption
<b>UDF</b>	UnDucted Fan
<b>UEET</b>	Ultra Efficient Engine Technologies
<b>UHC</b>	Unburned Hydro Carbons
<b>VBA</b>	Visual Basic for Applications
<b>VGW</b>	Variable Guide Vanes
<b>VITAL</b>	EnVIronmenTALly Friendly Aero Engine
<b>VIVACE</b>	Value Improvement through a Virtual Aeronautical Collaborative Enterprise
<b>WATE</b>	Weight Analysis of Turbine Engines

This document was created using L<sup>A</sup>T<sub>E</sub>X.

GasTurb® is a registered trademark of Dr. Joachim Kurzke.

ISight® is a registered trademark of Dassault Systèmes.

ModelCenter® is a registered trademark of Phoenix Integration, Inc.

Matlab® is a registered trademark of The Mathworks, Inc.

Excel® is a registered trademark of the Microsoft Corporation.

Windows® is a registered trademark of the Microsoft Corporation.

Visual Basic® is a registered trademark of the Microsoft Corporation.

Delphi® is a registered trademark of Embarcadero Technologies, Inc.

UDF® is a registered trademark of the General Electric Company.

# 1. Introduction

Commercial transport aircraft are complex, but highly efficient systems involving a large number of subsystems and components designed for minimum weight and energy consumption. The technological evolution of air transportation has led to a high degree of maturity of the existing system architectures. Probably the most sophisticated part of the aircraft is the power plant system which is tailored to meet a comprehensive set of performance, economic and ecological, as well as certification-related requirements. Starting from the high maturity level of today's propulsion systems, the search for new ways to significantly improve the economic and ecological efficiencies of future air transport systems requires the consideration of drastic changes to the overall system architecture. Today, pure evolutionary approaches to find new technical solutions are increasingly becoming limiting constraints in this endeavour. In turn, revolutionary design approaches including radical technological concepts add to the overall system complexity and - due to the connected lack of knowledge on real system behaviour - lower the confidence during technical decision-making. However, technical decisions during conceptual design phases are highly relevant to overall product development costs and performance characteristics, underlining the demand for methodological contributions to a sustainable assessment capability of advanced system concepts at early stages of technological development.

Challenging targets for aeronautical research and development were set by the Advisory Council for Aeronautics Research in Europe (ACARE) in the year 2001 [15]. Beside safety and economic ACARE's Strategic Research Agenda (SRA) involved ambitious environmental goals, i.e. reductions of 50% CO<sub>2</sub> and 80% NO<sub>x</sub>, as well as the halving of perceived noise by 2020 relative to the state-of-the-art in the year 2000. Contributions to the aimed CO<sub>2</sub> goals were expected from air traffic management (5-10%), airframe technological enhancement (20-25%) and from engine technology (specific fuel consumption) improvement (15-20%) [15]. Beyond that, the environmental goals declared within the "Flightpath 2050" vision [36], published by the European Commission in 2011, include the carbon-neutral growth of air traffic beginning in 2020, and a 50% overall CO<sub>2</sub> emission reduction by 2050.

In order to realise the required drastic improvements in energy efficiency, advanced ducted and more radical unducted ("open rotor") propulsion systems are being investigated as part of extensive research programmes. Ducted architectures have been subject to NASA's Energy Efficient Engine (EEE) [45] and Ultra Efficient Engine Technologies (UEET) [163] projects. Recent research within the European Union's 6th Framework Programme (FP) concentrated on innovative technologies for the improvement of thermal efficiency and emissions in New Aero Engine Core Concepts (NEWAC) [227] as well as the enhancement of propulsive efficiency and reduced noise based on new ducted propulsor designs in the EnVIronmenTALly Friendly Aero Engine (VITAL) project [92]. Open Rotor systems were addressed during the 1980s within NASA's Advanced Propfan Engine Technology (APET) [185, 176, 21] programme and the Advanced Turboprop Project ATP [76]. Today, open rotor engine architectures are being re-investigated, e.g. within FP7's validation of Radical Engine Architecture systems

(DREAM) project. Major research in advanced propulsion system integration was recently performed in the New Aircraft Concepts REsearch (NACRE) [56] project as part of FP6, as well as in NASA's the Fundamental Aeronautics Program [138].

### 1.1. Challenges in Advanced Propulsion Integration

In the past, lean interfaces between the airframe and the propulsion system constituted an efficient means of managing the enormous complexity involved in air transport system design. The strong decoupling of propulsion system and airframe design enabled the interchangeability of engines for a given aircraft. Hence, most commercial aircraft were offered to the customer including different propulsion system options provided by different engine manufacturers or alliances.

In order to utilise the additional efficiency potentials connected to the propulsion system integration, today, the classic role of engine design within the design of new aircraft is changing. Common practices in the past, often based on off-the-shelf engines or corresponding derivatives for the definition of aircraft concepts, become insufficient and are being replaced by engine designs tailored to the aircraft-specific characteristics from early stages of aircraft design. In current aircraft development programs (cf. Boeing's B787, the Airbus A350-XWB, and Bombardier's CSeries aircraft), engine manufacturers are more involved in the detailed aircraft design process and powerplant system development is tailored to a particular aircraft product.

Advanced propulsion systems will be key driving elements for the efficiency improvement of future aircraft. However, the enhancement of engine propulsion efficiency, i.e. the product of thermal and propulsive efficiencies, typically yields an increasing size of the propulsive device. In particular, new propulsor concepts stipulate stronger mutual couplings between powerplant system and airframe design. Moreover, advanced propulsion system concepts may have a significant impact on optimum system application and operational conditions [193]. In order to obtain maximum efficiency benefits from the application of advanced and unconventional propulsion system designs in the future, the close incorporation of propulsion system design starting from the very first steps in aircraft conceptual design will be vital.

In the past, a number of software frameworks for the integration of engine and aircraft-related codes were developed at NASA, including the Integrated Propulsion/Airframe Analysis System (IPAS) [110] and COMETSBOARD [71] frameworks. The development of these frameworks in the 1990s was tailored to high-speed respectively supersonic application cases which traditionally required a precise matching of engine and airframe design. Initiated as part of the European VITAL project, the Techno-economic and Environmental Risk Assessment (TERA) tool was introduced by Cranfield University and developed in collaboration with other European universities to a framework targeting the multidisciplinary assessment of engine environmental impact and cost of ownership [146]. While incorporating aircraft performance characteristics in the multidisciplinary engine assessment, the framework architecture treats aircraft conceptual design aspects in a less integrated way. Current effort towards a multidisciplinary aircraft preliminary design process, also aiming at the integration of engine preliminary design, is currently being expended at the German Aerospace Center (DLR) as part of the Technology Integration for the Virtual Aircraft (TIVA) project [120]. The system-level coupling of advanced engine and airframe design processes, however, has

not yet been reported. In summary, a rigorous methodological setup covering fast-responding integrated conceptual design of advanced transport aircraft including unconventional propulsion system architectures was not found in the literature. Therefore, the following research demands have been confirmed:

1. The development of a flexible methodological solution for an integrated conceptual design of airframe and propulsion system that enables fast-responding, full-parametric analyses of advanced and unconventional system architectures.
2. The introduction of a standardised concept for the integration of propulsion system design and operational (off-design) characteristics into the aircraft conceptual design process.
3. The formulation of a consistent aircraft and engine conceptual design methodology allowing for the mapping of future propulsion system technology, including the corresponding system installation implications, operational requirements and energy sources.

## 1.2. Research Objectives and Methodological Approach

The present research aims at enhancing the quality of engine design and technology mapping within aircraft conceptual design methodology. In particular, an increased level of detail of propulsion system design and integration aspects is targeted, while ensuring an efficient and traceable handling of the involved multidisciplinary design complexity. The methodological development, therefore, is intended to form the basis for the determination of the true efficiency potentials connected to advanced propulsion system architectures. Key requirements for the methodological development are listed below:

- Incorporation of state-of-the-art aspects of aircraft conceptual design in an automated sizing process with emphasis placed on the integration of advanced and unconventional propulsion system design and performance analysis capability, allowing for the further opening up of the aircraft design space.
- Appropriate mapping of the interactions between the propulsion system, the airframe and flight mission aspects at a conceptual system design level.
- Model extensibility for system zooming, e.g. the exchange of semi-empirical methods by physics-based models, as well as the mapping of new technologies, system architectures and analysis aspects.
- Comprehensive design analysis capability including sensitivity analysis, trade studies and constrained optimisation, thereby, enhancing the transparency of the multidisciplinary system behaviour, and allowing for the rapid identification of efficiency trends for advanced and unconventional propulsion technology at aircraft level.
- Applicability of typical figures of merit for aircraft conceptual design studies, such as Specific Air Range (SAR), mission fuel burn, green house gas emissions, such as CO<sub>2</sub> and NO<sub>x</sub>, and operational costs.
- Methodology verification, validation and demonstration based on representative design and analysis tasks.

The proposed methodology covers an efficient strategy for the decomposition of the targeted multidisciplinary design problem, including model integration and system analysis approach, as well as methods for the physics-mapping of advanced propulsion system design and integration, well-suited for fast-responding aircraft conceptual design studies. Therefore,

## 1. Introduction

important propulsion system design and performance aspects are incorporated within a rigorously discipline-oriented aircraft conceptual synthesis procedure, using surrogate modelling techniques based on artificial neural networks. For the modelling of propulsion system conceptual design and performance, the well-recognised software GasTurb is used. The developed methodological capabilities are demonstrated through aircraft-level design studies of representative turbofan and open rotor engine architectures.

### 1.3. Organisation of Thesis

In this thesis, a comprehensive approach to incorporating the design of advanced propulsion system concepts in the aircraft conceptual process is presented. Classic aircraft conceptual design methodology is extended by new methods to adequately allow for the design and integration of advanced propulsion system concepts.

In **Chapter 2**, the state-of-the-art in aircraft conceptual design and multidisciplinary analysis is characterised with particular focus on the handling of engine design aspects. Therefore, recent trends in Multidisciplinary Design Optimisation (MDO) are outlined and existing software frameworks for the concurrent treatment of aircraft and propulsion system design aspects are reviewed. Finally, a survey of conceptual design studies of open rotor and turbofan-powered aircraft is given. A formal analysis of the multidisciplinary problem of integrated engine and aircraft conceptual design is presented in **Chapter 3**, and potential approaches to efficient problem decomposition are discussed. Based hereon, a rigorous discipline-oriented procedure for the aircraft design synthesis is introduced, involving the surrogate model based integration of propulsion system design aspects within the disciplinary subtasks of the process. **Chapter 4** is dedicated to a newly developed approach to efficient engine design and performance data sampling using GasTurb 11 computer engine decks. In **Chapter 5**, a consistent set of aircraft and engine conceptual design methods is formulated, ensuring high-quality mapping of future propulsion system technology as part of aircraft conceptual design. The developed methods include the elaboration of basic propulsion system design aspects including the mapping of turbo components efficiencies, duct losses, swept-blade counter rotating propeller aerodynamics as well as turbo component length and weight estimation. The aircraft disciplinary implications connected to advanced turbofan and open rotor engine design and integration are discussed in detail and new methods for the prediction of powerplant structural installation weights are introduced. As part of **Chapter 6**, the proposed methodological approach is verified, and the implemented models for engine and aircraft design and performance mapping are validated. Moreover, the design and analysis capabilities of the developed methodology are demonstrated based on representative analysis tasks, i.e. the aircraft-level optimisation of engine design parameters, as well as the parametric aircraft-level comparison of advanced turbofan and open rotor propulsion system architectures. Finally, the developed methodology is critically reviewed. In **Chapter 7**, important results and findings gained from the elaborated methodological approach and conducted studies are summarised. To round of, starting points for follow-on research are identified.

Essential methodological aspects of the research presented in this thesis have been disseminated to the scientific community and discussed through four conference contributions [193, 189, 190, 191] and one journal article [192]. In Reference [189], the integrated framework of models was introduced, while References [193, 190, 191, 192] focused on insightful case studies.

## 2. State-of-the-Art in Aircraft Conceptual Design

The present work aims at advancing the capability of multidisciplinary analysis of aircraft conceptual design problems including the design of advanced propulsion system technology. The methodology described in the following chapters of the thesis involves essential aspects of aircraft conceptual design, multidisciplinary system modelling and optimisation, as well as the parametric mapping of the physics of advanced and unconventional propulsion system technology. In the present chapter, previous work in the affiliated fields of research is characterised, and the current state-of-the-art of aircraft conceptual design and recent advancements are discussed. Furthermore, the methodological frame of reference in multidisciplinary system modelling is outlined and a compact survey of existing methodological work towards an integrated treatment of aircraft and propulsion system conceptual design is given.

### 2.1. Current Practice in Transport Aircraft Development

The development of commercial aircraft is a challenging enterprise in systems engineering. The description of the Airbus A380 as an example of modern aircraft comprises approximately 1,000,000 technical drawings. The resulting commercial aircraft is a response to the manifold requirements of customer demands, company requirements and airworthiness regulations, and represents a compromise with respect to the knowledge, experience and creativity of the engineers from multiple disciplines involved in the development programme [152]. The current practice in the development of commercial aircraft at Airbus is described by Pardessus [152]. The structured development cycle, which is the baseline for all Airbus programmes, features five major phases, namely the “Feasibility”, “Concept”, “Definition”, “Development” and “Series” phases. While development and series production phases are dominated by industrial performance requirements, i.e. the linking of engineering and production, upstream phases (feasibility, concept and preliminary definition) constitute a considerable amount of interactive and iterative processes. In these early phases, efficient management of design freedom and disciplines is vital in order to ensure a robust baseline definition for succeeding development stages. More detailed design phases increasingly constrain design freedom from system architectural to local solutions [152].

A classic aircraft design procedure as presented by Torenbeek [221] is illustrated in Figure 2.1. Accordingly, in the conceptual design phase, initial design specifications are defined based on customer, contractor and airworthiness requirements and an aircraft design concept is established. Subsequent engine selection yields the initial design which serves as a baseline for parametric studies and configuration development in the preliminary design phase. The resultant technical description of the aircraft represents the basis for the subsequent detailed design phase. Similar process descriptions of the conceptual and preliminary design process

## 2. State-of-the-Art in Aircraft Conceptual Design

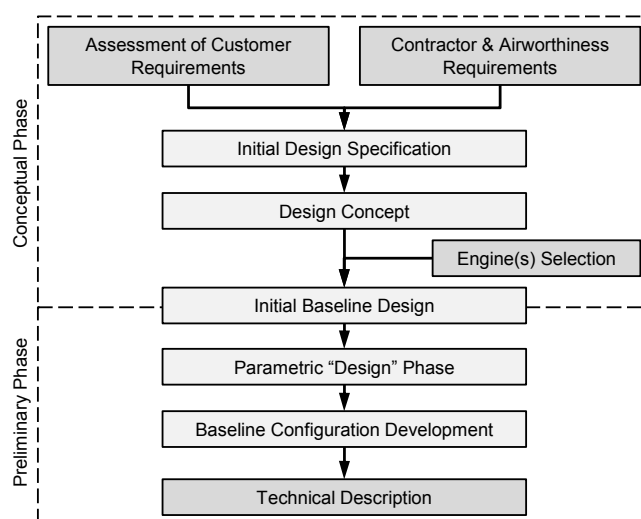


Figure 2.1.: Aircraft conceptual and preliminary design process according to Torenbeek [221, Fig. 1-3]

may be found in References [85] and [173]. These classic approaches to aircraft design may be correlated to current industry practice assuming conceptual design to be conducted during the feasibility phase, preliminary design to be finished after the concept phase and detailed design constituting the definition phase.

The role of engine design at aircraft conceptual design stages within modern aircraft programmes is explained by Remy [174]. During the feasibility phase, Top Level Aircraft Requirements (TLAR) such as payload, range, cruise speed and technology readiness at the expected entry into service date constitute the basis for the conceptual aircraft sizing yielding aircraft weights and wing area. Resulting take-off and climb performance requirements are then used to define the initial Top Level Engine Requirements (TLER). At this stage, engine manufacturers are provided with the TLER and the TLAR and propulsion system options are discussed. Trade-off studies for noise and fuel consumption are performed using component efficiencies, essential cycle parameters and bypass ratio as trade parameters. The gained trade-off results are fed back into the TLAR to ensure proper aircraft sizing. At the end of the feasibility phase, all major architectural decisions have been made and the aircraft concept including propulsion system is defined [174].

### 2.2. Significant Approaches to Sizing and Optimisation

Commercial aircraft have a long product life cycle of approximately 60 years from the established product idea until the last individual aircraft of the production series is out of service [174]. The commitment of product Life Cycle Costs (LCC) is strongly associated with the significance of design decisions. Large proportions of the overall programme expenditures are predetermined at very early stages of the product development cycle. Information on typically committed LCC shares at different design stages is given by Roskam [182] (cf. also Reference [211]). Approximately two-thirds (65%) of the aircraft LCC are defined during the feasibility phase, increasing to 85% during the concept phase. The severe cost impact of

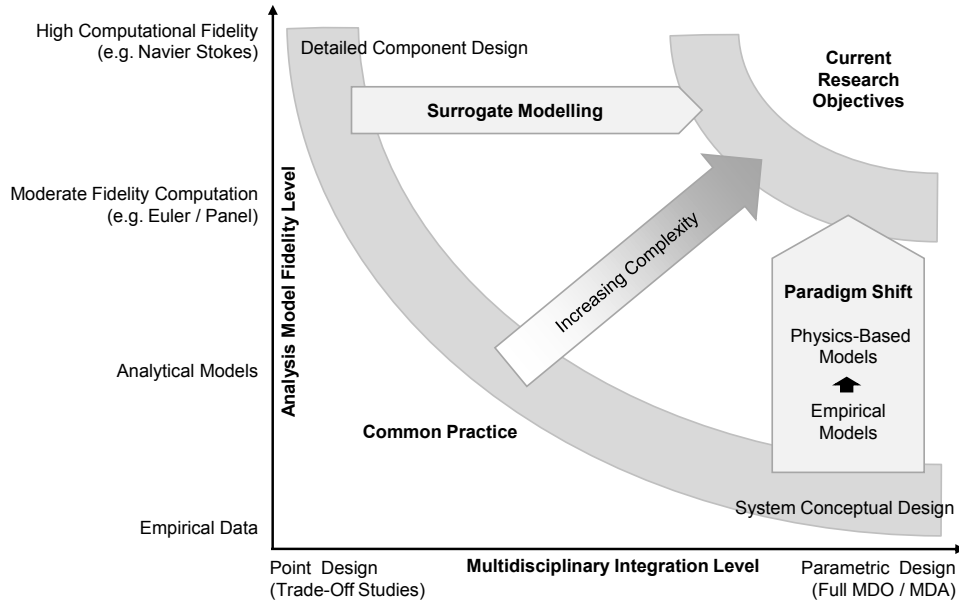


Figure 2.2.: Current trends in multidisciplinary design modelling and optimisation (cf. also References [40] and [88])

design decisions at aircraft conceptual design level underlines the necessity of drastic gain of knowledge on system behaviour at early stages of system design. Now, taking into account the extremely high safety and reliability requirements discussed in Reference [140] as well as the tremendous system complexity, the challenge of predicting the economic and ecological impact of important design decisions becomes clear.

A key requirement for product development at minimum cost and maximum throughput is to ensure maximum process efficiency during extensive development phases, i.e. detailed design and series production [152]. The knowledge on detailed design processes of aircraft, their subsystems and components is mainly owned by the Aircraft Integrators (AI) and supplier companies. Many research activities in the field of aircraft design focus on enabling methodologies to improve early stages of the product development cycle. Here, the aforementioned economic significance of conceptual design decisions has been triggering extensive methodological effort. Common research objectives aim at reducing the lack of knowledge on system behaviour, thereby increasing robustness and improving confidence whenever technical decisions take place.

Figure 2.2 visualises important trends followed during methodological development towards an enhanced system evaluation capability (cf. References [88, 40]). Here, two basic trends are apparent which increase the overall complexity of the design problem: firstly, the shift towards more sophisticated, physics-based disciplinary analysis models; and, secondly, the integration of more detailed component or subsystem design aspects into full parametric multidisciplinary studies.

In the following, essential fields of current research in the enhanced handling of the rising complexity during aircraft conceptual design phase are outlined. Significant methodological contributions forming the scientific environment for the present work are named and characterised.

### 2.2.1. Multidisciplinary Design Optimisation

Conceptual design decisions at aircraft level typically affect multiple parts of the system and implications extend to several design and analysis disciplines. These even include major design decisions at subsystem level, such as the propulsion system, which may have a significant impact on the best and balanced design of the overall aircraft [191]. In order to realistically evaluate the effect of (sub-) system design changes (e.g. by introducing new technologies) on an overall system level, design analysis and optimisation tasks have to incorporate the mutual couplings between system components as well as the affected intra- and interdisciplinary correlations in an adequate way. This challenge is tackled by multifaceted research activities embraced by the term Multidisciplinary Design Optimisation (MDO).

A comprehensive overview of methodological approaches to MDO problems as well as classic technical solutions and application cases is given in References [207] and [61]. A survey of state-of-the-art activity in MDO can be found in Reference [177], which summarises the capabilities of NASA's Integrated Design and Engineering Analysis (IDEA) environment. The MDO activities performed as part of the European Union co-funded Value Improvement through a Virtual Aeronautical Collaborative Enterprise (VIVACE) project are presented in Reference [88]. MDO techniques, particularly applied to the preliminary design of flight propulsion systems are summarised in Reference [151]. A comprehensive approach to MDO in aircraft conceptual design is illustrated in Reference [172]. Further trends in complex system engineering, involving the progress in computer science, system analytics and concurrent engineering can be found in Reference [189].

The progress in disciplinary analyses and the involved increase in information to be shared - disciplinary and interdisciplinary - adds to the communication challenges in multidisciplinary design. In order to keep optimisation problems to manageable sizes, an efficient management of models and codes involved in multidisciplinary design tasks is vital. Significant methodological effort was spent in the past in order to mitigate the problem of rapid complexity rise against increasing size of design or analysis tasks (cf. References [200, 199, 201, 93, 204, 203, 95, 205, 198, 206, 96]). Here, the time-honoured approach of decomposing large tasks into smaller, more manageable ones has proven to be a key factor to successfully handle complex design and analysis problems. The strategy followed by the approach of problem decomposition is outlined in Reference [199] as breaking large tasks into a number of smaller subtasks, while preserving the couplings among these subtasks. The objective of problem decomposition is to maximise the volume of information that is processed internally in a subtask, while minimising the coupling information between subtasks.

Decomposition schemes for particular engineering problems are numerous in the literature, some of them incorporate the hierarchical arrangement of the system nature (cf. multi-level decomposition [205]). Others treat problems encountered as non-hierarchical structures (cf. classic single-level decomposition, such as LU matrix decomposition [200]). An overview of common approaches to system decomposition involving physical boundary-based, discipline-based, mathematical property-based, sequence-based as well as combinatorial criteria is given in Reference [229]. A decomposition method based on combinatorial criteria is described in Reference [121, p.67ff] which considers different types of system attributes mapped within a multiple-domain matrix structure.

In the case of aircraft MDO problems, decomposition techniques facilitate the problem-oriented identification of adequate interfaces between subtasks within the overall design task. Hence, various decomposition-based approaches to optimising multidisciplinary design problems have been developed in the past, involving Global Sensitivity Equations (GSE) [202], System Analysis Equations (SAE) [23], the Concurrent SubSpace Optimization (CSSO) method [201], the Collaborative Optimization (CO) [95] approach as well as the Bi-Level Integrated System Synthesis (BLISS) technique [205, 206]. The BLISS approach represents a synthesis of methodological effort in dealing with complex, large-scale optimisation problems. BLISS is a method for path-building within system design space, by decoupling subtask optimization using local objectives and constraints from system level optimisation, while the latter only coordinates a relatively small number of design variables shared by the subtasks. The solution of the system level coordination task is guided by the derivatives of subtask behaviour and local design variables with respect to the shared global design variables [205]. Since its introduction in 1998 [205] the BLISS approach has been demonstrated for different fidelity levels of subtask analysis codes and applied to multidisciplinary aircraft design tasks [206, 89]).

A technique for problem decomposition closely related to BLISS is the Collaborative Optimization approach which was developed for and applied to distributed aerospace MDO tasks [94]. Both concepts, BLISS and CO, yield a decomposed design process involving individual disciplines each incorporating local analysis and design responsibilities while communicating with a system-level coordination routine. Intrinsic to the CO approach is the handling of global parameters exchanged between subtasks using so-called “compatibility constraints” [95] which are added as additional constraints to the convergence goal of the system-level optimisation procedure. Using compatibility constraints for feedforward and feedback correlations, this technique allows for full decoupling and parallelisation of subtasks. CO may be performed directly in a single software program or through communication via computer network [95]. Inherently connected to the CO approach, the size of the system-level optimisation problem increases against the number of parameters shared between subtasks. It is, therefore, considered primarily suitable for low dimensionality of subtask coupling [94]. Since its first presentation in 1994, CO has gained considerable importance in distributed design and optimisation tasks (cf. References [18, 96, 19, 20]).

Intelligent problem decomposition plays an important role in modern approaches to aircraft conceptual design synthesis and optimisation. Formalised problem decomposition based on the analysis of system semantics has been implemented in software solutions such as the DeMAID program [178], supporting an intelligent organisation of complex design processes. A comprehensive overview of MDO application to aircraft conceptual design including the characterisation of applied system decomposition techniques is given in Reference [53]. However, in order to increase the level of confidence during the search for global constrained optima of large-scale MDO problems, current research objectives have also focuses on an exhaustive design space exploration capability (cf. References [90, 116, 129, 113]). A most recent contribution to an advanced MDO of efficient aircraft concepts is presented in Reference [114], describing MDO application to integrated studies of advanced technologies at the aircraft conceptual design level.

### **2.2.2. Application of Surrogate Modelling Techniques**

Facilitating the capability of fast responding design space exploration, techniques for the approximation of complex system models through mathematical surrogates have proven to be key enabler for a successful handling of multidisciplinary design tasks.

A comprehensive state-of-the-art review of surrogate modelling methodology and its application to complex design problems is presented in Reference [169]. The issued contents include essential criteria for surrogate type selection and construction, design of experiments, sensitivity analysis, convergence and optimisation, highlighting practical concepts towards a Surrogate-Based Analysis and Optimisation (SBAO). A discussion of well-established approaches to surrogate modelling is also given in Reference [195], including the classic Design Of Experiments (DOE)-based Response Surface Methodology (RSM) as well as the Design and Analysis of Computer Experiments (DACE) which often employs Kriging [55] models.

The application of surrogate modelling techniques is best-suited for early design phases, when the ranges of parametric variation are large while the number of design variables is relatively small compared to more detailed design phases [205]. The effectiveness of surrogate model application is limited by the off-line computational effort required for surrogate model regression and validation which strongly increases with rising nonlinearity of system behaviour and number of free variables. A very early application to decision making in aero-engine design was reported by Boeing Commercial Airplane Company in 1975 [77]. Since then, RSM has been adopted to robust design space analysis [91] and various approaches to enhanced decision making such as represented by the Robust Concept Exploration Method (RCEM) [35].

Surrogate modelling techniques include linear and nonlinear regression approaches. In particular, the application of artificial neural network has gained popularity for aircraft MDO tasks. Here, important contributions were published by Patnaik et. al. who used neural network-based approximation for the design optimisation of (chronologically) high speed civil transport aircraft [157, 156], aero-engines [158, 159] and subsonic aircraft [155, 154]. RSM application in integrated engine and airframe studies may be found in References [30, 193, 188, 190, 190, 191]. An overview of further RSM application cases in aerospace engineering is given in Reference [196].

### **2.2.3. Enhanced Design Assessment Capability**

Various approaches for more efficient utilisation of design freedom towards enhanced product quality, i.e. economic profitability, environmental impact, development time-to-market etc., have been developed in the past. Recent methodology development has aimed at extending the scope of system design evaluation to environmental aspects [22, 51], enabling techniques for enhanced concept and technology assessment [90, 116, 129], as well as the exploration of complex design spaces [231]. Essential contributions are characterised in the following.

Recent methodological work concentrated on closing the “knowledge gap” during early phases of product development, i.e. the discrepancy between cost commitment and the confidence in design decisions (cf. [211, Fig. 1.1]), thereby, aiming at enhanced design freedom and reduced design uncertainty [127, 212]. Significant contributions towards enhanced capabilities for technology and system concept assessment [126, 184, 90, 31, 129] as well as conceptual

design decision-making [116] including the use of probabilistic correlations were developed at ASDL. Here, Reference [126] presents an Integrated Product and Process Design (IPPD) approach for military aircraft concept selection and evaluation. In Reference [90] a general approach to technology identification, evaluation and selection in conceptual aircraft design is developed, while Reference [129] focuses on the assessment of advanced propulsion concepts. The methodological treatment of risk and uncertainty in modern aerospace systems design is derived in Reference [184] which also emphasises propulsion system technology.

## 2.3. Integration of Airframe and Engine Design

Potential technical solutions for highly efficient future air transport involve engine architectures based on ducted and unducted, single and counter rotating, geared and directly driven propulsor concepts, each of which having essential implications on the optimum design of the overall aircraft system. A compact comparison of the characteristics of ducted and unducted propulsion system concepts is given in Reference [70].

In the present section, essential methodological contributions to an integrated treatment of engine and airframe design features are discussed. In particular, NASA activities in the past 20 years and the current European TERA developments will be emphasised. These have been identified to be most significant during the literature research conducted for the present work. Beyond that, well-established software solutions addressing aircraft conceptual design are reviewed towards the incorporation of propulsion design aspects. To round off, published studies on an integrated treatment of engine and airframe design are outlined.

### 2.3.1. Contemporary Methods

Significant methodological work towards a multidisciplinary optimisation of engine and airframe design was conducted at NASA Lewis Research Center. The methodological contributions published, mainly employed shared solutions for the disciplinary analyses, such as the FLIGHT OPTimization System (FLOPS) [131], the Weight Analysis of Turbine Engines (WATE) code [147] and the NASA Engine Performance Program (NEPP) [166]. Connecting these codes, the Integrated Propulsion/Airframe Analysis System (IPAS) [110] was introduced in 1992. IPAS allows for a concurrent optimisation of engine and airframe design parameters and was demonstrated for high-speed aircraft design case [110]. In 1996, the design code integration framework COMETSBOARD [71] was introduced as an optimisation engine for multidisciplinary aircraft and propulsion system design tasks [160, 162, 161]. Later, COMETSBOARD and the related decomposition-based cascade optimisation strategy were enhanced by surrogate model application (cf. References [157] and [156]).

Earlier, in 1994, an integrated method for engine cycle and aircraft configuration optimization was presented by K. Geiselhart (Lockheed Engineering & Sciences Company), This approach allowed for the incorporation of engine design parameters in aircraft design tasks and was demonstrated for supersonic civil transport application [60].

Current methodological effort towards an integrated aircraft preliminary design process is being made at the German Aerospace Center (DLR). Here, the integration of engine

## 2. *State-of-the-Art in Aircraft Conceptual Design*

preliminary design into the overall aircraft design process is aimed for as part of the Technology Integration for the Virtual Aircraft (TIVA) [120]. Here, for workflow integration the ModelCenter [164] framework is used. An overview of further software solutions for workflow management and tool chain integration is given in Reference [120, Table 2].

Initiated as part of the VITAL project and further developed within the NEWAC project [227], the tool TERA (Techno-economic and Environmental Risk Assessment) targets a multidisciplinary engine assessment of environmental impact and cost of ownership [146]. The TERA concept was introduced by Cranfield University and developed in collaboration with other European universities. TERA includes modules for aircraft and engine performance, engine weights, economics, environment, noise and emissions. For engine performance considerations, Cranfield University's in-house code TURBOMATCH [150] is used. Aircraft performance is simulated using the HERMES code, which computes typical performance characteristics for given aircraft geometry, weight information and mission profile [146]. Here, calculations are based upon handbook methods according to Jenkinson [85]. Engine operational characteristics are provided by TURBOMATCH [49]. A corresponding flow chart is given in Reference [49]. The modules of the TERA framework are embedded in an ISight [43] work flow scheme [29].

At Cranfield University, several dissertations related to the TERA development have been published in the recent past [49, 153, 170]. Here, Reference [49] focuses on the preliminary design methodology of advanced propulsion systems including cycle options, noise characteristics and weight mappings. Integration effects of an ultra-high bypass ratio, recuperated, intercooled-recuperated and constant volume combustion turbofans were studied for conventional airframe geometry. A novel aircraft concept featuring wing-embedded engine installation was investigated with respect to fuel burn and noise. Reference [153] describes the methodological approach to assessing risks and costs connected to advanced turbofan architectures as part of TERA. Based hereon, optimisation studies for the engine architectures investigated in VITAL (DD-TF, G-TF and CR-TF) were presented, targeting minimum fuel consumption and operating costs. In Reference [170], multi-objective assessments of advanced turbofan architectures tailored to new short range applications and benchmarked against an Airbus A320 baseline were presented. Objectives of the investigation involve the reduction of fuel burn, NO<sub>x</sub> emissions, engine Direct Operating Costs (DOC) and noise. A most recent overview of TERA capabilities is given in References [107] and [111].

A survey of distinguished propulsion system simulation software may be found in Reference [11]. The overview includes proprietary ("in-house") as well as commercially available software solutions. Characterisation is given for the PPropulsion Object Oriented SIMulation Software (PROOSIS), the Gas turbine Simulation Program (GSP), the Turbine Engine Real-Time Simulator (TERTS), the Numerical Propulsion System Simulation (NPSS) framework, the MODular Performance Synthesis program (MOPPS), the MODular Performance and Engine Design System (MOPEDES), the turbomatch scheme, the Sophisticated Aero Engine Performance Program (SAEPP) and the NASA's NEPP.

### 2.3.2. Engine Design Representation in Existing Aircraft Conceptual Design Software

Aircraft conceptual and preliminary design have been issued constantly in aeronautical research over the past decades and manifested in manifold types of software, including proprietary solutions and commercially available software tools. In the following, operative software solutions applicable for the early stages of aircraft design are characterised with emphasis placed on the incorporation of propulsion system design aspects. Here, it should be noted that the boundaries between software solutions for aircraft conceptual and preliminary design are not explicitly determinate, depending on the individual definition of the copyright owner.

#### **PIANO**

Piano is a commercial aircraft sizing and analysis software developed by Lissys Ltd. which is in use at numerous major aircraft and engine manufacturers worldwide [122]. Piano offers a database of calibrated models for more than 250 commercial aircraft. The calculation methods implemented as well as aircraft analysis and optimization features of the software are explained in Reference [194]. Engines are modelled in the form of data matrices. The software readily provides several scalable engine datasets for different propulsive systems including turbofans and turboprops at typical engine ratings. Comprehensive engine performance datasets as supplied by engine manufactures can be imported. Issues of engine synthesis or thermodynamic cycle analysis are not addressed by Piano.

#### **Pacelab APD**

Pacelab APD [13] (Aircraft Preliminary Design) is a commercial software package based on the Pacelab Suite [14] modelling environment offering a variety of predefined aircraft configuration options. Aircraft design computation refers to handbook methods, mainly implemented according to Torenbeek [221]. Engine performance characteristics are represented via thrust and fuel flow decks for typical engine ratings and part power settings [13]. The respective tabulated input files may be imported from external software / databases [149].

#### **PrADO**

The software PrADO (Preliminary Aircraft Design and Optimisation program) [78] is a modular framework developed at the Institute of Aircraft Design and Lightweight Structures (IFL), Technische Universität Braunschweig. PrADO comprises a pool of several hundred subprograms implemented in the Fortran programming language. The subprograms cover important aspects of multiple disciplines involved in aircraft preliminary design and can be applied according to the context of particular design and analysis capabilities involving unconventional aircraft configurations. The models and codes available in PrADO feature different levels of fidelity ranging from handbook methods to finite element analysis and high-order panel methods [226]. Engine performance characteristics in terms of thrust and specific fuel consumption are calculated as a function of flight speed and altitude using a “simplified thermodynamic cycle” [209].

#### **AAA**

The Advanced Aircraft Analysis (AAA) [46] program is developed by the Design, Analysis and Research (DAR) corporation and represents a comprehensive implementation of the

## 2. *State-of-the-Art in Aircraft Conceptual Design*

handbook methods according to Roskam. The software offers a variety of propulsion system installation options involving a variable number of engines, typical installation locations, as well as ducted and unducted propulsor types. [46] The calculation of propulsion system characteristics refers to Reference [183, Chapter 6].

### **RDS**

RDS-Professional [37] is an aircraft conceptual design software product of the Conceptual Research Corporation featuring a Computer Aided Design (CAD) module for aircraft layout as well as analysis modules for aerodynamics, weights, propulsion and cost. [171] RDS-Professional is based on the methods published by Raymer [173]. Raymer's handbook contains empirical correlations for turbo engine sizing including specific fuel consumption and thrust at cruise condition. The given formulas distinguish between afterburning and non-afterburning engines. [173, p.226f]

### **CEASIOM**

CEASIOM (Computerised Environment for Aircraft Synthesis and Integrated Optimisation Methods) is an aircraft conceptual design framework which was developed as part of the SimSAC (Simulating Aircraft Stability And Control Characteristics for Use in Conceptual Design) project within the European Commission's 6<sup>th</sup> framework programme [32]. CEASIOM is a freeware application developed in Matlab [216] and offers a set of modules facilitating aircraft geometry building, flight control system design as well as aerodynamics, aeroelastics, stability and control analysis [32]. The aircraft geometry building module offers a variety of engine installation options [175]. An interface for the input of basic propulsion system geometric parameters and performance data is provided [175].

### **2.3.3. Published Case Studies**

Advanced propulsion system architectures, in general, have been subject to scientific studies ever since powered flight exists. However, the challenge of propulsion system integration issues depends on the technological concept considered. The need for fuel burn reduction in commercial aviation - in the past and today - has been triggering extensive propulsion-technological and conceptual effort to increase thermal and propulsive efficiency.

In particular, the architecture of the propulsive device may have a great impact on the overall aircraft arrangement. Thus, ducted and unducted propulsor engine concepts have been subject to extensive comparative studies in the past as well as in current research investigations. Existing studies of propulsion system architectures at the aircraft conceptual design level are reviewed in the following, especially focussing on comparative investigations of propfan (also referred to as "open rotor") and turbofan engine architectures.

At the aircraft system level, several studies on open rotor propulsion systems have been performed in the past. Early analyses of mission fuel consumption of high-speed propeller-powered aircraft relative to turbofan-powered aircraft were conducted within the Reduced Energy for Commercial Air Transportation (RECAT) studies [1]. A corresponding summary of the sensitivity analyses performed for cruise Mach number and propeller tip speed is published in Reference [38]. Comparative design studies of technologically similar turbofan and open rotor-powered short range aircraft were also part of the Advanced Propfan Engine Technology (APET) programme studies [185]. In Reference [65], performance aspects of

potential open rotor installation arrangements based on the Douglas DC-9 Super 80 aircraft layout are compared. Existing publications, furthermore, include analytical approaches as well as numerous computational and experimental studies on the aerodynamic and aero-acoustic airframe integration of high-speed turboprop engines (cf. References [4, 3, 5, 76] and [57]).

An investigation of different cargo aircraft designs was performed by the Lockheed-Georgia Company under NASA contract [143] [144]. Here, the potential fuel burn and DOC benefits as well as airport noise penalties of turboprop propulsion were investigated relative to competitive turbofan technology. The technology considered was projected to be available in the mid-1980s. The aircraft design parameters investigated involved cruise Mach number, number of payload containers, initial cruise altitude, wing sweep angle, wing loading and aspect ratio. Varied propulsion system parameters were propeller tip speed, disc loading and blade number of the single rotating propeller and bypass ratio for the turbofan references. Three turboprop-powered aircraft were analysed and compared to three turbofan-powered aircraft yielding 17 to 21% fuel burn savings. [144]

In the more recent past, system integration aspects of ultra-high bypass ratio engines and corresponding environmental impact have been studied within NASA's Ultra Efficient Engine Technology (UEET) programme [41, 42]. In studies related to the present thesis, the implications of ultra-high bypass ratio engines on aircraft and mission design aspects were investigated with respect to fuel burn characteristics and emission characteristics as well as economic figures of merit [188, 190].

Recent studies on a multidisciplinary evaluation of advanced propulsion system architectures have been performed for a short to medium-range commercial aircraft application at Purdue University [112] based on the PASS (Program for Aircraft Synthesis Studies) framework [93]. Here, advanced technologies such as composite materials, natural laminar flow as well as direct-drive turbofan (DD-TF), geared turbofan (G-TF) and propfan engine concepts have been implemented in PASS using fudge factors [113]. Different designs of a counter-rotating ducted propfan engine concept have been comparatively evaluated at DLR, based on mission performance simulation [148]. A recent NASA study on advanced turbofan and geared turbofan technology for next generation single-aisle commercial aircraft is reported in References [74] and [73]. A related study focusing on a hybrid wing body aircraft for the long-range application can be found in Reference [219].

## 2.4. Reflection and Motivation of Presented Research

Classic design processes of commercial aircraft involve a lean interface for information exchange between airframe and engine conceptual design (cf. Section 2.1). Integrated design optimisation is subject to preliminary and detailed design phases. Therefore, the existing design freedom at conceptual aircraft design stages is not exploited in an optimum way. Here, intelligent problem decomposition and surrogate modelling techniques have been identified to be key enabling elements of a successful multidisciplinary design analysis and optimisation (see Sections 2.2.1 and 2.2.2).

Essential fields of recent and current research have been focusing on enhancing the system assessment capability for advanced technologies (see Section 2.2.3). Significant effort has been expended in connecting airframe and propulsion system design aspects (see Section 2.3).

## *2. State-of-the-Art in Aircraft Conceptual Design*

Several solutions, such as the IPAS and COMETSBOARD frameworks, have been developed by NASA and applied to multidisciplinary aircraft design problems including engine design aspects in the past. These software frameworks were essentially triggered by high-speed respectively supersonic application cases (cf. Section 2.3.1). The TERA activities include aircraft performance characteristics in the multidisciplinary engine conceptual design process. However, the tool architecture treats aircraft conceptual design aspects in a less integrated way. Existing software solutions for aircraft conceptual design do not offer the capability of an integrated consideration of propulsion system design (cf. Section 2.3.2). Based on aircraft design frameworks in current development such as aimed for in DLR's TIVA project, multidisciplinary coupling of engine and airframe conceptual design process has not yet been reported. Hence, a rigorous methodological setup covering fast-responding integrated design of advanced efficient aircraft concepts including unconventional propulsion systems concepts could not be found in the literature.

In summary, there is a lack of integrated treatment of propulsion system design in the aircraft conceptual design process. For a sustainable assessment of new propulsion system technologies, there is the need for an integrated design and operational simulation capability involving all relevant parts of the system considered. In terms of the aircraft conceptual design task, this includes the overall aircraft architecture and all subsystems affected by the introduction of a new technology, as well as operational aspects, such as mission design, flight envelope, operational flexibility and fleet design aspects. In the following chapters of this thesis, a comprehensive approach to tackling this research demand is introduced, elaborated and demonstrated.

## **3. Proposed Aircraft Conceptual Design Methodology**

Advanced and unconventional propulsion system technological concepts are considered as key drivers for further enhancements of aircraft environmentally friendliness as well as a key enabler for the profitability of future commercial aviation. However, an increasing challenge for the evaluation of new propulsion system architectures is connected to a reliable analysis of system integration aspects. The cross-coupling effects between engine and airframe require a multitude of design trade-offs, whose accurate assessment at overall system level is a key factor for the identification of promising candidate concepts for efficient future aircraft.

The core of the present methodological development is a new approach to the integration of multidisciplinary propulsion system design aspects into the aircraft conceptual design process. Therefore, a detailed analysis of the interrelations of airframe and propulsion system design is presented and a comprehensive approach to tackling the encountered, multidisciplinary design task is derived and elaborated. The proposed methodology facilitates rapid trend statements at overall system level without disregarding the involved system complexity, and thus, enables a quick gain of knowledge on system behaviour. Main elements of the proposed conceptual design approach are presented in Chapters 3, 4 and 5. While Chapter 4 focuses on the required integration of the considered engine design and analysis software, a consistent set of aircraft and engine conceptual design and analysis methods is introduced. The set of design laws and analysis methods is tailored to map the physics and integration aspects of next generation propulsion systems.

The current chapter emphasises on the modelling paradigms of the proposed aircraft conceptual design procedure. Essential parts of the discussion focus on the analysis of the physical problem and its mapping through an efficient organisation of the system design procedure. Furthermore, problem-tailored strategies for the integration of sophisticated disciplinary models, an efficient use of surrogate modelling techniques and aircraft design space analysis are presented.

### **3.1. Aircraft Conceptual Design Logic**

In the present section, the aircraft conceptual design task is analysed with respect to the particular influence of propulsion system design aspects. Based hereon, a new approach is derived, in order to map the role of propulsion system design as an integral part of the overall aircraft.

#### 3.1.1. Problem Formulation

Beginning from first steps in conceptual phases, the design of an aircraft is a formidable task involving the cross-correlated influences of a multitude of engineering disciplines and system parts. Therefore, computerised system design and analysis requires an adequate arrangement of the mathematical models that are applied to the physics mapping of the involved system parts and engineering disciplines.

The comprehensive modelling of flight propulsion systems involves various disciplines to be mapped, including aerodynamics, structures, mechanics, acoustics, thermodynamics, performance, LCC and many more. Similar multidisciplinary complexity applies to aircraft conceptual design tasks. A significant amount of additional system complexity is encountered when integrating both multidisciplinary design and analysis tasks, especially, if advanced propulsion system architectures as well as unconventional system integration concepts are taken into account.

A sustainable approach to managing the outlined complex multidisciplinary design problem is introduced in the following and elaborated in Section 3.2.

#### 3.1.2. Impact of Engine Conceptual Design at Aircraft Level

A sustainable integration of propulsion system conceptual design into the aircraft conceptual design process requires an appropriate identification of the interrelations between engines and airframe. In this section, essential coupling aspects between propulsion system and aircraft conceptual design are characterised and the relevance of propulsion system design as a contributor to important aircraft conceptual design and analysis disciplines is outlined.

In conventional commercial aircraft layouts, the interface between engine and airframe is reduced to a minimum, *inter alia*, taking advantage of full authority digital engine controllability and the modular exchangeability of competing powerplant system products. However, disciplinary interaction of propulsion system and other aircraft components include aerodynamics, structural mechanics, performance and interrelations of those disciplines.

Figure 3.1 visualises the basic structure of the aircraft conceptual design task including essential system components and analysis disciplines. It can be seen, that engine design impacts on all classic aircraft conceptual design disciplines, such as geometric arrangement, structures and weights, aerodynamics and performance. In the following, typical disciplinary commonalities and cross-couplings of engine and airframe design are listed, and thus, the considered scope and level of detail for the physics mapping during conceptual system design is outlined:

- **Geometry:** geometry parameterisation and component sizing, evaluation of design constraints, component positioning and aircraft balancing. Propulsion system geometric layout, integration and positioning may entail particular impact on landing gear height, tail plane configuration and sizing, as well as wing, fuselage and pylon structural geometry.

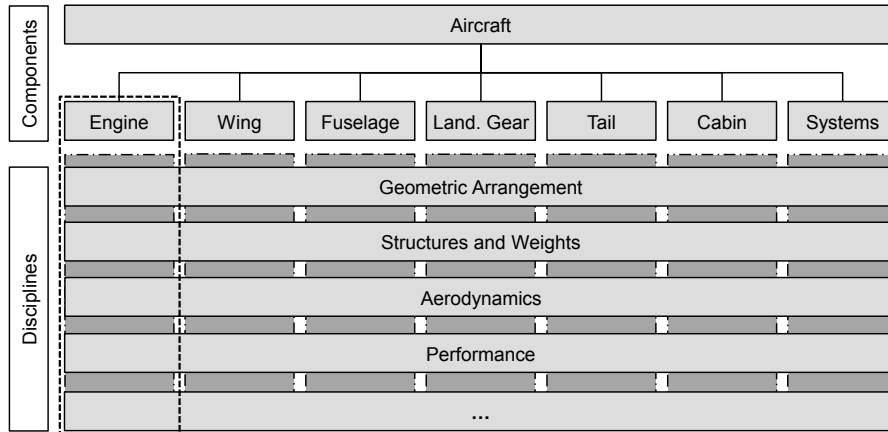


Figure 3.1.: Structural view of the aircraft conceptual design problem (the engine as a contributor to important aircraft design disciplines)

- **Structures and weights:** computation of structural loads and weights for main airframe components (e.g. wing, fuselage, landing gear, empennage, propulsion mounting structures) as well as engine mechanical design and weights (e.g. casings, discs, shrouds and blading, gearboxes, bearings and support structure, thrust reverser and other nacelle components).
- **Aerodynamics:** evaluation of aircraft high speed aerodynamics (e.g. lift and lift-induced characteristics, lift-independent drag characteristics, operational envelope, engine-airframe interference, maneuverability, wind milling characteristics) as well as low-speed characteristics (e.g. high-lift operation and high angle-of-attack aerodynamics, trim and handling qualities, one engine inoperative aerodynamics).
- **Performance:** simulation of typical point performances (e.g. drag polar, specific fuel consumption and specific air range at aerodynamic design conditions), airport operation (e.g. takeoff and landing performance, engine start- and warm-up time, cabin accessibility), manoeuvre (e.g. turning flight, acceleration and climbing ability, gust impact and diving characteristics), overall mission performance (e.g. block and trip fuel consumption and time, gaseous emissions, mission profile and trajectory).
- **Acoustics:** landing and take-off certification noise (e.g. extended landing gear, high-lift devices, fan, compressor, combustor, low pressure turbine and jet noise), in-flight cabin noise (e.g. propeller near-field acoustics, cabin noise damping properties).
- **Life cycle cost:** estimation of costs due to research and development investment, production, product ownership, maintenance and operation (e.g. crew, fuel, emissions) as well as end-of-life aspects (recycling, disposal).

Beyond these aspects, propulsion system technology also significantly influences upcoming aircraft conceptual design disciplines such as fleet design, operational scenario and environmental impact analysis. Now, considering the above listed disciplines, it becomes clear that propulsion system design directly contributes to the analyses performed in each and every discipline. The introduction of advanced or unconventional propulsion system concepts

### 3. Proposed Aircraft Conceptual Design Methodology

expands the interaction of engine and airframe in those typical disciplines and emphasises the consideration of additional disciplinary couplings such as heat transfer and energy management. Taking into account unconventional propulsion system installation options, disciplinary couplings being propagated across the physical components of the overall system may increase significantly.

#### 3.1.3. Discipline-Oriented Propulsion System Integration

In the preceding section, the impact of propulsion system design on an aircraft conceptual design level has been discussed. As shown, propulsion system design directly contributes to important aircraft analysis disciplines considered at conceptual design stages. Hence, for integrated conceptual design studies of airframe and engine, the consideration of the propulsion system as a contributor to aircraft design disciplines may have significant advantages over the classic treatment as a self-contained discipline. In the following, essential aspects of the proposed new approach to propulsion system integration are discussed.

The aircraft may be decomposed heuristically through examination of the system physical make-up. Alternatively, a formal decomposition may be derived by inspection of the functional relations that govern the problem [199]. Approaches, using the physical arrangement of the system components as a primary criterion for top-level problem decomposition are referred to as “component-oriented”, in the following. An alternative concept is based on the functional correlations of the system components, existing in different engineering disciplines, here referred to as “discipline-oriented” decomposition. In aircraft MDO, both approaches may be relevant, depending on the considered design task.

In a component-oriented approach to system decomposition, the arrangement of problem subtasks refers to the structure of the physical system components. The aspects of multiple design and analysis disciplines are handled component-internally, inside of the corresponding subtask. Hence, this type of decomposition facilitates the analysis of internal cross-disciplinary couplings of system components (cf. classic wing aero-elastics) without major system-level optimisation activity. However, the mapping of cross-component couplings requires significant information exchange at system level, typically involving extensive iteration effort. The detailed design of aircraft is typically organised according to the arrangement of the physical components, reflecting the expertise and the value creation structure of the involved product development partners. The same applies to the organisation of major engine development programmes (cf. Reference [81]). Towards production phases, the physical makeup of the system increasingly dominates the development process, being triggered by logistics and product assembly constraints. At this, the propulsion system, by its nature, is a self-contained, independent component of the overall aircraft.

For the present type of analysis problem the propulsion system has been identified as an important contributor to multiple disciplines involving significant cross-component coupling effects. In case of component-oriented system decomposition this implies significant iterative feedback of system design information for an adequate incorporation of propulsion system design into the aircraft system at conceptual design stages. However, all publications in the field of aircraft conceptual design found during literature research for the present work (cf. References [126], [205] and [89]) consider propulsion systems as a self-contained discipline besides structures, aerodynamics and performance.

The goal of efficient problem decomposition is the strengthening of the inner coherence within subtasks, while reducing subtask cross-coupling. Since engine conceptual design requires highly concurrent considerations of aspects connected to multiple engineering disciplines, the treatment of engine conceptual design as an integrated task seems appropriate. However, the integration of engine design aspects into the aircraft conceptual design as self-contained subtask involves a multitude of drawbacks. Taking the classic treatment of the propulsion system as a self-contained discipline within a discipline oriented aircraft conceptual design process, a large number of estimates on propulsion system design characteristics are necessary within aircraft disciplinary models. This, in turn, yields a highly iterative design procedure, if propulsion system design has to be incorporated adequately, and may constitute an important reason for the loose coupling of engine and aircraft conceptual design in the past.

Now, for a given level of propulsion system design integration, the required amount of information feedback is reduced dramatically, using rigorous discipline-oriented system decomposition. In the proposed discipline-oriented approach, propulsion system design and operational aspects are fully incorporated in the discussed aircraft conceptual design and analysis disciplines. This facilitates the direct analysis of the impact of propulsion system design changes at the aircraft system level. Moreover, the rigorous discipline-orientation of the aircraft conceptual design synthesis process, eases the incorporation of high-quality, disciplinary analysis codes, such as Computational Fluid Dynamics (CFD) for aerodynamics and Finite Element Methods (FEM) for structural design mapping. However, a major methodological challenge is connected to the discipline-oriented decomposition of propulsion system design aspects. Key elements of the proposed model integration strategy are discussed in Sections 3.2.2 and 3.3.

For propulsion system design and performance analysis in the present work, the software GasTurb 11 is used. Besides cycle design and off-design performance calculation GasTurb allows for basic engine design synthesis, well-suited for aircraft conceptual design level. GasTurb calculation yields propulsion system thermodynamic properties, relevant performance metrics such as the Specific Fuel Consumption (SFC) and thrust, as well as initial flow path dimensions and important mechanical design parameters such as the blade and disc-stress descriptive “AN<sup>2</sup>” metric<sup>1</sup>. Additionally, the software offers functionality for initial propulsion system weight estimation [105]. A detailed software characterisation, as well as workflow analysis and integration schemes are presented in Chapter 4.

## 3.2. Design Process Implementation

In the current section important aspects of the proposed methodological approach are presented. Therefore, the implementation of the aircraft synthesis procedure involving a discipline-oriented decomposition of propulsion system design aspects is illuminated and the resulting information flow scheme is discussed in detail. Furthermore, solutions for an intelligent integration of high-fidelity disciplinary models, as well as an efficient iteration strategy for consistent aircraft scaling are introduced. Finally, typical use cases of the proposed design process are outlined and direct starting points for further extension of the existing process implementation are characterised.

---

<sup>1</sup>AN<sup>2</sup> is defined by the local annulus cross-sectional area multiplied by the rotational spool speed squared.

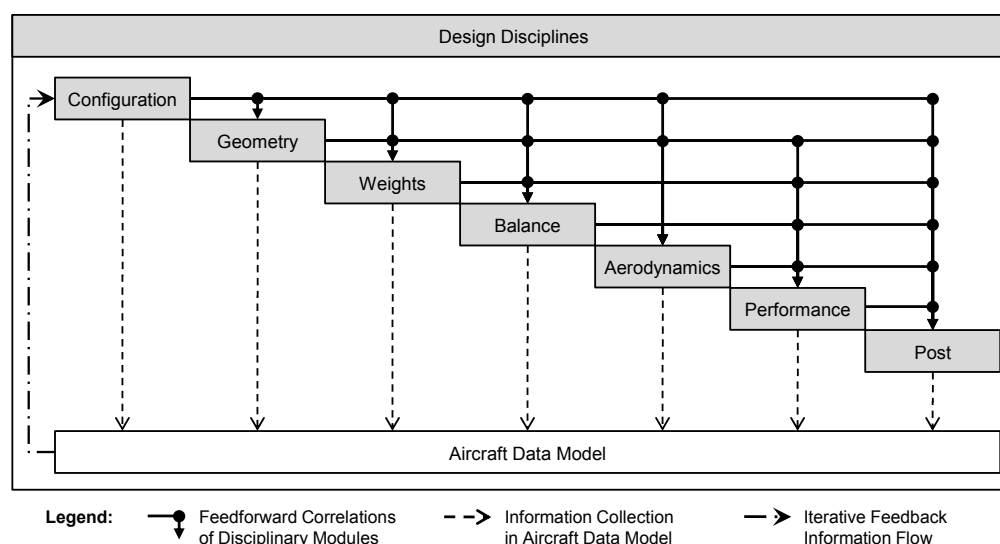


Figure 3.2.: Implemented discipline-oriented aircraft conceptual design scheme visualised in  $N^2$ -matrix view

### 3.2.1. Information Flow Scheme

A discipline-oriented setup of the overall aircraft design and analysis procedure including the discipline-oriented decomposition and incorporation of propulsion system design aspects has been identified as an efficient and sustainable approach for an integrated conceptual design of airframe and engine. The rigorous discipline-oriented problem decomposition offers optimum conditions for the utilisation of disciplinary design expertise. It also allows for a convenient exploitation of ideal correlations of innerdisciplinary parameters, thereby reducing the size of the system-level analysis problem dramatically without impacting on result quality. For propulsion system design aspects this modelling principle is consistently demonstrated in Chapter 5. In the present section the system-level information flow resulting from the proposed discipline-oriented decomposition of the aircraft conceptual design problem is discussed. Additionally, insight is given to the disciplinary module for aircraft weights calculation as a typical example for the inner workings of disciplinary subtasks.

#### 3.2.1.1. System-Level Information Flow

The information flow scheme resulting from the discussed aircraft conceptual design logic is shown in Figure 3.2. The parametric relationships between the disciplinary modules of the aircraft design process are visualised based on the commonly used  $N^2$ -matrix view. In the  $N^2$ -matrix view, the considered computational units (i.e. the disciplinary modules) are arranged along the matrix diagonal. Feedforward correlations between the computational units are shown as edges in the upper triangular matrix while feedback correlations are indicated in the lower triangular matrix.

At system level, information is exchanged between disciplinary modules - also referred to as subtasks in the following - based on a standardised interface. The computational results of every disciplinary module are compiled in a discipline-specific data model containing generic (independent from aircraft architecture) as well as system architecture-specific information. The handling of system architecture-dependent model parameterisation is performed inside the affected disciplinary modules, and thus, encapsulated against system-level interfaces. More information on the integration of disciplinary analysis models can be found in Section 3.2.2.

The resultant information flow follows a sequential procedure of disciplinary module calls. The returned Disciplinary Data Models (DDM) are successively compiled to the Aircraft Data Model (ADM) and, thus, available to any subsequent data processing (i.e. disciplinary modules). The resulting sequential arrangement of disciplinary modules ensures minimum iterative feedback at system level. As indicated in Figure 3.2, information feedback is managed using the ADM which allows for a flexible organisation of iterative system scaling (see Sections 3.2.3 and 3.2.4). Interdisciplinary feedback correlations are, therefore, not explicitly visualised in the system level  $N^2$ -matrix shown in Figure 3.2. The explicit number of feedback correlations strongly depends on the models and codes integrated in the disciplinary modules of the overall design procedure. Here, model types which may range from simple analytics to extensive computational methods, as well as model parameterisation play an important role.

For the reduction of response times during system design and analysis, the parallelised execution of subtask might be considered. Thus, subtask parallelisation is inherently supported by the proposed conceptual design process for the case of independent disciplinary modules, i.e. successive process modules without direct feedforward correlation may be evaluated separately from each other. However, the benefit from process parallelisation has to be evaluated carefully since representing a tradeoff between the gain of computational performance of the overall process and process parallelisation effort. Taking the CO approach to process parallelisation, a high number of compatibility constraints (cf. Section 2.2.1) are required during system level optimisation in order to handle the feedforward correlations between disciplinary subtasks. Thus, in the present approach, the paradigm of process parallelisation is disregarded in favour of a lean sequential process, tailored for minimum computational effort at given design and analysis qualities. Therefore, an efficient means of mitigating the necessity of process parallelisation is discussed in Sections 3.2.2 and 3.3.

#### 3.2.1.2. Outline of Disciplinary Subtasks

During aircraft conceptual design and analysis, the disciplinary subtasks involved in the proposed design procedure are repeatedly executed until a predefined set of feedback correlations is iteratively solved (cf. Section 3.2.3). At this, the system-level modules containing the involved subtasks are considered as black boxes for disciplinary design and analysis models of arbitrary complexity.

However, for the studies proposed as demonstration cases for the developed methodology, basic functionality was readily implemented to the modules shown in Figure 3.2. A generic overview of the corresponding operating modes is given in the following:

The “**Configuration**” module defines the aircraft architecture, its components and sub-systems, as well as important settings for the considered design mission such as mission

### 3. Proposed Aircraft Conceptual Design Methodology

profile, Landing and Take-Off (LTO) conditions. All aircraft configuration data are stored in a configuration file, which also contains information on application-specific iteration schemes and simulation settings. After successfully running through the aircraft conceptual design process, configuration files are supplemented by the correspondingly calculated aircraft data models and organised in a database system.

The “**Geometry**” module executes the geometric sizing of main components of the aircraft, i.e. wing, cabin and fuselage, empennage, landing gear, propulsion system and pylon in case of a conventional aircraft layout. Geometry definition is completely based on the configurational input and predefined design laws, both of which being subject to expert judgement during the conceptual design process. The innermodular sequence of component geometric definition is tailored to minimum iterative feedback. The geometric parameterisation of the aircraft and its components depends on the aspired design task, but also on the specific geometric inputs required by the succeeding disciplinary design and analysis models.

The “**Weights**” module computes the masses of main structural components of the aircraft, directly based on the geometric description supplied by the preceding geometry module. The calculated structural weights and weight information given in the configurational setup of the aircraft, such as payload, fuel and residual weights, are used to compile important aircraft weight figures such as Operating Weight Empty (OWE), Maximum Landing Weight (MLW) and Maximum Take-Off Weight (MTOW).<sup>2</sup> A more detailed discussion of the inner workings of the weights module can be found later in this section.

The “**Balance**” module adds to the geometric description of the aircraft by evaluating basic criteria for aircraft stability and control, thereby determining the exact positioning of the main aircraft components relative to each other. Based on the positioning of the considered components, their individual weights and local centers of gravity, the location of the aircraft’s overall center of gravity is calculated.

The “**Aerodynamics**” module computes important aerodynamic characteristics of the overall aircraft in clean configuration as well as in low-speed configuration yielding comprehensive drag polar information for the entire operational envelope. Therefore, parasite and lift-induced drag shares are evaluated at any requested operating condition. The evaluation of aerodynamics involves all externally exposed surfaces of the aircraft including the engine nacelles and pylons.

The “**Performance**” module computes arbitrary aircraft point performances within the predefined operational envelope as well as mission performance based on numerical simulation. Design-relevant operating conditions, such as take-off (rotation), top of climb and typical cruise (aerodynamic design) points, are determined as part of design mission simulation. The analysis of system performance includes the evaluation of aircraft weights and aerodynamics as well as engine performance characteristics at the referred operational condition. For aircraft operational analyses (off-design mission) operating point evaluation and mission simulation may be executed independently from the aircraft design procedure using the information contained in the aircraft data model (cf Section 3.2.4).

The “**Post**” module represents a black box for the modeling of additional aspects of aircraft conceptual design which are not explicitly addressed in the preceding modules. The number of post processing modules may be variable and modules may be calculated sequentially or

---

<sup>2</sup>MTOW is a transcendental function.

in parallel, if favourable. Typical aspects to be addressed in post processing modules may consider system noise evaluation, operational flexibility assessment, LCC modelling, aircraft fleet design or detailed environmental impact mapping.

Similar to the system-level process arrangement, the module-internal organisation of models and information flows is based on problem-oriented task decomposition. At this, the detailed inner workings of the disciplinary modules are defined by the applied models for the mapping the system physics. Thus, innerdisciplinary problem decomposition may be component-oriented, if favourable. In the following, insight is given to the weights module as a representative subtask example. The weights module is decomposed according to a component-oriented scheme.

#### 3.2.1.3. The “Weights” Module - A Typical Example for Subtask Decomposition

As an example for the inner workings of the disciplinary black boxes, Figure 3.3 shows the internal organisation of the “Weights” module. Here, the innerdisciplinary decomposition is aircraft component-oriented. The subtask inputs from upstream modules include aircraft geometric and configurational information (cf. Figure 3.2), the latter of which includes values for payload, fuel and aircraft residual weights as well as fuel fractions for relevant operating conditions. Disciplinary calculation results are fed downstream to succeeding modules of the overall process. It should be noted, that the explicit definition of the modular interfaces depends on the respectively implemented disciplinary models. The information flow shown in Figure 3.3 refers to the parametrics of the models for weights calculation presented in Chapter 5. For a fully physics-based approach to weights assessment only geometric information on system components would be necessary.

Depicted in the figure are the component breakdown and calculation sequence for a conventional aircraft layout allowing for under-wing as well as aft-fuselage engine mounting. The considered submodules refer to the aircraft’s main structural components, embraced by procedures for the preprocessing of module inputs as well as the postprocessing of component weight calculation. Here, the postprocessing submodule is used for the compilation of typical aircraft weight figures such as OWE, MLW and MTOW.

The sequence of component weight calculations is tailored for minimum module-internal feedback of information. Therefore, a component-specific assessment of the relevant load cases for component sizing and weight calculation is necessary with respect to the considered structural concepts and design requirements. However, the distribution of forces across component boundaries is an important metric for the determination of an adequate calculation sequence. Accordingly, the weights of peripheral components, such as empennage and engines, may be calculated independently, while the weights computation of central and conjunctive structural components, such as wing and fuselage, depends on the loads imposed by the connected peripheral components. Taking aft-fuselage mounted engines as an example, powerplant system weight directly affects engine pylon weight. Both component weights finally impact on fuselage weight. The  $N^2$ -matrix view in Figure 3.3 visualises the corresponding submodular interdependencies. Here, the calculation sequence is straight forward without any need for iteration.

### 3. Proposed Aircraft Conceptual Design Methodology

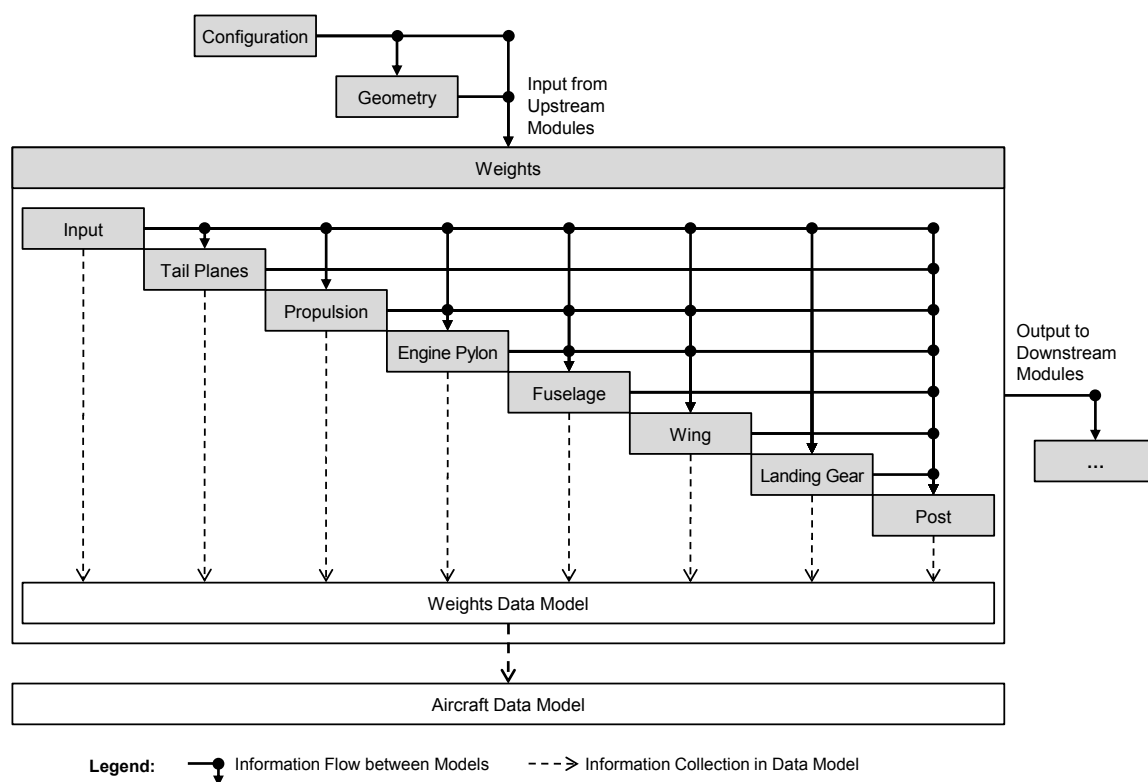


Figure 3.3.: Internal information flow scheme of weights module visualised in  $N^2$ -matrix view

#### 3.2.2. Integration of Propulsion System Aspects

The evident benefits of a discipline-oriented integration of propulsion design aspects into the aircraft conceptual design procedure proposed in this thesis have been outlined in the current chapter. Now, it is obvious that the propulsion system is a highly complex arrangement of functional components tailored to maximum efficiency and reliability as well as minimum weights, simultaneously. The conceptual design of propulsion systems, therefore, is a strongly interdependent, multidisciplinary process which requires an enormous amount of disciplinary expertise and knowledge on the involved interdisciplinary couplings. As a result of this high degree of inner coherence, propulsion system conceptual design aspects are typically provided en bloc by the used design synthesis and simulation model.

The decomposition of propulsion system design aspects requires particular consideration. A schematic overview of the methodological approach to this issue, which has been developed as part of present work, is illustrated in Figure 3.4. The figure shows a simplified diagram of the previously introduced aircraft conceptual design synthesis pattern (cf. Figure 3.2) as well as a wrapping process developed for the propulsion system synthesis model, framed by a dashed line.

The indicated wrapping process is based on the application of surrogate modelling techniques. The contained methodological elements and procedural steps are subject to in-depth discussion in the subsequent sections of this chapter. An explicit application case is demonstrated in detail in Chapter 4. However, a general overview of the proposed model integration approach

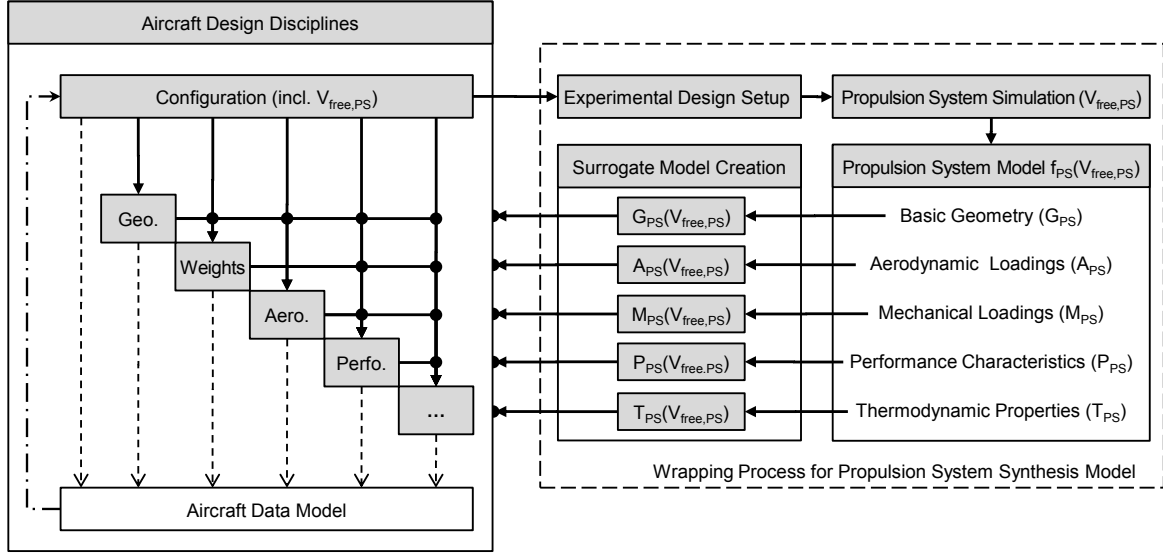


Figure 3.4.: Discipline-oriented integration of propulsion system aspects into the aircraft conceptual design process - a schematic overview

is given in the following.

Based on the considered aircraft design and analysis task, a set of propulsion system parameters  $\vec{V}_{free,PS}$ , required as free variables during the desired system-level studies, is defined. The propulsion system free variables may be an arbitrary subset of the set of input parameters used by the employed propulsion system synthesis model.  $\vec{V}_{free,PS}$  may include propulsion system design as well as operational (off-design) parameters.

Now, the functional mapping performed by the considered propulsion system synthesis model  $f_{PS}$  referred to in Figure 3.2 may be expressed as

$$Y_{PS} = f_{PS}(\vec{V}_{free,PS}), \quad Y_{PS} = \{G_{PS}, A_{PS}, M_{PS}, P_{PS}, T_{PS}\} \quad (3.1)$$

Here, the set  $Y_{PS}$  represents the total amount of results calculated by the propulsion system synthesis model  $f_{PS}$ .  $Y_{PS}$  integrally contains data of propulsion system geometry ( $G_{PS}$ ), aerodynamic loadings ( $A_{PS}$ ) and mechanical loadings  $M_{PS}$  of the turbo components, as well as performance characteristics ( $P_{PS}$ ) and thermodynamic cycle properties ( $T_{PS}$ ). Each of these shares of  $Y_{PS}$  contains multi-parametric information which may contribute to the aircraft overall design synthesis procedure at individual calculation steps in different disciplinary modules.

The application of surrogate modelling techniques is a convenient means of separating these design aspects for independent use, such as desirable for a discipline-oriented system-level design and analysis procedure. The functional transformation accordingly yields

$$y_{PS} = \hat{f}_{PS,y}(\vec{V}_{free,PS}) \quad \forall y_{PS} \in \{Y_{PS}\} \quad (3.2)$$

### 3. Proposed Aircraft Conceptual Design Methodology

where  $\hat{f}_{PS,y}$  represents the surrogate model function for a subset  $y_{PS}$  of the full set of propulsion system calculation parameters. The creation of surrogate models, i.e. the wrapping process for the propulsion system synthesis model, represents an off-line effort required prior the actual system-level studies. It, however, offers significant benefits for subtask quality assurance. The construction of surrogate model functions  $\hat{f}$  including the involved effort for experimental design setup and data sampling procedures (cf. “Propulsion System Simulation” in Figure 3.2) is issued in Section 3.3.

Parametric studies at the aircraft level, typically focus on particular system aspects. In most cases, a limited number of propulsion system free variables  $\vec{V}_{free,PS}$  is required. However, the propulsion system synthesis model needs to be parameterised adequately, in order to reduce the dimensionality of system-level optimisation tasks. For detailed information on the strategy for propulsion system design parameterisation implemented in the present work see Figure 4.2.

The number of calculated propulsion-specific parameters (contained in  $Y_{PS}$ ), which are relevant for aircraft disciplinary computation, may be quite large. Here, the proposed surrogate-based model integration facilitates a flexible treatment of propulsion system design aspects  $y_{PS}$  as input to system-level subtasks, constraints or objective functions. The evaluation of surrogate model functions  $\hat{f}_{PS,y}$  may be carried out on demand during the system-level design procedure. Therefore, the set of propulsion system free variables  $\vec{V}_{free,PS}$  as well as the correspondingly created surrogate model functions  $\hat{f}_{PS,y}$  are included in the configurational setup of the aircraft design synthesis process.

#### 3.2.3. Iteration Strategy for Aircraft Scaling

Iteration is a formal means of solving models or systems of models involving feedback correlations within the general information flow. Considering the model or system of models to be solved as a black box of nonlinear equations, iterative system solution refers to a classic root finding problem. For numerical application, a number of methods for nonlinear root finding are available, such as the derivative-using Newton-Raphson method [168]. The Newton-Raphson method works iteratively by extrapolating the local derivative of the nonlinear functional correlation to find the respective next estimate of the root location.

Taking a model or system of models featuring a number of  $n$  feedback correlations, for derivative-based iteration the determination of the  $n \times n$  Jacobi matrix of partial derivatives is necessary for every required step of the iterative root search. This implies the repetitive execution of model sensitivity analyses for each input estimation parameter of the considered iteration scheme involving the correspondingly required computational effort during model evaluation. However, in many practical cases of iterative analysis structures, a less generic but gradient-free problem solution strategy is suitable. Consider, therefore, the case of model calculation results that directly feed back as input parameters to preceding calculation procedures within a sequentially executed arrangement of design or analysis codes. This type of feedback correlation appears frequently within aircraft conceptual design and sizing tasks. Take, for example, the classic mass-performance-loop which requires an initial MTOW estimate in order to yield MTOW for the application-tailored aircraft, in the end.

In the present work, a simple gradient-free method is used for the solving of multidimensional iterative feedback at system level, i.e. the aircraft conceptual design sizing. The principle

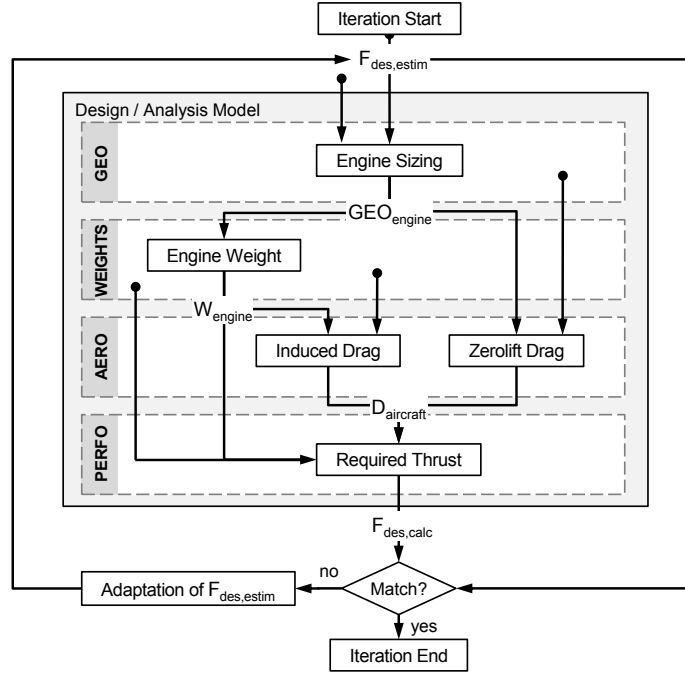


Figure 3.5.: Visualisation of iteration approach for aircraft conceptual design sizing (Example: Simplified nonlinear analysis structure for engine thrust sizing)

approach is visualised in Figure 3.5 showing a typical example of a design feedback correlation. The figure, therefore, illustrates a simplified scheme of the multidisciplinary model structure for engine thrust matching within an aircraft sizing procedure. Accordingly, the engine is geometrically sized based on an estimated design thrust value  $F_{des,est}$ . The engine's geometric description directly translates to weight information. Both, engine geometry and weight impact on aircraft aerodynamics which - in connection with aircraft weight information and operational requirements - defines the engine's required design thrust  $F_{des,calc}$ .

The implemented iteration solution is based on a set-actual comparison of iteration variable values estimated before running through the design disciplines  $\vec{V}_{it,est}$  and the corresponding physical values calculated during the disciplinary analyses  $\vec{V}_{it,calc}$ . The parameters used as iteration estimates  $\vec{V}_{it,est}$  are a subset of the aircraft configurational settings defined in the "Configuration" module (cf. Figure 3.2). The physically corresponding calculation results  $\vec{V}_{it,calc}$  are read from the aircraft data model. The set-actual comparison of feedback correlations is performed after a completed run through all disciplinary design and analysis modules. Using appropriate under-relaxation, new estimation values for the iteration variables  $\vec{V}_{it,est,new}$  are synthesised and fed back to the design process. The feedback information flow on system level is indicated in Figure 3.2. Adequate under-relaxation factor values  $\vec{\alpha}_{rel}$  result from the trade-off between computational performance and convergence stability of the process and may be tailored individually for every feedback correlation involved in the iterative system.

### 3. Proposed Aircraft Conceptual Design Methodology

The synthesis of new estimation values for the iteration variables is based on the following correlation:

$$\vec{V}_{it,est,new} = \vec{V}_{it,cal} \cdot \vec{\alpha}_{rel} + \vec{V}_{it,est} \cdot (1 - \vec{\alpha}_{rel}), \quad 0 < \vec{\alpha}_{rel} \leq 1 \quad (3.3)$$

The iteration convergence goal, here, is defined by the allowable relative mean squared error sum

$$E_{RMS} = \sqrt{\sum_{i=1}^n \left( \frac{V_{it,cal,i} - V_{it,est,i}}{V_{it,cal,i}} \right)^2}, \quad V_{it,cal,i} \neq 0 \quad (3.4)$$

where  $n$  represents the dimensionality of the iterative problem.

In general, increasing  $n$  adds to the numerical noise of calculation results. This effect is countered by using the error summation of the involved iterative correlations (cf. Equation 3.4) as a figure of merit for iteration convergence. For practical application, a convergence goal definition of  $E_{RMS} \leq 10^{-6}$  appears an adequate trade-off between numerical accuracy of results and computational effort during iteration.

A clear advantage of the used iteration scheme over classic derivative-based root finding methods is the omission of the sensitivity analyses at every iteration step. This advantage grows with increasing number of feedback correlations within the analysis structure. Iteration convergence characteristics may be tailored using adequate sub-relaxation settings. For the approach to solving the iterative problem of aircraft conceptual sizing implemented, here, the required premises of system response behaviour are similar to those of gradient-based iteration schemes. Classic risks connected to root searching methods, such as the encountering of local optima (i.e. the gradient of functional correlations within the set of iteration equations equals zero) or the case of nonconvergent cycles are discussed in Reference [168].

#### 3.2.4. Design Analysis Capabilities

The increasingly required detaching from evolutionary design strategies in aerospace engineering requires the exploration of new technologies and design options. Beside the required capability of mapping the principal system physics, a major challenge for the conceptual investigation of advanced and unconventional system configurations concerns the efficient extraction of usable knowledge from the complex design and analysis models.

The primary purpose of the proposed aircraft conceptual design procedure is the direct incorporation of engine conceptual design in order to facilitate integrated, comparative studies of advanced propulsion technological concepts. Due to the modular nature of the system-level procedure, disciplinary subtasks can be evaluated separately from each other, given that the individually required input information is available. This offers a multitude of system design and analysis options, including design synthesis, as well as operational analysis tasks.

Five basic application cases are characterised below:

1. **Performance analysis of given aircraft:**  
Recalculation and operational simulation of fixed aircraft design based on given geometry (wing area, etc.), engine performance characteristics and aircraft weight information (typical validation case).
2. **Optimum engine matching for given aircraft:**  
Engine conceptual design optimisation for given aircraft geometry (e.g. optimisation for minimum mission fuel burn); determination of aircraft re-engining benefit.
3. **Aircraft and engine design studies for given operational requirements:**  
Investigation of airframe and engine design trade-offs as well as the impact of new technologies on aircraft performance characteristics for fixed operational boundary conditions.
4. **Maximum transport efficiency:**  
Concurrent investigation of aircraft, engine and mission design parameters for minimum mission fuel burn, emission characteristics, operational cost, noise footprint or multi-objective considerations based on given system technology standards.
5. **Comparison of alternative system concepts:**  
Synthesis and parametric investigation of alternative aircraft and engine configurational arrangement using aircraft, engine and mission design aspects as free variables or optimisation parameters, respectively.

In the complex aircraft conceptual design space, the global prediction of system behaviour is desired in order to enable an efficient exploration capability aiming for a better understanding of the underlying functional principles. Now, the tracking of the response  $Y_i$  of a system to predefined input settings  $S_i$  ( $Y_i = f(S_i)$ ) is referred to as Design Space Exploration (DSE) [231]. The recording of data sampled from the system input space and the corresponding values from the response space ( $S_i$  and  $Y_i$ ) successively increases the available information on global system behaviour.

Central DSE challenges in aircraft conceptual design are connected to topological variations of system architecture, i.e. changes in the aircraft configurational arrangement, and, the efficient handling of the multiple design constraints at subtask and system level. The proposed discipline-oriented decomposition of the aircraft design synthesis procedure is widely independent from topological variations at system level (cf. Figure 3.2). The mapping of system topology and the geometric arrangement of the involved physical system components such as wing, fuselage and propulsion system is handled at disciplinary subtask level (cf. Figure 3.3). Now, the mapping of topological variation in parametric models means discrete parameter changes. In the present approach, all model input parameters  $V$  are treated as real numbers  $V \in \mathbf{R}$  at model interfaces. Discrete physical parameters are then type casted model-internally (i.e.  $V_{discrete} \in \mathbf{R} \rightarrow V_{discrete} \in \mathbf{Z}$ ), which conveniently allows for deterministic as well as statistical data sampling from the model input space.

In many practical cases of system analysis, the available design space is constrained by multiple constraints, which, normally, have to be evaluated independently. Here, the locations of constraint intersection often cause convergence problems during iteration and optimisation, since introducing discontinuities to the local gradients of model response. In the present

approach, multiple simultaneous constraints are mapped by single surrogate constraints, also referred to as “cumulative constraints” [199, p.353]) using the “Kreisselmeier-Steinhauser” function (cf. Reference [228]). Typical application of the Kreisselmeier-Steinhauser function involves the evaluation of the aircraft design performance constraint chart, landing gear height determination, the evaluation of engine operational envelope constraints, such as the  $AN^2$  values of the Low Pressure Turbine (LPT) and the maximum burner exit temperatures ( $T_4$ ), as well as the analysis of tail plane sizing constraints.

## 3.3. Surrogate-Based Model Analysis

The use of mathematical approximation techniques for the construction of surrogates for computationally expensive models essentially contributes to a quick gain of knowledge on system behaviour. Surrogate Modelling (SuMo) has, therefore, proven to be a key enabler for an efficient design and analysis of complex systems. Typical use cases include both design space scanning for robust design determination, as well as the high-accuracy response fitting of complex models. A literature survey of surrogate modelling application cases in the past is given in Chapter 2.

Considering surrogate modelling as an approach to predicting the output of a simulation-based model, the following problem formulation is applicable:

$$f_{pv}(\vec{x}) = \hat{f}(\vec{x}) + \epsilon(\vec{x}) \quad (3.5)$$

where  $f_{pv}(\vec{x})$  represents the expected prediction value for given model input settings  $\vec{x}$ . The error  $\epsilon_{pv}(\vec{x})$ <sup>3</sup> results from non-perfect value prediction by the surrogate model  $\hat{f}(\vec{x})$ . The selection of the surrogate model function  $\hat{f}$  is problem-specific and may range from simple polynomial approaches to complex non-parametric models (cf. Reference [168, Chapter 15]).

In particular, SuMo application has been identified beneficial for the analysis and integration of complex subtasks, i.e. high-fidelity disciplinary models. Previous work (cf. References [159, 193, 188] and [189]) has shown that the integration of propulsion simulation software using SuMo techniques may offer significant advantages over direct software system coupling. Thus, SuMo is considered a key enabler for the decomposition of propulsion system design aspects (cf. Section 3.2.2), hence, allowing for the convenient incorporation of the decomposed aspects into the proposed discipline-oriented aircraft conceptual design procedure. Beyond that, SuMo application appears an ideal solution for the global analysis and optimisation of the highly constrained overall aircraft design problem.

### 3.3.1. Problem-Tailored Data Sampling

The creation of surrogates requires detailed information on the original model to be approximated. The necessary information is gained from the original model by taking sample measurements, based on experimental sampling plans. Information is then extracted from

---

<sup>3</sup>also referred to as model appraisal [169]

the original model by successively simulating predefined model input conditions (sample points) and measuring the corresponding responses of the model. The model is, thereby, treated as a black box without detailed knowledge on the inner workings being required. The simulation of complex computational models may be very time-consuming. Hence, the goal of sampling plan definition is the reduction of simulation runs, necessary for the required amount of information on model response. Therefore, a reliable assessment of the goodness of the experimental plan is vital. In the present section, the developed strategy for an efficient data sampling is introduced. Essential aspects of the discussion include the problem-oriented definition and simulation of the experimental plan, as well as the quality assurance of sampled data.

### 3.3.1.1. On Sampling Plan Design Options

In order to maximise the amount of desired information extracted from such a black box data sampling requires appropriate planning. A sampling plan may be constituted by randomly generated or deterministically located sample points  $S_i$ , distributed in a predefined variable space  $F$ . The space  $F$  is defined by the set of considered input variables  $\vec{V} \in \mathbf{R}^p$  and their corresponding definition ranges  $\{\vec{V}_{min} \leq \vec{V} \leq \vec{V}_{max}\}$ , where  $p$  refers to the number of variables and, thus, represents the dimensionality of  $F$ .

Unlike pure random-distributed sampling plans, (cf. Monte-Carlo sampling [168]), deterministic, “designed” data sampling uses stratification of the considered  $p$ -dimensional variable space  $F$  in order to create unique sample point locations in  $F$ . The class of methods creating deterministic sampling plan is often referred to as the design of experiments (DoE). Here, classic Full Factorial Designs (FFD) produce  $p$ -dimensional rectangular grids in  $F$ , filled by sample points at all levels in all dimensions. The exponentially growing number of grid points against increasing dimensionality  $p$  of the variable space is also known as “the curse of dimensionality” [24]. FFD are therefore not applicable for many practical cases of SuMo, however, may be favourable for data interpolation purposes. In order to reduce the number of sample points required for grid-based space filling a variety of deterministic sampling methods, referred to as fractional factorial designs, have been developed. Overviews of these are in References [214] and [193].

Higher flexibility in space filling, including the decoupling of the number of sample points  $n$  from the dimensionality  $p$  of the variable space  $F$  is offered by so-called “quasi-random” or “sub-random” sampling sequences. Sub-random sequences<sup>4</sup>, at the same time, allow a for more uniform space filling than uncorrelated, random sampling distributions [168].

### 3.3.1.2. Latin Hypercube Sampling

Particular practical importance is attached to the Latin Hypercube Sampling (LHS) approach which has been first described by McKay in 1979 [133]. LHS allows for the highly flexible filling of multidimensional parametric spaces using freely choosable numbers of sample points  $n_{LHS}$ , independently from space dimensionality. It represents a quasi-random method, facilitating the simultaneous stratification of the  $p$  dimensions of the variable space  $F$ . The number of stratification levels in each dimension equals the number of predefined sample points  $n_{LHS}$ .

<sup>4</sup>e.g. Halton’s sequence and Sobol’s sequence (cf. Reference [168])

### 3. Proposed Aircraft Conceptual Design Methodology

The corresponding sampling plan matrix  $\mathbf{D}$  of  $n \times p$  size contains  $n$  sample points  $S_i \in \mathbf{R}^p$ . The space dimensionality  $p$  constitutes the column space of  $\mathbf{D}$ . In other words, a single sample point  $S_i$  is defined by its  $p$  coordinate values, constituting a full row vector in  $\mathbf{D}$ .

$$\mathbf{D} = \begin{pmatrix} S_{1,1} & \cdots & S_{1,p} \\ \vdots & \ddots & \vdots \\ S_{n,1} & \cdots & S_{n,p} \end{pmatrix} = S_{i,k}$$

A basic LHS design is generated through the column-wise<sup>5</sup> generation of  $n$  normalised random values. The samples contained in the resultant normalised sampling plan matrix  $\mathbf{D}_{norm}$  are distributed in the normalised Cartesian space  $F_{norm}$ .

Now, space stratification is realised in LHS plans by ensuring the uniqueness of sample point coordinate values in each dimension of the stratified space. Technically, this may be realised by identifying the ascending order of column-internal random values. Subsequently, each element of the column vector, the identified ranking is assigned back to, and finally divided by the number of vector elements (cf. Reference [214]). As a result of this, the column-internal spacing of sample point coordinate values is uniform and the dimensional ranges are retained normalised. However, satisfying the space stratification criterion does not inherently ensure proper space filling<sup>6</sup>.

For the generation of space filling LHS plans, significant effort may be undertaken, since representing a multi-degree-of-freedom optimisation problem, strongly depending on the number of sample points  $n$  and variable space dimensions  $p$  involved. As an example for this, an evolutionary approach to LHS optimisation is presented in Reference [55]. However, adequate sampling plan generation is a trade-off between optimisation effort the required uniformity of the sample point distribution. For the purposes of the present work a rather simple approach to achieving useful space filling according to Reference [214] has shown good results and was, therefore, used for LHS plan generation throughout the studies present in this thesis. Here, the commonly used ‘‘maximin’’ metric (cf. Reference [55]) is employed for the assurance of LHS space filling quality. A typical example of an optimised four dimensional, 10 points LHS design is shown in Figure 3.6.

The figure shows a matrix of scatter plots  $\mathbf{M}$  representing all possible two-dimensional projections of the  $p$ -dimensional ( $p = 4$  in this example) variable space, filled by the LHS plan outlined above. The plots along the matrix diagonal  $\mathbf{M}(i, i)$  show the self-projections of the space dimensions  $\vec{V}$ . The upper and lower triangular matrices  $\mathbf{M}(i, j), \forall i \neq j$  show the LHS plan mapped to the projection planes defined by the pairwise combinations of variable space dimensions  $V_i$  and  $V_j$ . The plots in the lower triangular matrix  $\mathbf{M}(i, j), \forall i > j$  contain the transposed views of the LHS plan projections in the upper triangular matrix  $\mathbf{M}(i, j), \forall i < j$ . The matrix of two-dimensional projections allows for a comprehensive assessment of the multidimensional distribution of sample points in the hypercubic space. It thus represents a powerful tool for the visual inspection of the space filling quality of LHS and is used for visualisation of LHS plans in the following.

<sup>5</sup>i.e. separately for each dimension of  $F$

<sup>6</sup>Consider a placing of sample points along the diagonal of  $F$ .

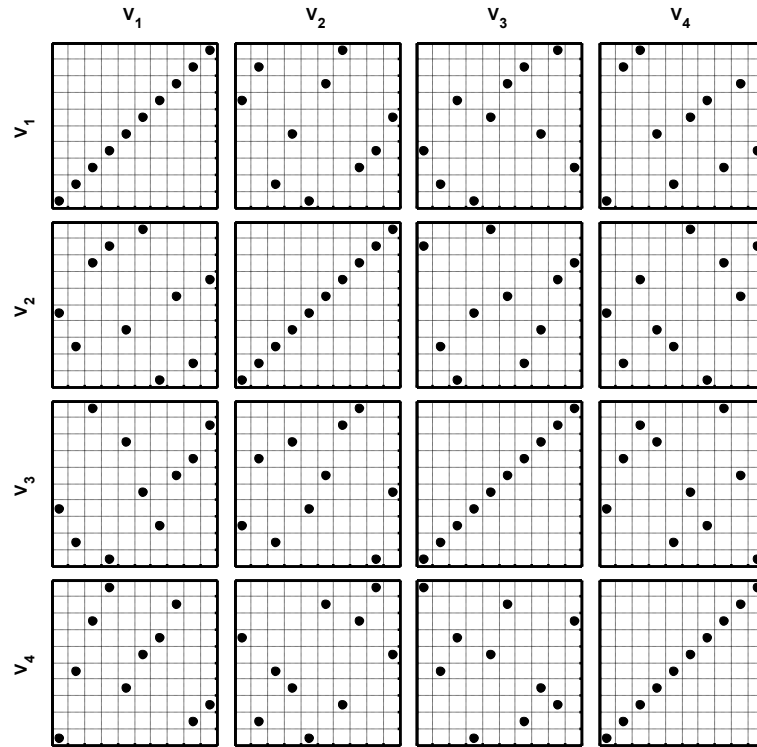


Figure 3.6.: Matrix of 2-dimensional projections of Latin hypercube sampling plans (Example: 4 dimensions, 10 sample points, 100 repetition cycles)

### 3.3.1.3. Simulation of Sampling Plans

The sampling of data required for surrogate model regression and validation represents the most time-consuming aspect of the surrogate model creation effort. Essential elements of the data sampling process include the experimental design setup, the simulation itself, as well as adequate capabilities for the assessment of simulation results.

The standardised procedure for data sampling, implemented during the present work, is illustrated in Figure 3.7 (overleaf). The starting point for the shown flow diagram is the initial “Experimental Design Setup” including the determination of essential setting for the data sampling process, i.e. the description of the variable space  $F$  by defining the variables  $V_i$  and their corresponding ranges to be investigated during data sampling. The DoE settings also include the choice of data sampling strategy, i.e. space stratification and number of sample points. Based on the DoE settings, the sampling plan  $\mathbf{D}$  is generated. For the studies presented in the following chapters of this thesis, the previously discussed LHS strategy was used. This also included the presented strategy for visual sampling plan inspection (cf. Figure 3.6) in order to ensure appropriate space filling.

The most time-consuming procedural step shown in Figure 3.7 is the “Sampling Plan Simulation”. Here, the single simulation input settings  $S_i$  contained in the predefined and sorted sampling plan  $\mathbf{D}$  are successively computed based on the simulation model. The

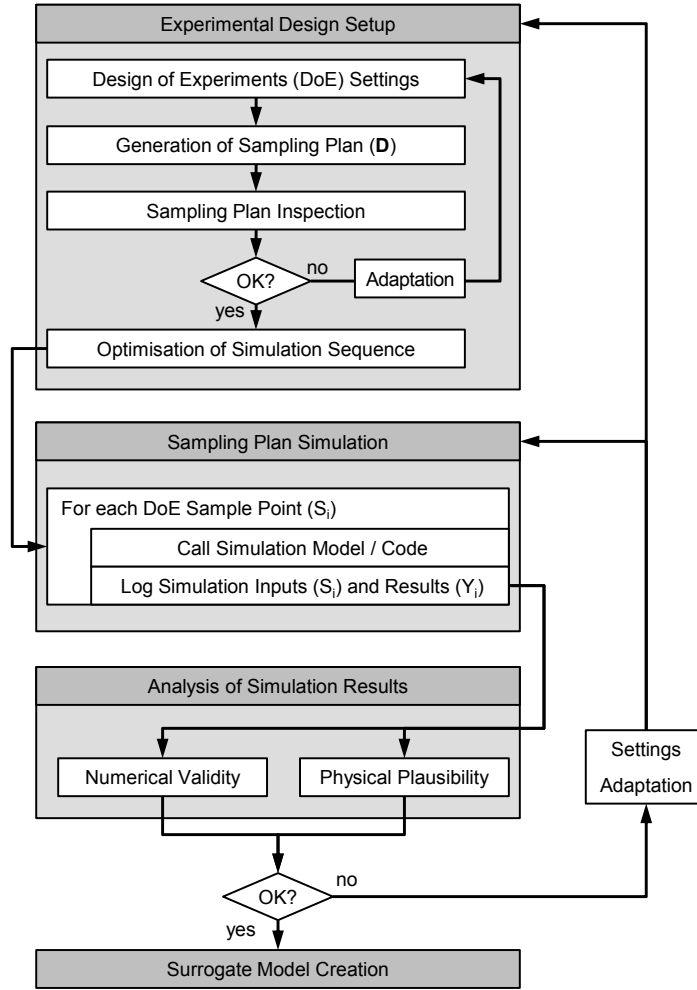


Figure 3.7.: Information flow scheme of implemented input data sampling process for surrogate model creation

returned results  $Y_i$  are recorded in combination with the corresponding input settings  $S_i$ . Both,  $S_i$  and  $Y_i$  constitute a simulation sample set

$$U_i = \{S_i, Y_i\}, \quad S_i \in \mathbf{R}^p, Y_i \in \mathbf{R}^q \quad (3.6)$$

where  $p$  and  $q$  refer to the number of simulation input variables  $V_i$  and the number simulation result parameters, respectively. In order to significantly reduce the computational effort during simulation, the sequence of sample points  $S_i$  in  $\mathbf{D}$  may be re-organised prior to sampling plan simulation. A corresponding sorting strategy which was developed as part of the present research is presented in Chapter 4.

The subsequent “Analysis of Simulation Results” involves checks for the numerical validity of the results, e.g. based on a numerical status indication returned by the executed model (cf. Section 4.2.4), as well as the data inspection by disciplinary experts, in order to ensure

physical plausibility of the gained information. As a result of the result analysis, modification of both, the parameterisation of the simulation model as well as the sampling plan setting may be required for adequate, problem-oriented mapping of the model physics. In fact, the adaptation of DoE Settings after expert analysis can be used for the heuristic allocation of sample points to enhance local sampling density in variable space regions of particular interest, i.e. strong non-linearity of system response or elevated requirements for surrogate model accuracy.

### 3.3.2. Surrogate Model Creation

Existing mathematical methods to model a given response function  $f(\vec{x})$  include parametric and non-parametric approaches.<sup>7</sup> Parametric models use a fixed inner structure, i.e. the functional correlation of model inputs and response  $\hat{f}(\vec{x})$  is predefined and data fitting is based on the proper estimation of predefined parameters. Parametric models include classic associative combinations (polynomial) and non-linear regression methods. The application of non-parametric models also includes the estimation of the functional correlation  $\hat{f}(\vec{x})$ . In the following, the implemented process for surrogate model creation is presented. The discussion is focused on Artificial Neural Networks (ANN) in the form of Feedforward Neural Networks (FNN).

#### 3.3.2.1. Feedforward Neural Networks

During research related to the the present work alternative solutions for surrogate model generation have been applied and evaluated (cf. References [193, 189] and [191]), indicating feedforward neural networks as a convenient and versatile data fitting approach for the present types SuMo problems. FFN facilitate a well-balanced trade-off between non-linear data fitting quality and required computational effort during surrogate model evaluation. In Figure 3.8 (overleaf), the typical structure of single hidden layer FFN is visualised. The shown FFN involves  $n$  neurons in the layer,  $p$  neurons representing the network input parameters  $x_i$  in the input layer, as well as  $q$  neurons for the network outputs  $\hat{f}_k$  in the output layer. The model function in tensor notation yields:

$$\hat{f}_k(\vec{x}, w) = w_{k0}^{(2)} + \sum_{j=1}^n w_{jk}^{(2)} f_{TR} \left( w_{j0}^{(1)} + \sum_{i=1}^p w_{ij}^{(1)} x_i \right) \quad (3.7)$$

where  $w = \{w_{10}^{(2)}, \dots, w_{q0}^{(2)}, w_{11}^{(2)}, \dots, w_{nq}^{(2)}, w_{10}^{(1)}, \dots, w_{n0}^{(1)}, w_{11}^{(1)}, \dots, w_{np}^{(1)}\}$ . The absolute parameters  $w_{k0}$  and  $w_{j0}$  are called “bias” or “threshold” parameters, while  $w_{jk}$  and  $w_{ji}$  represent the weight matrices connecting the individual layers of the network. The term  $f_{TR}$  refers to the transfer or activation function of the neurons in the hidden layer.

The FNN model function given in Equation 3.7 allows for structural adaptation of the network and its response to incoming information through the variation of number of hidden layers and corresponding numbers of neurons, as well as the choice of transfer functions in the hidden layers. Hence, FNN are non-parametric models and, by their nature, offer a

<sup>7</sup>A comprehensive overview of various approaches to surrogate model creation is outlined by the contents given in References [40, Chapter II], [169], [168, Chapter 15] and [55, Chapter 3].

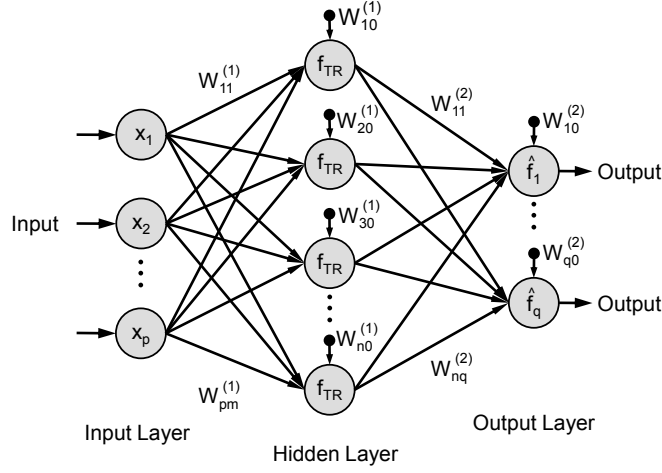


Figure 3.8.: Typical structure of single-layer feedforward neural network

high flexibility for data fitting. However, an FNN behaves like a parametric model, once its inner structure is determinate, i.e. the number of hidden layers and neurons per layer, their respective biases and transfer functions, as well as the coupling weight matrices have been fixed. The appropriate determination of these network structural properties is briefly explained in the following.

In the present context, only single hidden layer FNN are considered. In practice, the number of neurons in the layer is determined empirically, considering the optimum number of neurons in the hidden layer to be dependent on multiple aspects, including

- the dimensionality of inputs and outputs, i.e. the number of neuron in the input and output layers,
- the “degree of non-linearity” of model response(s), i.e. the strength of model response changes against small variations of the input settings, including discrete steps and not continuously differentiable correlations, and the correspondingly required data sampling density in  $F$ ,
- the noise of the model response to be predicted, as well as
- the chosen neuron transfer function  $f_{TR}$ .

For the present FNN application cases, hyperbolic tangent sigmoid (tansig) transfer functions are used (cf. Reference [213]). The determination of the neuron biases and the weighting values corresponds to a classic nonlinear regression task, referred to as ANN “training”. In the present context, training is conducted as “supervised learning” (cf. References [213] and [40]), i.e. a predefined learning rule is provided through a set of examples showing the proper model response. The set of proper examples - the training data  $\mathbf{U}_{tr}$  - consists of previously generated sample points  $S_{tr,i}$  and the corresponding model simulation results  $Y_{tr,i}$  (cf. Section 3.3.1) in the form given in Equation 3.6.

After initialisation, the network’s weights and biases are iteratively adjusted in order to optimise a given performance function  $f_{pf}(\mathbf{D}_{tr})$ . This typically refers to the minimisation of the overall FNN prediction error calculated for the sampling data used during training. The number of iterations during training is often referred to as “training epochs”. After each epoch,

a training performance function representing the mean squared sum of FNN prediction errors for the set of training samples  $S_{tr,i}$  is evaluated. The used algorithm for the optimisation of the performance function is gradient-based. The gradient is determined by performing computations backward through the network [213] [50]. Here, the back propagation method of K. Levenberg [115] and D. Marquardt [125] is employed.

### 3.3.2.2. Implemented Surrogate Model Creation Process

For the creation of high-quality surrogate models a standardised iterative process has been implemented during the present work. The basic flow diagram illustrating important process characteristics is given in Figure 3.9 (overleaf). The routine includes a heuristic approach to model refinement through an iterative adaptation of the surrogate model setup and successive supplementation of sampling data, controlled by the increasing knowledge of the human expert on model behaviour.

The procedure involves the data sampling procedure as presented in Figure 3.7, supervised surrogate model training involving expert-in-the-loop checks of training results, as well as the evaluation of the response prediction at independent sample point locations in  $F$ . For the studies presented in this thesis, the shown process was employed for FNN creation and validation, however, the implemented patterns are generic and, thus, may also be applied to alternate SuMo approaches.

During “Input Data Sampling”, the data sets for surrogate model training  $\mathbf{U}_{tr}$  and validation  $\mathbf{U}_{val}$  are extracted from the simulation model to be approximated, the former of which are used for “SuMo Creation”. Now, surrogate model creation is an iterative procedure requiring expert-in-the-loop activity to ensure data fitting quality. Starting from initial “SuMo Settings”, i.e. the definition of the surrogate model type, structure and training setup, the regression procedure is performed. Training is stopped, once a predefined training (performance) goal, such as the  $f_{pf}(\mathbf{D}_{tr}) < 10^{-6}$  is reached. Subsequently, visual inspection of the surrogate model response behaviour is required, in order to allow for plausibility checks by disciplinary experts. Therefore, the capability of multidimensional space exploration (cf. Figure 3.10) is employed. Based hereon, adequate adaptation of surrogate model settings can be conducted as part of the inner feedback loop shown in Figure 3.9, if required.

In the case of FNN, the determination of network structure, i.e. number of hidden layers, the respective numbers of neurons per layer, as well as the choice of neural transfer functions, has to be balanced between high accuracy of training data fitting and the risk of data over-fitting. Originating from a misallocation of non-linear neuron behaviour, i.e. the inadequate determination of input weightings and neuron biases for the expected model response, data over-fitting of FNN normally appears in the form of oscillating network responses. Here, the experience gained during the present work indicates that for practical application during conceptual design phases, the number of hidden neurons should be tailored to reach training performances  $f_{pf}(\mathbf{D}_{tr})$  of the order of  $10^{-6}$  within an adequate number of training epochs. Performances being significantly better than  $10^{-6}$  turned out as a clear indicator of data over-fitting for the analysed model approximation tasks. Typical numbers of training epochs, chosen as stop criteria for FNN training during the studies presented in this thesis, ranged from 500 to 2000.

### 3. Proposed Aircraft Conceptual Design Methodology

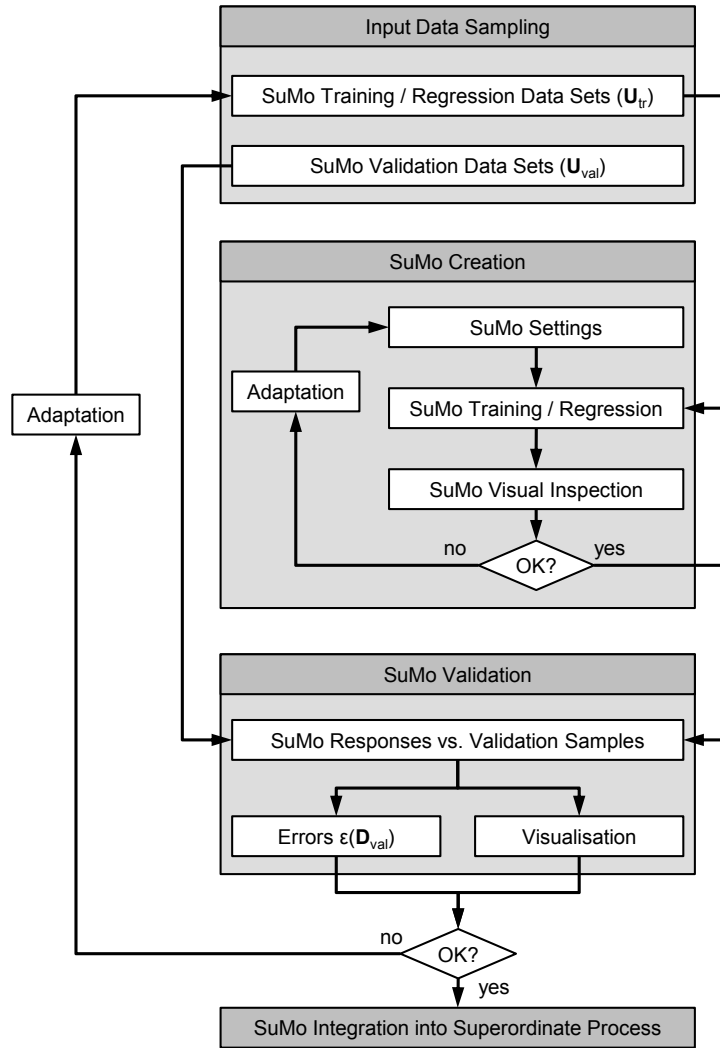


Figure 3.9.: Information flow scheme of implemented generic surrogate model creation process

After its successful creation, the surrogate model is validated using the independent data sets  $\mathbf{U}_{val}$  previously extracted from the simulation model. Therefore, the surrogate model prediction values  $\hat{f}(S_{val,i})$  for the validation samples  $S_{val,i}$  are compared to the expected responses  $f(S_{val,i})$ . The analysis of validation results includes both, the calculation of the error values of the surrogate model responses  $\epsilon(\mathbf{D}_{val})$ , as well as the location of badly approximated validation samples  $S_{val,i}$ . The identification of regions in  $F$  that are badly approximated by the surrogate is essential for the heuristic refinement of training data. Therefore, sampling density in  $F$  can be increased locally, e.g. in order of account for strong non-linearity of simulation response. Adaptive data sampling is conducted until sufficient surrogate model accuracy is reached across the variable space (cf. the outer loop in Figure 3.9). The actual metrics used for the evaluation of the validation results are presented in Section 3.3.3.

### 3.3.3. Validation and Quality Assurance

The physical accuracy of surrogates for disciplinary subtasks as well as system-level simulation results, in principle, relies on the quality of the underlying model. SuMo validation and quality assurance, thus, refers to proving that the errors induced by the surrogate ( $\epsilon(\vec{x})$ , cf. Equation 3.5) are small against the physical uncertainty of the approximated model, which includes the proper sampling of training data (cf. Figure 3.7) as well as the problem-tailored SuMo creation (cf. Figure 3.9). Typically, the confidence in surrogate model predictions is high in the vicinity of training samples, but declines with increasing distance to the nearest training sample. The use of independent space-filling LHS plans of surrogate model validation enhances the trust regions of surrogates significantly. Thus, meaningful figures of merit for the surrogate model quality can be derived from the SuMo approximation error at LHS-distributed validation samples in  $F$ . Now, the relative deviations of SuMo prediction  $\hat{f}(S_{val,i})$  and expected values of the  $k$ th response parameter  $Y_{val,i,k}$  for the  $i$ th validation Point  $S_{val,i}$  are defined as:

$$\epsilon_{val,i,k}(S_{val,i}) = \frac{Y_{val,i,k} - \hat{f}(S_{val,i})}{Y_{val,i,k}} \quad (3.8)$$

The resulting relative validation errors  $\epsilon_{val,i,k}$  may be evaluated statistically, in order to distinguish systematic errors from random errors.

#### 3.3.3.1. An Insightful Example

After the discussion of the underlying methodological approach to creating high-quality surrogates of complex simulation models, the validity of the produced results is demonstrated using a scalable turbofan engine deck based on GasTurb 11. Therefore, the mapping of engine net thrust  $FN$  and  $SFC$  for a wide cruise envelope is considered. The chosen input variables are the design net thrust of the engine and three basic operational parameters: flight altitude, flight Mach number and power lever setting. Design laws and parameterisation of the GasTurb 11 simulation model refer to the contents presented in Chapter 5.

Based on independent LHS plans, 1000 training data sets  $\mathbf{U}_{tr}$  and 100 validation data sets  $\mathbf{U}_{val}$  were simulated using the methodology introduced in Chapter 4. Based hereon, a single-hidden-layer FNN was created and validated as previously described in the present section. Here, the maximum relative errors identified for the set of validation samples  $\mathbf{U}_{val}$  as well as arithmetic mean values are given for the exemplary response parameters. Accordingly, the maximum relative errors amount to 1.15% for the net thrust approximation, and 0.49% for the specific fuel consumption, respectively. Both mean relative errors are of the order of  $10^{-3}$ , representing conservative values relative to the accuracy of the surrogate models employed for the studies presented in Chapter 6. However, the numbers demonstrate, that the uncertainty of system-level conceptual design studies induced by SuMo application is negligible against the general level of uncertainty at this stage of aircraft design. A synopsis of all relevant settings of the validation example are given in Table B.1 in Appendix B.

### 3. Proposed Aircraft Conceptual Design Methodology

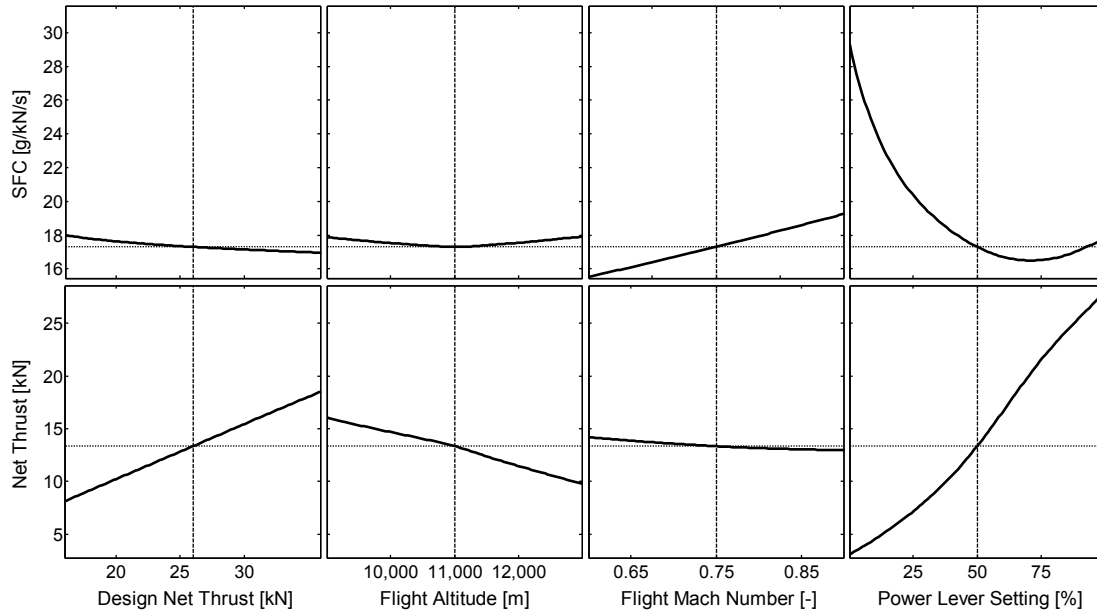


Figure 3.10.: Matrix of partial dependencies for an interactive exploration of surrogate model behaviour (Shown example: Surrogate model-based turbofan engine deck including net thrust based on GasTurb 11 simulation)

#### 3.3.3.2. Detailed Exploration of Model Behaviour

Still, the confidence in surrogate models is limited due to the complex multidimensional dependencies which complicate direct insight to model behaviour, in the first instance. Therefore, an adequate visualisation scheme is required, enabling the human expert to rapidly examine SuMo responses, thereby gaining knowledge on model behaviour in a highly efficient way.

Figure 3.10 shows a screenshot of an active graphical element allowing for the interactive exploration of SuMo behaviour in the mapped variable space  $F$  by horizontally dragging the indicated vertical lines in the shown plots. The graphical visualisation responds within the order of milliseconds, on a standard desktop computer. Depicted in the figure is the Matrix of Partial Dependencies (MPD) mapped by the underlying surrogate model. The size of the matrix refers to the external parametric interfaces of the surrogate, the input parameters defining its column space and response parameters defining its row space, respectively. The explicitly shown plots refer to the application case outlined in Table B.1 in Appendix B.

The interactive MPD is a powerful tool for design space analysis enabling an extremely rapid gain of knowledge on model behaviour and readily implemented for polynomial-based response surfaces in Reference [214]. During the present work, the basic visualisation approach was adapted for the interactive exploration of FNN, and used for the visual assessment of SuMo quality during SuMo creation (cf. “SuMo Visual Inspection” in Figure 3.9) as well as for subsystem and system-level design space exploration. This type of interactive visualisation has, in particular, proven to be helpful for the identification of potential optimisation variables, since the characteristics of the parameter-specific optima of a given objective function can

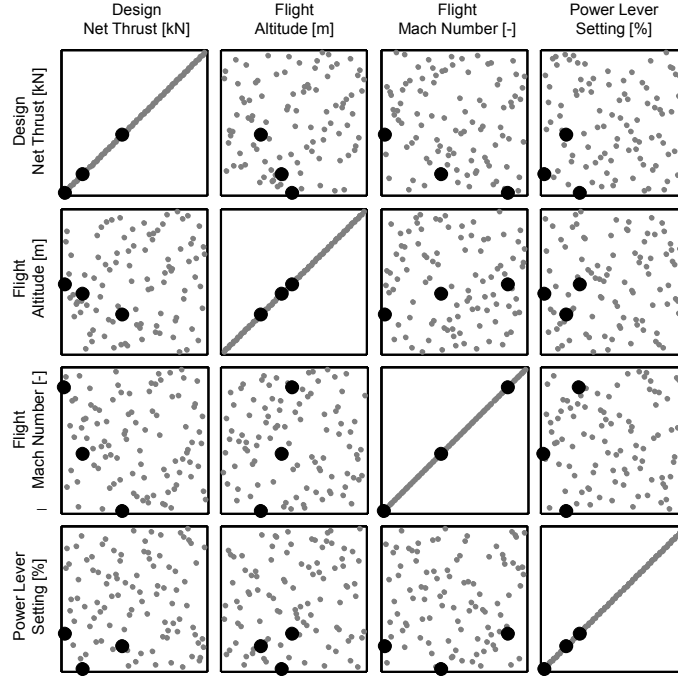


Figure 3.11.: Visualisation of LHS-distributed validation points according to Table B.1: Sample showing SuMo relative errors  $\epsilon_{val} > 0.8\%$  for the prediction of engine net thrust are highlighted.

be analysed efficiently. Taking, for instance, the partial dependencies of SFC shown in Figure 3.10, it is apparent that the power lever setting during cruise may be optimised for minimum SFC.

For the purpose of surrogate model refinement the gain of more insight to the validation results is required. Therefore, in Figures 3.11 and 3.12, matrices of 2-dimensional projections are depicted for the variable space  $F$  considered in the present example, showing the LHS-distribution used for SuMo validation. It can be seen that the validation results are representative, as the space is appropriately filled by validation samples. In the figures, the worst approximated validation samples are highlighted, for FN (cf. Figure 3.11) and for SFC (cf. Figure 3.12), respectively. This type of visualisation allows for a more detailed analysis of the validation results including the identification of potential causes and eligible counter measures. Here, the information on the location of badly approximated validation samples in  $F$  is of primary importance for the interpretation of the validation results.

Inspection of Figure 3.11 reveals that all of the highlighted (bad) validation points are located close to the outer boundary of  $F$  in at least one dimension. Examination of Figure 3.12 shows, that the highlighted, badly approximated validation points, here, occur at similar flight altitudes centrally located in  $F$  (cf. the second column of the matrix).

Reasons for bad data fitting of FNN, typically, originate from locally insufficient sampling density of training data, which either manifests in over-fitting (oscillating network response) or the underestimation of nonlinear behaviour of the original model. As can be seen from Figure 3.10, over-fitting is not an issue in the present example case. On the other hand,

### 3. Proposed Aircraft Conceptual Design Methodology

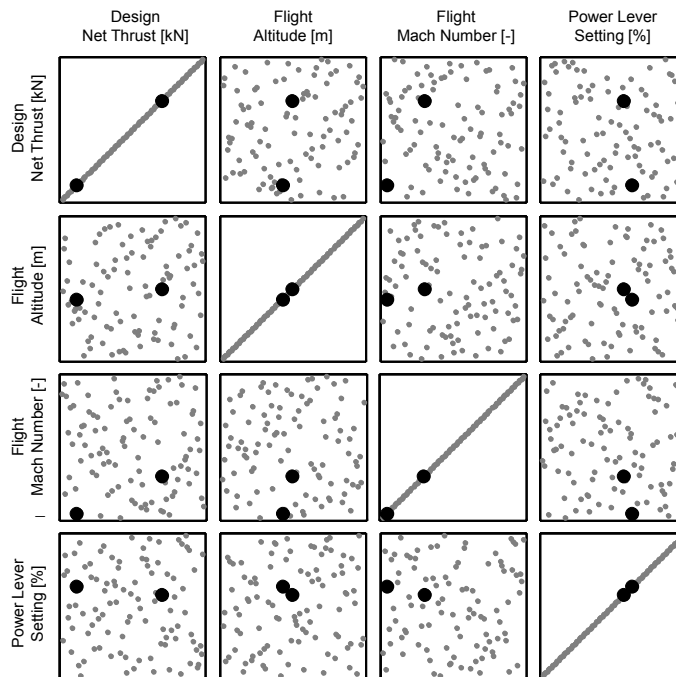


Figure 3.12.: Visualisation of LHS-distributed validation points according to Table B.1: Sample showing SuMo relative errors  $\epsilon_{val} > 0.4\%$  for the prediction of specific fuel consumption are highlighted.

insufficient training information at the boundary of the sampled space  $F$ , leads to bad approximation of net thrust characteristics, here. Thus, for given parameter ranges required for valid approximation by the surrogate ( $\{V_{i,min} \leq V_i \leq V_{i,max}\}$ ) a convenient counter measure against bad approximation in the boundary areas of  $F$  is to include sample sets located outside of  $F$  into the SuMo training procedure.

Insufficient local training information is also the reason for the centrally located, bad validation points in Figure 3.12: The used standard atmospheric conditions for the engine performance simulation produce a kink in the partial dependencies of FN and SFC against flight altitude due to the tropopause. In Figure 3.10, it can be seen that corresponding local non-linearity in model response is captured by the FNN, however, identified most critical for the approximation of SFC during validation. Now, an increase of local sampling density for SuMo training is capable of enhancing FNN accuracy, here. Again, additional local training sampling may lead to unbalanced regression results, and thus, requires a problem-oriented trade-off for maximum SuMo quality, guided by the human expert.

### 3.4. Verification of Methodological Approach

The proposed discipline-oriented aircraft design procedure represents a multi-level decomposition approach such as followed by the BLISS and CO approaches discussed in Chapter 2. However, the approach to system-level analyses is tailored to even stronger human design control, since the tasks of design space exploration and design optimization are decoupled. The

key enabler, here, is the application of surrogate models derived from a set of scaled aircraft configurations which have been subject to expert-judgement before further processing.

In summary, the methodological setup presented in this chapter is essentially based on three elements:

1. the rigorous discipline-orientation of the aircraft synthesis procedure,
2. the discipline-oriented incorporation of propulsion system design aspects into the aircraft conceptual design process, and
3. the problem-tailored application of surrogate modelling techniques for model integration and analysis.

In order to verify the proposed methodological approach, the discipline-oriented aircraft conceptual design process has been programmed in Matlab [215]. The applicability of the overall design approach to an integrated analysis of unconventional system architectures including advanced propulsion system concepts is demonstrated in Chapter 6.

The proposed surrogate-based solution for a discipline-oriented integration of propulsion system aspects can be found verified in all relevant aspects, involving

- the demonstration of the applicability of the implemented surrogate modelling process to the approximation of engine simulation models (cf. Section 3.3.3),
- the software integration of the engine design and performance programme GasTurb 11 (see Chapter 4),
- the detailed description of the conceptual design physics of advanced propulsion system and important airframe integration aspects (see Chapter 5), as well as
- validation studies at aircraft conceptual design level involving variations of propulsion system design parameters, technology level and architectural arrangement (see Chapter 6).

The software programmed in Matlab is organised and separated in three layers (cf. [208, Chapter 11]): firstly, a database containing the aircraft configuration files, surrogate model information, a number of auxiliary models and functions as well as important natural constants, secondly, the discipline-oriented design process including the modularly arranged subtasks, as well as the overall process logics and the iterative solver, and lastly, a user interface for the convenient analysis of system design and operational behaviour. The second and third software layers are widely independent from each other, only exchanging information through the predefined aircraft configuration files.

Intelligent human interfacing and problem-tailored, visual analysis capabilities are key factors for a quick gain of knowledge on system behaviour. The implemented graphical user interface enables convenient manipulation of configuration files and multidimensional analysis of model behaviour, all at a glance. The well-arranged visualisation and the fast response of the programmed process have, therefore, established as a key support for the confidence in results and design decisions during the present work. A typical representation of the graphical user interface is shown in Figure A.1 in Appendix A.



## 4. Integration of Propulsion System Simulation Software

For propulsion system conceptual design and performance analysis tasks in the present work, the commercial software GasTurb 11 is used. GasTurb is a well-established solution for engine performance simulation and in broad use in industries and academia [104] during early phases of engine design [193]. The software offers a high level of user-friendliness and a comprehensive set of engine design and performance analysis capabilities for a large number of predefined propulsion system architectures including many concept candidates considered for next generation aero engines. Therefore, in the first part of this chapter a detailed characterisation of GasTurb is given, including important features, recent extensions and available software interfaces options.

Also, important methodological elements for the surrogate-based integration of GasTurb engine models into the aircraft conceptual design process are elaborated. In particular, the generic data sampling process for the acquisition of surrogate model training and validation data, presented in Section 3.3.1, is applied to GasTurb simulation models. Therefore, sustainable solutions for the individual process elements shown in Figure 3.7 are introduced and discussed.

### 4.1. The Software GasTurb 11

In this section a brief overview of GasTurb's software features and capabilities during engine design and analysis is given. In particular, the typical workflow in the software as well as the principles of model parameterisation, implemented during the present work, are outlined. Finally, the available options for connecting GasTurb simulations to external applications are characterised.

#### 4.1.1. Basic Characterisation

The software GasTurb is a gas turbine performance program comprising the evaluation of the thermodynamic cycle of common gas turbine architectures, both for engine design and operational behaviour (off-design). The latest version of the program, GasTurb 11, furthermore covers preliminary flow path sizing and disk stress calculation capabilities. A package of auxiliary software, GasTurb Details [101], allows for the design and analysis of specific aspects of engine conceptual design such as turbine cooling, user-defined fuels based on NASA's CEA (Chemical Equilibrium with Applications) program (cf. References [67] and [128]), heat exchangers and turbine velocity triangles. For the studies presented in this thesis a recent release of GasTurb (version 11, compiled on 27th January 2010) [105] was used.

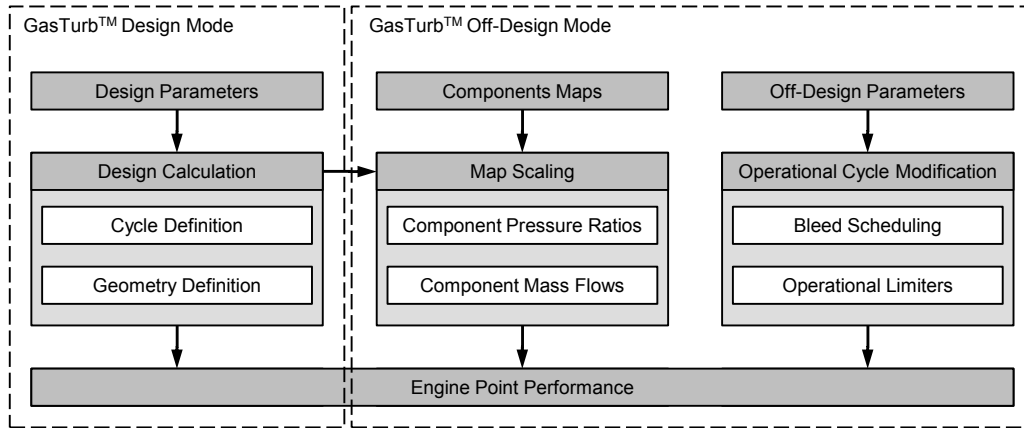


Figure 4.1.: Basic visualisation of GasTurb general work flow

GasTurb provides more than 20 different predefined propulsion system types ranging from turbojets to variable cycle engines. Configurations for the mapping of important candidates for next generation flight propulsion systems are readily included:

- Advanced conventional turbofan (2-spool and 3-spool)
- Geared turbofan
- Intercooled and/or recuperated turbofan
- Turboprop / open rotor engines

The software’s graphical user interface provides convenient guidance for the user and comprehensive model analysis capabilities involving 2D parametric studies, sensitivity analysis, optimisation and Monte Carlo studies. For model supplementation and post-processing GasTurb provides so-called “composed values”, iteration capability and free “input parameters”. Composed values can be used for the implementation of figures of merit for iterative correlations and model post-processing. “Iterations” are available for the implementation of additional heuristics to system design and operational characteristics. “Input parameters” may serve as additional free model variables or as part of iteration targets.

The software provides external interfaces involving export functionality to Microsoft Excel [135] for the results of 2D parametric studies, sensitivity analyses or batch job calculation. More recently, engine performance deck applications in the form of Dynamic Link Libraries (DLL) have become available for selected GasTurb engine configurations [104].

#### 4.1.2. Analysis of Typical Work Flow

The software GasTurb distinguishes between geometry definition (“design”) mode and operational analysis (“off-design”) mode. The isolated handling of design and off-design modes enhances user friendliness in a manner of separation of concerns and allows for the neglect of component maps during design mode as can be seen in Figure 4.1.

However, different operational conditions may act as critical design drivers for individual aspects of aero engine design. The most important engine operating conditions to be

considered during conceptual design phases involve typical cruise conditions (often representing the aircraft's Aerodynamic Design Point, ADP), maximum climb (MCL) and take-off (MTO) conditions at which given thrust and efficiency requirements have to be met. Thus, the required aerodynamic capacity of turbo components is typically defined at top of climb and maximum rating conditions. At cruise operation maximum thermal and propulsive efficiency is the predominant requirement (especially for long range applications, cf. Reference [193]). Maximum temperature levels in turbofan engines occur at maximum take-off conditions. The involved maximal thermal loadings of materials strongly determine the required turbine cooling air mass flows, which have an essential impact on component sizing and cycle definition. The high level of interdependence between cruise, maximum climb and take-off conditions, all influencing the engine's geometric layout necessitates iterative procedures during conceptual design.

The iterative computation of engine design in GasTurb design mode as used for the present work is shown in Figure 4.2 (overleaf). The shown work flow involves four succeeding steps: the proper assignment of input parameters, the corresponding evaluation of the internal model yielding the straight-forward design results, model post processing using the provided number of composed values, and finally the definition and solution of required iterative correlations in order to exploit ideal correlations of model parameters. Standard in- and output parameters of the calculation are intrinsic to the chosen engine architecture, however, nomenclature is common for all types of engines available in the software [105].

For the studies of the present work, special attention was paid to an adequate model parameterisation allowing for comparative studies, while retaining technological similarity of designs within the aspired space of parametric variation (cf. Chapter 6). The definition of composed values, therefore, included the processing of flow path geometry and turbo component aerodynamics, yielding a set of engine architecture-dependent design laws. Accordingly, the iteration setup was defined to satisfy these design laws. Converged design solutions included a comprehensive data set of engine design point performance, basic flow path geometry, turbo component sizing and aerodynamic loading characteristics as well as the considered aircraft installation effects such as cabin power and bleed air off-takes. A detailed discussion of the physical aspects mapped during the present work is given in Chapter 5.

### 4.1.3. GasTurb Computer Decks

In the past, the integration of GasTurb simulation results into superordinate processes was realised through the exchange of tabulated data based on GasTurb's built-in export functionality [193]. Today, an application of the available computer engine decks [104] instantly allows for the simulation of operational characteristics for a given engine design outside of the GasTurb environment. Computer engine decks are defined according to the SAE Aerospace Standard AS681 [102] and available for selected GasTurb engine model types.

#### 4.1.3.1. Basic Functionality

The engine simulation functionality is contained in individual dynamic link libraries for each engine type available as a computer deck. The calculation of engine characteristics using

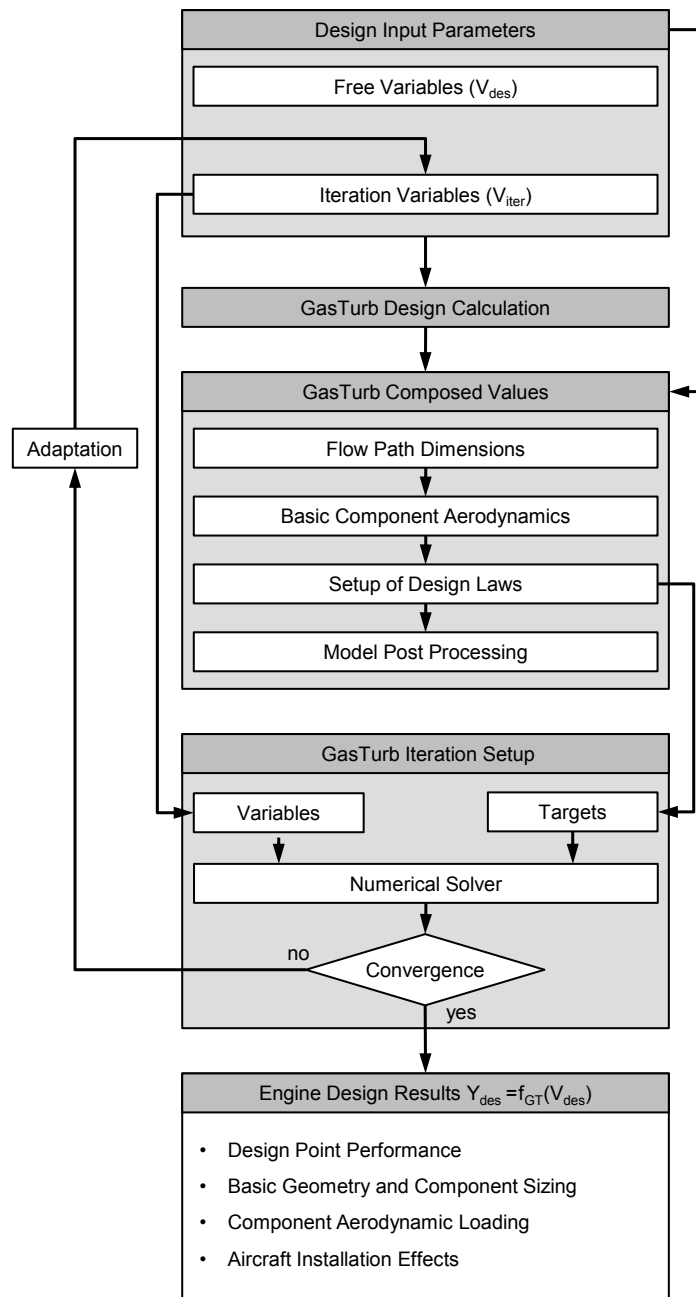


Figure 4.2.: Visualisation of engine design calculation process as used in GasTurb design mode

GasTurb computer decks is based on the information given in respective, type-specific Engine Model File (EMF) which is created by GasTurb 11 [102] and incorporates all necessary engine design information.

The initialisation of GasTurb computer decks requires properly defined EMF including appropriate minimum and maximum limiter settings for steady-state and transient operation as well as proper bleed schedule settings. Detailed requirement formulations for the EMF creation in GasTurb connected to the engine deck application are given in the corresponding user manuals (cf. References [102] and [103]). After initialisation, engine operational behaviour can be simulated through call of engine deck functionality [102]. Thus, engine deck libraries are a convenient means of integrating GasTurb in superordinate software environments.

During initialization the EMF is read from file and evaluated [102] which corresponds to the calculation of a “single cycle” [105] in GasTurb 11 design mode including the computation of the defined “composed values” and evaluation of design iteration scheme. After the initialisation, off-design simulations as defined for the considered type of engine model may be conducted. These may involve for steady state or transient operation as well as model based test analysis [103].

### 4.1.3.2. Dynamic Link Library Connection

The functionality of GasTurb engine decks is wrapped in the form of 32-bit Windows [136] DLLs. As a part of the engine deck documentation, interface definitions for DLL connection to external software are provided for Visual Basic for Applications (VBA) [134] and Delphi [52], see References [102, 103].

The framework used for model integration in the present work is Matlab. For external software communication, Matlab features a generic interface based on the C programming language [215] which allows for the translation between Matlab and external code. Corresponding header files working as a connector between engine deck DLLs and Matlab internal functionality have been implemented during the present work. The resulting software interface allows for an efficient control of DLL functionality out of Matlab.

## 4.2. Implemented Data Sampling Process

Studies related to the present work [193, 189, 190, 191] have shown the high potential of SuMo application concerning the integration of GasTurb simulation results in aircraft conceptual design processes. However, the large amounts of sampling data required for the creation of multidimensional, high-quality surrogates of GasTurb engine models represented a rigorous limiter, in the past. Now, the application of GasTurb 11 computer engine decks allows for an efficient sampling of multidimensional propulsion system simulation data. The present section, therefore, focuses on the proposed methodological approach to gaining arbitrary amounts from GasTurb simulation models. The presented methodology is applicable to the data sampling of both, propulsion system design and operational characteristics.

The aspects discussed in the following apply to arbitrary sampling plans within a properly defined, i.e. numerically and physically valid, parameter space. However, the given examples

focus on LHS plans which have been identified most significant for the efficient regression and validation of surrogate models (cf. Section 3.3.1).

The proposed and implemented Data Sampling Process (DSP) for the available GasTurb engine decks directly corresponds to the generic scheme shown in Figure 3.7. An overview of the sampling procedure is illustrated in Figure 4.3, it accordingly incorporates four essential elements:

1. the “**Engine Modelling in GasTurb 11**” based on the full spectrum of design and analysis capabilities provided by the software (see Section 4.2.1),
2. the “**Process Setup**” including the definition of the simulation and the experimental Design settings (cf. Section 3.3.1), as well as parametric input space  $F$  for the sampling plan (see Section 4.2.1),
3. the “**Experimental Design Preparation**” including the generation of the sampling plan based on the predefined DoE settings, as well as the optimisation of the sampling sequence for minimum computational effort during simulation(see Section 4.2.2), and
4. the “**Sampling Plan Simulation**” allowing for an error tolerant simulation of predefined sampling plans including the logging of relevant simulation data (see Section 4.2.3).

In the following, the introduced procedural elements will be emphasised in detail.

##### 4.2.1. Engine Modelling and Process Setup

Basis for the proposed sampling process is a properly defined EMF, created by GasTurb 11. The EMF results from the definition of propulsion system design and its parameterisation according to the implemented design laws (see Chapter 5), the chosen component maps and adequate off-design parameter settings.

Off-design parameterisation includes adequate limiter settings and bleed scheduling for the engine model, and results from extensive analyses of engine operational behaviour in the desired operational envelope. For integrated design and off-design parametric studies, the effect of design variations has to be incorporated properly in the off-design parameterisation of the EMF. The parameterised engine model is developed iteratively using GasTurb in design as well as in off-design mode.

All relevant information on the propulsion system model is contained in the EMF. The setup of the data sampling process is subsequently tailored to the range of parametric variation covered by the design laws  $f_{GT}(\vec{V}_{des})$ , chosen component map and off-design parameterisation  $f_{GT}(\vec{V}_{des}, \vec{V}_{off})$ . Now, the process setup includes

- the definition of free design and off-design variables  $\vec{V}_{des}$  and  $\vec{V}_{off}$ , as well as their corresponding ranges to be included in the experimental design,
- the setting of simulation options, and
- the defining settings for the experimental design generation.

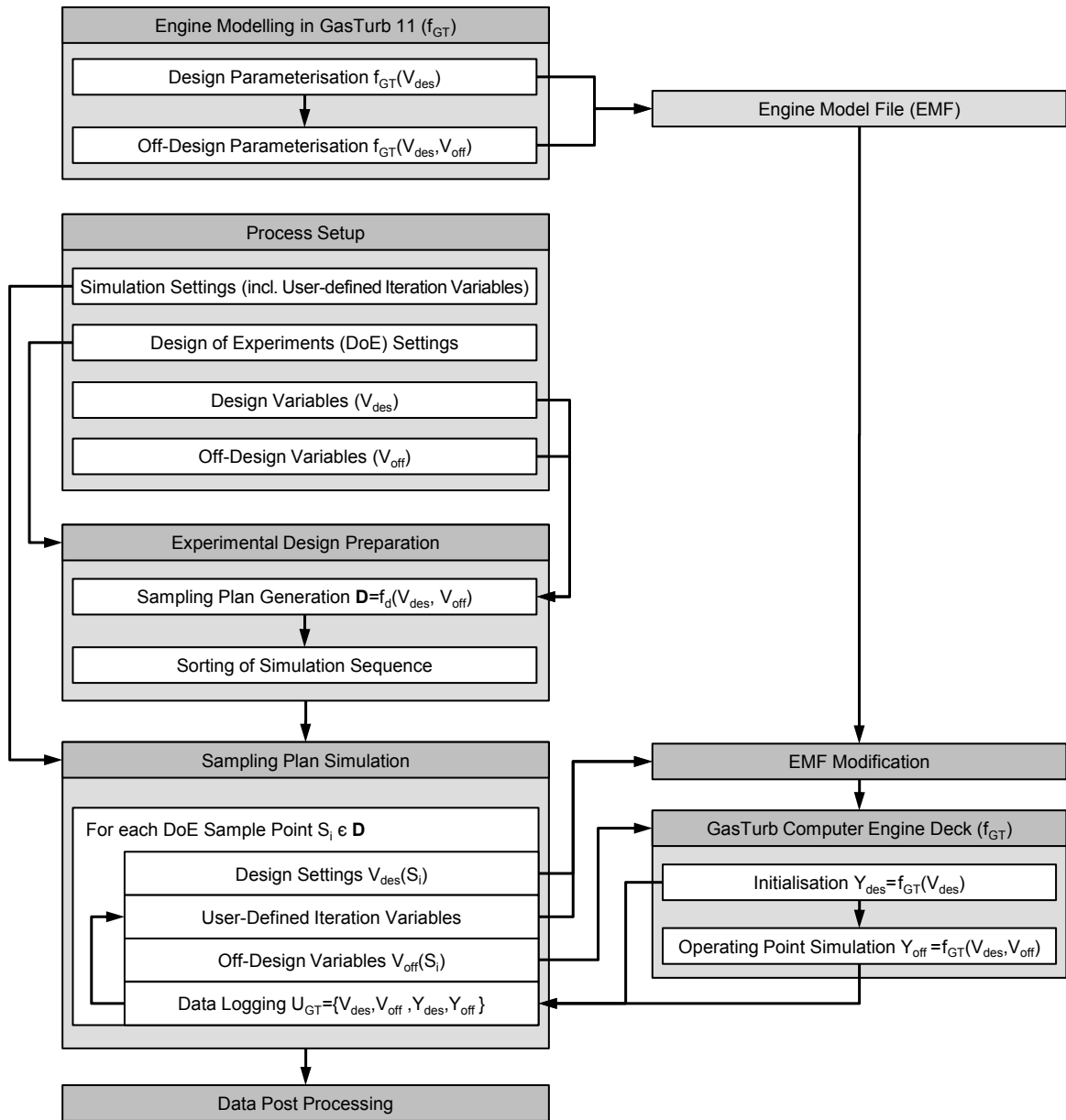


Figure 4.3.: Visualisation of implemented engine data sampling process using GasTurb dynamic link libraries

The number of parameters included in the experimental design is variable and depends on the desired study. The list of free parameters may contain GasTurb design as well as off-design parameters. Typical design variables involve design thrust, altitude and Mach number, design component efficiencies and pressure losses, design cycle parameters such as the burner exit temperature and compressor pressure ratios, fuel properties, customer power and bleed air off-takes as well as the design bypass ratio in case of turbofan engine architectures. Off-design variables typically include flight altitude and Mach number, power lever setting, atmospheric parameters such as standard temperature deviation and relative humidity as well as operational power and bleed air off-takes. The definition of free parameters  $V_j$  contains a type flag, denoting the parameter as design or off-design variable, the parameter name as used by GasTurb, the range of variation defined through the corresponding minimum and maximum values  $\{V_{j,min} \leq V_j \leq V_{j,max}\}$  as well as an empirical parameter  $c_{crit,j}$  describing the maximum allowable (critical) distance between succeeding simulation points.

The simulation setup contains a list of calculation result parameters to be read from the DLL, including all iteration and user-defined off-design iteration variables as used in the referred engine model as well as basic settings for data logging and buffering intervals.

### 4.2.2. Experimental Design Preparation

Taking the predefined experimental design settings, the design and off-design parameter definitions a sampling plan can be calculated (cf. Section 3.3.1). The parametric space  $F$  covered by the sampling plan is defined by the considered input variables  $V_j \in \mathbf{R}^p$  and their respective definition ranges  $\{V_j : V_{j,min} \leq V_j \leq V_{j,max}\}$ , where  $p$  represents the total number of design and off-design variables  $\vec{V}_{des}$  and  $\vec{V}_{off}$ . It should be noted, that in case of physical parameters the interval  $[V_{j,min}, V_{j,max}]$  may be a function of other input parameters, as encountered when considering a typical flight envelope.

For the purpose of multidimensional surrogate model regression and validation, the computation of large numbers of sample points is required. In order to significantly reduce the involved computational effort, adequate preparation of created sampling plans is necessary. In the following, important aspects to be considered for experimental design preparation for simulation are discussed.

#### 4.2.2.1. Influence of Initial Values on Convergence

Depending on the parameterisation of the underlying GasTurb engine model including number and setup of iterative feedback correlations for design, off-design and transient conditions, the convergence radii, i.e. the allowable deviation of initially estimated and finally determined values for the iteration variables, may vary significantly. The convergence challenge encountered is a classic starting value problem.

Assuming the existence of bijective solutions for the system of iterative correlations, two ways of ensuring a proper estimation of iteration variable values are apparent:

- a direct estimation of iteration variables as a function of the varied free parameters, or

- the stepwise approaching of the free parameter target settings, using the iteration variable values determined at the preceding convergent solution, while keeping the variation free parameters within model convergence radii.

The direct estimation of iteration variables involves significantly reduced parametric flexibility, since requiring extensive off-line preparation. The second approach is referred to as “search with correlated values” [168, Chapter 3.1.1] in the literature. It is considered of primary relevance for practical application, and thus, emphasised in the following.

#### 4.2.2.2. A Traveling Salesman Problem

Considering the existence of a convergence radius  $r_i$  at a given location  $S_i$  within the parametric space  $F$ , the values of the iteration variables connected to a preceding location  $S_{i-1}$  have to meet the  $r_i$  constraint to ensure calculation convergence at  $S_i$ . Accordingly, the maximum allowable distance between succeeding calculation points  $R_{crit,i-1 \rightarrow i}$  is given as a function of  $r_i$ :  $R_{crit,i-1 \rightarrow i} = f(r_i)$ . The convergence radius  $r_i$ , again, is a function of the input variable settings  $V_j$  included in the experimental design. Since both,  $r_i$  and  $f(r_i)$  are initially unknown, convergence sensitivity has to be mapped implicitly. Hence in the present approach, empirical parameters  $c_{crit,j}$  are employed to map the model convergence sensitivities connected to the individual input variables  $V_j$  to the maximum allowable distance between succeeding calculation points  $R_{crit,i-1 \rightarrow i}$ :

$$R_{crit,i-1 \rightarrow i} = \sqrt{\sum_{j=1}^p c_{crit,j}^2} \quad (4.1)$$

Now, taking a sampling plan matrix  $\mathbf{D}$  of  $n \times p$  size<sup>1</sup>, the actual distance  $R_i$  between succeeding sample points  $S_{i-1}$  and  $S_i$  is defined as

$$R_{i-1 \rightarrow i} = \sqrt{\sum_{j=1}^p (D_{i,j} - D_{i-1,j})^2} \quad (4.2)$$

A single sample point  $S \in \mathbf{R}^p$  is defined by its  $p$  coordinate values, constituting a full row vector within  $D$ . In case the distance between succeeding sample points  $R_{i-1 \rightarrow i}$  exceeds the maximum allowable distance between succeeding calculation points  $R_{crit,i-1 \rightarrow i}$ , intermediate calculation steps between  $S_{i-1}$  and  $S_i$  are necessary. Neglecting variations of  $R_{crit,i-1 \rightarrow i}$  between  $S_{i-1}$  and  $S_i$  and assuming the intermediate calculation steps to subdivide  $R_{i-1 \rightarrow i}$  into equidistant intervals, the minimum number of required auxiliary calculation points  $n_{aux,i-1 \rightarrow i}$  yields

$$n_{aux,i-1 \rightarrow i} = \left\lceil \frac{R_{i-1 \rightarrow i}}{R_{crit,i-1 \rightarrow i}} \right\rceil \quad (4.3)$$

The total number of required calculation points  $n_{total}$  for a given number of sample points finally includes the number of sample points  $n$  and the summation of auxiliary calculation

<sup>1</sup> $n$  represents the number of sample points  $S$  in  $\mathbf{D}$ ,  $p$  refers to the number of input variables.

points  $n_{aux}$ . It is apparent, that the number of required calculation points depends on the length of the actual simulation path, which corresponds to the classic “Traveling Salesman Problem” (TSP) [168]. Here, re-organisation of the sample point sequence may yield significant reductions of required auxiliary calculation points.

#### 4.2.2.3. Proposed Sorting Procedure

For the sorting of full factorial design sampling plans, applied to multidimensional parameter studies in GasTurb, a useful procedure is presented in Reference [193]. For the case of random or quasi-random sample point distributions, an efficient approach to sorting sample point sequences was implemented during the present work: The sorting algorithm executes a straight-forward, row-wise re-organisation of the sampling matrix  $D$ . Starting from a given location in  $F$ , the nearest neighbour out of a given set of eligible sample points  $\mathbf{D}_{res}$ , also located  $F$ , is identified.  $\mathbf{D}_{res}$  represents the residual set of sample points resulting from the initial design matrix  $\mathbf{D}$  reduced by the set of already sorted sample points  $\mathbf{D}_{sort}$ . For the subsequent step of the sorting procedure, the previously determined nearest neighbour is removed from  $\mathbf{D}_{res}$ , becoming the starting point for the following nearest neighbour search. Sample points identified as nearest neighbours are accumulated in chronological order in the matrix of sorted sample points  $\mathbf{D}_{sort}$ . The search for nearest neighbours is repeated until the sample point set  $\mathbf{D}_{res}$  is empty. It can be shown that the required computational effort correlates quadratically to the number of sample point contained in  $\mathbf{D}$ , for a given number of space dimensions  $p$ .

The criterion for the nearest neighbour identification during the presented sorting procedure refers to the minimum value of  $n_{aux}$  (cf. Equation 4.3) required to reach the next sample point  $S \in \mathbf{D}_{res}$ . Now, the total number of calculation points is a direct indicator for the overall computational effort required during the simulation of a given experimental sampling plan. The effectiveness of the sorting procedure, accordingly, can be measured by comparing the number of required calculation points before sorting  $n_{total,unsorted}$  and after sorting of the sampling plan sequence  $n_{total,sorted}$ :

$$\eta_{sort} = 1 - \frac{n_{total,sorted}}{n_{total,unsorted}} \quad (4.4)$$

In case adequate values for  $c_{crit,j}$  are unknown or the calculation convergence behaviour is independent across  $F$ , the (virtual) length of the simulation path  $L$  represents a convenient abstraction for  $n_{aux}$ -value.  $L$  results from the accumulation of the vector of distances  $R_{i-1 \rightarrow i}$  of succeeding sample points in  $\mathbf{D}$ :

$$L = \sum_{i=2}^n R_{i-1 \rightarrow i} \quad (4.5)$$

Thus, in parameter spaces  $F$  featuring variable-independent, isotropic convergence behaviour, the effectiveness of the sorting procedure may be defined using the ratio of simulation path lengths before sorting  $L_{unsorted}$  and after sorting of the sample point sequence  $L_{sorted}$ :

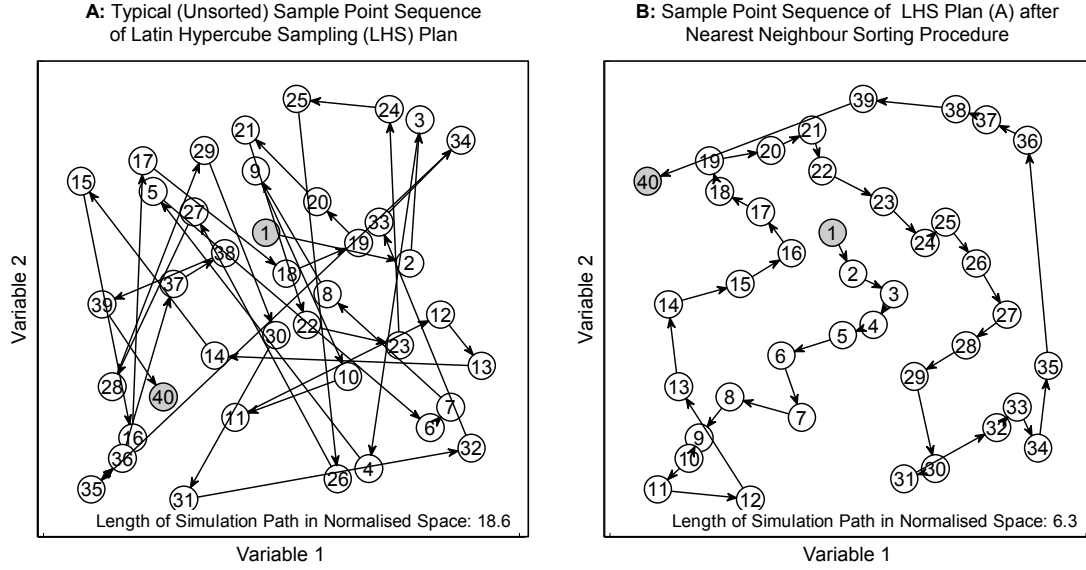


Figure 4.4.: Visualisation of implemented experimental design sorting procedure for reduced simulation time (Example: 40 sample points, 2 variables latin hypercube sampling)

$$\eta_{sort} = 1 - \frac{L_{sorted}}{L_{unsorted}} \quad (4.6)$$

Exemplary results produced by the sorting algorithm are shown in Figure 4.4. As an indication of the sorting effectiveness, the simulation path lengths before and after sorting  $L_{unsorted}$  and  $L_{sorted}$  are given. For the shown 2-dimensional LHS example case the above-described functional principle of the nearest neighbour sorting approach can be followed easily. Furthermore, it can be seen that the algorithm performs suboptimal towards the end of the sorting procedure. This phenomenon may be explained intrinsically due to the continuously reducing freedom of choice for decreasing number of sample points remaining in  $\mathbf{D}_{res}$ . However, the resulting effect on sorted simulation path length diminishes against rising number of sample points.

The results of systematic analysis of algorithm performance are shown in Figure 4.5 for normalised LHS designs. Since LHS designs represent quasi-random distributions of sample points, sorting efficiency is starting value dependent. Therefore, five independent LHS designs were generated and sorted for each combination of number of sample points and design variables shown in Figure 4.5. It can be seen, that the sorting procedure yields significant reductions of simulation path lengths especially for large numbers of sample points. The sorting algorithm, inherently, is starting value dependent. However, it can be seen from Figure 4.5 that the impact of alternative starting values on sorting efficiency diminishes for large numbers of sample points. Against increasing number of dimensions of the hypercube, sorting effectiveness decreases due to the stratification scheme of LHS designs.

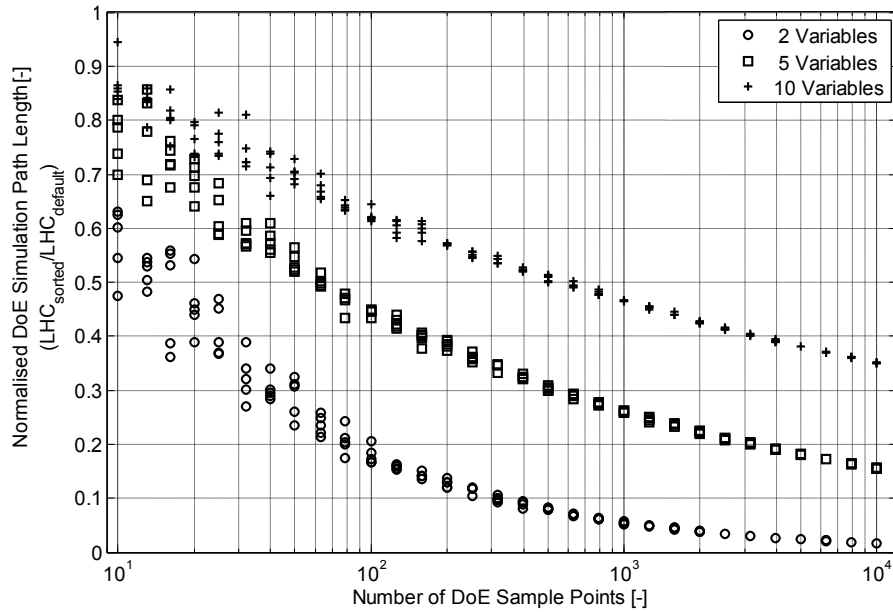


Figure 4.5.: Performance of implemented algorithm for sample plan sequence optimisation plotted against number of sample points (Example: latin hypercube designs for 2, 5 and 10 variables)

### 4.2.3. Sampling Plan Simulation

Central part of the proposed data sampling process is an automated routine for the sequential simulation of predefined sampling plans. The interfaces of the simulation routine refer to Figure 4.3. Accordingly, the simulation of sampling plans requires a consistent setup of inputs comprising the experimental design plan, a properly defined EMF, as well as realistic simulation settings defined during process setup.

Simulation may include design and off-design calculation. The engine simulation at off-design conditions is based on straight forward application of GasTurb engine deck functionality. For design calculation, modification of the EMF is required. GasTurb 11 EMFs are saved in plain text format. Value assignments for input parameters in the engine model file are unique, hence, design parameter settings may be applied to the baseline EMF through text parsing. Besides the settings of the free design variables, also the user-defined iteration variable values determined at the preceding convergent design point are assigned to the EMF. After modification of the EMF design point calculation is triggered while the engine deck library is initialised. Subsequently, operating points for the new defined engine may be evaluated.

During simulation, experimental design plan information and the corresponding data gained from the engine deck library are recorded. Calculation results include the standard output value of the library as well as the additional calculation result values defined during process setup. According to the predefined intervals, recorded data are buffered to prevent loss of information in case of simulation abort.

#### 4.2.3.1. On Simulation Options

The simulation routine is capable of running integrated design and off-design parametric studies as defined by the referred sampling plan. Design point calculation is triggered in case the variation of at least one engine design input parameter is identified between succeeding sample points within the experimental design plan. An overview of typical study cases is listed below:

- pure design points
- pure off-design points (fixed engine design)
- mixed mode (design- and off-design mode)
- iterative mixed mode (integrated design- and off-design iteration)

Beside multidimensional design studies, data sampling may be conducted to produce tabulated off-design data as used in existing aircraft design software (cf. Section 2.3.2). More importantly, mixed mode studies allow for studies involving design points and the corresponding operational points which is essential for the generation of integrated design / off-design surrogate models. Additionally, the simulation algorithm allows for an automated iterative procedure between design and off-design calculation which enables the consideration of essential operational characteristics such as temperature levels, as well as aerodynamic and mechanical design constraints during engine geometry optimisation in GasTurb design mode.

#### 4.2.3.2. Solution Strategies for Convergence Problems

By default, the simulation procedure uses predefined step width settings between succeeding calculation points  $\Delta_{i-1 \rightarrow i}$ , based on the experience on typical model convergence behaviour. However, in case of local “bottlenecks” in convergence behaviour, i.e. local narrowing of the convergence corridor due to strong non-linearity of model response, calculation may not converge. A useful strategy for this type of convergence problem is schematically shown in Figure 4.6 (overleaf). If the step width  $\Delta_{i \rightarrow i+1}$  exceeds the local convergence radius  $r_{i \rightarrow i+1}$ , a temporary reduction of step width ( $\Delta \rightarrow \delta$ ) may help in successfully approaching the target parameter settings ( $S_{i+1}$ ). Determination of the optimum default step width is empirically based and may be tailored to minimum simulation response times through appropriate adaptation of the referred process settings.

In case the step width reduction strategy does not successfully lead to the targeted sample point  $S_{i+1}$  and alternate, secondary strategy visualised in Figure 4.7 (overleaf) has been identified successful during practical application. Here, the approach to  $S_{i+1}$  is started from the initial point of the simulation  $S_1$  which should be centrally located within the parameter space  $F$ . As indicated in Figure 4.7, this strategy is also suitable for convergence problems caused by temporary boundary violation of the defined parameter space  $F$  such as possible in case of concave-shaped parts of the boundary (cf. typical flight envelope visualisation as given in Figure A.7).

#### 4.2.3.3. Integrated Handling of Design and Off-Design Modes

For the approximation of propulsion system design and operational characteristics in surrogate models, GasTurb’s design and off-design mode can be treated collectively, acknowledging the

#### 4. Integration of Propulsion System Simulation Software

**Legend:**

- DoE Sample Points (S)
- Auxiliary Calculation Points using Standard Step Width
- ◇ Auxiliary Calculation Point using Reduced Step Width
- Boundary of Convergence Corridor
- R Distances between Succeeding Sample Points
- r Convergence Radii at Sample Points (S)
- $\Delta$  Calculated Standard Step Width for Simulation Progression
- $\delta$  Reduced Step Width for Simulation Progression

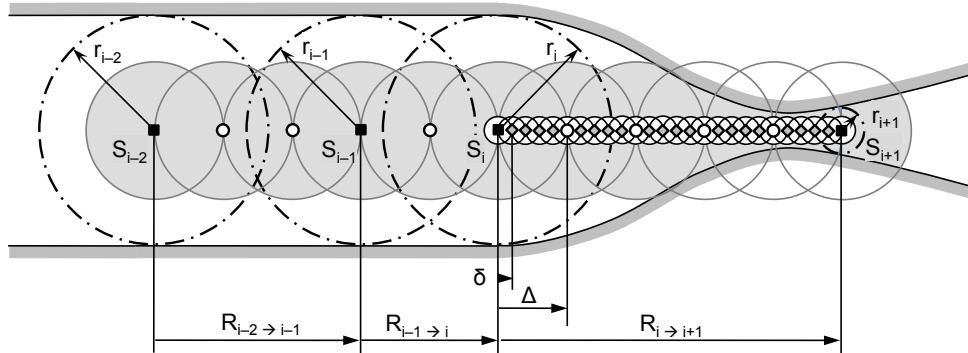
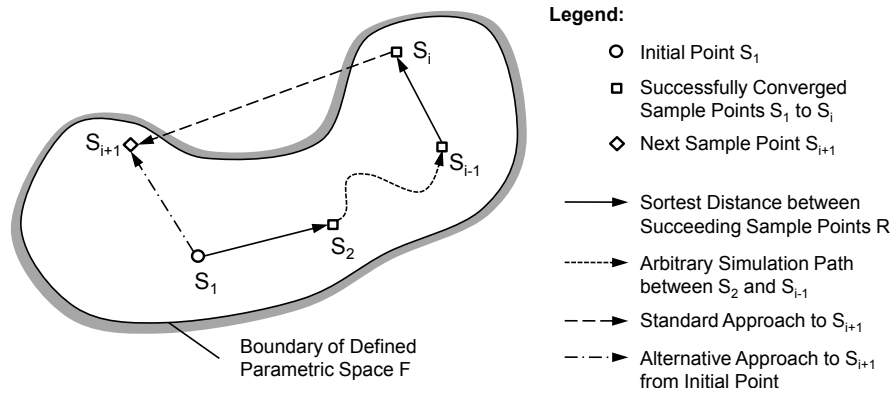


Figure 4.6.: Solution strategy for convergence bottle necks in design space



**Legend:**

- Initial Point  $S_1$
- Successfully Converged Sample Points  $S_2$  to  $S_i$
- ◇ Next Sample Point  $S_{i+1}$
- Shortest Distance between Succeeding Sample Points R
- > Arbitrary Simulation Path between  $S_2$  and  $S_{i-1}$
- - - -> Standard Approach to  $S_{i+1}$
- · · · ·> Alternative Approach to  $S_{i+1}$  from Initial Point

Figure 4.7.: Solution strategy for convergence problems due to temporary violation of design space boundaries

fact that off-design variables typically do not have an impact on engine geometry except for parts explicitly defined as variable geometry such as variable guide vanes, pitch blades or nozzle areas.

For parameters occurring as design as well as off-design free inputs, such as free stream Mach number or altitude, two free variables are introduced describing the design condition and as well as the actual operating condition independently. At design conditions the values of both variables match. Finally, in surrogate models containing both, design and off-design variables, a general independence of engine geometry from off-design parameter variations has to be ensured.

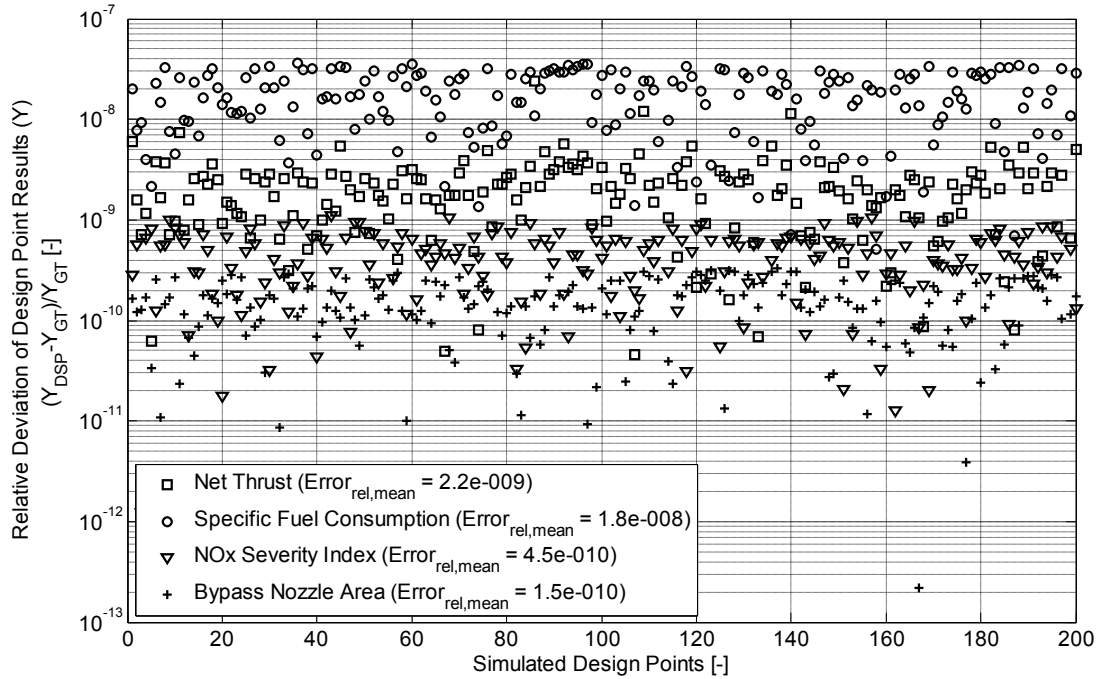


Figure 4.8.: Comparison of design point calculation results: GasTurb 11 versus the presented data sampling process (Example: 200 points, 10 variables latin hypercube design)

#### 4.2.4. Validity of Results

In this section, validation results for the proposed data sampling process are presented. Beyond that, best practices for the handling of sampled data ensuring high quality engine simulation results are discussed.

##### 4.2.4.1. Process Validation

The functionality of the presented data sampling process extends the functionality of the GasTurb 11 engine deck libraries to the capability of integrated design and off-design propulsion system parametric studies. New elements of the discussed process focus on the automation of the “design” part of these studies and, therefore, require validation.

In Figure 4.8, representative validation results are shown for the presented data sampling process. Here, 200 quasi-random engine design points distributed in a 10 dimensional space of typical design parameters were computed using both the software GasTurb 11 and the proposed data sampling process. The shown results refer to a boosted two-spool turbofan architecture based on Gasturb’s “Geared Unmixed Flow Turbofan” model. The used engine model refers to the standard demonstration file without additional parameterisation as delivered with the software GasTurb 11.

It can be seen, that the observed relative deviation of calculation responses, defined as  $(Y_{GT} - Y_{DSP})/Y_{GT}$  stays clearly below the order of  $10^{-7}$  for the considered exemplary calculation output values (design net thrust, specific fuel consumption,  $\text{NO}_x$  severity index

and bypass nozzle area). The occurring relative deviations are considered numerical errors, since being orders of magnitude smaller than the physical effects correlated to the imposed variation of design parameters.

##### 4.2.4.2. Quality of Produced Results

The use of surrogate modelling for the integration of disciplinary models into superordinate optimisation and analysis processes allows for previous check of calculation results by disciplinary experts.

The procedural patterns followed to ensure adequate quality of simulation data involve the check of numerical validity as well as comprehensive investigation of physical plausibility based on expert knowledge. An initial measure for numerical validity of results is the Numerical Status Indicator (NSI) which is part of the engine deck library standard output [102]. For the assurance of the physical plausibility of results, visual data analysis by disciplinary experts plays an important role. Therefore, appropriate data mining capability, such as provided by commercial software solutions (cf. Reference [9]), is required. Typical aspects of physical plausibility involve

- the check of potential violations of physical constraints,
- the evaluation of trends and distributions of system responses against input parameter variation, as well as
- the comparison of sample point result values against empirical expectation.

Finally, data regression during surrogate model generation may be utilised to reveal “bad” sample points which have not been indicated before. In order to ensure physically valid information to be used for surrogate model creation, an iterative procedure of adapting engine model design and off-design parameterisation and subsequent comprehensive data analysis may become necessary.

### 4.3. Recapitulation

Due to its philosophy of strictly distinguishing between design and off-design mode, the software GasTurb is limited concerning an integrated, multidimensional analysis of engine variants both at design and off-design operating conditions. Thus, for the complexity arising from the goals of the present research, powerful analysis capabilities going beyond the readily available functionality are required. The data sampling process presented in this chapter allows for the desired gathering of multidimensional information on system behaviour. It enables the convenient sourcing of information required for the regression and validation of surrogate models and therefore represents a key element for a high-performance, quality-ensured integration of propulsion system design and operational characteristics into the aircraft conceptual design process.

The presented process is applicable to conventional as well as unconventional propulsion system architectures available in the form of GasTurb engine decks and has been implemented for important propulsion system concepts being currently in discussion for next generation aircraft, such as advanced direct drive turbofan (A-TF), geared turbofan (G-TF), intercooled recuperated turbofan (IR-TF) and open rotor (OR) architectures.

## 5. Conceptual Design Methods for Aircraft and Propulsion System

As the third major part of the methodological development presented in this thesis, a consistent set of methods for the synthesis of aircraft and propulsion system conceptual design is introduced in the present chapter. The organisation of the chapter is directly geared to the discipline oriented aircraft synthesis procedure introduced in Chapter 3 (cf. Figure 3.2). The conceptual design and analysis methods presented in this chapter allow for a full-parametric integrated aircraft and propulsion system design and performance analysis. The discussion of propulsion design and integration aspects focuses on two alternative engine technology candidates, here, an advanced conventional turbofan and an advanced counter rotating turboprop (“open rotor”)<sup>1</sup> configuration. The results gained from initial case studies are presented in Chapter 6.

### 5.1. Overview of Implemented Methods

The synergistic incorporation of advanced propulsion systems involving the numerous unconventional installation options possible, yields a significant number of potential aircraft configurational arrangements. An overview of exotic engine/airframe integration options can be found in Reference [230]. However, for the validation of the methodological approach of the present work, it is more appropriate to demonstrate the developed capabilities for eligible system concepts. Hence, in the first instance, aircraft layouts refer to the conventional fuselage and cantilever wing (“tube & wing”) arrangements. Aircraft topological variations focus on the propulsion system layout, its installation location and the potentially required changes of the tail plane configuration.

The propulsion system layouts featured by GasTurb 11 include ducted and unducted architectures. Now, the determination of adequate propulsion system installation options depends on the air transport application under consideration of, i.e. the size and corresponding thrust demand of the aircraft, safety requirements, cabin internal noise, passenger comfort, external noise radiation, as well as powerplant accessibility during maintenance. The installation options, emphasised in this chapter involve classic under-wing mounting as well as aft-fuselage engine installation.

The aircraft layouts considered appropriate for the demonstration of the proposed aircraft conceptual design approach are shown in Figure 5.1. Both configurations shown, represent twin-engine, medium range (M/R) commercial aircraft layouts, featuring under-wing mounted turbofan engines and aft-fuselage mounted open rotor engines, respectively.

---

<sup>1</sup>in the past referred to as counter rotating unducted “propfan”

## 5. Conceptual Design Methods for Aircraft and Propulsion System

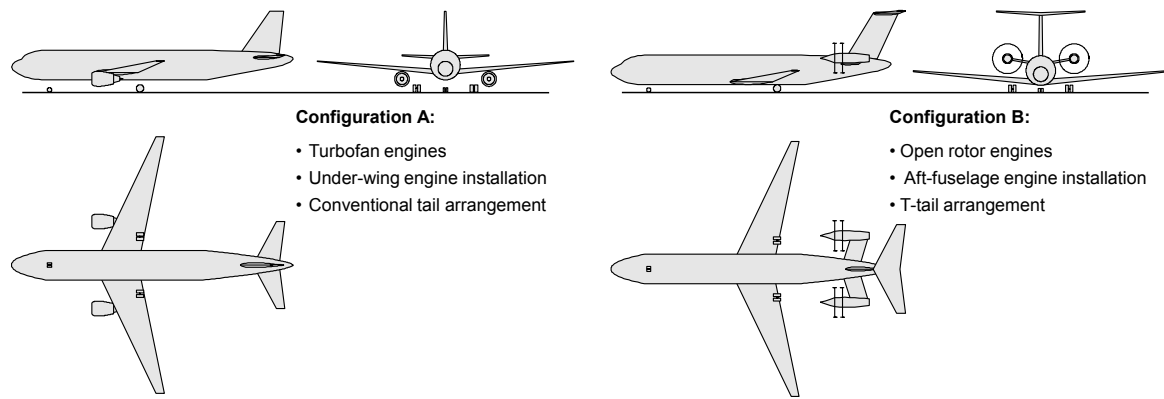


Figure 5.1.: Exemplary aircraft layouts considered for the demonstration of the proposed methodological approach

The resolution of the physical problem and the corresponding analytical fidelity of models is tailored to ensure a consistent treatment of these alternate propulsion system architectures and installation options on a conceptual level of system design. The system-level design and performance, therefore, focuses on

- the concept-specific propulsion system design aspects,
- engine operational performance characteristics, e.g. thrust lapse and part load behaviour,
- powerplant installation position,
- the aerodynamic interaction of propulsion system and airframe components, e.g. propeller slipstream effects,
- the geometric sizing of affected aircraft components, such as
  - engine pylon,
  - wing,
  - fuselage,
  - empennage, and
  - landing gear
- component weight effects caused by the engine installation, e.g. wing root bending moment relief in case of wing-mounted engines or increased fuselage longitudinal bending moment during touch down in case of aft-fuselage mounted engines, as well as
- the impact on ideal mission parameters, e.g. climb trajectory and optimum cruise conditions (Mach number and altitude).

Aircraft design aspects not directly affected by the propulsion system design and integration are not explicitly modelled, and treated as invariant residuals of weight and drag.

The implemented set of disciplinary design and analysis models comprises semi-empirical methods, the physics-based extension of textbook methods, as well as simple physics-based methods. For demonstration purposes, established textbook methods for aircraft design have been widely adopted. The selection of methods is based on the experience of the author. However, the classic empirically based methods are limited for the parametric mapping of conventional system architectures. Hence, a number of custom methods are presented for an

adequate mapping of the physical effects emanating from the targeted unconventional system arrangements.

The presented set of methods for the design and performance analysis of aircraft and propulsion system is implemented to the methodological framework presented in Chapter 3. The mapping of propulsion system design and performance is synthesised using the software GasTurb 11 and subsequently integrated into the discipline-oriented system-model based on the surrogate modelling techniques discussed in Section 3.3. The required data sampling is based on the methodology presented in Chapter 4. In the following, the proposed methods for system design and performance modelling are discussed in detail.

## 5.2. Propulsion System Design Aspects

Aircraft efficiency is influenced by propulsion system design through a number of effects either referring to engine-specific design and performance characteristics or relating to the integration of the powerplant in the airframe. The present section focuses on the methodology for propulsion system conceptual design and performance modelling. Propulsion integration aspects are addressed in the subsequent sections of the chapter. In the following, an overview of the implemented methods for propulsion system modelling is given, before the mapping of the specific design aspects is elaborated in detail.

### 5.2.1. Overview of Propulsion System Modelling

The multidisciplinary conceptual design of flight propulsion systems is an engineering task of fabulous complexity, and thus, has been subject to extensive research work in the past. Best practices for the initial layout of aero engine aspects are substantially published in well-known textbooks, such as by Walsh and Fletcher [225] and Grieb [69]. Now, the present approach focuses on the parametric mapping of essential propulsion system design aspects while aiming at the implications on aircraft design and performance and vice versa. Attention is paid to the implementation of adequate design laws, in order to allow for system-level parametric studies of technologically similar engine designs, as well as comparative studies of alternative system architectural arrangements. The proposed methods for propulsion system modelling are summarised in Table 5.1.

For the studies presented in Chapter 6, a classic 2-spool boosted turbofan is chosen as a baseline engine configuration. Besides, the presented methodology is applied to a geared counter rotating turboprop engine architecture, also referred to as open rotor concept.

Most propulsion system design methods introduced and discussed in the present section employ basic physical principles and are, therefore, widely independent from the chosen system architecture: The basic geometry of turbo components is modelled based on the local corrected mass flows, axial Mach numbers and hub-to-tip ratios. Based on the geometric definition and the representative blade speeds, the aerodynamic loading conditions are calculated, and correlated with technology-dependent loss coefficients, yielding the component efficiencies. Efficiency corrections for tip clearance and Reynolds number effects are superimposed. The impact of cooling air mass flow on turbine efficiency is captured. Duct losses are modelled as a function of inlet Mach numbers and shape-specific loss coefficients. Different technology

Table 5.1.: Overview of methods used for the mapping of propulsion system conceptual design aspects

Aspect	Method
<b>Synthesis Model<sup>a</sup></b>	GasTurb 11
<b>Mapping of Turbo Component Design</b>	
Geometric description	GasTurb 11, custom adapted (see Section 5.2.3.1)
Mechanical loadings <sup>b</sup>	GasTurb 11 (see Section 5.2.3.2)
Turbo component efficiencies	custom (see Section 5.2.3.3)
Turbine cooling air <sup>c</sup>	custom (see Section 5.2.3.4)
<b>Ducts and Associated Losses</b>	
Duct losses	GasTurb 11, custom parameterised (see Section 5.2.4)
Nozzle calculation	GasTurb 11, parameterised acc. to Grieb [69]
<b>Propeller Aerodynamics</b>	
Analysis Model Type	strip line calculation
Geometry Parameterisation	custom (see Section 5.2.5)
Induced Characteristics	acc. to Theodorsen [217, 39, 44]
Blade Profiling	NACA16-Series, data read from Reference [75]
<b>Operational Characteristics</b>	
Component Maps	GasTurb 11 standard
Bleed Scheduling	custom (see Section 5.2.6)

<sup>a</sup> incl. engine architecture, cycle parameterisation and operational simulation

<sup>b</sup> Mechanical design parameters (i.e.  $AN^2$  of turbo components resulting from flow path sizing and component aerodynamics) are treated as nonlinear constraint parameters during system-level design studies. Typical values and technical limits can be found in References [69, 225].

<sup>c</sup> incl. cooling air mass flow determination and turbine efficiency impact

levels are mapped by consistently increasing or reducing the used loss coefficients. Propulsion system operational behaviour is simulated using GasTurb standard component maps.

For the mapping of new system architectures, such as the aforementioned open rotor engine configuration, the development of additional methods for the concept-specific system components is presented. In order to parametrically incorporate the design characteristics of the counter rotating propellers at an appropriate level of fidelity, a stripline method for the swept propeller aerodynamics is presented. The prediction of the characteristics of the involved propeller drive gearbox refers to the extensive studies performed as part of NASA's APET programme (cf. References [176, 185]). The mechanical efficiencies of spools are considered invariant during the targeted studies. Efficiency values are very close to unity.

The modelled design aspects primarily focus on the aero-thermodynamic characteristics of the propulsion system, consistently mapped against varying technology status. The selection of design aspects modelled is based on their SFC impact. Therefore, SFC sensitivity analyses were conducted for typical input parameters to engine performance simulation. The obtained results are shown in Figure A.2 in Appendix A. The elaboration of mechanical design details is not part of the present focus. However, geometric parameters, mechanical loads and local temperature levels gained from system sizing and performance simulation are used as inputs

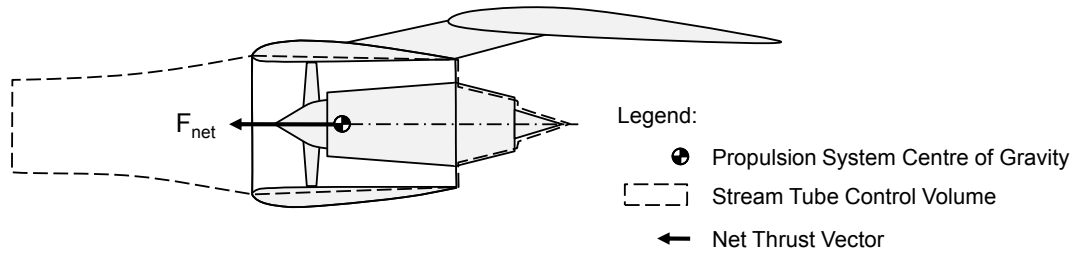


Figure 5.2.: Visualisation of control volume considered for the mapping of propulsion system design aspects

to propulsion system weight estimation. Detailed characteristics of the developed methods are discussed in the following sections.

### 5.2.2. Engine Design Strategy

In the present section, an outline of the paradigms followed during propulsion system modelling is given. Therefore, the interfaces between the engine model implemented in GasTurb and the disciplinary models of the overall aircraft are defined including the resulting installation effects to be considered during engine design and performance mapping. Furthermore, the propulsion system design strategy is outlined, involving essential engine-specific figures of merit, the considered sizing requirements as well as the handling of basic cycle parameters and the implemented engine design laws.

#### 5.2.2.1. Control Volume of Engine Modelling

The consistent mapping of propulsion system design aspects requires an adequate interface definition for the coordination of the involved models. The control volume for the modelling of propulsion system design and performance aspects used for the present purposes is shown in Figure 5.2. The chosen control volume definition is geared to the engine's stream tube. All physical effects imposing on the stream tube ahead of the propulsion system are incorporated in the propulsion system design and performance mapping. For the presently considered types of propulsion system installation, upstream disturbances, such as temperature and pressure distortion, are assumed small and, thus, not explicitly modelled. Also, effects due to the interaction of engine jet stream and aircraft components located downstream the engine which may act repercussive on engine operation are neglected, in the first instance. However, it should be noted that the aerodynamic and aeroelastic interaction of propeller-wing-configurations may have significant impact on the design and performance of both system components.

The proposed control volume definition results from the rigorous discipline-oriented integration of the propulsion system into the aircraft conceptual design process. All external nacelle effects are treated as part of the respective aircraft design disciplines, i.e. external drag of fan cowling and pylon are considered as contributors to the overall aerodynamic drag of the aircraft, which has to be overcome by the net thrust  $FN$  produced by the installed engines.

The book keeping for unducted (turboprop or open rotor) engines is handled identically by mapping the additional drag of the external wetted areas of the nacelle (as well as all other aircraft components affected by the propeller slipstream) caused by the induced velocities of the propeller.

The mapping of aircraft installation effects during engine conceptual design is discussed in References [69, Section 5.11] and [97, p.7-16ff]. In the present work, all losses and drag shares inside the propulsion system control volume are covered by the parameterised GasTurb 11 engine models used. The incorporated effects, furthermore, include mechanical power and bleed air offtakes required for engine auxiliaries, aircraft systems and cabin air conditioning (cf. Reference [100]).

### 5.2.2.2. Metrics for System Design and Performance Evaluation

Aiming at aircraft performance, in the first instance, mission fuel burn is a meaningful metric being used for system-level optimisation in Chapter 6. However, essential metrics for the evaluation of propulsion system design can be directly demonstrated from the definition of the “Specific Air Range” (*SAR*). Describing the distance the aircraft can cover per unit fuel consumed, *SAR* represents a meaningful figure for aircraft point performance. *SAR* is defined as

$$SAR = \frac{V_0}{SFC} \cdot \frac{L/D}{W_{a/c} \cdot g} = \frac{V_0}{SFC \cdot FN_{req}} \quad (5.1)$$

where  $V_0$  represents the operational velocity of the aircraft (True Air Speed, TAS). It can be seen that propulsion system design and performance have multiple implications on aircraft performance. *SAR* is degraded by increasing *SFC* and total thrust required  $FN_{req}$ . The latter results from the ratio of aircraft weight force  $W_{a/c} \cdot g$  and its aerodynamic efficiency  $L/D$ .

As a measure for the energy conversion efficiency of engines, *SFC* either relates the provided fuel flow to the produced thrust (Thrust Specific Fuel Consumption *TSFC*) or to the delivered shaft power (Power Specific Fuel Consumption *PSFC*, as normally used for turboshaft engines). Since from an aircraft propulsion point of view *PSFC* is only an intermediate figure for the description of engine efficiency, in the present context, the term *SFC* exclusively refers to the thrust specific fuel consumption

$$SFC = \frac{V_0}{\eta_{ov} \cdot FHV} = \frac{V_0}{\eta_{th} \cdot \eta_{pr} \cdot FHV} \quad (5.2)$$

where *FHV* (Fuel Heating Value) refers to the lower calorific value of the employed fuel. The overall efficiency of the engine  $\eta_{ov}$  is constituted by its thermal efficiency  $\eta_{th}$  and the propulsive efficiency  $\eta_{pr}$  [100]. It should be noted that the balancing of thermal and propulsive efficiencies is different for turbofan-type (ducted) and turboprop-type (unducted) propulsion systems. A comparison of turbofan and turboprop efficiency bookkeeping is presented in Reference [179].

### 5.2.2.3. Cycle Definition

The thermodynamic cycle of today's flight gas turbines refers to the classic Joule or Brayton cycle, characterised by the sequential processes of compression, heat addition at (almost) constant total pressure and subsequent expansion of the working fluid. The ideal cycle efficiency, i.e. no entropy rise during compression and expansion, no pressure during heat addition, is directly defined by the compression ratio. In technical application, the law of increasing cycle efficiency for increasing compression ratio is compromised by the allowable temperatures after heat addition, i.e. burner exit temperature  $T_4$ , before the working fluid enters the aero-thermodynamically and mechanically high-loaded turbine section. In fact, the choice of compressor overall pressure ratio ( $OPR = p_3/p_2$ ) and  $T_4$  is a complex trade-off between cycle efficiency, compressor efficiency and material selection, secondary mass flow required for turbine cooling, and combustor emission levels.

The  $NO_x$  emissions produced by the combustion chamber (cf. typical definition of  $NO_x$  severity index [100, Section 4.9.5]) are directly influenced by the conditions of the working fluid at the compressor exit  $p_3$  and  $T_3$ . A discussion of combustion efficiency, pressure losses and Low- $NO_x$  combustor concepts is given in Reference [69, p.291ff].

Methodical approaches to the choice of design  $OPR$  and  $T_4$  are discussed in References [186] and [176]. The introduction of additional cycle elements, such as intercooling or recuperating components may have significant impact on the optimum choice of both parameters (cf. Reference [27, Figure 4]). Based on the presently introduced methodology, the system impact of cycle design parameters including  $OPR$  and  $T_4$  may be analysed and optimised at aircraft level. They are, therefore, considered free variables, in the first instance.

### 5.2.2.4. Implemented Design Laws

For the demonstration of the overall methodological approach of the present work, the comparative investigation of technologically similar unducted and ducted propulsion concepts at the aircraft system level is considered (see Chapter 6). This requires the application of a rigorous common methodological approach for the engine design and performance mapping. The software GasTurb allows for the implementation of iterative correlations for the parameterisation of engine design and off-design characteristics (cf. Figure 4.2). For the present purposes, a set of design heuristics was compiled, ensuring the feasibility of engine design computation as well as the technological similarity against the variation of design parameters. Therefore, the performance implications emanating from the variation of essential design parameters are traced back to the underlying physical mechanisms. The implemented design laws capture the turbo component efficiency implications due to varying aerodynamic loading conditions, ducting and nozzle loss characteristics, as well as heuristics defining essential design settings for the propulsive device.

The technological similarity of the mapped propulsion system design aspects is ensured against design parametric studies using identical

- turbo component loss coefficients,
- duct loss coefficients
- turbine cooling settings
- material properties, and

## 5. Conceptual Design Methods for Aircraft and Propulsion System

- spool mechanical efficiencies.

The geometric similarity of turbo components is based on identical hub/tip ratios and axial Mach numbers at the component inlets and exits. Turbine blade and spool rotational speed are defined by connected compressor tip speeds. For a constant technology level, the tip speeds of Intermediate Pressure Compressors (IPC) and High Pressure Compressors (HPC) are considered invariant against design parametric changes. In case of turboprop architectures the handling of LPC tip speed corresponds to the IPC and HPC mapping. Boosters tip speeds in turbofan architectures are mechanically connected to the fan tip speeds. In order to ensure similar conditions for the comparison of alternative system designs, common laws for bleed scheduling as well as the definition of maximum and minimum power settings are implemented (see Section 5.2.6).

The plausibility of generated component designs is controlled based on the inspection of essential engine design and performance constraints including geometric figures (blade height at HPC exit and HPC bore radius), critical mechanical and aerodynamic loads ( $AN^2$  values and stage loadings, see Reference [69, Section 5.2]) and operational boundaries (compressor surge margins, cycle temperature levels, mechanical and corrected spool speeds, flight envelope, and idle conditions).

For turbofan engines the efficiency of the propulsive device is the product of fan efficiency  $\eta_{fan}$ , duct total pressure ratio  $p_{16}/p_{13}$  and propulsive efficiency  $\eta_{pr}$ , the latter of which closely coupled to the ratio of flight and jet velocity. Here, the exit velocity of the bypass nozzle is correlated to the average outer fan pressure ratio and a trade-off between propulsive efficiency and net thrust production. The most significant design parameter affecting the optimum of the mentioned trade-off is engine bypass ratio ( $BPR = \dot{m}_{13}/\dot{m}_{22}$ ), i.e the amount of inlet air mass flows passing through the bypass duct  $\dot{m}_{13}$  relative to the core engine mass flow  $\dot{m}_{22}$ . Since strongly imposing on the fan diameter, the variation of  $BPR$  has major implications on the architecture of the propulsion system and its installation on the aircraft. For separate flow turbofan engines, ideal  $\eta_{pr}$  is a direct function of the ratio of flow velocities in the bypass and core nozzle jets ( $V_{18}/V_8$ ). The optimum ratio  $V_{18}/V_8$  can be derived analytically (cf. Reference [58]), it is used for the iterative determination of the outer fan pressure ratio (FPR)  $p_{13}/p_2$ . The determination of outer FPR in case of mixed flow nozzle arrangements is based on the equality of total pressures after the turbine exit duct  $p_6$  and at the exit of the bypass duct  $p_{16}$  when entering the mixer ( $p_{16} = p_6$ ) [186] [100]. The inner FPR  $p_{21}/p_2$  is iterated as a function of the outer FPR. An important influence parameter for the relative variation of inner and outer FPR is the bypass ratio. The implemented design law, here, is based on the area averaged specific works of the inner and outer fan regions derived from Reference [69, Figure 5.2.2.12]). Fan speed is mapped as a function of outer fan pressure ratio according to Reference [69, Figure 5.2.2.6a].

In case of unducted propulsors, the efficiency of the propulsive device primarily refers to the propeller efficiency  $\eta_{prop}$  which is a function of the losses due to the blade induced velocities, and the drag effects on the blades. When installed on the aircraft, the additional drag of wetted surfaces being exposed to the propeller slipstream has to be taken into account. Important propeller design parameters, such as propeller power loading and blade tip speed, are considered as free variables. The corresponding impact on system efficiency, geometric dimensions and the corresponding installation challenges, as well as weights and noise characteristics is mapped according to Section 5.2.5. The propulsive efficiency  $\eta_{pr}$  of unducted engine concepts is dominated by the propeller efficiency  $\eta_{prop}$ . The residual thrust

produced by the exhaust of the turboshaft core, however, yields an enhancement of  $\eta_{pr}$  over  $\eta_{prop}$ . Core residual thrust is calculated from the mass flow and excess velocity at the core nozzle exit. The ideal velocity of the turboshaft exhaust stream for minimum *SFC* can be derived analytically (cf. Reference [222]). In order to achieve maximum  $\eta_{pr}$ , the core nozzle pressure ratio  $p_8/p_0$  is iterated to ensure equality of ideal and actual jet velocities ( $V_8 = V_{8,id}$ ).

### 5.2.2.5. Engine Thrust Sizing

During detailed design phases, performance simulation covers all potential engine operating conditions. For conceptual design purposes the most important design driving operational requirements take-off (*T/O*), maximum climb (*MCL*) and typical cruise are considered significant. Traditionally, required thrust at these operating conditions set by the aircraft and airworthiness requirements are input to engine conceptual design studies. Based hereon, geometric constraints as well as efficiency, noise, emissions and weight targets have to be met. Due to the conceptual design approach proposed in the present thesis, thrust requirements are not given as fixed values but result from an integrated design and performance of aircraft and propulsion system characteristics.

At the *MCL* operating point, i.e. Top Of Climb (*TOC*) and given requirements for aircraft climb capability (e.g.  $300\text{ft}/\text{min}$ ), component corrected air mass flows respectively axial Mach numbers are maximum, therefore, constituting the constraining operational condition for flow path sizing. At take-off conditions maximum cycle temperatures occur for turbofan engines, forming essential constraints for engine mechanical design involving choice of materials and turbine cooling system dimensioning. At typical cruise condition maximum efficiency is desired for minimum mission fuel burn. The term “typical cruise condition”, here, refers to the aircraft’s *ADP*.

For engine conceptual aerodynamic sizing two strategies are common practice:

1. geometry definition at *ADP* condition while checking component flow capacity requirements at *MCL* and *T/O* conditions.
2. geometry definition at *MCL* condition representing maximum corrected component air mass flows while checking efficiency targets at *ADP* conditions and component flow capacity requirements at *T/O* thrust settings.

Both strategies may be followed using the methodology elements described in Chapter 4. However, in order to reduce process complexity while ensuring design validity, the latter design strategy based on flow path sizing at maximum climb conditions was chosen for studies presented in Chapter 6.

### 5.2.3. Mapping of Turbo Component Design

For classic aero engine architectures the design of the internal flow path is essentially driven by the involved turbo components.<sup>2</sup> In the following, the proposed methodology for the mapping

<sup>2</sup>In case of elaborate cycle concepts such as intercooled and/or recuperated engines architectures, ducting and the involved additional system components may gain considerable significance for flow path layout.

of turbo component design aspects is presented. The discussion includes the component geometric description, as well as the modelling of component efficiencies.

### 5.2.3.1. Geometric Description

In reality, turbo component design results from the evaluation of manifold, partly counter-acting requirements involving

- the working fluid including its aero-thermodynamic properties,
- temperature and pressure levels between component inlet and exit,
- the implications of potentially required component cooling,
- the aerodynamic interaction between succeeding components along the flow path,
- the mechanical interaction of components mounted on the same shaft,
- required operational envelope and transient operability,
- the geometric boundary conditions imposed by the mechanical design of the overall engine,
- the available materials and design technologies, to ensure structural integrity and to meet defined weight goals,
- noise emission requirements,
- available technology, as well as
- goals towards production effort and maintainability.

When aiming at turbo component “design-from-scratch”, the comprehensive implementation of such requirements implies the detailed description and multidisciplinary analysis of turbo component geometry. In particular, critical design characteristics such as noise emission behaviour or compressor surge margin require extensive 3-dimensional aerodynamics modelling or rig-testing for reliable assessment.

In the present work, however, system-level parametric studies of similar turbo component designs are targeted. Therefore, it is useful to reduce the geometric description to a basic parameterised model. For the subsequent prediction of component efficiencies and weights, semi-empirical methods are employed based on the geometric description.

In Figure 5.3, an overview of the geometric mapping of the engine flow path is shown. Here, the definition of turbo component lengths is illustrated. Based on the fan and the HPC, the definition of representative component diameters are displayed. In the following, the methodological approach to determining the relevant diameters  $D_i$  as well as the component lengths  $L_{comp}$  is discussed.

For a given number of component stages  $n_{st}$  the pressure ratio of a turbo component  $\Pi_{comp}$  can be calculated from the mean stage pressure ratio  $\Pi_{st,m}$  as follows

$$\Pi_{comp} = \Pi_{st,m}^{n_{st}} \quad (5.3)$$

Equation 5.3 corresponds to the classic form of  $f(x) = a^x$  which can be conveniently written as  $x = \ln f(x) / \ln(a)$ . Now, assuming ideal gas behaviour, i.e. the specific volume  $v$  is inversely proportional to the pressure  $p$ , yields a logarithmic dependency of annulus cross sectional area  $A$  against pressure. Neglecting the effects of varying axial flow velocities in the annulus,

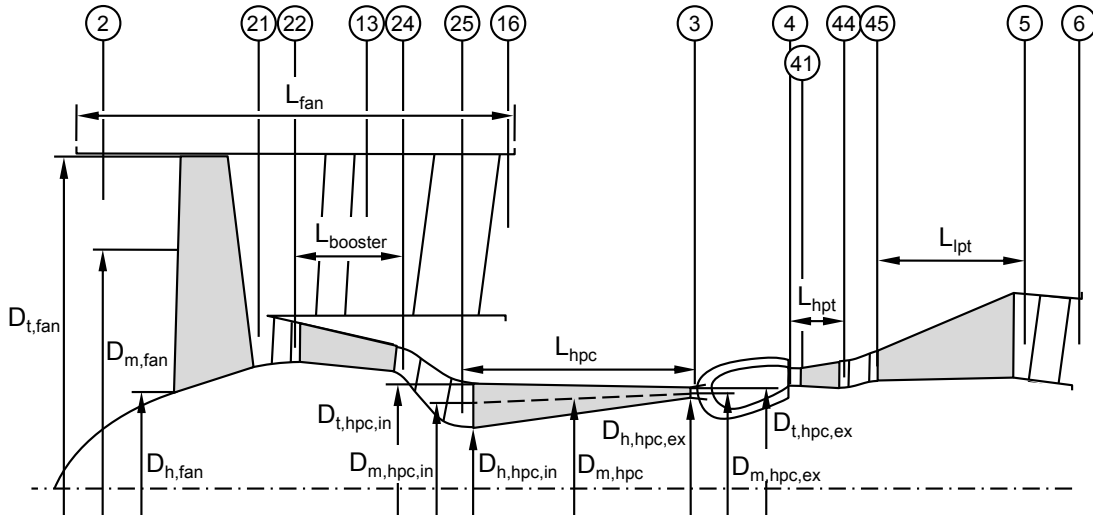


Figure 5.3.: Basic parameterisation of flow path geometry including thermodynamic station nomenclature (Example: 2-spool turbofan)

in the first instance, the distribution of the annular cross sectional areas between component inlet and exit can be expressed as

$$A_{st,i} = A_{in} - (A_{in} - A_{ex}) \cdot \frac{\ln(i)}{\ln(n_{st})} \quad \forall n_{st} > 1 \quad (5.4)$$

where  $A_{st,i}$  represents the annular cross sectional area at the  $i^{th}$  stage of the component. Equation 5.4 is applicable to multi-stage compressors and turbines. For single-stage components  $A_{st}$  refers to the mean value of component inlet and exit areas ( $A_{in}$  and  $A_{ex}$ ).  $A_{in}$  and  $A_{ex}$  refer to the component inlet and exit cross sectional areas which directly result from the evaluation of the thermodynamic cycle performed in GasTurb 11. The values of  $A_{in}$  and  $A_{ex}$  are essentially affected by the local mass flows  $\dot{m}$ , the mean axial flow velocities  $C_{ax}$ , the pressure  $p$  and temperature  $T$  levels.

Now, the calculation of the component length  $L_{comp}$  is based on the summation of stage lengths  $L_{st,i}$

$$L_{comp} = \sum_{i=1}^{n_{st}} L_{st,i} = \sum_{i=1}^{n_{st}} c_{L,st} \cdot \frac{h_{st,i}}{\Lambda_{R,i}} \quad (5.5)$$

where,  $\Lambda_{R,i}$  refers to aspect ratio of the rotor blades in the  $i^{th}$  stage, based on the axial blade chord length  $c_{R,i}$ . The mid-chord height of the rotor blades  $h_{st,i}$  is assumed equal to the local duct height, i.e. tip clearances are neglected. For given local hub/tip ratios  $(h/t)_i$ , blade height result from the following correlation

$$h_{st,i} = \sqrt{\frac{A_{st,i}}{\pi} \cdot \frac{(1 - (h/t)_i)}{(1 + (h/t)_i)}} \quad (5.6)$$

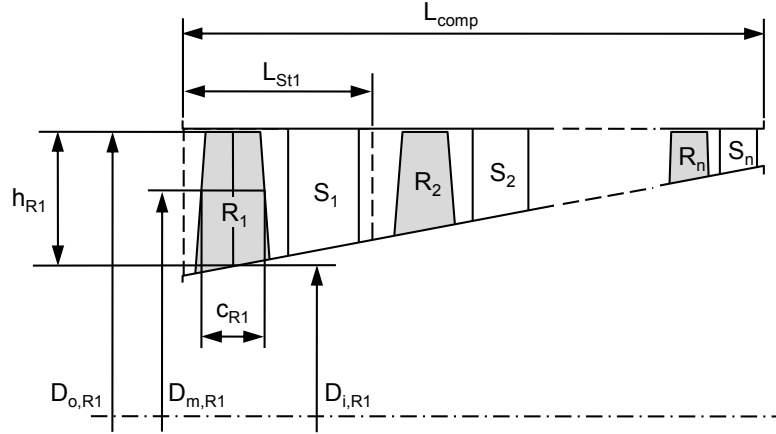


Figure 5.4.: Basic parameterisation of turbo component geometry including the nomenclature used for stage description

The parameter  $c_{L,st}$  in Equation 5.5 is an empirical factor representing the average stage length per rotor chord length  $c_{R,i}$ . For the studies presented in Chapter 6, values for  $c_{L,st}$  were derived from Reference [48, Appendix A-1]. Here, compressors, turbines and fan components were handled individually. The geometric parameters used in the presented method for turbo component length estimation are illustrated in Figure 5.4.

Based on the given annulus areas  $A_i$  and the hub/tip ratios  $(h/t)_i$  the local hub  $D_{h,i}$  and tip  $D_{t,i}$  diameters of the component can be derived from basic geometric considerations. The area averaged local diameter  $D_{m,i}$  accordingly yields

$$D_{m,i} = \sqrt{\frac{2 \cdot A_i}{\pi} \cdot \frac{(1 + (h/t)_i^2)}{(1 - (h/t)_i^2)}} \quad (5.7)$$

where the index  $i$  may represent any axial location between component inlet and exit planes.

In the engine synthesis model implemented in GasTurb 11, component inlet and exit hub/tip ratios  $(h/t)_{in}$  and  $(h/t)_{ex}$ , as well as the axial flow Mach numbers  $M_{ax,in}$  and  $M_{ax,ex}$  were treated as input parameters for flow path geometric sizing. Typical values therefore, can be found in the literature (cf. References [69], [225] and [186]). For the determination of the local hub/tip ratios  $(h/t)_i$  used in Equations 5.6 and 5.7, a proper design law is required. For the studies presented in Chapter 6, either the outer or inner diameters are linearly interpolated between component inlet and exit planes. Based hereon,  $(h/t)_i$  values are calculated. Through the definition of the radial contour of the annulus, individual turbo components shapes of can be approximated.

### 5.2.3.2. Aerodynamic and Mechanical Loadings

Based on the previously described geometric parameterisation, the aerodynamic and mechanical loadings of turbo components can be derived. Therefore, essential metrics describing the

aerodynamic flow conditions as well as the stresses due to the centrifugal forces induced by the high blade tip speeds of the component rotors.

For the estimation of component efficiency trends against design variation, the consideration of the aerodynamic loading conditions is essential. Here, the introduction of the stage loading  $\psi$  and stage flow  $\phi$  coefficients allows for full control over the aerodynamic velocity triangles replacing the explicit evaluation of angle relationships [117]. The proposed aerodynamic assessment uses the mean values of  $\psi$  and  $\phi$ , averaged between component inlet and exit conditions. Hence, mean stage loading parameter  $\psi_m$  is defined as

$$\psi_m = \frac{\Delta h}{n_{st} \cdot \frac{U_m^2}{2}} \quad (5.8)$$

where  $\Delta h$  denotes the component's specific work,  $n_{st}$  represents the number of component stages, while equal specific works are assumed for all stages, and  $U_m$  is the blade velocity at representative mean diameter of the component  $D_m$  which is defined as (cf. Figure 5.3)

$$D_m = \frac{D_{m,in} + D_{m,ex}}{2} \quad (5.9)$$

involving the area averaged mean annulus diameters at component inlet and exit planes  $D_{m,in}$  and  $D_{m,ex}$ .

Component blade tip speeds  $U_t$  are treated as inputs to the aerodynamic loading analysis. In GasTurb 11, compressor tip speeds are free input parameters each in case the compressor “design” option is activated [105]. The corresponding spool rotational speeds and turbine blade speeds are calculated as dependent values, based on the geometric configuration. Compressor blade tip speeds result from multidisciplinary considerations involving the local temperatures and allowable stress levels for discs and blades, the blade profiling and transonic behaviour of the blade cascades, as well as noise characteristics. The tip speeds are often limited by the allowable stress levels in the rotor blades and discs, and therefore, strongly dependent on the available material technology. Indication for maximum rim and blade tip speed for compressor and turbine design are given in Reference [225, p.165].

A meaningful figure for the mechanical loading of turbo component rotors is the  $AN^2$  metric which is a direct measure for the disc rim stress due to the acting centrifugal forces induced by the rotor blading (cf. Reference [100, Section 4.10.4]). Allowable  $AN^2$  values can be derived from the statistical analyses of existing turbo components presented Reference [69, Sections 5.2.2 and 5.2.3]. Beside its consideration as a component design constraint, the  $AN^2$  metric is essentially used for the mapping of turbo component weights (see Section 5.4.2).

Now, based on the cross sectional areas, total pressures and temperatures at the component inlet and exit planes, the corresponding meridional velocities can be determined. The dimensionless metric describing the ratio of meridional flow velocities and circumferential blade speeds is the stage flow coefficient. Assuming small radial velocity components, the representative stage flow coefficients at component inlet and exit planes can be defined as

$$\phi_{in} = \frac{C_{ax,in}}{U_{m,in}} \quad \phi_{ex} = \frac{C_{ax,ex}}{U_{m,ex}} \quad (5.10)$$

where  $C_{ax,in}$  and  $C_{ax,ex}$  denote the mean axial flow velocities at component inlet and exit.  $U_{m,in}$  is determined at  $D_{m,in}$  and  $U_{m,ex}$  at  $D_{m,ex}$  respectively. Component mean stage flow coefficient  $\phi_m$  yields

$$\phi_m = \frac{\phi_{in} + \phi_{ex}}{2} \approx \frac{C_{ax,in} + C_{ax,ex}}{2 \cdot U_m} \quad (5.11)$$

For a proper aerodynamic design of turbo components, the aerodynamic loading values of  $\psi_m$  and  $\phi_m$  resulting from the component geometric definition and the circumferential blade speeds have to be maintained in feasible boundaries. Typical ranges of  $\psi_m$  and  $\phi_m$  for existing compressors and turbines are given in Reference [69, Sections 5.2.2 and 5.2.3].

### 5.2.3.3. Component Efficiency

For conceptual design studies on a high system level, the efficiency of flow path components as a function of flow path design is of primary interest. Efficiency mapping for turbo components therefore should cover the inherent first order effects. The approach presented below incorporates the following aspects:

- the level of technology applied, e.g. flow path shaping, blade shape, casing treatment, active flow control etc.,
- the aerodynamic loading conditions,
- effects due to cooling air, typical for High Pressure Turbines (HPT) and Intermediate Pressure Turbines (IPT), as well as
- component size implications, i.e. Reynolds number and tip clearance effects.

In the literature, empirical correlations for the determination of turbo component design efficiency against average stage loading (cf. References [225, Chart 5.1ff] and [69, Section 5.2]). A semi-empirical method for efficiency calculation of multi-stage axial compressors is presented in Reference [63]. Included herein are recommendations for size corrections compressor polytropic efficiency. The defined threshold for compressor size equals a corrected compressor inlet mass flow of  $10lb/s$  below which efficiency has to be degraded. Comparable conceptual design and analysis methods for axial flow turbines are also available in the literature (cf. References [210] and [62]).

The proposed mapping of turbo components presented in the following yields polytropic efficiencies expressed in the form

$$\eta_{pol} = f(\phi, \psi, \zeta) \quad (5.12)$$

Where  $\phi$  and  $\psi$  represent the aerodynamic stage duty and  $\zeta$  indicates the technology dependent losses associated with the considered component design. The loss term  $\zeta$  may include component size influences as well as cooling air impacts on turbine aerodynamic efficiency. For the studies presented in Chapter 6  $\zeta$  is used as a calibration factor for different technology levels.

In Reference [117] the isentropic efficiencies of turbine and compressor stages are analytically derived as functions of  $\phi$ ,  $\psi$  and  $\zeta$  at annulus mean line based on linear cascade theory.

Assuming stage reaction of 0.5 which can be analytically shown as optimum<sup>3</sup>, and equal loss coefficients for stator and rotor, turbine stage isentropic efficiency  $\eta_{is,st,t}$  yields (cf. [117, Equation 3.33b])

$$\eta_{is,st,t} = \frac{1}{1 + f_L(\phi, \psi) \cdot \zeta_t} \quad (5.13)$$

The isentropic efficiency of compressor stages  $\eta_{is,st,c}$  is calculated similarly as (cf. [117, Equation 4.18a])

$$\eta_{is,st,c} = 1 - f_L(\phi, \psi) \cdot \zeta_c \quad (5.14)$$

The aerodynamic duty term  $f_L$  is an expression for the velocity triangle environment representing the aerodynamic conditions for the blading and therefore acts as a scale factor for aerodynamic losses.  $f_L$  is defined as (cf. [117, Equation 3.34])

$$f_L = \frac{1}{\psi} \left( \phi^2 + \frac{1}{4} \left( \frac{\psi}{2} + 1 \right)^2 \right) \quad (5.15)$$

Theoretically derived by Lewis [117],  $f_L$  is similar to the correlation published by Smith [197]. It yields similarly shaped contour lines as the well-known Smith diagram in a  $\phi$ - $\psi$  coordinate system.

Equation 5.15 is adapted from the definition given in Reference [117] to match with the definitions of  $\phi$  and  $\psi$  given above. In the following,  $f_L$  is calculated for representative stages of the considered turbo components using  $\phi_m$  and  $\psi_m$  according to Equations 5.11 and 5.8. Here, for the determination of basic loss factors  $\zeta$  simple empirical models are employed. The turbine loss factor  $\zeta_t$  is treated proportional to Soderberg's correlation [47, Equation 4.12]. For the initial estimation of the compressor loss factor  $\zeta_c$ , a profile loss correlation based on Lieblein's diffusion factor [119] given in Reference [118] is employed. Both loss coefficients are subsequently calibrated to account for 3-dimensional flow effects, as well as transonic losses.<sup>4</sup> Technology related effects are mapped by linear scaling of the component-specific loss factors  $\zeta_i$  (where  $i$  refers to the  $i^{th}$  component) using the loss scaling coefficient  $f_{tech,ps}$ . The resulting isentropic stage efficiencies (cf. Equations 5.13 and 5.14) are treated representative for the overall polytropic component efficiencies of turbines  $\eta_{pol,t}$  and compressors  $\eta_{pol,c}$ . Resultant generic aerodynamic design charts for compressors and turbines are visualised in Figure 5.5. The shown characteristics are in good qualitative agreement with the charts given in reference [117, Figures 3.12 and 4.4]. The values and shape of the shown efficiency contours are subject to loss correlation and technology adaptation. The shown efficiency maxima for compressors appear at slightly to high values of  $\psi_m$ . Statistics of  $\psi_m$  for existing compressors are given in Reference [69, Figures 5.2.2.8ff].

Model input parameters are the mean stage pressure ratios  $\Pi_{st,m}$  correlated to the defining conditions of  $\phi_m$  and  $\psi_m$  for core compressors and stages counts  $n_{st}$  for turbines.

<sup>3</sup>velocity triangles are symmetrical [117]

<sup>4</sup>Correlations for transonic loss correction are given in Reference [69, p.744].

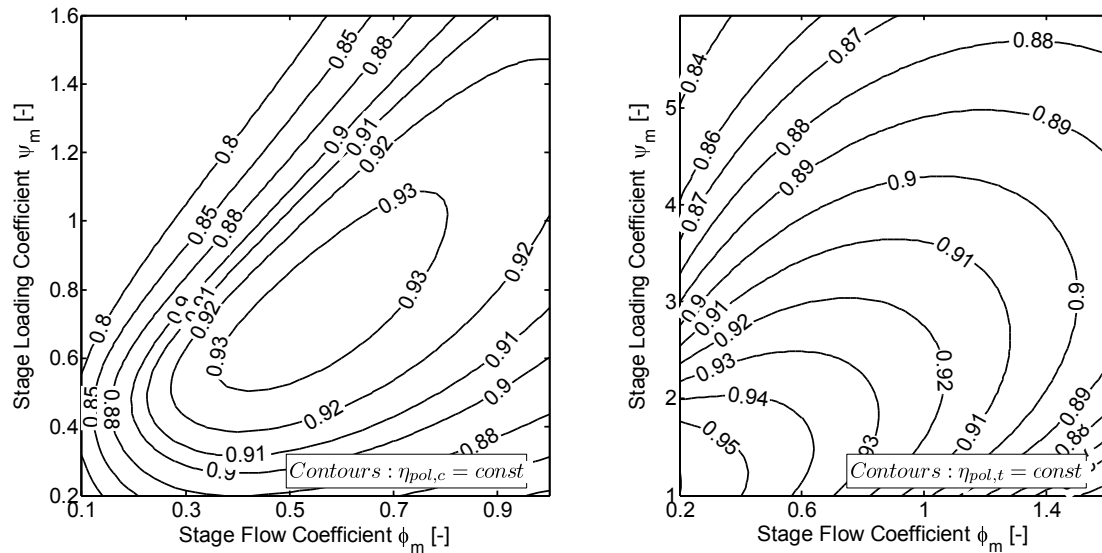


Figure 5.5.: Exemplary aerodynamic design charts for compressors (left) and turbines (right) as calculated based on the presented methodology

Comparative studies of similar aircraft designs involving different thrust requirements and inherently varying engine component sizes requires the capability for mapping size implications on component efficiencies. Important physical effects leading to efficiency penalties for turbo machinery below a certain geometric size are summarised in Reference [69, p.155] as

- the quality of blade profile due to manufacturing allowances relative to blade size,
- the aspect ratio in case of turbine blades,
- tip clearance effects, and
- smoothness of hub and shroud contours and surfaces.

In the developed model, the implications of Reynolds number and relative blade tip clearance on component polytropic efficiency are included. For tip clearance related effects, component specific loss factors  $\zeta_t$  and  $\zeta_c$  are adapted to match the efficiency trade factors given in Reference [225, p.176f, p.209]. For the Reynolds number correction of component efficiencies, application of the approach presented in Reference [69, Eq. 5.2.1.8] is considered. Further effects that may be covered through loss factor adaption include influences of casing treatment on tip loss characteristics as indicated in Reference [97, Figure 1] as well as turbine efficiency losses due to inlet temperature distortion, see Reference [97, Figure 20].

#### 5.2.3.4. Turbine Cooling Air

As discussed in Section 5.2.1, optimum gas temperature levels in aero engine turbines are a trade-off between multiple aspects involving thermodynamic cycle concept, compressor pressure levels, weight, cost and life cycle requirements. However, resulting turbine gas inlet temperatures in most cases are significantly above maximum allowable material temperatures, which necessitates elaborate cooling mechanisms for gas-exposed turbine parts. Existing flight gas turbine engines use compressor bleed air for turbine cooling. The application

of compressor bleed air is essential for turbine material life, however, involves significant detrimental effects on the thermodynamic cycle:

1. The introduction of secondary air mass flows at lower total enthalpy levels affects the turbine's aerodynamic efficiency in the flow path.
2. Since cooling air is bypassed around the combustion chamber it is not fully available as a working fluid for the thermodynamic cycle, therefore reducing thermal efficiency (cf. also Figure A.2 in Appendix A).
3. Cooling air mass flow strongly influences engine size and weight for given thrust requirements, which again interferes with aircraft design.

Now, turbine cooling air mass flow depends upon a multitude of effects including required turbine life, technology level (both materials and cooling), temperature distortion at combustor outlet (see Reference [69, p.292f]), cooling air temperature, corrosive environment<sup>5</sup>, turbine reaction ratio<sup>6</sup>, centrifugal stress due to rotational speed causing creep (blades only) as well as the blade configuration (shrouded versus unshrouded) (cf. Reference [225]).

Cooling air for the first stage of high pressure turbines is typically extracted at the HPC exit. Cooling air required for downstream turbine stages may be extracted from HPC inter-stage bleed ports. Basic equations for cooling air mass flow determination on a conceptual design level can be found in the literature (cf. References [59] and [139]). A more detailed mapping of the turbine cooling air system is given in Grieb [69, p.255ff].

In the present context, a correlation taken from Reference [59] is employed for the determination of the relative cooling air mass flows of each grid of cooled turbines (cf. Equation 5.17). The correlation is essentially based on the efficiency definition for heat exchangers expressed by the term cooling effectiveness  $\eta_{cool}$  which is defined as

$$\eta_{cool} = \frac{T_{HG} - T_M}{T_{HG} - T_{CA}} \quad (5.16)$$

where  $T_{HG}$ ,  $T_{CA}$  and  $T_M$  refer to the representative temperature of working fluid at considered turbine blade row ( $T_{HG}$ ), the temperature of cooling air ( $T_{CA}$ ) and allowable bulk temperature in the turbine material ( $T_M$ ). For  $T_{HG}$  the respective grid total inlet temperatures at maximum take-off conditions are taken representative for both, nozzles and rotors. For more detailed design studies, a number of temperature increments have to be considered for cooling mass flow determination in order to account for effects due to production scatter (minimum engine relative to average new engine), development risk (confidence on component performance), engine growth potential (product family design), the operational environment (atmospheric temperature, humidity, particle pollution etc.), as well as deterioration and component lifing [187].  $T_{CA}$  is a function of the required cooling air pressure, depending on the local pressures at the thermodynamic station to be cooled, possible cooling air cooling mechanisms, cooling air ducting losses, turbine pumping potentials, as well as compressor efficiency. In more complex cycle architectures additional pressure losses or heat transfer effects, e.g intercooling and recuperation, may have to be taken into account.

Using  $\eta_{cool}$  the required cooling air mass flow  $\dot{m}_{cool}$  relative to HPC inlet mass flow  $\dot{m}_{25}$  can be derived from the correlation:

<sup>5</sup>depending of the fuel type and the potential presence of salt in the atmosphere

<sup>6</sup>Low reaction reduces blade metal temperature for a given stator outlet temperature(SOT).

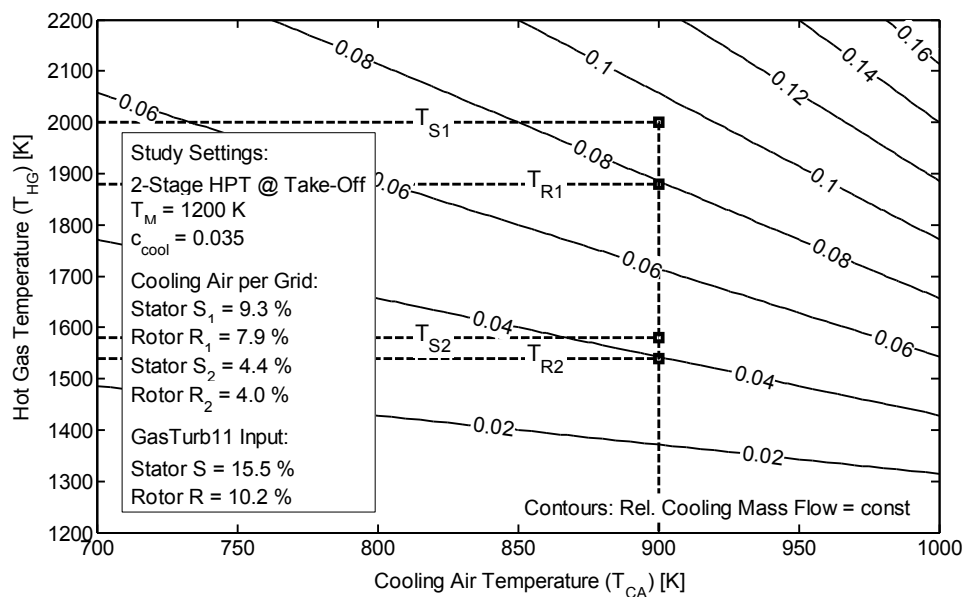


Figure 5.6.: Turbine cooling air determination (Example case: 2-stage cooled high pressure turbine featuring  $T_4 = 2000K$ ,  $T_3 = 900K$  at max. take-off conditions)

$$\frac{\dot{m}_{cool}}{\dot{m}_{25}} = c_{cool} \cdot \left( \frac{\eta_{cool}}{1 - \eta_{cool}} \right) \quad (5.17)$$

Here,  $c_{cool}$  represents a technology-dependent, empirical factor. In the literature (cf. References [139] and [59]) different values for  $c_{cool}$  can be found. In Reference [59]  $c_{cool}$  factors for typical turbine blade cooling concepts involving convection-, film- and transpiration-based configurations are given. A more recent technological status representation for turbine cooling efficiency is given in Reference [69, p.265]. Auxiliary cooling air demands such as for shroud, platform and rim cooling, are included in  $c_{cool}$  by (cf. Reference [59]).

The software GasTurb uses an equivalent single-stage model for the mapping of turbines [102]. However, in case of large pressure ratios of the HP system, two-stage HPTs are commonly employed in aero engines (cf. IAE-V2500 [81], GP7000 [142], GENx [141]). Now, the thermodynamic matching of single- and multi-stage cooled turbines may differ significantly. Hence, for a unified treatment in GasTurb a consistent model conversion from multi-stage cooled turbines to the equivalent single-stage model used in GasTurb is required. For model conversion and the corresponding impact on cooling air bookkeeping the methodology presented in Reference [98] is used. For the conversion from multi-stage cooled turbines to the equivalent single-stage, in particular, turbine expansion ratios, the sum of cooling mass flows, and the balance of cooling air work potentials have to be kept consistent. Typical work potential assignments for single- and multi-stage turbines are given in Table B.2 in Appendix B. Here, cooling air of upstream grids is assigned with full work potential (i.e. the same work potential as the primary air flow of the working fluid) in downstream rotors.

Now, Figure 5.6 illustrates a typical example of a 2-stage cooled HPT. In the figure, the relative cooling air mass flows  $\dot{m}_{cool}/\dot{m}_{25}$  determined for each grid of the 4 grids is denoted, as well as the equivalent single-stage input used for GasTurb simulations. Indication for allowable

material temperatures  $T_M$  can be obtained from existing uncooled LPT (cf. Reference [12]). The cooling factors  $c_{cool}$  of rotor and stator grid may differ. For the shown example these differences are disregarded, in the first instance. The selected value for  $c_{cool}$  is based on Reference [139] which has been reduced by one third to account for advancements of cooling technology. Furthermore, an equal distribution of specific works is assumed across the involved HPT stages.

Cooling air reduces the attainable turbine efficiency levels and may not be neglected. In the literature diverse trade factors for cooling air impact on turbine efficiency can be found. Individual efficiency debits for suction surface film cooling, shroud cooling by upstream injection, trailing edge cooling as well as leading edge or pressure surface cooling for NGVs and blades are given by Walsh and Fletcher [225]. Efficiency trade factors for different overall airfoil cooling concepts can be found in Reference [59]. A more integrated correlation for cooling air impact on turbine efficiency is illustrated by Grieb [69, Figure 5.2.3.18] which is well-suited for comparative studies of technologically similar turbine designs, and thus superimposed on the turbine polytropic efficiencies previously determined in this section.

#### 5.2.4. Ducts and Associated Losses

Ensuring the proper air supply of the engine, interconnecting the working turbo components and containing engine's exit flow, ducts represent essential elements in the flow path of air-breathing propulsion systems. Typically primary flow path ducting includes the air intake, compressor and bypass ducts, turbine interduct(s), as well as the propelling nozzle(s). Beside the guiding of the air flow, ducts provide structural support and allow for vital services such as cooling air and oil supply through integrated struts. Turbine interducts may include nozzle guide vane functionality.

##### 5.2.4.1. Mapping of Pressure Losses

Pressure losses in engine ducts may have significant impact on overall efficiency as can be seen from the sensitivity analysis shown in Figure A.2 in Appendix A. Based on the assumption of adiabatic walls, commonly used for air ducts, losses are a function of duct geometry, inlet swirl angle and inlet Mach number respectively dynamic head (ram pressure). The first two of these influences are typically accounted for by a loss coefficient. Accordingly, relative duct pressure losses  $(p_{in} - p_{ex})/p_{in}$  can be expressed as a function of inlet Mach number  $M_{in}$

$$\frac{p_{in} - p_{ex}}{p_{in}} = \lambda_d \cdot \left( 1 - \left( 1 + \frac{\gamma - 1}{2} M_{in}^2 \right)^{\frac{\gamma}{1-\gamma}} \right) \quad (5.18)$$

The duct loss coefficient  $\lambda_d$  includes wall friction as well as turbulence effects, while  $\gamma$  refers to the representative isentropic exponent. Apart from turbine exit ducts most ducts have a constant inlet swirl angle of zero degrees [225, p.221]. Therefore,  $\lambda_d$  may be considered mainly a function of duct geometry, i. e. duct contour shaping, duct wetted wall area and representative Reynolds number. Additional impact is superimposed by the presence of struts, splitting or mixing structural elements.

Representative loss coefficients for different duct types are given in References [225] and [69]. Pressure losses are finally determined through appropriate choice of axial flow Mach numbers. Characteristic Mach number values are indicated in the literature (see References [225] and [186]) A more decided treatment of losses is required for bypass ducts and air intakes. Corresponding calculation basis and empirical data are given for bypass ducts in Reference [69, section 5.5.3] showing decreasing losses against increasing bypass ratio.

### 5.2.4.2. Air Intake

For engine air intakes, duct exit conditions are taken representative for loss calculation according to Equation 5.18. This is due to occurring very low duct entry Mach numbers at sea level static conditions [225, p.222]. An alternative method for air intake pressure ratio calculation frequently found in the literature is based on the ram respectively inlet recovery factor (cf. References [225] and [69]). For propeller engines, the pressure rise near the hub caused by the propeller approximately equals losses due to the typically required intake swan neck intakes (cf. Reference [176, Table 4.4-I]).

Distortion of the air in-flow field is immanent for aero engines in operation. Inhomogeneity of temperature and pressure in the intake flow field may have a significant impact on intake efficiency as well as fan respectively LPC performance. The consideration of in-flow distortion in case of pod-mounted engines is primarily relevant for off-design operation at high angle of attack. Unconventional propulsion system installation involving stronger aerodynamic interaction between engine and airframe such as boundary layer ingesting intake concepts require careful evaluation of the acting aerodynamic, structural and coupling effects at design and off-design operating conditions. The software GasTurb 11 allows for inlet distortion simulation based on the parallel compressor theory. Specific air intake characteristics may be evaluated using tabulated data in the form of intake maps [100]. For the studies presented in this thesis, however, inlet flow distortion effects are considered second order and are not explicitly evaluated. Diffusion effects upstream of the turbofan engines air intake at high flight velocities are accounted for using an adequate stream tube factor during net thrust calculation.

### 5.2.4.3. Nozzle Calculation

In principle, propelling nozzles may be regarded as internal ducts. However, due to their broad aero-thermodynamic range of operation nozzles require decided consideration. As can be seen from *SFC* sensitivity analyses (cf. Figure A.2 in Appendix A), nozzle effectiveness has a major impact on engine fuel efficiency.

The implemented model for the calculation of nozzle characteristics is based on the evaluation of nozzle gross thrust coefficients  $c_F$  and discharge coefficients  $c_D$  as used in GasTurb 11. Nozzle gross thrust coefficient  $c_F$  relates the obtained effective jet velocity at the nozzle exit to the ideal jet velocity yielding from isentropic nozzle expansion (for derivation of coefficient see Reference [69, p.17]). Nozzle efficiency  $\eta_{noz}$  is therefore directly correlated to nozzle gross thrust coefficient in the form of  $\eta_{noz} = c_F^2$ . Blockage effects due to aerodynamic separation at nozzle walls yields a reduction of nozzle exit area that is available for the nozzle mainstream

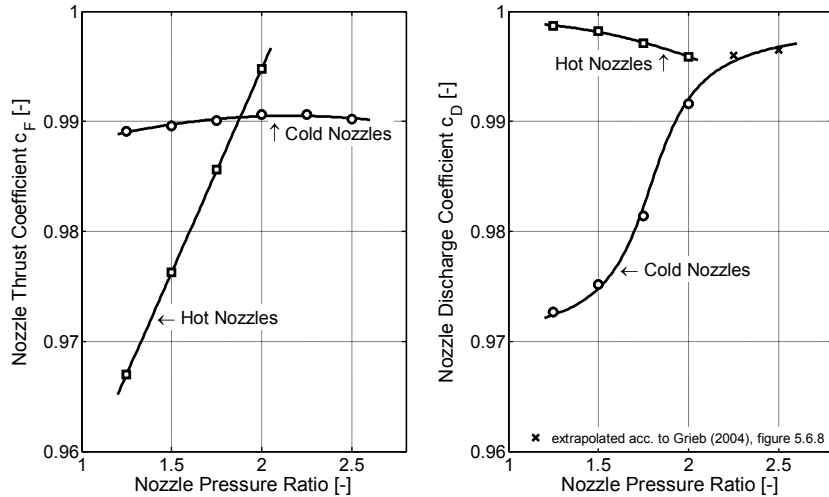


Figure 5.7.: Fitted characteristics of important nozzle coefficients against nozzle pressure ratio according to Grieb [69, Figure 5.6.7]

flow. The ratio of effective and geometric nozzle exit area is described by the nozzle discharge coefficient  $c_{Dis}$ .

In Figure 5.7, the nozzle gross thrust coefficients  $c_F$  and discharge coefficients  $c_D$  of hot respectively cold nozzles are given as functions of nozzle pressure ratio ( $p_{ex,noz}/p_0$ ). The herein depicted characteristics refer to separate flow civil turbofan and ducted propfan engines featuring external core nozzle plug. While “cold nozzles” represent bypass nozzles, the term “hot nozzles” applies to core engine exhaust nozzles.<sup>7</sup> For the mapping of the exhaust nozzles of turboprop engines, “hot nozzle” characteristics are assumed. The shown fitting nodes refer to measured and interpolated values taken from the information given in Reference [69, Figure 5.6.7]. For nozzle pressure ratios greater than  $p_{ex,noz}/p_0 \approx 2$  effects due to choked respectively super-critical nozzle conditions such as the additional pressure term for thrust calculation are considered herein. Fitting nodes for cold nozzle discharge coefficient at super-critical conditions are derived from information given in Reference [69, Figure 5.6.8]. It should be noted, that bypass nozzle pressure ratios, which are dominated by fan pressure ratio and the effect ram pressure recovery, typically are operated supercritical at cruise conditions.

### 5.2.5. Propeller Aerodynamics and Design

The efficiency mapping of ducted turbo components is based on the aerodynamic loadings resulting from the flow conditions described by the representative velocities of the mass flow and rotor blades. For the targeted open rotor engine concept the propulsive device is formed by a pair of counter rotating propellers. The counter rotating propeller arrangement allows for a significant reduction of swirl losses, therefore yielding 5 to 10% increased efficiency levels [137] relative to single rotating configurations. For single rotating airscrews, swirl losses may be reduced by the application of stationary contra vanes (cf. Reference [26]), also referred to

<sup>7</sup>The hot nozzle characteristics shown in Figure 5.7 may also be used for mixed flow turbofan engines [69, p.375].

as Swirl Recovery Vanes (SRV). These, however, do not yield efficiency the levels of counter rotating propellers.

In order to parametrically map the efficiency of the counter rotating propellers at an accuracy level similar to the methodology presented for ducted turbo components, an aerodynamic model based on the ideal induced characteristics of heavily loaded propellers is introduced. Essential aspects hereof are discussed in the following.

### 5.2.5.1. Theoretical Basis

The theoretical basis for the design and analysis of counter rotating propellers essentially refers to the work of L. Prandtl, C.N.H. Lock, A. Betz, S. Goldstein, H. Glauert, and T. Theodorsen. For the identification of ideal propeller efficiencies, i.e. minimum induced losses, the ideal circulation functions according to Goldstein [66] and Theodorsen [217] are available. Both approaches are based on classical momentum theory, i.e. the induced fluid velocities in the far wake are twice the induced fluid velocities in the propeller plane. For the mapping of heavily loaded airscrews, Theodorsen's circulation function is of primary importance which differs from Goldstein's approach by defining the circulation distribution in the ultimate wake. The ideal circulation distribution  $\Gamma$  along the relative radial blade coordinate  $x_B$  yields from Theodorsen's circulation function  $K(x_B)$  as follows (cf. Reference [217, Vol.I, p.36])

$$\Gamma(x_B) = \frac{2\pi \cdot (V_0 + w_a) \cdot w_a}{B \cdot \omega} K(x_B) \quad (5.19)$$

where  $V_0$  is the free stream velocity and  $w_a$  represent the axial displacement velocity in the ultimate wake, induced by the propeller.  $B$  and  $\omega$  refer to the number of propeller blades and the propeller's angular velocity, respectively. The relative radial blade coordinate  $x_B$  is defined by the ratio of local radius  $r$  and the radius of the blade tip  $R$  ( $x_B = r/R$ ,  $\forall r : r_h \leq r \leq R$ , where  $r_h$  is the propeller hub radius).

According to Betz' criterion [25] for minimum induced propeller power loss, the optimum blade loading distribution occurs when the rearward wake displacement velocity  $w_a$  is radially constant.<sup>8</sup>

The ideal circulation function according to Theodorsen as well as Betz' criterion for minimum induced losses are applicable to both, single and counter rotating airscrews (cf. References [39] and [44]). The interaction of induced effects of a close pair of counter rotating airscrews is described by Lock [123]. Davidson [44] presents a methodological approach to translate tip loss factor introduced by Lock to Theodorsen's ideal circulation distribution, using Betz's criterion for blade shape optimisation.

---

<sup>8</sup>in analogy to Prandtl's wing theory yielding minimum induced drag for constant down wash velocity along wing span [167]

### 5.2.5.2. Implemented Propeller Design Code

The model implemented for the sizing and efficiency prediction of counter rotating propellers is based on Davidson's methodology presented in Reference [44]. The method is essentially based on the initial estimation of the axial displacement velocity in the ultimate wake  $w_a$ , and the subsequent calculation of the overall power absorbed ( $P_{prop}$ ) and thrust produced ( $FN_{prop}$ ) by the pair of propellers. The ratio of  $FN_{prop}$  and  $P_{prop}$  is significant for the resultant propeller efficiency  $\eta_{prop}$  which may be also expressed in terms the corresponding dimensionless coefficients

$$\eta_{prop} = \frac{V_0 \cdot FN_{prop}}{P_{prop}} = \frac{J \cdot c_T}{c_P} \quad (5.20)$$

where  $J$  refers to the geometric advance ratio of the propeller blade tips, and  $c_P$  and  $c_T$  represent the propeller power and thrust coefficients.<sup>9</sup>

Taking Equation 5.19, it can be seen that  $w_a$  has a significant impact on the ideal circulation distribution  $\Gamma(x_B)$  which is directly correlated to the propeller element load characteristics  $\sigma(x_B)$ , i.e. the product of propeller solidities  $s(x_B)$ <sup>10</sup> and profile lift coefficients  $c_l(x_B)$  (cf. Reference [44, Equation 14]). Radial flow effects are incorporated by the tip loss factor derived for counter rotating propeller pairs in Reference [44]. The element load coefficient  $\sigma(x_B)$  is a central input to the calculation of propeller power absorption and thrust production. The initial  $w_a$  estimate may be iteratively adapted to match a predefined value of the dimensionless power coefficient  $c_P$ . For actual thrust sizing, the diameter of the propeller  $D_{prop}$  is iterated simultaneously.

The code implemented during the present work uses spanwise discretisation of the propeller blades, i.e. all radially dependent parameters are evaluated predefined at spanwise locations  $x_B$ . Based hereon, the power absorbed and thrust produced by the propeller pair are calculated by numerical integration of the corresponding radial derivatives expressed in Reference [44, Appendix E, p.38]. Beside the evaluation of the pure induced effects, Davidson's methodology allows for the incorporation of blade drag characteristics. Therefore, the spanwise lift-to drag distribution  $c_l/c_d(x_B)$  is included in the evaluation of power absorption and thrust production (cf. Reference [44, Equation 12]). The application of airfoil characteristics is discussed below.

In order to account for the transonic helical Mach numbers  $M_{hel}(x_B)$  occurring for the targeted high-speed propellers, the mapping of blade sweep effects is necessary for an adequate prediction of propeller efficiency. The radial distribution of helical Mach numbers is defined as  $M_{hel}(x_B) = \sqrt{M_0^2 + M_{cir}(x_B)^2}$ , where  $M_{cir}(x_b)$  represents radial distribution of blade circumferential Mach numbers, and  $M_0$  is the free stream Mach number. Blade sweep reduces the effective Mach number perpendicular to the blade's aerodynamic center line. Davidson's strip line method was extended using the theory of the infinite sheared wing, i.e. a simple cosine correction was applied to the helical Mach numbers  $M_{hel,corr}(x_B) = \cos(\Lambda(x_B)) \cdot M_{hel}(x_B)$ . Now, the criterion applied to the optimisation of the radial circulation distribution refers to the ideal induced characteristics in the ultimate wake, i.e. the ideal circulation distribution

<sup>9</sup>For the mathematical derivation of  $c_P$  and  $c_T$  see Reference [224, p.4f].

<sup>10</sup> $s(x_B) = B \cdot c(x_B)$ , where  $c(x_B)$  represents the radial distribution of blade chord lengths

$\Gamma(x_B)$  is independent from variations of blade sweep  $\Lambda(x_B)$ . Thus, in order to map the effect of blade sweep on the propellers capability to absorb power and produce thrust, cosine correction was also applied to the element load coefficients  $\sigma_{corr}(x_B) = \cos(\Lambda(x_B)) \cdot \sigma(x_B)$ .

### 5.2.5.3. Results and Discussion

For the studies presented in this thesis, the presented model for ideal propeller design was applied to a 6 + 6 bladed counter rotating propeller configuration. The corresponding characteristics of Theodorsen's circulation function are FNN-approximated based on the data read from Reference [39, Figure 4]. Based hereon, ideal induced efficiencies were calculated for a wide range of propeller power loadings  $P_{prop}/D_{prop}$ . The calculated results were compared to the corresponding data given in Reference [132, Figure 2], showing very good agreement of computed values. In Figure A.3 in Appendix A, the obtained validation results are displayed.

In order to include airfoil drag characteristics in the propeller efficiency prediction, a full set of 2-D NACA 16-series airfoil data was read from Reference [75, Vol. III, Figures 85ff] allowing for corrected helical Mach numbers of up to 1.5, lift coefficients  $c_l$  up to 0.8 for a range of relative thicknesses between 2.0% and 18%. The airfoil data include the full 2-D drag rise characteristics. The gained data were interpolated and subsequently approximated by a FNN-based regression model for convenient integration into the propeller design model.

Basic blade shape characteristics of the F7/A7 rotors of GE's UDF are taken from References [4] and [57]. Here, the spanwise distribution of relative profile thickness  $t/c(x_B)$  refers to Reference [4, Figure 5.7]. The lift coefficient distribution  $c_l(x_B)$  is taken from Reference [57, Figure 20]. The blade sweep distributions  $\Lambda(x_B)$  are given in Reference [57, Figure 23]. The implemented design model does not account for individual characteristics of each blade row of the counter rotating pair of airscrews. Therefore, the averaged properties of the F7/A7 forward and aft blade rows are used for both propeller rotors. Assuming given  $t/c(x_B)$ , the blade sweep distribution  $\Lambda(x_B)$  is a trade-off between transonic drag rise mitigation, the reduction of the capability of thrust production (see above) and structural weight implications. In order to allow for the adaptation of blade sweep during propeller design, a parametric model for the interpolation of the sweep distribution between propeller hub and tip radii is introduced

$$\Lambda(x_{sw}) = (\Lambda_t - \Lambda_h) \cdot \frac{\ln(c_{sw} - (c_{sw} - 1) \cdot x_{sw})}{\ln(c_{sw})} \quad \forall x_{sw} : 0 \leq x_{sw} \leq 1 \quad (5.21)$$

where  $x_{sw}$  is the relative spanwise blade coordinate defined between hub and tip of the propeller rotor.  $\Lambda_t$  and  $\Lambda_h$  represent the sweep angles at the propeller hub and tip radii. Setting the sweep interpolation coefficient  $c_{sw} = 0.02$  yields good qualitative agreement between the logarithmic interpolation approach and the sweep distributions of the F7/A7 rotors.

Based on the described blade and air airfoil properties, the propeller design model was validated against the F7/A7 propeller configuration. The corresponding validation data refer to Reference [4, Tables 5-1 and 5-2]. The efficiency of the F7/A7 propeller configuration is overestimated by +1.9% which may refer to the neglect of hub choking effects (cf.

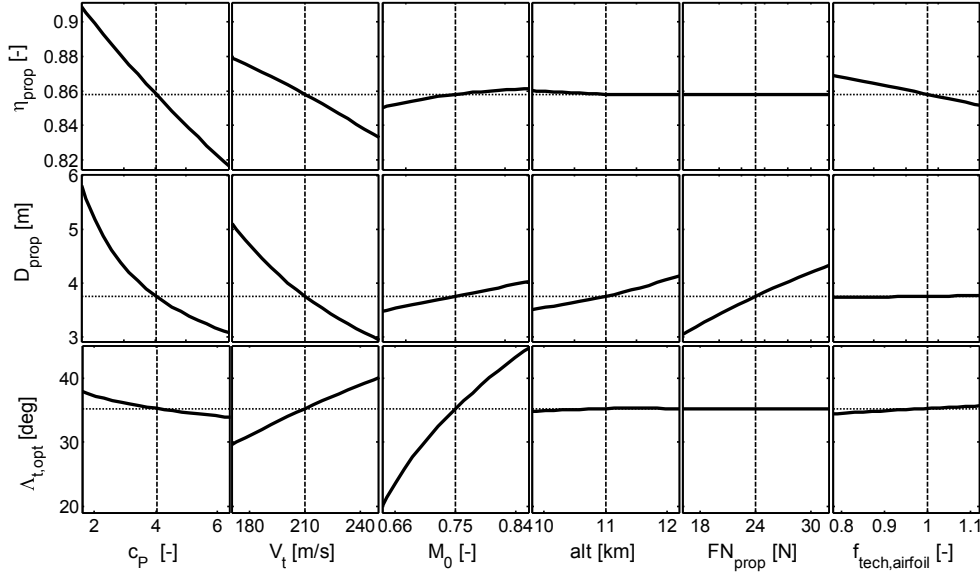


Figure 5.8.: Matrix of partial dependencies view for counter rotating propeller design model (Example: 6 + 6 bladed rotors, F7 / A7 blade shaping, NACA-16 series airfoil characteristics, propeller hub/tip ratio 0.3, blade sweep optimised for maximum propeller efficiency)

Reference [57]) and the insufficient mapping of losses caused by 3-dimensional flow in the blade passage. However, the efficiencies calculated from the presented propeller design model feature an adequate accuracy for the targeted aircraft conceptual design studies. A summary of the validation results is presented in Table B.3 in Appendix B.

Typical propeller design characteristics produced by the presented model are visualised in Figure 5.8 using the MPD view (cf. Section 3.3.3). The figure shows the trends of propeller efficiency  $\eta_{prop}$ , propeller diameter  $D_{prop}$  and optimum blade tip sweep angle  $\Lambda_{t,opt}$  as partial functions of essential propeller design parameters including the power coefficient  $c_P$ , the blade tip speed  $V_t$ , the free stream Mach number  $M_0$ , the design altitude  $alt$ , propeller design thrust  $FN_{prop}$  and the airfoil technology factor  $f_{tech,airfoil}$ . The latter is defined as a scaling factor for the profile drag coefficients gained from the NACA 16-series data. The propeller blades are discretised by 100 spanwise strips. Blade tip sweep is optimised for maximum propeller efficiency using the correlation given in Equation 5.21. Here, hub sweep is kept constant ( $\Lambda_h = -20^\circ$ ).

The majority of partial dependencies gained from the model exhibit intuitively obvious trends, such as the increasing  $\eta_{prop}$  and  $D_{prop}$  against decreasing  $c_P$  and  $V_t$ . Similarly, the expected increase of  $\Lambda_{t,opt}$  against increasing  $V_t$  and  $M_0$  can be seen. Further essential findings are listed in the following:

- Propeller design thrust  $FN_{prop}$  only affects  $D_{prop}$ , but has no impact on  $\eta_{prop}$ .
- The effect of  $FN_{prop}$  on  $D_{prop}$  is clearly exceeded by power loading implications, i.e.  $c_P$  and  $V_t$ .
- The impact of the power loading conditions implications  $c_P$  and  $V_t$  on  $\eta_{prop}$  and  $D_{prop}$  demonstrate the design trade-off between propeller efficiency and weight for aircraft

## 5. Conceptual Design Methods for Aircraft and Propulsion System

design studies.

- The adaptation of blade sweep is dominated by the nonlinear airfoil drag rise. Therefore, the airfoil technology factor  $f_{tech,airfoil}$ , which linearly scales the airfoil drag, does not significantly impose on the optimum tip sweep  $\Lambda_{t,opt}$ .
- Enabled by the adaptation of blade sweep,  $\eta_{prop}$  increases slightly against increasing  $M_0$ . This effect is caused by the reduction of the relative axial displacement velocity against increasing Mach number. The connected reduction of  $FN_{prop}$  is compensated by the simultaneous increase of  $D_{prop}$ .

For the studies presented in Chapter 6, the propeller design model was connected to the open rotor engine model defined in GasTurb. Therefore, both models were approximated by FNN and subsequently integrated in aircraft synthesis procedure.

### 5.2.6. Engine Operational Behaviour

In the present work, operational performance characteristics, are simulated using the “off-design” mode of the software GasTurb. The simulated operational characteristics are treated as constraints during engine design analysis and optimisation. The constraint parameters considered involve

- the maximum  $AN^2$  values for the critical stages of the turbo components, i.e. the first stages of compressors and the last stages of turbines,
- the allowable temperature levels at HPC exit and turbine inlets,
- maximum and minimum corrected rotational speeds in component maps, and
- the compressor surge margins.

The simulated characteristics focus on steady state performance, in the first instance. In the following, essential aspects of the implemented mapping of engine operational behaviour are presented. In particular, the application of component maps, the implemented laws for bleed scheduling and the definition of maximum and minimum allowable power settings are emphasised.

#### 5.2.6.1. Component Map Application

For the mapping of turbo component operational characteristics, GasTurb standard component maps [105] are employed. The component maps are automatically scaled by GasTurb (cf. Reference [100, Sections 3.1.2 and 3.1.3]). The Cycle reference point positioning within component maps refers to GasTurb default settings [100] (cf. also Reference [106]). Component map Reynolds corrections are disregarded, in the first instance.

For a precise mapping of the operational behaviour of variable pitch propellers multiple maps are required. In propeller maps, typically, propeller efficiency is given as function of propeller advance ratio  $J$  and power coefficient  $c_P$  at a given operating Mach number  $M_0$ . Thus, an accurate coverage of the flight envelope implies the interpolation of propeller efficiency from a set of maps referring to different operational Mach numbers  $M_0$ .<sup>11</sup> However, for the focus of the present work, use of generic propeller map characteristics is considered feasible. Therefore,

---

<sup>11</sup>Extensive experimental data sets for counter rotating propeller configurations investigated for GE’s UDF are given in Reference [57, Section 7.2.1].

propeller map data taken from Reference [224, Figure 10ff] and provided by GasTurb 11 are used. Since, here, variable pitch behaviour is not included, particular consideration of propeller operability at low advance ratios is necessary. Therefore, the propeller map is scaled for each propeller design as a trade-off between low-speed and high-speed operational efficiency.

### 5.2.6.2. Compressor Handling Bleed Mapping

In order to ensure proper operability throughout the projected operational envelope, aero engines are typically equipped with variable geometry features. Here, compressor designs often include Variable Guide Vanes (VGV) and valves for handling bleed extraction, to ensure sufficient surge margins. For ultra-high  $BPR$  ducted propulsor engines variable nozzle geometry respectively variable pitch fan blades may be necessary to meet the full operability goals.

In the present context, the mapping of VGV, variable blade pitch and nozzle geometries is disregarded, in the first instance. Effects due to strong nozzle throttling during take-off are modelled using of correlations for nozzle gross thrust and discharge coefficients given in Figure 5.7. For the operability assurance of compressors, a parameterised model for the scheduling of handling bleed extraction is used. Compressor handling bleed is of particular importance to the operability of boosters whose operating line is essentially determined by the downstream compressor, i.e. the HPC [99], while being mechanically connected to the propulsor. For decreasing engine power settings, the HPC inlet mass flow decreases and boosters are throttled. When mounted to a constant speed spool (cf. variable pitch propellers), booster operating lines quickly approach the surge line, unless bleed air is discharged behind the booster.

In GasTurb, the schedules for compressor handling bleed are typically expressed as a function of relative corrected spool speed  $n_{corr} = n_{rel}/\sqrt{T}$ , where  $n_{rel}$  refers to the component-specific mechanical spool speed) [100]. However, this approach is inconvenient for constant speed boosters. For the present work, a unified approach to mapping the handling bleed schedules for all compressor types is used. The approach is based on the beta values  $\beta_i$  which are auxiliary coordinates used by GasTurb in order to avoid ambiguities during numerical map evaluation [100, Section 4.19.2.3]. Albeit the  $\beta$ -values do not have a direct physical meaning, they well-describe the operational envelope defined by the component map. Therefore, an investigated engine operating point can be uniquely identified in the component maps based on  $n_{corr,i}$  and the corresponding  $\beta$ -values. In the present context, the  $\beta$ -values are considered as first indications for compressor surge margin. A synopsis of different definitions of compressor surge margin used in the aero engine industry is given in Reference [100, 4.19.2.4]. Now, the required handling bleed air mass flow  $\dot{m}_{bl}/\dot{m}_c$  is iterated to match the following bleed correlation

$$\frac{\dot{m}_{bl}}{\dot{m}_c} = c_{zbl} \cdot \frac{\beta_i}{\beta_{crit}} + \begin{cases} c_{bl} \cdot (\beta_i - \beta_{crit})^{c_{beta}} & , \beta_i > \beta_{crit} \\ 0 & , \beta_i \leq \beta_{crit}. \end{cases} \quad (5.22)$$

where  $\beta_i$  refers to the beta value of the actual operating point in the considered compressor map. The critical beta value  $\beta_{crit}$  defines the maximum beta value below which bleed air valve

are closed. The bleed coefficient  $c_{bl}$  and exponent  $c_{beta}$  of the beta-term have to be tailored problem-specifically in order to ensure adequate surge margin throughout the operational envelope. The linear term in Equation 5.22 has no physical meaning, but is essential to prevent numerical problems during iteration. The coefficient  $c_{ZBl}$ , therefore, should have a very small value, such as  $10^{-6}$ , in order to reduce its physical impact.

### 5.2.6.3. Engine Operational Envelope

The operational envelope investigated during the studies presented in Chapter 6 includes three basic parameters describing the operational conditions of the engine: flight altitude  $alt$ , flight Mach number  $M_0$  and power setting. The envelope of operational altitudes and Mach numbers, considered during engine design evaluation corresponds to the aircraft operational envelope definition (see Section 5.6). Hence, in the following, the boundaries considered for the definition of maximum and minimum engine power settings are discussed.

In GasTurb, the Power Lever Angle (PLA) is directly connected to the relative mechanical spool speed  $n_{rel}$  of the first compressor, in case of jet engines. For turboshaft engines, PLA is correlated to the standard day corrected shaft power [102, Section 3.10.2.1]. For the present purposes, the maximum power settings are limited by the relative corrected spool speed of the first independent compressor  $n_{corr,c1}$ , i.e. the fan in case of turbofan engines. In case of a 2-spool turboprop engine with a booster mounted to the power turbine spool, the first independent compressor refers to the HPC. Accordingly, PLA 100% is defined by  $n_{corr,c1} = 1$ , which allows for a full utilisation of the component maps. However, the corresponding maximum mechanical spool speeds  $n_{rel}$  have to be monitored in order to retain blade and disc stresses within the allowable boundaries. For the precise definition of engine operational envelope, classic rating schedules may be adopted through adequate limiter settings in GasTurb 11. The concepts of engine de-rating and flat-rating which play an important role in product family design, may be included for system-level optimisation as multi-faceted constraint functions.

Minimum power settings, i.e. idle settings, are defined by the minimum feasible engine power or thrust output produced when the ideal requirement of the application effectively equals zero. Here, the minimum feasible power or thrust setting depends on different engine aspects including combustor stability, levels of temperature, pressure and compressor surge margin. The paramount idle constraint at low altitudes typically refers to the acceleration times to higher power or thrust settings as required e.g. during missed approach operation [225, p.411]. For a classic mix of cabin bleed air and power offtakes, an important constraint for engine idle rating at high altitudes is the minimum compressor pressure ratio for required cabin bleed air pressure [188, p.42]. During idle operation the use of  $SFC$  as a metric for the evaluation of engine fuel consumption is infeasible. Therefore, the minimum feasible fuel flow determined based on the aforementioned evaluation criteria is considered representative for the computation of fuel consumption (cf. Section 5.6).

## 5.3. Aircraft Geometric Description

The geometric description of the aircraft and its component forms the basis for the succeeding disciplinary analyses performed during the proposed aircraft design procedure (cf. Section 3.2),

i.e. the computation of system aerodynamics, weights and performance characteristics. In the present section, central aspects of aircraft geometric synthesis and the implemented design laws for component geometric sizing are introduced. In particular, the geometric parameters relevant for propulsion system integration are discussed and determined.

### 5.3.1. Overview of Component Geometric Synthesis

The system configurations targeted for the methodological demonstration presented in Chapter 6 refer to the aircraft layouts displayed in Figure 5.1. Thus, aircraft geometrical synthesis, here, focuses on classic wing-fuselage layouts. The system components considered during geometric synthesis and subsequent aerodynamic, structural and performance analysis involve all major structural groups of the aircraft: the wing, the fuselage, the horizontal and vertical tail planes, the propulsion system, the engine pylon, and the landing gear. System topological options include propulsion system type and installation location, tail plane arrangement and landing gear configuration. The topological arrangement including the positioning of system components relative to each other is defined as part of the “Configuration” module at the beginning of the overall aircraft design procedure (cf. Figure 3.2). The geometric mapping of the individual components of the aircraft is based on elementary forms. The aspects of component geometric modelling include the parameters used for component shape description, as well as the rules used for determining the parameters adequately to ensure the feasibility of the component’s basic layout. An overview of the modelled component geometric aspects is given in Table 5.2 (overleaf).

In the following, the determination of the basic parameters for components geometric description is elaborated. The discussion includes geometric constraints considered as well as the design laws implemented for aircraft component sizing. A detailed description of the geometric integration of the propulsion system is given in the subsequent section.

#### 5.3.1.1. Fuselage Shape

In classic “tube & wing” aircraft layouts the geometric sizing of the fuselage is essentially based on the volume required for the payload compartment. In the present context, cabin sizing is disregarded in favour of an empirical definition of fuselage dimensions considered adequate for the transport tasks studied in the present work. Fuselage size is based on the definition of the length  $L_{fus}$  and diameter  $D_{fus}$ . The basic geometric shape of the fuselage includes nose ( $x < x_{no}$ ) and aft-sections ( $x > x_{af}$ ) approximated by paraboloids of rotation, and a cylindric center section of diameter  $D_{fus}$ . The length of nose and aft-sections, as well as the longitudinal extent of the payload compartment inside the fuselage is defined relative to  $L_{fus}$ . During the studies presented in Chapter 6, the position of the cabin’s rear pressure bulk  $x_{pb}$  is considered significant for the longitudinal positioning of aft-fuselage mounted open rotor engines, due to cabin safety and passenger comfort reasons. Potential implications of the open rotor installation on the required length of the fuselage aft-section are neglected, in the first instance.

The fuselage is a significant contributor to the aircraft’s skin friction drag, i.e. 60 to 70%. The fuselage’s wetted area  $S_{wet,fus}$  results from the surface areas of the used basic shapes, reduced by the fuselage / wing intersection.

Table 5.2.: Overview of methods for the description of aircraft geometry

Component	Aspect	Method <sup>a</sup>
<b>Fuselage</b>	length	input
	diameter	input
	cabin dimensions	relative to fuselage length
	center-section shape	cylindrical
	nose-section shape	paraboloid
	aft-section shape	paraboloid
	wetted area	custom (see Section 5.3.1.1)
<b>Wing</b>	reference area	input
	planform	trapezoidal
	profiling	generic
	taper ratio	acc. to Torenbeek [221]
	sweep angle	input
	aspect ratio	input
	dihedral	input
	relative thickness at MAC	input
	MAC length	see Figure A.4
	wetted area	acc. to McCormick [130]
	tank volume	obelisk shape approximation
<b>Empennage</b>	shape parameterisation <sup>b</sup>	see “Wing”
	sizing	volume coefficient <sup>c</sup>
<b>Propulsion System</b>	propulsor diameter <sup>d</sup>	GasTurb simulation
	flow path diameters <sup>e</sup>	acc. to GasTurb simulation
	flow path length	custom (see Section 5.3.2.1)
	nacelle thickness	input
	nacelle length	custom (see Section 5.3.2.1)
	nacelle wetted area	acc. to Torenbeek [221]
	positioning	see Figures 5.10 and 5.11
<b>Engine Pylon</b>	shape parameterisation	see Figures 5.10 and 5.11
<b>Landing Gear</b>	height	see Figure 5.9
	positioning	see Figure 5.9

<sup>a</sup> Input parameters may be subject to additional design laws or system-level optimisation (cf. Section 3.3).

<sup>b</sup> Tail plane taper ratio is an input parameter. Vertical fin taper ratio is calculated according to the root chord length of the horizontal stabiliser in case of a t-tail arrangement.

<sup>c</sup> The tail plane volume coefficients may be either inputs or result of sizing constraint evaluation.

<sup>d</sup> The propulsor may refer to ducted or unducted devices.

<sup>e</sup> Including turbo components, ductings and propulsor reduction gearbox, if applicable.

### 5.3.1.2. Wing Planform

The wing is modelled based on a simple trapezoidal shape being parameterised by the reference area  $S_{ref}$ , the aspect ratio  $\Lambda_{wing}$ , the taper ratio  $\tau_{wing}$ , the sweep angle  $\varphi_{wing}$  and the dihedral angle  $\vartheta_{wing}$ . The design rules implemented for wing parametric shaping are discussed in the following.

For high subsonic Mach numbers wing sweep-back is required in order to reduce the severity of the transonic drag rise. However, optimum sweep angle is a trade-off between the reduction of wave drag, the simultaneous increment of induced losses due to the rising 3-dimensional flow effects, and the growing wing structural weight connected to an increasing sweep angle. The design law for the determination of the sweep angle at the aerodynamic center (AC) line  $\varphi_{AC,wing}$  is based on the simple sweep theory, i.e. employing cosine correction of the free stream Mach number

$$\varphi_{AC,wing} = \begin{cases} \cos^{-1} \left( \frac{M_{eff,wing}}{M_{ADP}} \right) & , M_{ADP} \geq M_{eff,wing}, \\ 0 & , M_{ADP} < M_{eff,wing}. \end{cases} \quad (5.23)$$

where  $M_{ADP}$  refers to the aircraft's aerodynamic design point Mach number.  $M_{eff,wing}$  is the component of the free stream velocity vector perpendicular to the AC line. The allowable value of  $M_{eff,wing}$  depends on the airfoil technology applied to the wing. Besides,  $M_{eff,wing}$  is essentially influenced by wing loading and relative airfoil thickness  $t/c_{wing}$ . Typical values of  $M_{eff,wing}$  derived from the geometric analysis of existing swept-wing aircraft range from 0.7 and 0.75.

Wing taper ratio  $\tau_{wing}$  is balanced to approximate elliptical spanwise lift distribution as a function of  $M_{ADP}$ ,  $\Lambda_{wing}$  and  $\varphi_{wing}$  according to Reference [221]. The determination of wing wetted surface area  $S_{wet,wing}$  is based on the exposed planform region  $S_{exp,wing}$ , i.e.  $S_{ref}$  reduced by the fuselage intersection.  $S_{exp,wing}$  is translated to  $S_{wet,wing}$  using an empirical correlation given by McCormick [130, p.152f]. Wing shape definition, furthermore, includes the determination of the following parameters:

- the mean aerodynamic chord (MAC) length  $c_{MAC,wing}$  which is considered representative for the wing's aerodynamic characteristics and horizontal tail sizing,
- the wing and center tank volume  $V_{tank}$  which is treated as constraint parameter during system-level optimisation, and
- the longitudinal position of wing aerodynamic center  $x_{AC,wing}$  which is required for aircraft balancing

The reference area  $S_{ref}$ , the aspect ratio  $\Lambda_{wing}$ , dihedral angle  $\vartheta_{wing}$  and the effective perpendicular Mach number  $M_{eff,wing}$  are treated as input to the wing planform sizing method. These parameters may be subject to system-level optimisation. A schematic of wing planform parameterisation is given in Figure A.4 in Appendix A.

### 5.3.1.3. Empennage

For the targeted methodological demonstration, the considered tail plane configurations include a conventional tail layout featuring a fuselage mounted horizontal stabiliser, and

a T-tail arrangement. The geometric parameterisation of the empennage corresponds to the wing's planform description. Tail plane sweep angles are geared to the wing's sweep angle using relative increments of  $5^\circ$  respectively  $8^\circ$  for the horizontal and vertical stabilizers. Empennage sizing is based on predefined volume coefficients ( $c_{V,ht}$  for the horizontal stabiliser and  $c_{V,vt}$  for the vertical fin), see also Reference [173, Equations 6.28 and 6.29]:

$$S_{ht} = c_{ht} \cdot c_{MAC,wing} \cdot \frac{S_{ref}}{L_{ht}} \quad S_{vt} = c_{vt} \cdot b_{wing} \cdot \frac{S_{ref}}{L_{vt}} \quad (5.24)$$

where  $S_{ht}$  and  $S_{vt}$  represent the trapezoidal planform areas of the horizontal and vertical tails. The corresponding lever arms  $L_{ht}$  and  $L_{vt}$  represent the longitudinal distances between the individual tail planes' aerodynamic centers and the wing's aerodynamic center location (cf. Figure A.4). The values of  $L_{ht}$  and  $L_{vt}$  are initially unknown in the proposed discipline-oriented aircraft sizing procedure, resulting from aircraft balancing (see Section 5.4.4).

The tail volume coefficients  $c_{V,ht}$  and  $c_{V,vt}$  are treated as model inputs. For the studies presented in Chapter 6 empirical values are chosen in order to adequately account for One Engine Inoperative (OEI) cases, directional, longitudinal and trim stability. In case of a T-tail arrangement both tail volumes may be reduced relative to the conventional arrangement due the undisturbed incidence flow of the horizontal stabiliser and the end-plate effect of the vertical fin [173, p.23]. For the studies presented in Chapter 6, T-tail volume coefficients are reduced by 5% relative to the conventionally arranged empennage. For the sizing of the horizontal tail, potentially stabilising effects due to the large pylons of aft-fuselage installed open rotor engines are neglected. General effects on horizontal tail volume connected to the aft-fuselage installation of propeller engines are discussed in Reference [173, p.485].

### 5.3.1.4. Landing Gear

A comprehensive overview of landing gear integration in aircraft conceptual design is given in Reference [33]. In the present context, landing gear geometric description and its integration in the aircraft primarily focuses on the positioning of landing gear legs and the landing gear height (see Figure 5.9). Leg positioning is primarily based on stability considerations during taxi, liftoff and touchdown [33, p.15].

Landing gear height results from the required geometric freedom in the pitch-wise and roll-wise direction during takeoff and landing manoeuvres. The longitudinal positioning of both, nose and main landing gear legs results from aircraft weight balancing. Here, relative load of nose landing gear is treated as a calculation input parameter (see Section 5.4.4). The lateral positioning of main landing gear legs results from the consideration of aircraft roll stability during ground operation, the transmission of landing shock loads into the airframe structure, as well as the aircraft topology. For landing gear height determination, the consideration of the multiple geometric boundary conditions is required. Here, the roll clearances of engine nacelle and wing tip, as well as the pitch clearances of the fuselage contour are considered. In case of under-wing mounted turbofan engines the roll clearances of the installed engine nacelles is accounted for. In case of aft-fuselage open rotor engines, propeller diameters are treated as an additional pitch clearance constraint. The coupling of roll and pitch clearance constraints is neglected, in the first instance. The individual landing gear height constraints are derived from the geometric parameters given in Figure 5.9. The subsequent cumulative

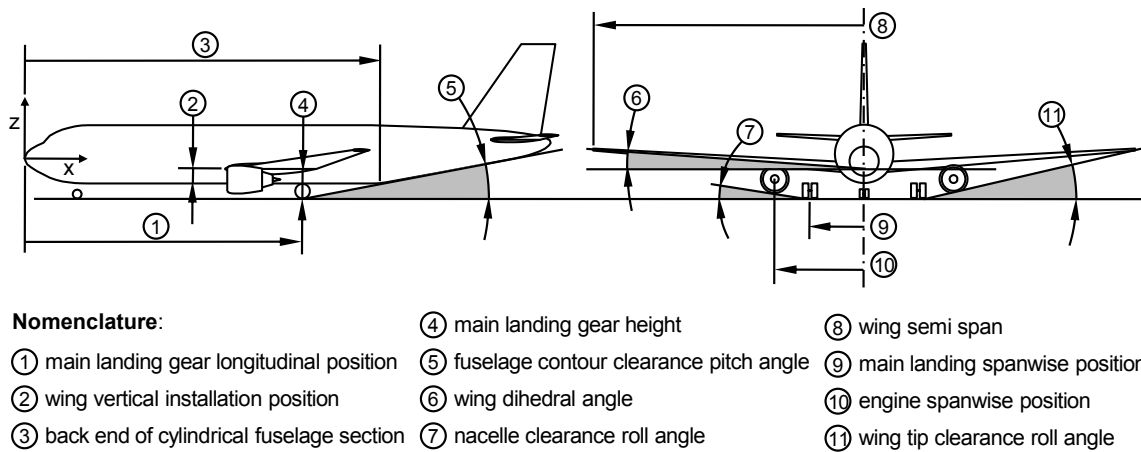


Figure 5.9.: Geometric relations considered in the determination of main landing gear height

evaluation of the calculated constraints based on the Kreisselmeier-Steinhauser function (cf. Reference [228]). For all studies presented in Chapter 6 roll freedoms of  $8^\circ$  and pitch freedoms of  $11^\circ$  were assumed.

### 5.3.2. Propulsion System Geometric Integration

Beside considerations of the available geometric free space, optimum propulsion system installation position results from the evaluation of multidisciplinary aspects including

- the aerodynamic interference between engine and airframe,
- the installation weights due to aircraft component sizing effects, the structural loads introduced by the installed engines, as well as aeroelastic interaction of engine and airframe,
- system safety aspects, e.g. containment against blade-off,
- passenger comfort including cabin noise, vibration and visual disturbance,
- external noise emission characteristics, and
- engine maintainability, i.e. engine accessibility.

For the installation of open rotor propulsion systems, various options have been investigated in the past, including wing-mounted and fuselage-mounted, tractor and pusher arrangements. Comparisons of different potential installation options for open rotor engines are given in References [64] and [65]. For passenger safety and cabin comfort reasons, a longitudinal separation of the unducted rotor planes and the payload compartment is desirable. Therefore, aft-fuselage mounting is considered most appropriate for the aircraft integration of open rotor engines.

For turbofan-type engines classic under-wing mounting is considered, acting as a baseline for the system-level comparative studies. In the following, essential geometric aspects for the aircraft integration of both alternative propulsion system options are discussed.

### 5.3.2.1. Nacelle Dimensions

The geometric description of engine nacelles, here, is essentially based on the determination of nacelle lengths  $L_n$  and diameters  $D_n$ . For the mapping of Short Duct Separate Flow (SDSF) nacelle (fan cowling) shaping, an empirical model describing the ratio of nacelle length and diameter was derived based on the data given in Reference [42, Figure 3.6]. Therefore, it is assumed that the contraction of the nacelle contour towards the exit plane of the bypass nozzle has to be balanced between skin friction, form and wave drag. Here, the fan pressure ratio  $p_{13}/p_2$  is considered significant for mass flow specific bypass nozzle area, and thus, for the contraction of the nacelle contour. The resultant correlation for the nacelle shape parameter  $L_n/D_n$  is based on the design outer fan pressure ratio

$$\frac{L_n}{D_n} = 0.95 \cdot \frac{p_{13}}{p_2} - 0.09 \quad (5.25)$$

The correlation was validated for a CFM56-5A nacelle. Here, Equation 5.25 is in very good agreement with the nacelle dimensions measured from Reference [8]. A summary of the model validation is visualised in Figure A.5 in Appendix A. The model is considered valid for fan pressure ratios between 1.3 and 1.9.

The length of Long Duct Mixed Flow (LDMF) turbofan nacelles results from lengths of the air intake, the bare engine and the common nozzle assembly. Here, nacelle length represents the overall length of installed propulsion system  $L_{ps}$ . For SDSF turbofan engines installed propulsion system length  $L_{ps}$  results from the length of the bare engine  $L_{ps,dry}$ , the fan cowling length  $L_n$  and the axial position of the fan relative to  $L_n$ .

Bare engine length  $L_{ps,dry}$  results from the summation of lengths calculated for the turbo components, the interconnecting ducts, the combustor and the exhaust.  $L_{ps,dry}$  includes the axial dimension of the propulsor including the spinner. Due to the compact assembly of turbofan engines, half of the propulsor axial dimension is considered to overlap with the core engine. In case of counter rotating propeller arrangement in tractor configuration shown in Figure 5.11, propulsor axial dimensions are fully accounted in  $L_{ps,dry}$ . The calculation of turbo components lengths refers to the methods presented in Section 5.2.3. The lengths of ducts, combustors and exhaust nozzles are extrapolated from reference values (cf. also References [69, p.296ff] and [225, p.193f]). In case of turboprop-type engines, bare engine length additionally contains the typically required propeller drive gear system. Gearbox dimensions refer to the correlations given in Reference [176, Vol.2, Table 4.3.3-23]. Installed propulsion system length  $L_{ps}$ , here, is essentially equal to bare engine length  $L_{ps,dry}$  (see Figure 5.11).

Nacelle diameters  $D_n$  result from the maximum diameters of the contained turbo components, i.e. fan diameter  $D_{fan}$  in case of turbofan-type engines, and nacelle thickness  $t_n$ . Apart from fan cowlings, nacelle diameters are defined based on the diameter of the low pressure turbine  $D_{lpt}$ , in the present context. Flow path geometric parameters including the turbo component diameters and nozzle area refer to the engine design calculation performed in GasTurb 11. Using the discussed geometric description, nacelle external wetted surfaces are calculated according to Torenbeek [221, p.449].

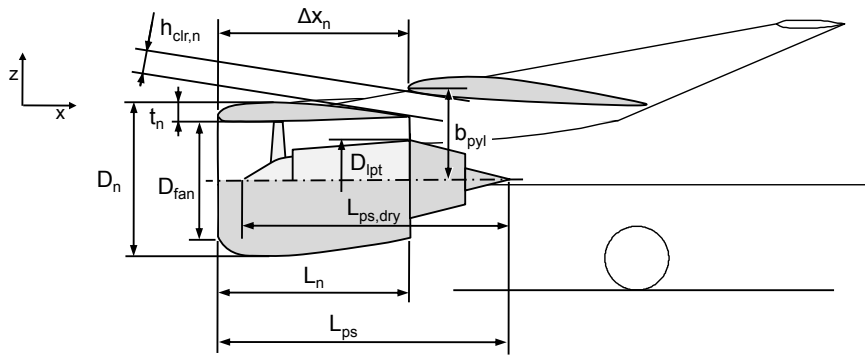


Figure 5.10.: Under-wing geometric integration of turbofan propulsion system

### 5.3.2.2. Turbofan Installation

Advanced turbofan engines are tailored to high propulsive efficiency which is typically achieved for a given thrust requirement by reducing the specific thrust and simultaneously increasing the fan mass flow, yielding increasing fan diameters. The most decisive engine design parameter, here, is the bypass ratio  $BPR$  defined in Section 5.2.1. For classic low-wing aircraft configurations, the geometric free space under the wing is typically constrained by the height of the landing gear. Therefore, fan diameter and maximum bypass ratio are strongly limited. In the present context, propulsion system geometry is treated as an input to the geometric sizing of the landing gear, allowing for full parametric studies of propulsion system design characteristics while maintaining the physical feasibility of results. The implication of  $BPR$  on aircraft design and performance is analysed in Chapter 6.

However, under-wing turbofan installation requires the consideration of multiple aspects concerning the lateral installation location, as well as the axial and vertical positioning relative to the wing (see References [221, Section 6.5.3] and [42, Table 3.1]). In the present context, the engine installation is parameterised by its spanwise installation location  $y_{ps}$ , as well as the vertical and longitudinal positioning relative to the wing ( $h_{clr,n}$  and  $\Delta x_n$ ). The mapping of engine installation angles (cf. Reference [221, Figure 6-20]) and the corresponding aircraft design and performance implications<sup>12</sup> is disregarded, since preliminary analyses showed insignificant impact for the targeted studies. The geometric parameters describing the under-wing installation of turbofan engines are visualised in Figure 5.10.

Now, the shape of the channel between nacelle and wing is considered the decisive factor for the interference drag between these components [221, p.209]. Here, the shape-describing parameter is the clearance between wing and nacelle contour  $h_{clr,n}$ , also referred to as “gully height”. The longitudinal installation position of the engine is defined by the distance between nacelle front face and the wing’s leading edge  $\Delta x_n$ . The definition of  $\Delta x_n$  requires the consideration of aerodynamic shaping of the nacelle / wing channel, the torsional load introduced into the wing structure, the location of the last LPT rotor disc relative to the wing structure in case of uncontained disc failure, as well as thrust reverser operability

<sup>12</sup>i.e. the tradeoff between incremental lift and inlet pressure recovery

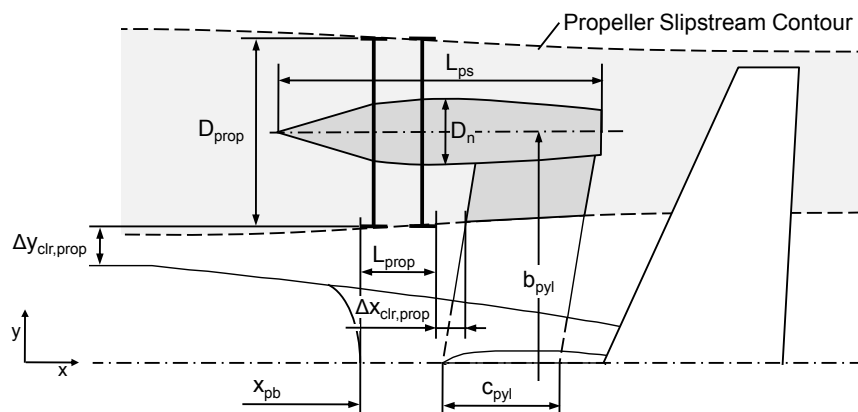


Figure 5.11.: Aft-fuselage geometric integration of open rotor propulsion system

(effectiveness, plume impact and door clearances [42, Table 3.1]). The pylon span  $b_{pyl}$  is defined as the vertical distance between the center line of the local wing cross section and the engine's rotational axis.

The spanwise engine position  $y_{ps}$  represents the trade-off between lateral trim in OEI cases, lateral separation from main landing gear legs and ground clearance aspects, and requires appropriate matching with the wing's strut and flap designs [42, Table 3.1]. For the studies presented in Chapter 6, an empirically-derived constant value is used describing the relative spanwise ( $y_{ps}$  per wing semi-span) engine installation position.

### 5.3.2.3. Open Rotor Installation

The driving aspects for the positioning of open rotor engines at the rear section of the fuselage include cabin internal noise as well as the propellers' aero-mechanical and aero-acoustic interference with aircraft components. The main parameters determining the the open rotor aft-fuselage installation are illustrated in Figure 5.11. Due to the reduced complexity of the engine internal flow path, the undisturbed propeller incidence flow and tail-strike avoidance in case of rotor blade-off, a tractor configuration is preferred over a pusher arrangement. The longitudinal engine positioning is defined so that the plane of the forward rotor of the counter rotating unducted propulsor is located behind the location rear pressure bulk  $x_{pb}$ . The positioning of the engine is tailored to reduce the aero-mechanical interference of the propeller rotors and the adjacent structural components of the airframe, i.e. the engine pylon and the fuselage. The relevant parameters, therefore, describe the axial clearance between the propeller discs and the pylon  $\Delta x_{clr,prop}$ , as well as the lateral clearance between propeller blade tips and the fuselage contour  $\Delta y_{clr,prop}$ . For the studies presented in the following a radial rotor tip clearance of  $\Delta y_{clr,prop} = 0.5m$  is chosen in order to account for the impact of the fuselage boundary layer on rotor aerodynamics. For the axial spacing  $\Delta x_{clr,prop}$  a tentative correlation for wing-mounted propeller engines given in Reference [185, Figure 4.7-5] is used.

The installation space required for the propeller rotors is analytically approximated through a cylinder defined by the propeller diameter  $D_{prop}$  and longitudinal extend  $L_{prop}$  resulting

from the axial projection of blade shapes and the axial spacing of the rotors. Propeller diameter  $D_{prop}$  is strongly affected by engine thrust requirement and propeller disc loading. Both parameters and their corresponding impact on aircraft design and performance are analysed in Section 6.3. In order to minimize aero-mechanical interference between propeller slipstream, wing wake flow field and tail incidence flow, a low wing installation position and T-tail arrangement is chosen, and the vertical engine installation position  $z_{ps}$  is tailored to ensure sufficient vertical separation.

Pylon geometry is approximated by a swept, untapered wing segment. The pylon span  $b_{pyl}$  is a dependent parameter which results from the lateral distance between the rotational axes of the engines installed on both sides of the fuselage. Pylon chord length  $c_{pyl}$  and relative profile thickness  $t/c_{pyl}$  are treated as inputs to the model. An adequate definition of  $c_{pyl}$  represents a trade-off between  $t/c_{pyl}$  pylon aerodynamic drag and pylon structural weight (see Section 5.4.3). For nacelle shaping laws, aerodynamics and air inlet design of open rotor engine configurations see Reference [185, Section 4.7].

## 5.4. Weights and Balance

In this section, the implemented models for aircraft component weight estimation are presented. The detailed discussion focuses on the newly developed methods for the mapping of power plant system and propulsion installation weights. The considered aircraft configurational arrangements refer to Figure 5.1 including the engine installation options displayed in Figures 5.10 and 5.11.

### 5.4.1. Overview of Weight Estimation Methods

A variety of analytical techniques for aircraft component weight estimation on a conceptual level are described in the literature, ranging from the parameterised interpolation of data known from existing aircraft (cf. References [10, 173, 181, 221]) to more elaborate theoretically-derived analytical models (cf. References [108, 79, 34]). Correspondingly, a number of analytical methods for the preliminary estimation of propulsion system component weights can be found in the literature (cf. References [147, 165, 185, 218, 220]).

For the parametric mapping of component weights within conventional aircraft layouts, the application of established textbook methods offers a convenient basis for comparative studies yielding high confidence of results due to the underlying empirical database. However, the applicability to unconventional system layouts is limited due to the neglect of new physical aspects which may act as central design drivers. Thus, for a number of aspects involving the prediction of propulsion system components as well as installation effects, custom models based on first order physical principles were developed during the present work. An overview of the methods implemented for the purpose of the present work is given in Table 5.3. The modelled structural component listed in Table 5.3 directly corresponds to the inner structure of the “Weights” module discussed in Section 3.2.1 (cf. also Figure 3.3). The calculation of component weights  $W_i$  is based on the component sizing and arrangement discussed in Section 5.3. For studies implying different technology levels, the calculated aircraft component weight  $W_i$  are linearly scaled using the technology dependent coefficient  $f_{W,tech,i}$  (cf. Table 6.3, Chapter 6).

Table 5.3.: Overview of methods for the prediction of aircraft component weights

Component	Aspect	Method <sup>a</sup>
<b>Empennage</b>	horizontal stabilizer	acc. to Torenbeek [221]
	vertical fin	acc. to Torenbeek [221]
<b>Propulsion System</b>	turbo components	custom (see Section 5.4.2.2)
	ductings	custom (see Section 5.4.2.1)
	shafts	custom (see Section 5.4.2.1)
	auxiliaries	custom (see Section 5.4.2.1)
	propeller	acc. to LTH [10], adapted
	propeller drive gearbox	acc. to Pratt & Whitney [176]
	nacelle	custom (see Section 5.4.2.1)
<b>Engine Pylon</b>	aft-fuselage engine mounting	custom (see Section 5.4.3.1)
	under-wing engine mounting	custom (see Section 5.4.3.1)
<b>Fuselage</b>	structure	acc. to LTH [10], adapted
	cabin and systems	input
<b>Wing</b>	structure	acc. to LTH [10]
	systems	input
<b>Landing Gear</b>	main gear	acc. to Raymer [173]
	nose gear	acc. to Raymer [173]
<b>OWE Residual<sup>b</sup></b>	cabin and systems	input

<sup>a</sup> Custom methods are described in Section 5.4.

<sup>b</sup> The residual includes all OWE items not explicitly modelled.

#### 5.4.2. Propulsion System Components

Due to the sensitive geometric response of propulsion system components to aerodynamic and mechanical design changes, as well as the complex thermal environment, the estimation of propulsion system weights at early design stages is an immanent critical task. Especially for the involved Life Limiting Parts (LLP), such as turbine discs, blades and nozzle vanes the use of material, and thus, component weight represents a complex trade-off between, cycle design, stage cooling, aerodynamic component efficiency, component sizing constraints and maintainance-relevant lifing implications.

A number of methods targeting engine conceptual weight prediction have been published in the past (cf. References [147, 165, 185]): The Weight Analysis of Turbine Engines (WATE) computer code, was developed by Boeing's Military Airplane Division under NASA contract [147]. The software GasTurb 11 offers built-in weight prediction functionality which can be found evaluated in Reference [48]. A detailed comparison of published methods for engine preliminary weight prediction including the WATE code is given in Reference [186]. The applicability of existing methods is limited since in most cases a substantial amount of information on engine component sizing is required. Hence, during the present work new methods for propulsion system weight estimation appropriate for aircraft conceptual design tasks were developed and implemented.

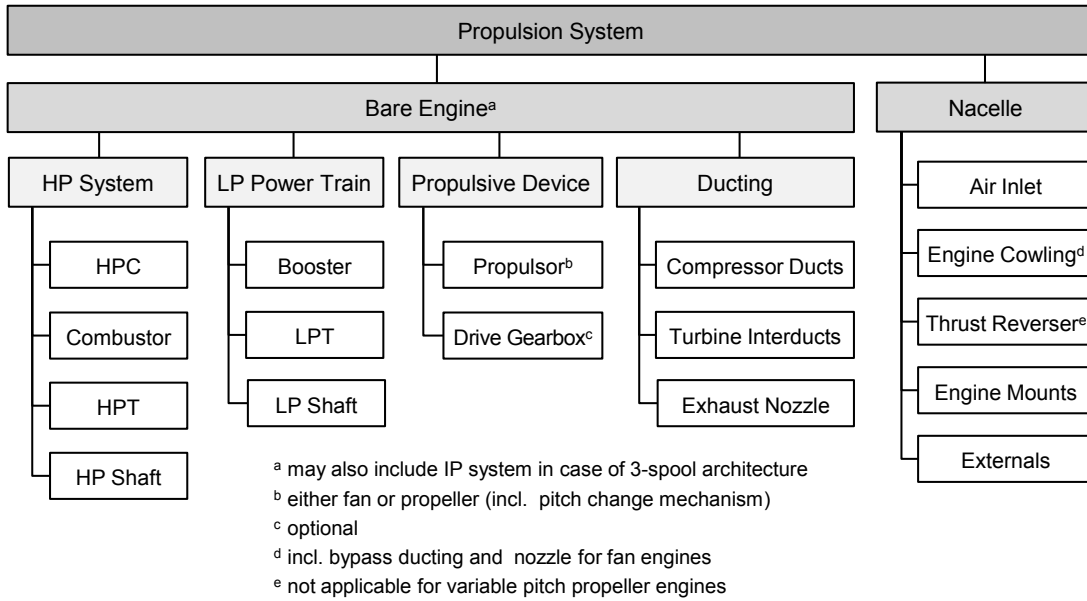


Figure 5.12.: Visualisation of component build-up used for propulsion system weight estimation

#### 5.4.2.1. Component Build-Up Method

In order to consistently map the aspired propulsion system concepts, a common approach to capturing the alternative architectural arrangements is necessary. Now, the book keeping of component weights is strongly dependent on the definition of interfaces within the system architecture, and may vary significantly for existing engines. The present work essentially focuses on the integral results of the propulsion system weight prediction. The discussion in this section, therefore, does not go into the details of component interface definitions. However, in order to separate the impact of essential engine design aspects on the resulting propulsion system weight  $W_{ps}$ , a hierarchical breakdown of major system components is used for the assembly of  $W_{ps}$ . Therefore, a generic component build-up is employed for the mapping of both propulsion system architectures targeted for the studies presented in Chapter 6. The component build-up used is illustrated in Figure 5.12. The component structure shown, refers to 2-spool engine architectures. However, the structural principles are also applicable to 3-spool arrangements.

According to Figure 5.12, the propulsion system is composed of the bare engine and the nacelle.<sup>13</sup> The latter includes the air inlet, engine cowling, thrust reverser system, engine mounts and nacelle externals, i.e. the engine build-up units (EBU), accessories and buyer furnished equipments (BFE). The bare engine consists of the HP system, the low pressure (LP) power train, the propulsive device and the involved additional ducts. The weight of the bare engine is referred to as engine dry weight  $W_{ps,dry}$ , in the following.

For the proposed comparative studies, a convenient way of the mapping the acting component weight trends is to extrapolate given reference data based on variation of representative design parameters. Hence, the weight of all components of the propulsion system except

<sup>13</sup>Operating fluids such as oil for hydraulics, lubrication and cooling are included.

the turbo components are mapped by parametric scaling of engine weight information given in the literature. Typical component weight breakdowns for turbofan engines are given in References [48] and [28].<sup>14</sup> The applied component weight scaling laws include the following proportionalities:

- shafts proportional to shaft torque
- ducting proportional to corrected inlet mass flow
- air inlet proportional to inlet diameter
- engine cowling proportional to cowling diameter, cowling length
- thrust reverser proportional to maximum take-off thrust
- engine mounts proportional to maximum take-off thrust
- externals proportional to cabin power off-take

For propeller weight estimation the statistical method according to LTH [10, MA 615 10-01] is used after calibration for the propeller weight and design information given in Reference [176, Vol.2, Table 4.1.2-3]. The used method is applicable to both single and counter rotating propellers. Propeller drive gearbox is estimated based on the scaling laws presented in Reference [176, Vol.2, Table 4.3.3-23]. For the mapping of the involved turbo components including fan, compressors and turbines, a more detailed approach was developed and implemented during the present work. Essential aspects hereof are presented in the following parts of this section.

#### 5.4.2.2. Approach to Turbo Component Weight Mapping

Turbo components include rotating as well as stationary masses. The rotating shares are essentially composed of the disc and blade masses, while the stationary shares include the masses of component casing, vanes, air sealings and additional structural elements such as struts, bearings, support and gearbox elements. The basic approach developed and implemented for turbo component weight estimation, here, is formulated accordingly

$$W_c = W_{c,rot} + W_{c,stat} \quad (5.26)$$

where  $W_{c,rot}$  and  $W_{c,stat}$  represent the component's rotating and stationary mass shares. Both mass shares are evaluated based on stage-wise operations conducted on the component's annular volume and material properties. The stationary mass share  $W_{c,stat}$  is treated proportional to the component's annular volume. It is calculated using the following correlation

$$W_{c,stat} = f_{c,stat} \cdot \sum_{i=1}^{n_{st}} L_{st,i} \cdot A_{st,i} \cdot \rho_{M,st,i} \quad (5.27)$$

The determination of stage axial length  $L_{st,i}$  and mean annular area  $A_{st,i}$  is discussed in Section 5.2.3. The rotating mass share  $W_{c,rot}$  is calculated from the following correlation

$$W_{c,rot} = f_{c,rot} \cdot \sum_{i=1}^{n_{st}} c_{rot,st,i} \cdot L_{st,i} \cdot A_{st,i} \cdot \rho_{M,st,i} \quad (5.28)$$

<sup>14</sup>Comparative breakdowns showing the differences between turbofan and open rotor architectures are given in References [176, Table 4.4-II], [185, Table III-3] and [21, Table D-III].

where the nondimensional rotating stage mass coefficient  $c_{rot,st,i}$  is defined as

$$c_{rot,st,i} = \frac{A_{st,i} \cdot n_{sp}^2 \cdot \rho_{M,st,i}}{\sigma_{M,st,i}} \quad (5.29)$$

Here,  $\rho_{M,st,i}$  and  $\sigma_{M,st,i}$  represent the properties of the material (density  $\rho_M$  and yield strength  $\sigma_M$ ) used for the  $i^{th}$  stage of the component. Material properties modelled as functions of local bulk temperature  $T_{M,st,i}$  based on data are taken from Reference [101]. In case of uncooled components  $T_{M,st,i}$  values are directly derived from linear interpolation of component inlet and exit total temperatures across the number of component stages  $n_{st}$ . The assumed operating condition representative for the evaluation of cycle temperatures refers to maximum take-off (MTO). In the range of typically occurring material temperatures, the choice of materials depends on the specific strength  $\rho_{M,st,i}/\sigma_{M,st,i}$ .<sup>15</sup> In case the stage temperature value  $T_{M,st,i}$  exceeds a cut-off value of  $1250K$ , stage cooling is assumed and the cut-off temperature is used for the analysis of material properties.

The rotating stage mass coefficient  $c_{rot,st,i}$  is a measure for the material mass required to bear the centrifugal forces caused by the rotational motion of blade and disc masses. The physical meaning of  $c_{rot,st,i}$  is based on the  $AN^2$  metric referred to in Section 5.2.3, and the basic properties of the employed rotor material. Accordingly,  $c_{rot,st,i}$  increases with increasing annular area  $A_{st,i}$  and spool rotational speed  $n_{sp}^2$ , but decreases for enhanced specific material strength  $\rho_{M,st,i}/\sigma_{M,st,i}$ . The dimensionless coefficients  $f_{c,rot}$  and  $f_{c,stat}$  are used for model calibration.

For the studies presented in Chapter 6, typical splits of rotating and stationary weight shares were derived for different types of turbo components, i.e. fan, booster, HPC, HPT and LPT, by clustering and averaging the data given in Reference [48, Appendices C and D]. Based hereon, and by using the averaged component weight breakdown given Reference [48, Figure 5-3] the model was calibrated for the engine weight information given in Reference [82].

Now, Figure 5.13 (overleaf) shows the engine dry weight  $W_{ps,dry}$  trends gained from a hypodimensional design study for a generic 2-spool turbofan engine. The results are displayed using the MPD visualisation (cf. Section 3.3.3) based on neural network regression. The design study includes typical design operational conditions, i.e. design Mach number  $M_{des}$  and altitude  $Alt_{des}$ , engine design thrust  $FN_{des}$  and bypass ratio  $BPR_{des}$ , the engine's aerothermodynamic technology factor  $f_{tech,ps}$  described in Section 5.2.3, as well as the discrete number of LPT stages  $N_{st,LPT}$ . The depicted partial dependencies feature a high degree of plausibility, displaying the expected magnitudes of engine weight increase against  $Alt_{des}$ ,  $FN_{des}$  and  $BPR_{des}$ . Beyond that, the effect due to the discrete number of LPT stages  $N_{st,LPT}$  is adequately captured by the presented engine weight model. It can be seen that the step changes of  $W_{ps,dry}$  against  $n_{st,LPT}$  are accurately approximated by the created FNN.

### 5.4.3. Propulsion Installation Effects

Beside the propulsion system's own weight, the loads introduced into the airframe caused by its installation may have significant implications on the design and sizing of major structural components of the airframe. In the present section, the methods developed for pylon, wing

<sup>15</sup>For the studies presented in this thesis, Ti-6Al-4V, INCONEL 718 and Rene 41 alloys were employed.

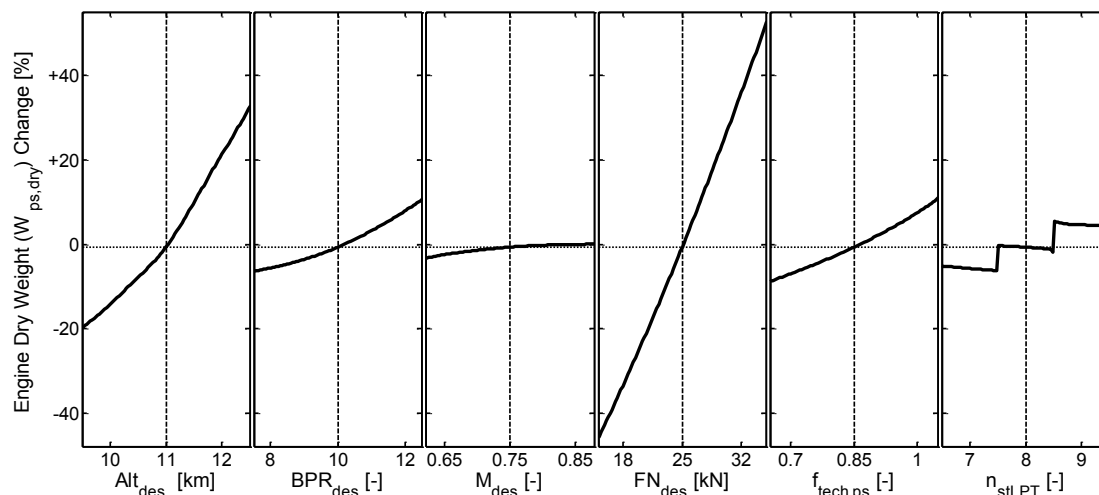


Figure 5.13.: Matrix of partial dependencies for feedforward neural networks created from proposed engine weight model (Example: bare engine weight of 2-spool boosted turbofan)

and fuselage structural weight estimation are discussed under special consideration of the propulsion system installation impact.

#### 5.4.3.1. Engine Pylon

The targeted propulsion system types and installation options necessitate particular consideration of the connected weight implications on airframe structural components. Especially, for aft-fuselage mounted open rotor engines (cf. Figure 5.11), the empirical database is small. However, according to design report for GE's UDF engine [4] significant pylon structural weights are expected (cf. [4, p.315ff]).

A feasible method allowing for the parametric estimation of pylon structural weight was not found during the literature research conducted as part of the present work. Therefore, a simplistic physics-based method for pylon weight estimation was developed which is applicable to pylons for under-wing engine mounting as well as aft-fuselage engine mounting. Key aspects of the method are discussed in the following.

For the structural layout of the engine pylon, a detailed analysis of the relevant load cases is required. Here, the inertial, thrust, and gyroscopic loads induced by the engine, high and low cycle fatigue margins as well as the dynamics caused by propulsor blade out cases represent significant criteria for the design and sizing of pylon structural components. A summary of load assumptions and safety margins used for UDF pylon design can be found in Reference [4, Table 12-1]. For the present purposes, the consideration of the static loads caused by propulsion system weight  $F_{w,ps}$  and maximum (take-off) thrust  $F_{T/O,max}$  forces are considered satisfactory, in the first instance. Aerodynamic forces are assumed small, and thus, neglected. Now, the considered forces acting on the pylon structure are illustrated in Figure 5.14 for both engine installation cases shown in Figures 5.10 and 5.11. The basic approach for pylon weight calculation assumes the pylon weight to be constituted as

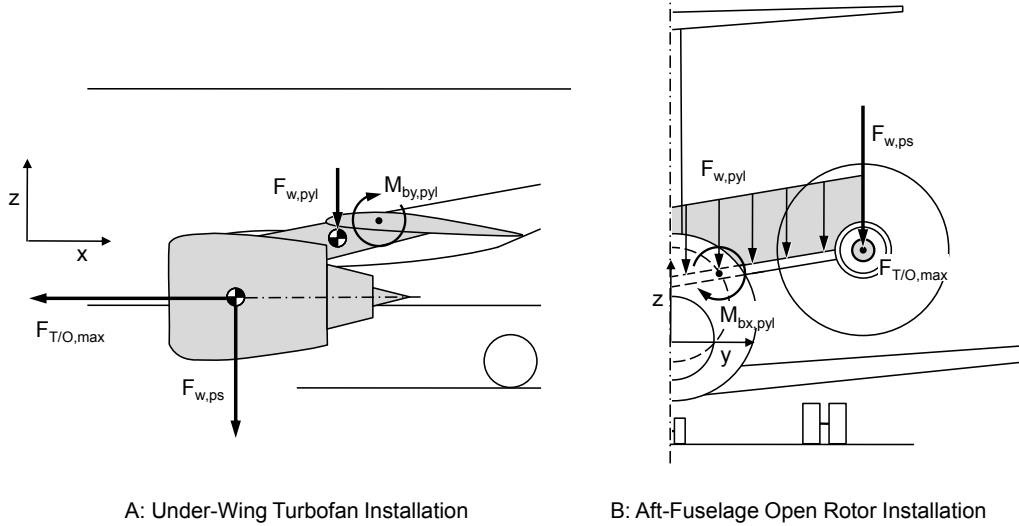


Figure 5.14.: Schematic of acting forces considered during pylon structural weight estimation

$$W_{pyl} = W_{pyl,box} + W_{pyl,sht} + W_{pyl,res} \quad (5.30)$$

where  $W_{pyl,box}$  represents the weight of load-carrying inner structure of the pylon which is approximated by a simple hollow beam model.  $W_{pyl,sht}$  refers to the weight of the pylon's surface sheeting which is assumed not to be load-carrying, here.  $W_{pyl,res}$  incorporates weight items, such as hydraulics, bleed air ductings and additional systems located inside the pylon.

The residual weight share  $W_{pyl,res}$  is assumed proportional to pylon span  $b_{pyl}$ . The other weight shares are calculated from the volume and density of the material used. Here, the sheeting volume results from the pylon's wetted area and a predefined sheeting thickness. The volume of the load-carrying structure is calculated from the considered load conditions (cf. Figure 5.14). Based on the acting forces the resulting 2-dimensional (polar) bending moment is determined at a representative cross section along the pylon's spanwise coordinate. The representative cross sections position is considered to be located at the pylon / fuselage respectively pylon / wing intersection.

The hollow beam representing the pylon box is parameterised by its cross section which is defined by its outer dimensions (the chordwise length  $L_{beam}$  and height  $h_{beam}$ ) and the beam thickness  $t_{beam}$ , and  $b_{pyl}$ . For aft-fuselage engine installation, the pylon beam is considered to run through the fuselage. The outer dimensions of the beam cross section are constrained by the pylon's aerodynamic profile. The beam thickness  $t_{beam}$  is considered uniform in the cross section and across the pylon's spanwise coordinate, in the first instance. For predefined  $L_{beam}$ ,  $h_{beam}$  and  $t_{beam}$  the directional moments of inertia of the beam are determined according to the formulation given in Reference [173, p.427]). Based on the beam's moments of inertia and cross-sectional area the stress in the representative cross system  $\sigma_{beam}$  is calculated by superposition of the partial stresses due to the acting bending moments as well as shear forces respectively normal forces (cf. configurations A and B in Figure 5.14). The acting forces are, therefore, scaled by a structural load factor  $n_{des}$  representing the ultimate design loads. Additional pitchwise torsional moments emanating from pylon sweep and the axial

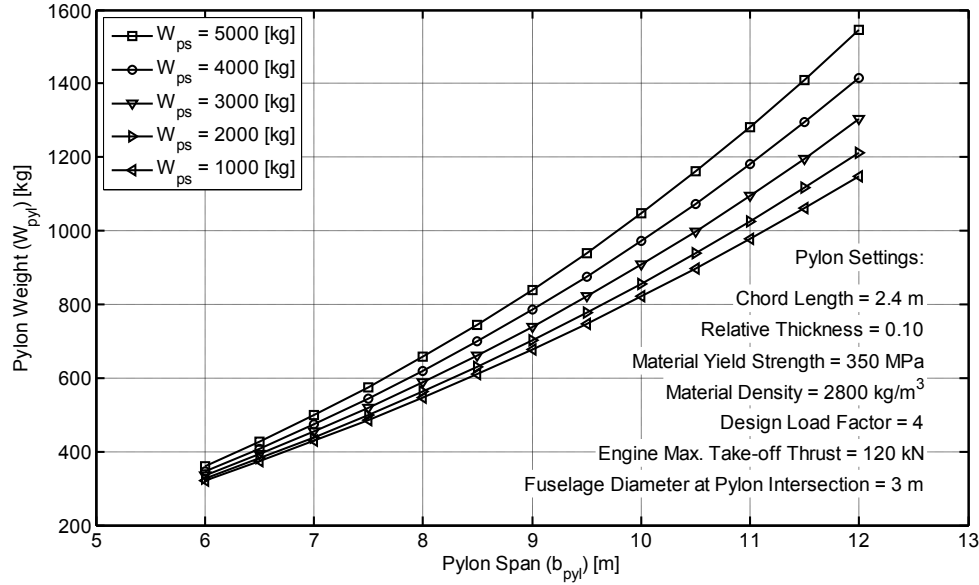


Figure 5.15.: Parametric study of aft-fuselage pylon weight for a wide range of potential load cases (Study parameters: pylon span and propulsion system weight)

eccentricity of acting propulsion system weight forces are neglected in case of aft-fuselage mounted engines, in the first instance. The evaluation of the 2-dimensional stress conditions is based on the basic mechanical methods presented in Reference [145, Section 3.3.3].

Now, material yield strength  $\sigma_{M,pyl}$  and density  $\rho_{M,pyl}$  are input parameters to the model. Hence, due to the fact that the pylon's own weight force which is a result of the beam calculation, imposes on the stress condition  $\sigma_{beam}$ , the model requires iterative solving. Therefore, the beam material thickness  $t_{beam}$  is varied until  $\sigma_{beam}$  equals the prescribed material strength  $\sigma_{M,pyl}$ . A solution can not be found if  $t_{beam}$  exceeds  $h_{beam}/2$  during iteration. However, iteration success can be ensured by choosing appropriate material properties, limiting pylon span, increasing pylon chord length or relative profile thickness. For the studies presented in Chapter 6, material properties typical for aluminum alloys are chosen ( $\sigma_{M,pyl} = 350MPa$ ,  $\rho_{M,pyl} = 2800kg/m^3$ ), irrespectively for further potential choices of material, such as titanium.

The pylon weights calculated as part of a parametric study of pylon span  $b_{pyl}$  and propulsion system weight  $W_{ps}$  for aft-fuselage installed open rotor engines are displayed in Figure 5.15. The shown range of  $b_{pyl}$  is representative for typical open rotor installations. The figure displays the significant impact of propulsor diameter on the engine's primary installation weights. The nonlinearity against  $b_{pyl}$  results from the repercussive impact of the pylon's own structural weight.

#### 5.4.3.2. Secondary Installation Weights

Beside the engine mounting structure, i.e. the pylon, which is directly affected by the propulsion system design and installation concept, secondary but by no means negligible

effects act on the wing and fuselage structures. Here, propulsion system installation may reduce but may also significantly increase component-specific structural loads. Taking for example the conventional case of under-wing mounted engines, the weight of the installed engines reduces the maximum bending moment at the wing root due to manoeuvre loads. Increasing the relative spanwise coordinate of the installed engine may yield structural weight benefits (cf. Reference [10, MA 501 12-01]). In contrast, the pitchwise torque moment at the wing root is strongly affected by the longitudinal position of the engines relative to the wing front spar, yielding structural weight penalties if the engines are moved forward.

For the studies presented in Chapter 6, the weight correlation according to LTH [10, MA 501 12-01] is used. The method captures important aspects of the propulsion system installation, i.e. a relief factor for the wing root bending incorporating propulsion system weight, takeoff-thrust and spanwise installation position. Due to its simplicity, the LTH method was favoured over more complex analytical models for wing weight estimation such as the theoretically-based ‘‘F Method’’ according to Howe [79].

Fuselage structural design is essentially driven by the pressurisation of payload cabin as well as the longitudinal distribution of bending moments [34, p.9]. The latter load condition is assumed to be most significantly affected by the optional installation of engines at the rear-section of the fuselage. Here, the increased bending moment during landing shock is crucial for fuselage structural design (cf. Torenbeek [221, p.464]). Established methods available in the literature, typically account for this using a constant offset coefficient describing the weight penalty for the fuselage structure (cf. LTH [10, MA 508 12-02], Torenbeek [221, Appendix D], Howe [80, p.350]). However, for significant variations of propulsion group weight such as resulting from the wide range of propulsion system design changes encountered in the present context, a constant penalty factor appears inappropriate.

During the present work, a simple method for the parameterisation of the fuselage structural weight penalty due to the propulsion system installation was developed. The method is based on a comparison of the bending moments  $M_{by,fus}$  acting in the fuselage cross section located at the longitudinal position of the main landing gear  $x_{mlg}$ , with and without fuselage-installed propulsion group. The forces considered for bending moment determination are visualised in Figure 5.16. Cabin, payload and fuselage weight forces are assumed constant line forces over the fuselage’s longitudinal axis. Fuselage nose and aft section weights are approximated as triangular line forces. The weight forces of the engines, pylons and empennage are treated as point forces acting in the corresponding component centres of gravity. The reacting force during touch down, i.e. the landing shock load, is introduced into the fuselage structure through the wing’s rear spar which is assumed to be located at  $x_{mlg}$  (cf. Figure 5.16). The representative fuselage bending moment  $M_{by,fus}$  equals the sum of moments induced by weight force contributors located behind the main landing gear<sup>16</sup>

$$M_{by,fus} = \sum_{i=1}^{n_w} F_{w,i} \cdot (x_{w,i} - x_{mlg}) \quad \forall (x_{w,i} > x_{mlg}) \quad (5.31)$$

where  $n_w$  refers to the number of acting weight forces either including the propulsion group (*Case II*) or not (*Case I*).  $x_{w,i}$  represent the locations of the acting weight forces. Inspection

<sup>16</sup>The balance of moments at  $x_{mlg}$  is ensured by the wing’s pitching moment.

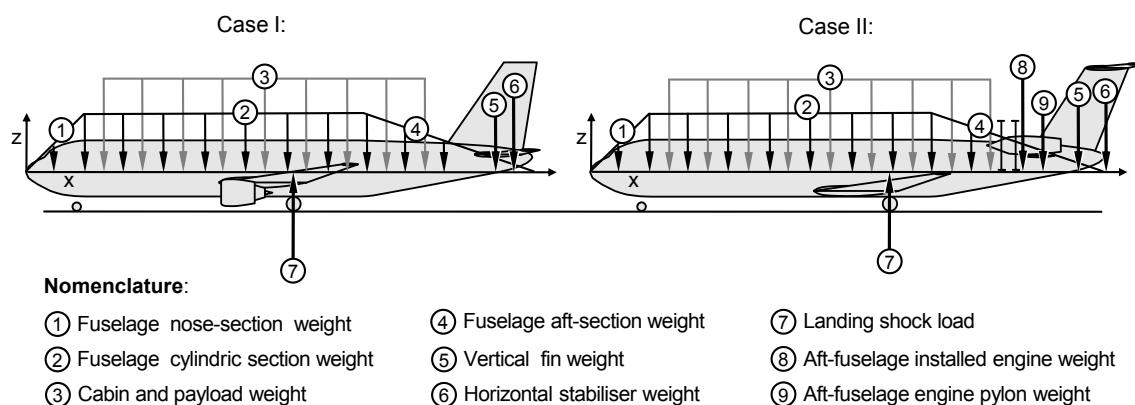


Figure 5.16.: Schematic of forces contributing to fuselage bending load in landing shock load scenario: under-wing engine installation (left), aft-fuselage engine installation (right)

of Equation 5.31 shows, that the ratio of the bending moments calculated for both cases is independent from the actual load factor.

For fuselage structural weight prediction, the statistical method according to LTH [10, MA 508 12-02] was chosen, forming a consistent setup of fuselage and wing weight calculation. The LTH method for fuselage structural weight prediction parametrically includes the effects of essential design fuselage attributes such as the slenderness ratio, cabin pressurisation and payload mass. The optional aft-fuselage installation of engines is treated using the term  $(1 + k_{FT})^{0.367}$  as a constant factor in the overall statistical equation. The addend  $f_{FT}$  equals 0.2 if the engines are fuselage-mounted (otherwise  $f_{FT} = 0$ ) [10, MA 508 12-02] in the case of wing-mounted main landing gear. Now, taking existing aircraft featuring aft-fuselage mounted engines, the impact of the installed propulsion group on the fuselage bending moment  $M_{by,fus}$  can be analysed. As a figure of merit, here, the ratio of bending moments  $R_{Mb,fus}$  between *Case I* and *Case II* is used

$$R_{Mb,fus} = \frac{M_{by,fus,I}}{M_{by,fus,II}} \quad (5.32)$$

In the present context two existing aircraft have been analysed as described above with respect to their geometric arrangements and published weight data: the Douglas DC9-15 and the McDonnell Douglas MD-81. The required information is taken from References [2], [6] and [181]. Based on the analysis of the DC9-15 and MD-81 aircraft, the engine installation coefficient  $k_{FT}$  used in the LTH method is correlated to  $R_{Mb,fus}$ . Therefore, the correlation between  $k_{FT}$  and  $R_{Mb,fus}$  was calibrated using the  $R_{Mb,fus}$  value calculated for the DC9-15 aircraft and validated based on the corresponding value determined for the MD-81 aircraft. For the validation, the weight penalty term  $(1 + k_{FT})^{0.367}$  as calculated from the calibrated correlation of  $k_{FT}$  and  $R_{Mb,fus}$  was evaluated for the MD-81 configuration and compared to the statistical reference ( $f_{FT} = 0.2$ ). The validation result as well as the extrapolation characteristics against the variation of propulsion group installed weight  $W_{pg}$  and lever arm  $(x_{w,pg} - x_{mlg})$  calculated for the MD-81 configuration are shown in Figure 5.17.

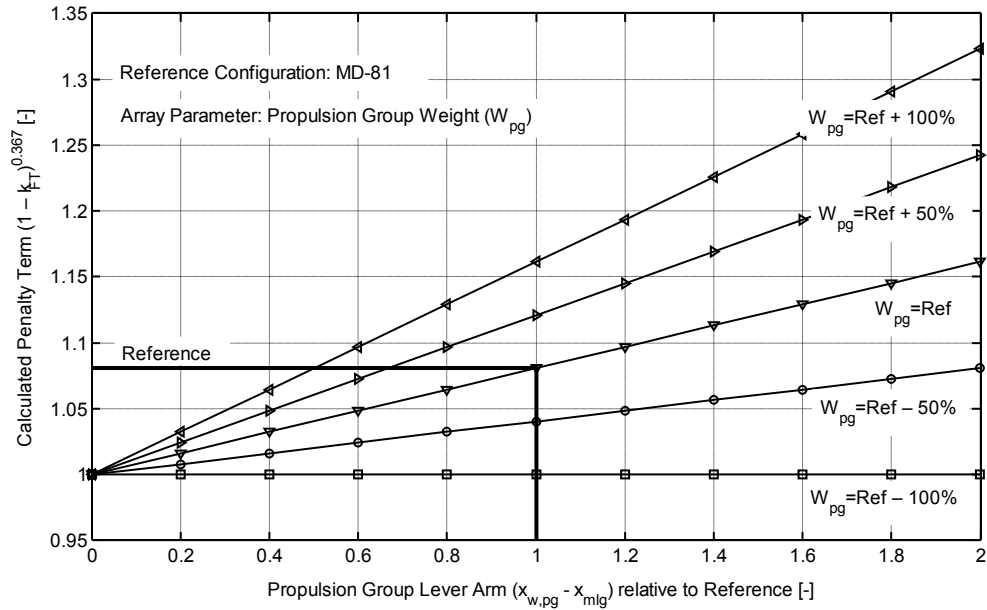


Figure 5.17.: Parametric study of fuselage structural weight penalty term due to propulsion installation

The weight penalty term calculated for the MD-81 is in good agreement with the corresponding statistical value according to LTH. The relative deviation amounts to 1.1%. The intuitively obvious trends of the weight penalty term shown in Figure 5.17 reflect the increasing structural bending loads caused by increasing propulsion group weight and lever arm. According to the model, the weight penalty vanishes in case  $x_{w,pg}$  equals  $x_{mlg}$  (cf. Figure 5.17).

The presented fuselage weight penalty approach represents an enhancement of the statistical method for fuselage structural weight prediction according to LTH. The approach allows for a convenient extrapolation of the weight penalty term  $(1 + k_{FT})^{0.367}$  including variations of propulsion group weight and longitudinal installation position. The fuselage weight penalties calculated using the presented approach may significantly exceed the values suggested by LTH, especially for high propulsion group weights such as encountered for propulsion systems featuring large diameters. In most cases, the derived penalties are, however, moderate compared to the tentative correlation suggested by Torenbeek [221, p.464].

The weights of the horizontal and vertical stabilizers are calculated according to Torenbeek [221, p.281]. The weights prediction for nose and main landing gear refers to Raymer [173, p.459]. All other OWE shares are treated as technology-dependent offset values during parametric design studies.

#### 5.4.4. Aircraft Balancing

The implemented methods for aircraft balancing include static longitudinal stability requirements based on wing and tail plane sizing as well as the longitudinal positioning of wing and landing gears based on the predefined topology of the aircraft, its components weights

## 5. Conceptual Design Methods for Aircraft and Propulsion System

and local centres of gravity. Stability calculation uses the correlation given by Torenbeek (cf. [221, Eq. (9-5)]) which has been simplified and rearranged to yield the wing's longitudinal position  $x_{AC,wing}$  for a given stability margin  $dc_m/dc_L$

$$x_{AC,w} = x_{NP,a/c} - \frac{\left(1 - \frac{d\varepsilon}{d\alpha}\right) \cdot \frac{V_{ht}}{S_{ref}}}{1 + \frac{S_{ht}}{S_{ref}} \cdot \left(1 - \frac{d\varepsilon}{d\alpha}\right)} \quad (5.33)$$

In Equation 5.33, the lift curve slopes of wing and horizontal tail plane as well as the dynamics pressures at wing and horizontal tail plane are assumed similar. The wing induced downwash gradient  $d\varepsilon/d\alpha$  and required static longitudinal stability of the aircraft  $dc_m/dc_L$  are input to the model. Values for  $d\varepsilon/d\alpha$  can be derived from Raymer [173, Fig. 16.12]. Taking the calculated wing longitudinal position  $x_{AC,wing}$  and considering the geometric constellation given in Figure A.4 in Appendix A, the actual lever arms of the horizontal and vertical tails ( $L_{ht}$  and  $L_{vt}$ ) can be derived.

The longitudinal position of the aircraft's center of gravity  $x_{CG,a/c}$  directly results from the balance of moments in the spanwise direction. Therefore, the afore-calculated weight forces  $F_{w,i}$  and local center of gravity locations of the aircraft's structural components, mission fuel and payload ( $x_{CG,i}$ ) are evaluated with respect to their positioning in the aircraft coordinate system (cf. also Figure 5.16). Based on the balance of moments and the predefined load split between nose and main landing gear, the longitudinal positioning of the landing gear legs is determined.

In the overall aircraft design and sizing procedure the aircraft center of gravity position, as well as the lever arms of horizontal and vertical tails are inputs to the sizing methods of landing gear and empennage. Therefore, the calculated  $x_{CG,a/c}$  and  $L_{ht}$  and  $L_{vt}$  are treated as feedback parameters in the aircraft conceptual design process.

## 5.5. Aerodynamics

The detailed mapping of aerodynamics is not in the focus of the present work. Therefore, the application of classic semi-empirical methods for the estimation of aircraft aerodynamic characteristics is preferred, in the first instance. In the following, an overview of the implemented methods is given. Subsequently, the mapping of the involved aircraft drag shares and the corresponding aspects related to propulsion system integration are discussed.

### 5.5.1. Overview of Methods

The methods implemented for the mapping of aircraft aerodynamics refer to the textbook methods according to References [173, 130, 180, 72] and [80]. A synopsis of the aerodynamics modelling is given in Table 5.4. Hence, a symmetric approach is used to map the aircraft drag polar. The aerodynamic model includes the drag shares due to skin friction and pressure, component interferences, transonic compressibility as well as lift-induced effects. The calculation of induced drag is focused on the wing, whose induced efficiency is estimated based on the correlation given by Howe [80]. Induced drag emanating from fuselage or engine nacelle angles of attack are neglected, in the first instance. Trim drag is not modelled

explicitly, but considered within a constant offset ( $c_{D,res}$ ) in the aircraft's drag coefficient. It is, however, relatively small and constitutes only 1 to 2% of the total aircraft drag at typical cruise conditions [130, p.182]. The drag report given in Reference [194, Chapter 5] indicates the trim share to be even less than one percent (0.4%) at typical cruise conditions. Additional and miscellaneous drag shares, e.g. due to leakages and protuberances, are also treated as constant offsets in the aircraft's drag coefficient.

Table 5.4.: Overview of implemented methods for the mapping of aircraft aerodynamics

Drag Share <sup>a</sup>	Aspect	Method
<b>Skin Friction and Form</b>	external wetted surfaces <sup>b</sup>	acc. to Raymer [173]
	<b>Wave</b>	lifting surfaces
<b>Induced</b>	non-lifting surfaces	acc. to Roskam [180]
	polar approach	symmetrical
	lift distribution	Oswald factor acc. to Howe [80]
<b>Interference</b>	representative wing section	MAC <sup>c</sup>
	nacelle integration	input (cf. Reference [194])
	propeller slipstream effects	custom (see Section 5.5.2.2) <sup>d</sup>
	drag bookkeeping scheme	custom (see Figure 5.2)

<sup>a</sup> Additional parasite drag shares are included in a residual drag offset.

<sup>b</sup> Includes fuselage, wing, empennage, engine nacelles and pylons.

<sup>c</sup> Mean Aerodynamic Chord (MAC)

<sup>d</sup> The underlying propeller aerodynamic model is described in Section 5.2.5.

The approach used for skin friction, form and interference drag prediction refers to References [130] and [173]. Interference drag mapping emphasises on typical propulsion system installation constellations. Component interference factors are chosen according to Reference [194]. Wave drag estimation for lifting surfaces based on Korn's equation [72], for the mapping of the wave drag of non-lifting surfaces generic characteristics given by Roskam [180, Part I] are employed. Fuselage and nacelles are considered non-lifting surfaces. The characteristics of lifting surfaces are based on the aerodynamic conditions at the corresponding mean aerodynamics chord (MAC). For technology studies, the wing's chordwise location of laminar-turbulent flow transition  $x_{trans,wing}$ , Korn's empirical airfoil factor  $K_{Korn}$ , and a linear scaling factor for the calculated induced efficiency  $f_{OS,tech}$  is used.

In case of unducted propulsor engine configurations, propeller-induced axial velocities are incorporated in the parasite drag calculation of wetted surfaces in propeller slip stream. Low-speed aerodynamic characteristics are calculated according to Loftin [109]. For wind milling drag estimation in case of engine failure, i.e. One Engine Inoperative (OEI), a simple parametric model was derived from information provided in Reference [42]. An overview of the modelled drag build-up is given in Figure 5.18 (overleaf).

A representative polar plot for a generic M/R aircraft configuration as calculated using the implemented methods for drag prediction is depicted in Figure A.6 in Appendix A, showing is the aircraft's aerodynamic efficiency ( $L/D$ ) against for a wide range of high-speed operating conditions.

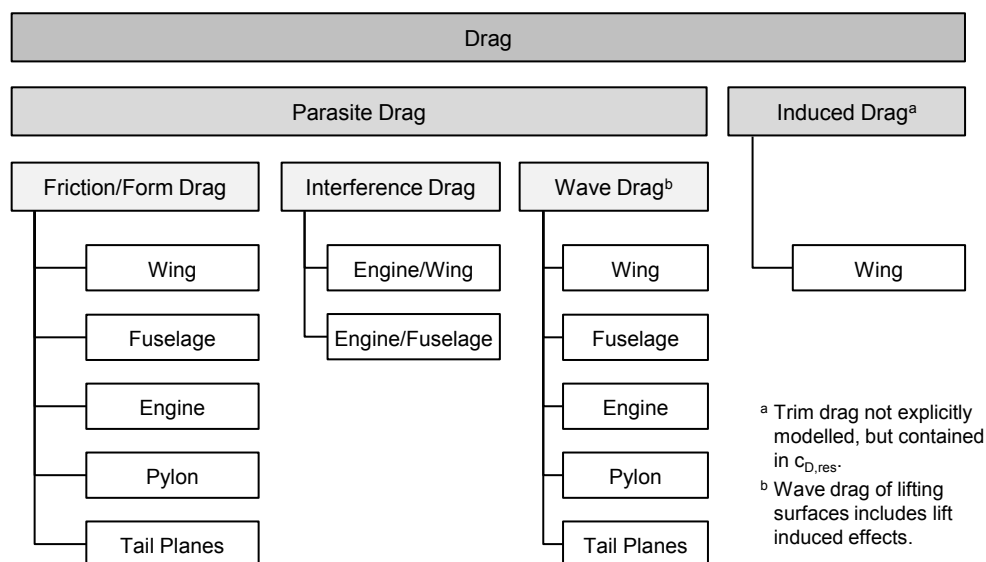


Figure 5.18.: Component build-up of implemented models for aerodynamic drag estimation (clean configuration, landing gear retracted, all engines operative)

## 5.5.2. Propulsion Integration Aspects

The installed propulsion system is a major contributor to the overall drag of aircraft. The drag share is sensitive to propulsion system design variations. Thus, for an adequate evaluation of advanced propulsion system design aspects, an accurate mapping of the implications on aircraft aerodynamics connected to the engine installation is required.

The methods presented in the following focus on major effects impacting on mission performance. The discussion includes the aerodynamic interference of propulsion system and airframe during high-speed operation, as well as the additional drag caused by engine failure during low speed operation. In particular, the mapping of propeller slipstream effects in case of the considered open rotor engine installation option is emphasised.

### 5.5.2.1. Engine / Airframe Aerodynamic Interference

For a low aerodynamic drag of the propulsion system, an adequate nacelle contour shape is essential, that well balances the occurring skin friction, pressure and wave drag shares (cf. References [42, Figure 3.5] and [185, Section 4.7.8]). Assuming proper contouring (see Section 5.3.2) nacelle drag essentially scales with nacelle wetted area, the latter of which is a direct function of nacelle diameter  $D_n$  and length  $L_n$ . The influence of engine fan diameter on aircraft interference drag is shown in Reference [42, Figure 3.9] assuming constant gully height  $h_{clr,n}$  (cf. Section 5.3.2). The results obtained from the present methodology are in good agreement with these characteristics.

An additional share of the overall drag caused by the installed propulsion system emanates from the aerodynamic interference of the nacelle and the adjacent airframe components. Interference drag in case of under-wing mounted turbofan engines is largely characterised by

the changed flow conditions around the wing caused by the presence of the nacelle and the pylon [42, figure 3.5]. This includes the powered effects caused by the jet exhaust below the wing. According to Reference [194, Chapter 5.9] an allowance for interference drag of 10% is added to the drag coefficients calculated for the isolated nacelles and pylons. Pylon drag, in case of wing-mounted turbofan engines, is largely a function of the wetted area of the strut, typically, rarely generating wave drag if proper integration is realised [42, p.19].

### 5.5.2.2. Propeller Slipstream Effects

For the aerodynamic evaluation of the considered counter rotating propeller installation, the drag shares of nacelle (including propeller spinner) and pylon at free stream conditions are superimposed by propeller slipstream effects (see Figure 5.11).

The induced velocities in the propeller slipstream are directly derived from the propeller aerodynamic design code presented in Section 5.2.5. Since a counter rotating pair of propellers is considered, the induced velocities are considered purely axial. Induced vorticity effects and periodical velocity fluctuation due to the finite number of propeller blades are neglected. Instead of the radial distribution of induced velocities  $w_a(x_B)$ , the mean axial induced velocity  $\bar{w}_a$  is treated representative for the flow conditions in the slipstream.

The additional drag of engine nacelle and pylon caused by the propeller slipstream is evaluation after superposition of the free stream velocity  $V_0$  at flight altitude and  $\bar{w}_a$ . The resulting Mach number in the slipstream  $M_{sl}$  is applied to the calculation of skin friction, form and wave drag for the surfaces wetted by the slipstream. Effects due to slipstream contraction are neglected, in the first instance. Different from the external nacelle and pylon aerodynamics of ducted propulor engines, here, wave drag effects are encountered for high flight Mach numbers and propeller power loadings. Again, interference drag is accounted for by applying identical interference factors to the resulting isolated drags of nacelle and pylon as used for the turbofan installation.

### 5.5.2.3. Wind Milling Drag

For the mapping of low speed aerodynamics, the additional drag caused by engine failure, i.e. OEI cases, is considered. This drag increment consists of the engines windmilling drag and the drag due to the asymmetric flight condition. The additional trim drag due to the asymmetric flight condition is not modelled, in the first instance. The former is composed by the external drag share due to spillage of the inlet and the internal pressure losses caused by the windmilling of the turbo components [221, p.553]. Low speed operational wind milling drag for ultra high bypass ratio engines ranges from 1 to 2% of engine takeoff thrust, increasing with growing fan diameter [42]. Besides these low-speed operational modes for long range twin-engine aircraft wind milling drag at cruise conditions has to be considered during design for Extended-Range Twin-Engine Operations (ETOPS) certification [42].

Using the information given in Reference [42, Tables 2.2 and 2.3] a simple empirical model for engine wind milling drag was derived assuming wind milling drag proportional to fan

frontal area. The wind milling drag of propeller engines is, in the first instance, assumed similar to the wind milling drag of ducted propulsor engines.<sup>17</sup>

## 5.6. System Performance and Sizing

Important characteristics to be considered for a comprehensive assessment of aircraft and propulsion system design qualities were presented in Section 3.1.2, including the evaluation of system performance, noise, cost, life-cycle and fleet compatibility aspects. The present section focuses on classic measures for the evaluation of aircraft performance qualities including the performances at relevant operating conditions such as during take-off, climb, cruise, descent and ground operation, as well as overall mission performance. Moreover, the evaluation of essential aircraft sizing constraints and the proposed aircraft scaling procedure are discussed.

### 5.6.1. Typical High-Speed Point Performances

For the studies presented in Chapter 6, three basic operating conditions are considered relevant, including steady level flight, climb and acceleration flight as well as descent / gliding conditions. The formulation used for the evaluation of these operating conditions is summarised in Table 5.5. Flight conditions connected to curvilinear and/or accelerated manoeuvring are not considered, in the first instance.

Table 5.5.: Basic formulation of flight conditions considered during aircraft performance analysis

Operating Condition	Basic Formulation
<b>Stationary level flight</b>	$FN_{req} = D \quad L = W_{a/c} \cdot g$
<b>Climb / acceleration flight<sup>a</sup></b>	$P_s = \frac{dH}{dt} + \frac{V}{g} \cdot \frac{dV}{dt} \approx \frac{V \cdot (FN_{avail} - D)}{W_{a/c} \cdot g}$
<b>Descent / gliding</b>	$L/D = \frac{1}{\tan\gamma} \quad FN_{req} = \begin{cases} \text{Idle} & ,  \gamma_{desc}  \geq \gamma, \\ D & ,  \gamma_{desc}  < \gamma. \end{cases}$

Nomenclature:

$FN_{req}$ - total thrust required	$D$ - total drag
$L$ - total lift required	$W_{a/c}$ - actual aircraft weight
$g$ - gravitational constant	$P_s$ - specific excess power
$V$ - true air speed	$dh/dt$ - climb rate
$dV/dt$ - acceleration rate	$FN_{avail}$ - total thrust available
$\gamma$ - glide angle	$\gamma_{desc}$ - descent angle

<sup>a</sup> Transient load factors and corresponding influences on drag prediction neglected.

<sup>17</sup>Basic characteristics and scaling laws for propeller wind milling drag (feather drag) are given in Reference [185, p.152ff]. A prediction method for the drag caused by a feathered, stopped propeller can be found in References [221, Eq. G-83] and [173, Eq. 12.40].

Beyond the basic flight mechanics, point performance calculation may incorporate the evaluation of system operational characteristics, such as

- the emission indices for  $NO_x$ ,  $CO$  and Unburned Hydro Carbons (UHC),
- essential engine temperature levels (e.g.  $T_3$ ,  $T_{4X}$ ),
- the aerodynamic and mechanical loadings of turbo components, or
- varying cabin power and bleed air demand.

Point performance characteristics can be calculated based on the full set of aircraft and engine design parameters previously determined during the system synthesis procedure. Inputs potentially required from downstream disciplinary analyses are supplied through iterative feedback.

### 5.6.2. Mission Simulation

In order to exploit the optimum fuel burn and emission reduction potentials of advanced aircraft and propulsion system configurations, the design operational conditions have to be considered. Therefore, the implemented methods emphasised on the full parametric, numerical simulation of typical mission profiles including a parameterised 4-segment climb schedule:

1. Climb and acceleration at constant calibrated air speed (CAS): Below Flight Level (FL) 100, CAS is limited to  $250KCAS$  due to Air Traffic Control (ATC) laws [17, p.155].
2. Acceleration to CAS of 3<sup>rd</sup> climb segment.
3. Climb and acceleration at constant CAS until cruise Mach number  $M_{cr}$  is reached: Optimum CAS depends on a number of parameters including actual aircraft weight, cruise speed and considered objective function, e.g. fuel burn or operating costs. Recommended CAS schedules above 10,000 *ft* altitude are given in Reference [16, Table 9].
4. Climb at initial cruise Mach number  $M_{cr}$  above crossover altitude until the top-of-climb (TOC) point, i.e. initial cruise altitude, is reached.

The CAS for climb segments 1 and 3 are input parameters to the model. The simulation of cruise flight includes multiple options. The standard cruise schedule represents a constant level flight at initial cruise altitude and Mach number until the Beginning Of Descent (BOD) point is reached. Besides, the implemented mission model allows for the simulation of step-climb phases during cruise, as well as varying cruise speed. During descent flight, a Continuous Descent Approach (CDA) is assumed and simulated at constant descent angle  $\gamma_{desc}$ <sup>18</sup>, while checking maximal allowable descent rates. A typical mission profile, as well as the considered aircraft flight envelope are indicated in Figure A.7 in Appendix A. Engine design characteristics and aircraft disciplinary models are prepared to allow for system performance simulation throughout the operational envelope. In order to minimise numerical scatter, the discretisation of mission segments is tailored to ensure consistent flight states at the transition points between succeeding segments along the flight trajectory. The numbers of simulation nodes per mission segment are treated as individual inputs to the model.

The series of simulated flight states between departure and arrival constitutes the database of mission information. During mission simulation, trajectory information as well as aircraft and

<sup>18</sup>For the studies presented in Chapter 6,  $\gamma_{desc}$  is chosen  $3^\circ$ .

engine performance characteristics are tracked (cf. Section 5.6.1). Based hereon, characteristic mission operating points, such as take-off (T/O), TOC, ADP and BOD points are evaluated with respect to important design and performance constraints. Based on the series of simulated flight states, cumulative metrics for aircraft mission performance can be computed, including block fuel and time (gate-to-gate).

The fuel burned during flight phases  $W_{F,trip}$ , is calculated from a simple numerical integration scheme, i.e. summing up the product of time  $\Delta t_i$  and representative fuel flow  $\dot{m}_{F,i}$  for the simulated flight intervals:

$$W_{F,trip} = \sum_{i=1}^{n_I} \Delta t_i \cdot \dot{m}_{F,i} = \sum_{i=1}^{n_I} \Delta t_i \cdot FN_{req,i} \cdot SFC_i \quad (5.34)$$

where  $n_I$  represents the number of simulated intervals.  $FN_{req,i}$  and  $SFC_i$  refer to the total required thrust and the engines' specific fuel consumption calculated for the representative flight state of the  $i^{th}$  simulation interval. For the computation of block fuel  $W_{F,block}$ , fuel burn during taxi-out, take-off, landing and taxi-in is added based on constant fractions of aircraft  $MTOW$ .  $W_{F,block}$  forms the basis for the prediction of aircraft exhaust emission characteristics. Gaseous emissions of hydrocarbon-fueled aircraft primarily consist of  $CO_2$ , water vapour ( $H_2O$ ),  $NO_x$ ,  $UHC$  and soot (cf. also Reference [100, Section 4.9.5]).

The mission model is applicable to the simulation of aircraft design and off-design mission simulation. Off-design missions within the payload-range envelope may be compiled to operational scenarios in order to investigate the robustness and flexibility of a predefined aircraft design with respect to the expected operational portfolio. As part of the overall aircraft design and sizing procedure, the mission model provides a number of results that are used for feedback correlations to iterate initially estimated values, such as engine design thrust  $FN_{des}$  and aircraft  $MTOW$ .

### 5.6.3. Mapping of Aircraft Sizing Constraints

For the identification of feasible design solutions, a number of operational requirements resulting from airworthiness regulations have to be considered as system sizing constraints during aircraft design. In the present context, the airworthiness standards for transport category aircraft (cf. Reference [54]) apply. Hereof, the minimum required climb rates for take-off with OEI, missed approach with OEI, and TOC point, as well as the stall speed margins during take-off and approach are taken into account for the basic sizing of the wing and the engines. Central system performance characteristics, including the required Take-Off Field Length ( $TOFL$ ) and Landing Field Length ( $LFL$ ), the aircraft aerodynamic efficiencies and stall speeds, aircraft weights and engine thrust lapse behaviour are obtained from the preceding disciplinary analyses.

Engine geometric sizing refers to MCL at TOC conditions (cf. Section 5.2.2) which are normally most critical for flow path dimensioning in case of transport aircraft powered by very high bypass turbofan engines (i.e.  $BPR_{des} > 5$ ). However, thrust demands during take-off or OEI operation may supersede the engine sizing requirements at TOC, e.g. in case of strict  $TOFL$  targets. Moreover, turbine temperature limits may stipulate reduced thrust

availability during low-speed operation. In order to account for this during aircraft design optimisation, the thrust scaling factor  $c_{FN,MCL}$  is introduced as

$$c_{FN,MCL} = \frac{FN_{req,TOC}}{FN_{des}} \quad (0.8 \lesssim c_{FN,MCL} \leq 1) \quad (5.35)$$

where  $FN_{des}$  refers to the thrust value used for engine sizing, and  $FN_{req,TOC}$  represents the actual TOC thrust requirement per engine for the aircraft design mission. Accordingly,  $c_{FN,MCL} = 1$ , if  $FN_{req,TOC}$  is most critical to engine sizing. In case take-off or OEI minimum thrust constraints are active,  $c_{FN,MCL} < 1$ , yielding oversized engines with respect to the TOC point.

The formulation of the aircraft's performance metrics during low-speed operation are summarised in Table 5.6, yielding balanced  $TOFL$  and  $LFL$  (cf. Reference [223, p.7f].), as well as the achievable climb gradients for the relevant OEI cases ( $\gamma_{AP,OEI}$  and  $\gamma_{TO,OEI}$ ). During system-level design optimisation studies, these metrics are translated to nonlinear constraint functions (cf. Section 6.2.1).

Table 5.6.: Basic formulation of aircraft performance metrics during low-speed operation

Operating Condition	Formulation
<b>Landing</b>	$LFL = \frac{c_{LFL}}{c_{L,AP}} \cdot \frac{MTOW}{S_{ref}} \cdot \frac{MLW}{MTOW} \cdot \frac{\rho_{SL}}{\rho_{LTO}}$
<b>Nominal Take-Off</b>	$TOFL = \frac{c_{TOFL}}{c_{L,TO}} \cdot \frac{MTOW}{S_{ref}} \cdot \frac{MTOW \cdot g}{n_{EI} \cdot FN_{TO}} \cdot \frac{\rho_{SL}}{\rho_{LTO}}$
<b>Take-Off (OEI)</b>	$\gamma_{TO,OEI} = \frac{n_{EI}-1}{n_{EI}} \cdot \frac{n_{EI} \cdot FN_{TO} - D_{WM}}{MTOW \cdot g} - \frac{1}{(L/D)_{TO}}$
<b>Missed Approach (OEI)</b>	$\gamma_{AP,OEI} = \frac{n_{EI}-1}{n_{EI}} \cdot \frac{n_{EI} \cdot FN_{TO} - D_{WM}}{MTOW \cdot g} \cdot \frac{MTOW}{MLW} - \frac{1}{(L/D)_{AP}}$
Nomenclature:	
$LFL$ - landing field length	$c_{LFL}$ - empirical landing parameter
$c_{L,AP}$ - approach lift coefficient	$MTOW$ - maximum take-off weight
$S_{ref}$ - wing reference area	$MLW$ - maximum landing weight
$\rho_{SL}$ - air density at sea level	$\rho_{LTO}$ - ambient air density at airport
$TOFL$ - take-off field length	$c_{TOFL}$ - empirical take-off parameter
$c_{L,TO}$ - take-off lift coefficient	$\gamma_{AP,OEI}$ - climb gradient for missed approach (OEI)
$FN_{SLS}$ - engine SLS thrust	$\gamma_{TO,OEI}$ - climb gradient for take-off (OEI)
$D_{WM}$ - OEI wind milling drag	$(L/D)_{TO}$ - lift-to-drag in take-off configuration
$n_{EI}$ - no. of installed engines	$(L/D)_{AP}$ - lift-to-drag in approach configuration

The evaluation of sizing constraints, here, is based on the equivalent take-off thrust  $FN_{TO}$  per engine (at Sea Level,  $M_0 = 0.2$ ) which is determined as a function of engine design thrust  $FN_{des}$  according to the definitions made in Section 5.2.6. The thrust lapse during take-off roll (for  $M_0 < 0.2$ , i.e.  $FN_{TO}/FN_{SLS}$ ), is accounted for using the empirical take-off parameter  $c_{TOFL}$  (cf. Reference [109, p.104ff]) which is adjusted for the thrust low speed thrust lapse of different types of propulsion systems as given in Reference [173, Figure 5.4]. The empirical landing field length parameter  $c_{LFL}$  is derived from Loftin [109, p.104ff]. The lift coefficients in take-off  $c_{L,TO}$  and approach  $c_{L,AP}$  configuration directly result from

the airworthiness requirements [54] as a function of the maximum lift coefficient  $c_{L,max}$  in low-speed configuration which is treated as an input to the model.

#### 5.6.4. Aircraft Scaling Procedure

At the beginning of the aircraft design synthesis procedure (cf. Section 3.2), a number of design parameters have to be estimated which, in fact, result from calculations performed later on during the process. The correspondingly required feedback correlations are handled using a gradient-free iteration strategy (cf. Section 3.2.3). For a given sequence of the disciplinary modules (cf. Figure 3.2), the number of feedback correlations to be handled in the iterative scheme for aircraft design scaling depends on the following aspects:

- the parameterisation of the employed methods for the physics-mapping,
- the considered system architecture / topology, as well as
- the considered aircraft design / analysis application (cf. Section 3.2.4)<sup>19</sup>

As an example, a typical scheme of feedback correlations used for aircraft design scaling during the studies presented in Chapter 6 is discussed in the following. The scheme includes 8 parameters  $V_{it,i}$  that require initial estimation, and subsequent iterative solving. Accordingly, aircraft  $MTOW$ , longitudinal center of gravity position  $x_{GC,a/c}$ , design mission block fuel  $W_{F,Block}$ , required engine thrust at TOC conditions  $FN_{req,TOC}$  and take-off conditions  $FN_{TO}$ , the lever arms for the horizontal  $L_{HT}$  and vertical  $L_{VT}$  tails, as well as aircraft minimum stall speed  $V_{stall}$  are iterated. The scheme of feedbacks is summarised in Table 5.7, including the sources of calculated iteration values  $V_{it,cal,i}$  (cf. “Output from”) and corresponding models requiring iterative input of initial estimation parameters  $V_{it,est,i}$  (cf. “Feedback to”).

Table 5.7.: Typical scheme of feedback information used for aircraft scaling during the present studies

Parameter	Output from	Feedback to
$MTOW$	design mission simulation	→ wing geometry
$x_{GC,a/c}$	aircraft balancing	→ landing gear geometry
$W_{F,Block}$	design mission simulation	→ wing geometry
$FN_{req,TOC}$	design mission simulation	→ engine geometry
$FN_{TO}$	design mission simulation	→ pylon weight
$L_{HT}$	aircraft balancing	→ horizontal tail geometry
$L_{VT}$	aircraft balancing	→ vertical tail geometry
$V_{stall}$	low-speed aerodynamics	→ landing gear weight

The feedback scheme shown in Table 5.7, as well as the implemented models for the disciplinary subtasks of the aircraft conceptual synthesis procedure are subject to comprehensive validation in the following chapter.

<sup>19</sup>i.e. the number of applied design laws, such as additional heuristics for the geometric scaling of system components, as well as the mass-performance-loop

## 6. Demonstration of the Methodology

In this chapter, a number of integrated aircraft and propulsion system design studies are presented and discussed in order to demonstrate the validity of the methods introduced in the previous chapters, as well as the additional insight in system behaviour enabled by the overall methodological approach elaborated in this thesis. The methodology, therefore, is applied to selected design aspects including the identification of optimum bypass ratios for turbofan engines, as well as a parametric design comparison of turbofan and open rotor powered aircraft. The presented results are based on the integrated evaluation of the design analysis methods discussed in Chapter 5 which have been implemented in the disciplinary subtasks and the aircraft synthesis scheme introduced in Chapter 3. Propulsion system design aspects are integrated in the disciplinary analyses using FNN-based surrogate models, created from comprehensively parameterised GasTurb 11 engine models. The required data sampling refers to the approach presented in Chapter 4. The presented studies focus on mission fuel characteristics, in the first instance. Initial results on important emission characteristics including  $CO_2$ ,  $NO_x$  and noise can be found in References [191] and [192] which are closely related to the present work.

### 6.1. Validation of Models

The proposed discipline-oriented integration of engine design aspects in the aircraft synthesis process has been verified through the successful implementation of the methods introduced in Chapter 5. The process used for engine data sampling based on GasTurb 11 Engine Decks can be found validated in Chapter 4. The validity of results obtained from the custom-developed methods for aircraft and propulsion system mapping is discussed and evaluated in Chapter 5. Supplementary validation figures and tables can be found in Appendices A and B. However, validation of the overall aircraft conceptual design synthesis is yet required. In the following, the numerical validity of the proposed aircraft iteration strategy is demonstrated. Subsequently, the physics of the implemented models are validated using an Airbus A320 aircraft equipped with IAE<sup>1</sup> V2500 engines.

#### 6.1.1. Verification of System Iteration Strategy

For the training and validation of system-level surrogate models, the simulation of multidimensional sampling plans is required. Here, consecutively simulated sample points take the respectively preceding convergent results as iteration starting points. Therefore, the independence of iteration convergence from iteration starting values is vital. In the present section, the validity of the implemented iterative scheme for aircraft design scaling is shown. Thereby,

---

<sup>1</sup>IAE (International Aero Engines)

## 6. Demonstration of the Methodology

its robustness against bad estimation values and potential starting value dependencies are analysed.

For the verification of the iteration strategy, quasi-random start value settings  $V_{it,est,i}$  were applied to independent quasi-random aircraft design settings  $V_{free,i}$  applicable to generic M/R configurations. Therefore, individual LHS-designs were generated for  $V_{it,est,i}$  and  $V_{free,i}$ , each featuring 10 samples. The generated start value cases  $S_{SV,j}$  characterised by the parameters listed in Table 5.7 are displayed in Table B.4 in Appendix B. A large space of iteration start settings was covered by the cases  $S_{SV,j}$ . The scatter of iteration starting values relative to the finally converged iteration values  $V_{it,conv,i}$  reached up to 25%.

The considered aircraft design cases  $S_{AD,i}$  are displayed in Table B.5. Here, 12 typical aircraft design parameters were varied, producing continuous as well as topological design changes:

- Mach number  $M_{ADP}$  and altitude  $alt_{ADP}$  at aerodynamic design point,
- propulsion system installation location  $PS_{loc}$  and tail plane configuration  $Tail_{con}$ ,
- the technology scaling factor for aircraft structural weights  $f_{tech,W}$ ,
- aircraft maximum structural payload weight  $W_{pl}$  and its design range at  $R_{des}$ ,
- wing reference area  $S_{ref}$  and aspect ratio  $AR_{wing}$ ,
- fuselage length  $L_{fus}$ , as well as
- engine design thrust scaling factor  $c_{FN,MCL}$  and design bypass ratio  $BPR_{des}$ .

The set of iteration start cases  $S_{SV,j}$  was applied to each aircraft design cases  $S_{AD,k}$  and the iterative solving procedure was performed on the design synthesis process. The under-relaxation parameter  $\alpha_{relax}$  (cf. Equation 3.3) was chosen 0.4 for all  $V_{it,est,i}$ . The convergence goal  $E_{RMS}$  (cf. Equation 3.4) was defined as  $1.0 \times 10^{-6}$ . All combinations of  $S_{SV,j}$  and  $S_{AD,k}$  converged within a maximum number of 30 iteration steps.

In order to assess potential starting value dependencies of the obtained convergent results, the scatter  $E_{SC}$  of converged iteration values  $V_{it,conv,i}$  between the investigated start value cases  $S_{SV,j}$  was analysed for each aircraft design case  $S_{AD,k}$ . Therefore, the mean converged iteration values  $V_{it,mean,i}$  were calculated for each  $S_{AD,k}$

$$V_{it,mean,i} = \frac{\sum_{j=1}^{n_{SV}} V_{it,conv,i}(S_{SV,j})}{n_{SV}} \quad (6.1)$$

where  $n_{SV}$  refers to the number of different start value settings  $S_{SV,j}$ . Taking mean converged iteration values  $V_{it,mean,i}$ , the convergence scatter  $E_{CS,j}$  for the individual  $S_{SV,j}$  was determined using the root mean squared error definition introduced in Equation 3.4.<sup>2</sup>

In Figure 6.1, the convergence scatter characteristics  $E_{CS,j}$  obtained for the investigated aircraft design cases  $S_{AD,k}$  are depicted. The determined  $E_{CS}$  values range from approximately  $6.0 \times 10^{-9}$  to  $5.0 \times 10^{-6}$ . These orders of magnitude demonstrate that the convergence behaviour for the investigated aircraft design cases  $S_{AD,k}$  is independent from the studied start value settings  $S_{SV,j}$ . In Figure 6.2 (overleaf), 3-view drawings of the aircraft configurations calculated for the design settings  $S_{AD,k}$  are shown.

<sup>2</sup>Due to the nonlinear nature of the  $E_{CS}$  metric with respect to the defined convergence goal  $E_{RMS}$ , the obtained maximum values of  $E_{CS,j}$  may exceed  $E_{RMS}$ .

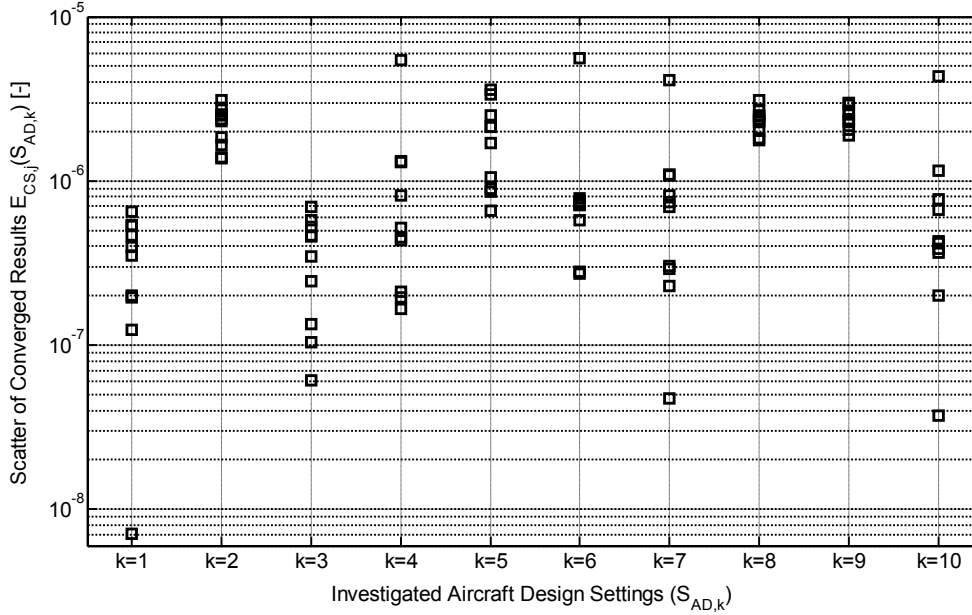


Figure 6.1.: Analysis of iteration convergence behaviour for the aircraft configurations shown in Figure 6.2

The significance of the results shown in Figure 6.1 is based on the fact, that for both groups of setting cases ( $S_{AD,k}$  and  $S_{SV,j}$ ) quasi-random sample plans were used, ensuring a high probability of result validity. However, system convergence and bijective response behaviour, still, depend on the nonlinear behaviour of the implemented models. Thus, in case starting value dependency occurs, the best convergent solution (with respect to the targeted design objective) may be adopted for further use.

In order to investigate the overall numerical accuracy of the implemented models, a study of the convergence behaviour during aircraft sizing was performed. Therefore, an arbitrary aircraft configuration was used, and iteration starting values  $V_{it,est,i}$  were initialised 10% below the expected convergent values  $V_{it,conv,i}$ . The iteration system corresponded to Table 5.7. Convergence of the iterative aircraft sizing procedure could be shown for convergence goals  $E_{RMS} < 10^{-8}$ . Thereby, the mission simulation procedure could be verified to produce adequately smooth results, i.e. a low level of numerical noise, due to the chosen discretisation of flight segments. The smooth response behaviour of the employed FNN-based surrogate models was of particular importance, in this context. In summary, the proposed gradient-free iteration strategy proved to be efficient and robust during the studies conducted as part of the present work.

### 6.1.2. Propulsion System

The powerplant chosen for the validation of the implemented propulsion system design and performance models is IAE's V2500 Series, which represents high bypass ratio turbofan engines featuring long duct mixed flow (LDMF) nacelles. V2500 engines are in service on the Airbus A320 family and on the Boeing MD-90 twinjet [83]. Available ratings range from

6. Demonstration of the Methodology

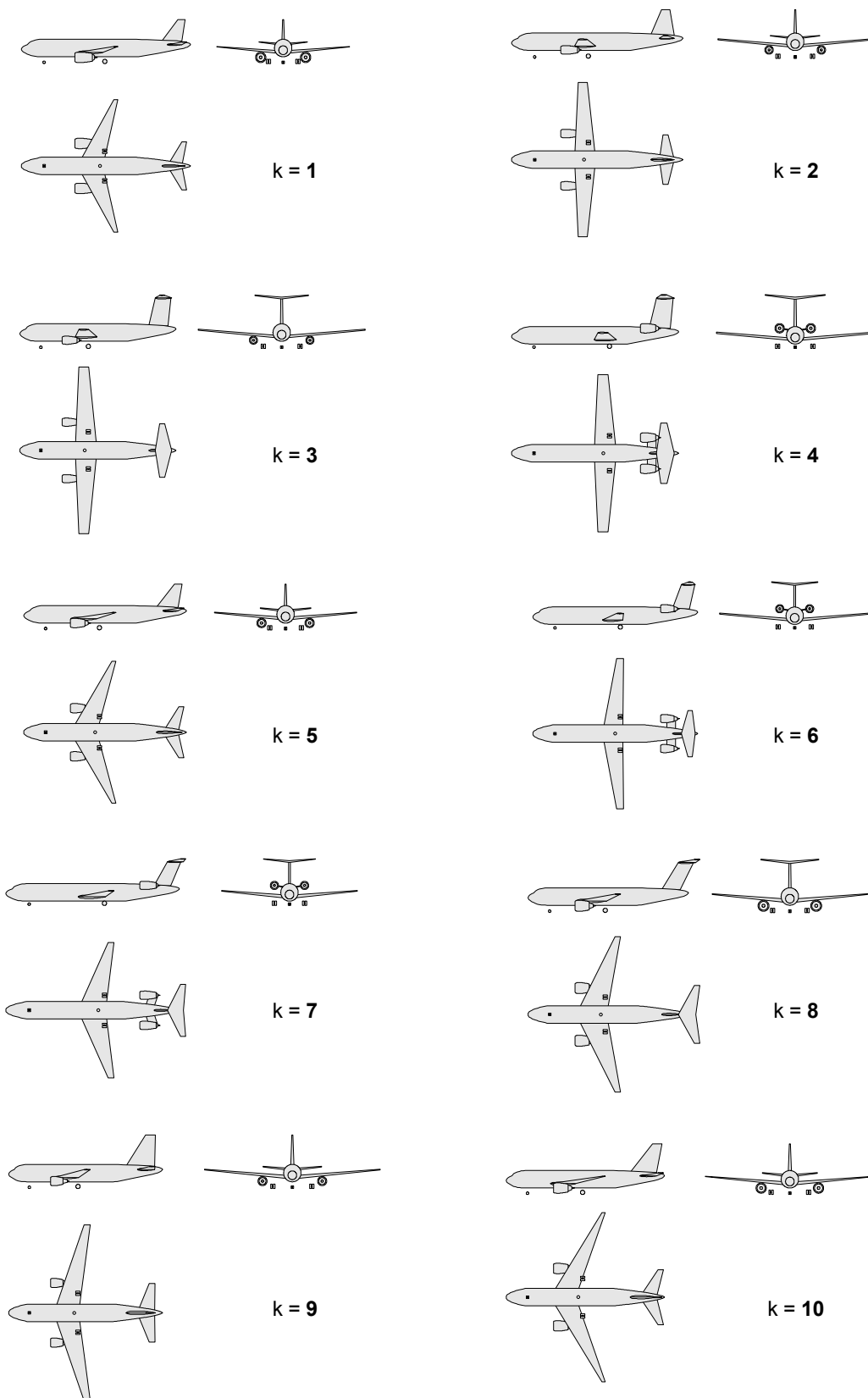


Figure 6.2.: 3-view drawings of the aircraft configurations calculated from the investigated design cases  $S_{AD,k}$

102kN to 142kN (23000lbf to 32000lbf) take-off thrust [83]. For the Airbus A320-200, two evolution options of V2500 are available: the V2500-A1 type which was certified in 1988 and the V2530-A5 series types which were launched in 1995 [83]. The latter feature a 4-stage booster and a 0.5" increased fan diameter relative to V2500-A1 baseline.

The validation results presented in this section refer to a full parametric mapping of the design and performance based on the methods presented in Section 5.2. Therefore, component loss coefficients were calibrated to match the pressure losses and component efficiencies given in Reference [186, Table 5-6f]. Turbo component axial Mach numbers referred to Reference [186, Table 5-9], while turbo component hub/tip ratios were measured from an engine 2-dimensional general arrangement given in Reference [81]. HPT cooling air mass flows were chosen according to Reference [48, Figure 2-4]. GasTurb standard fuel featuring a lower caloric value ( $FHV$ ) of  $43.124 MJ/kg$  [105] was used.

For the validation of engine geometric mapping, turbo component diameters were considered significant. The check parameters used for the assessment of computed performance characteristics included the specific fuel consumption at design conditions, as well as bypass ratio, fan pressure ratio, overall pressure ratio, net thrust and engine inlet mass flow at take-off conditions. The turbo component stage configurations as well as essential design settings at MCL conditions were treated as inputs during model validation.

A synopsis of representative design and performance characteristics calculated for the V2530-A5 engine is given in Table 6.1 (overleaf). The relative deviation of computed results from the data given in References [83, 186] and [81] is denoted in percent. The comparison of calculated characteristics and literature data exhibits good agreement of values. Turbo component diameters are slightly underestimated, yielding a maximum error at HPC inlet of  $-2.7\%$ . The largest error of calculation results concerns the overall pressure ratio at take-off conditions which deviates by approximately 12% from the value given in the literature (cf. Reference [83]). This, however, has only a minor impact on the targeted performance characteristics, here. The errors identified for all other check parameters are of the order of 2% or less.

### 6.1.3. Overall Aircraft

In order to assess the validity of the implemented methods for aircraft design and performance mapping an Airbus A320 aircraft configuration was used. The Airbus A320 is a classic twin-engine, cantilever low-wing, conventional tail aircraft configuration. Two alternative engine options are available including the SDSF nacelle CFM56-A5 and LDMF nacelle V2530-A5 series powerplants. The latter type of engines was considered for aircraft model validation, in the current context. Therefore, FNN were generated for essential design characteristics of the previously validated V2530-A5 model. The FNN were parameterised for flight Mach number  $M_0$ , flight altitude  $alt$  and power setting  $PLA$ , as well as engine design thrust  $FN_{des}$  in order to allow for automated engine thrust scaling during aircraft design.

The validation results presented in the following include the models implemented for all design disciplines discussed in Chapter 5. Therefore, the full aircraft sizing procedure was performed, including mass-performance-loop, as well as engine, tail plane and landing gear sizing, based on the iteration scheme given in Table 5.7. An A320 design mission calculation was considered representative for the assessment of model quality. The validation data required for the

Table 6.1.: Model validation: Overview of IAE V2530-A5 design synthesis results

Stage Configuration	Ref.	Validation Results		
		Value <sup>a</sup>	Unit	Error <sup>b</sup> [%]
Fan	[83]	1	–	<i>n/a</i>
Booster	[83]	4	–	<i>n/a</i>
HPC	[83]	10	–	<i>n/a</i>
HPT	[83]	2	–	<i>n/a</i>
LPT	[83]	5	–	<i>n/a</i>
<b>Turbo Component Diameters</b>				
Fan	[83]	1.609	<i>m</i>	–0.3
Booster Inlet <sup>c</sup>	[81]	0.925	<i>m</i>	–1.2
HPC Inlet <sup>c</sup>	[81]	0.572	<i>m</i>	–2.7
HPT Exit <sup>c</sup>	[81]	0.668	<i>m</i>	–1.5
LPT Exit <sup>c</sup>	[81]	0.936	<i>m</i>	–1.2
<b>Performance at Maximum Climb Point</b>				
Mach Number	[186]	0.78	–	<i>n/a</i>
Altitude	[186]	10668	<i>m</i>	<i>n/a</i>
Bypass Ratio	[186]	4.60	–	<i>n/a</i>
Net Thrust	[186]	26.69	<i>kN</i>	<i>n/a</i>
SFC	[186]	17.33	<i>g/kg·s</i>	+0.8
<b>Performance at Max. Takeoff Point (Static Sea Level, ISA+15K)</b>				
Bypass Ratio	[83]	4.52	–	–1.7
Overall Pressure Ratio	[83]	35.8	–	+11.9
Fan Pressure Ratio	[83]	1.78	–	–1.1
Net Thrust	[186]	140.01	<i>kN</i>	+0.2
Engine Inlet Mass Flow	[83]	394.2	<i>kg/s</i>	+1.3

<sup>a</sup> Calculated values are based on fully parameterised engine design synthesis according to Section 5.2.

<sup>b</sup> errors of calculated values relative to reference values, errors of input parameters are marked as *n/a*

<sup>c</sup> reference values measured from 2-dimensional general arrangement

assessment of the computed A320 characteristics were taken from References [10, 8, 84] and [194]. The settings and conditions used for A320 design mission simulation involved

- the simulation of maximum range at maximum structural payload for  $MTOW = 73500kg$  (cf. Reference [8, Chapter 2.1.1]), including 200nm diversion flight, 30min hold<sup>3</sup> and 10% final fuel reserves,
- the application of A320 standard climb law as given in Reference [16, p.44],
- cruise at constant Mach number ( $M_{cr} = 0.78$ ) and altitude ( $alt_{cr} = FL350$ ),
- a continuous descent from BOD conditions at 3° descent angle (cf. Figure A.7),
- the use of constant fuel weight fractions for ground operational phases as defined in Section 5.6.2,
- considered field lengths for take-off and landing:  $TOFL = 2200m$  and  $LFL = 1800m$  (cf. Reference [8, Chapters 3.3.2 and 3.4.1]), as well as
- the assumption of ISA, still air conditions.

Validation was performed in two steps, allowing for an individual validation of the methods used for structural weight estimation and system performance prediction. In the first step, aircraft characteristics were directly computed based the input of essential geometric parameters, an overview of which is given in Table B.6 in Appendix B. This type of investigation allowed for the assessment of the validity of structural weight prediction.<sup>4</sup> In a second step, the calculated OWE value was corrected in order to match the OWE value given in the literature. Therefore, the OWE residual weight value  $W_{res}$  is adapted. The second step allowed for the validation of the implemented performance model. In Table 6.2 (overleaf), a summary of representative validation results is given. Here, the first step of validation is referred to as “Weights Validation”, while the second is labeled as “Performance Validation”.

More detailed synopses of the results are listed in Tables B.6 and B.7 in Appendix B. Here, the mapping of geometric characteristics, as well as the calculated break downs of structural and operational weights are compared to the corresponding data available in the literature. The comparison of calculated structural weights and validation data reveals that major structural groups such as wing and fuselage are underestimated by the implemented methods. The resulting underestimation of OWE imposes aircraft performance characteristics. Therefore, design mission fuel  $W_{F,TO}$  is predicted 3.9% to low during weights validation. After OWE calibration,  $W_{F,TO}$  calculation deviates by only 0.5% from the reference value derived from Reference [8, Chapters 2.1.1 and 3.2.2]. The computed aerodynamic efficiencies  $L/D$  at typical cruise conditions exhibit good agreement with the data given in Reference [194, Chapter 5.1]. The absolute value of aircraft maximum thrust loading  $FN_{SLS,tot}/MTOW$  is sensitive to  $L/D$  at TOC condition as well as the considered  $TOFL$  requirements (cf. Table 5.6). The obtained relative error of approximately  $-7\%$  for  $FN_{SLS,tot}/MTOW$ , therefore, results from the small absolute values of both, calculated and validation data. Additional plausibility is added to the obtained validation results, considering the computed aircraft geometry which is shown as a 3-view drawing in Figure 6.3 (overleaf).

<sup>3</sup>Hold is simulated using the performance characteristics determined at BOD point of diversion flight.

<sup>4</sup>The results obtained, here, were slightly influenced by the repercussive effects of the underestimated  $MTOW$ .

## 6. Demonstration of the Methodology

Table 6.2.: Summary of model validation results for Airbus A320 / IAE V2500

Weights	Ref.	Unit	Weights Validation		Performance Validation	
			Value <sup>a</sup>	Error <sup>b</sup>	Value <sup>a</sup>	Error <sup>b</sup>
<i>MTOW</i>	[10]	<i>kg</i>	70,665	-3.9	73,565	+0.1
<i>OWE</i>	[8]	<i>kg</i>	37,971	-6.1	40,429 <sup>c</sup>	±0.0
<b>Aerodynamics<sup>d</sup></b>						
<i>L/D</i> ( $c_L = 0.4$ )	[194]	-	15.7	+2.5	15.6	+1.8
<i>L/D</i> ( $c_L = 0.5$ )	[194]	-	17.1	+1.3	17.0	+0.7
<i>L/D</i> ( $c_L = 0.6$ )	[194]	-	17.6	+1.4	17.5	+0.9
<b>Performance</b>						
<i>MTOW/S<sub>ref</sub></i>	[84]	<i>kg/m<sup>2</sup></i>	577.3	-3.9	601.0	+0.1
<i>FN<sub>SLS,tot</sub>/MTOW</i>	[84]	-	0.305	-6.7	0.303	-7.3
<i>W<sub>F,TO</sub></i> <sup>e</sup>	[8]	<i>kg</i>	12,415	-2.9	12,857	+0.5

<sup>a</sup> Calculated values are based on full aircraft design and sizing procedure.

<sup>b</sup> Error values are given relative to reference values according the relative error definition introduced in Equation 3.8.

<sup>c</sup> OWE is calibrated for performance validation using OWE residual value  $W_{res}$  (cf. also Table 5.3).

<sup>d</sup> aerodynamic efficiencies for typical cruise conditions:  $FL350$ ,  $M = 0.78$  (reference data taken from Reference [194, Chapter 5.1])

<sup>e</sup> 1550nm mission, maximum payload, 200nm diversion, 30min hold and 10% fuel reserves

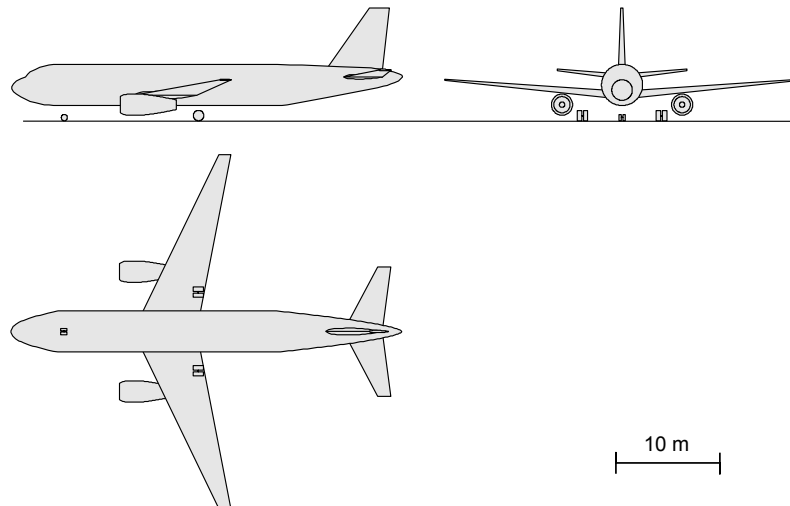


Figure 6.3.: 3-view drawing of the calculated Airbus A320 / IAE V2500 aircraft configuration

## 6.2. Parametric Design Studies

In the present section, the applicability of the proposed methodological setup to integrated system-level design studies is demonstrated. At first, the handling of aircraft performance constraints and the handling of typical objectives for design optimisation is discussed and demonstrated. Subsequently, optimum constellations for exemplary system design parameters are investigated. For the present purpose, the design bypass ratio  $BPR_{des}$  of turbofan engines and aircraft aerodynamic design Mach number  $M_{ADP}$  are considered as insightful parameters:  $BPR_{des}$  is an engine design parameter with significant system-level impact, affecting multiple aircraft disciplines including the geometric sizing of major components and propulsion system integration options, aircraft balancing and aerodynamics, as well as overall system performance. The identification of adequate  $BPR_{des}$  requires system-level analyses and, therefore, represents a meaningful subject for the targeted methodological demonstration. The particular significance of  $M_{ADP}$  in terms of mission fuel consumption and emission characteristics has been indicated by numerous studies in the past (cf. References [191] and [193]). The effect of cruise speed on aircraft operational cost is not in the focus of studies presented in the following chapter, however, the the methodological framework allows for the incorporation of operational cost as well as life cycle cost mapping in the aircraft conceptual design and analysis process.

Finally, the impact of varying technology status on optimum system characteristics is investigated. Therefore, 4 technological scenarios are introduced and comparatively studied. All studies performed, focus on a generic M/R transport task which is outlined in Table B.8 in Appendix B. The studies presented in this section focus on a classic M/R aircraft layout featuring a low-wing installation, under-wing mounted turbofan engines, wing-mounted main landing gear and a conventional tail arrangement. The considered type of engine refers to a SDSF-nacelle, 2-spool boosted turbofan architecture with directly-driven fan.

### 6.2.1. Setup of Optimisation

System design optimisation may focus on different objective functions, including classic performance, operating costs, noise, or environmental impact metrics, aircraft family and life cycle considerations as well as multi-share composed objective functions.<sup>5</sup> Practically, aircraft are designed for low operating costs, which include the aircraft ownership, crew and fuel cost, as well as navigation charges and landing fees. Due to the high share of fuel costs on long-haul flights, long range (L/R) aircraft are typically optimised for minimum fuel consumption. For short range (S/R) aircraft, the high number of cycles is a major design driver. Here, system optimisation often targets minimum *MTOW*.

In the present context, for system-level design analyses a surrogate-based optimisation strategy (cf. also References [87] and [86]) is used. Based on LHS-distributed starting points in the parametric input space  $F$ , the algorithm performs local gradient-based search according to Reference [214], thereby, realising a simplistic global search strategy. The fast responding behaviour of surrogate model approximations allows for parametric “optimisation-in-the-loop” studies. Before optimisation can be conducted, the generation of surrogate models is required for targeted system characteristics. The first step of optimisation preparation, therefore, is

---

<sup>5</sup>multi-objective optimisation

## 6. Demonstration of the Methodology

the selection of free parameters for the study  $\vec{V}_{free}$ . The free parameters used for the studies in this section are listed below:

- design cruise Mach number  $M_{ADP}$
- design altitude  $alt_{ADP}$
- wing reference area  $S_{ref}$
- engine MCL thrust scaling factor  $c_{FN,MCL}$
- engine design bypass ratio  $BPR_{des}$
- engine aerodynamic loss scaling factor  $f_{tech,ps}$

The preparation for optimisation subsequently involved the LHS-based simulation of aircraft designs  $S_i(\vec{V}_{free})$ . For the simulated aircraft designs the necessary result characteristics  $Y_i$  for surrogate model training and validation were recorded. While data recording may apply to all parameters that are available in the aircraft data model (cf. Section 3.2.1), the parameters  $Y_i$  of primary interest for the studies presented in the following include:

- design mission block fuel  $W_{F,block,des}$
- maximum take-off weight  $MTOW$
- engine design thrust  $FN_{des}$
- engine take-off thrust  $FN_{TO}$
- engine thrust requirement  $FN_{req,TOC}$  at TOC conditions
- the aerodynamic efficiency  $L/D$  at TOC conditions
- the aerodynamic efficiency  $L/D$  at ADP conditions
- the engines' specific fuel consumption  $SFC$  at ADP conditions
- required take-off field length  $TOFL$
- required landing field length  $LFL$
- achievable climb gradient during missed approach (OEI)  $\gamma_{AP,OEI}$
- achievable climb gradient during take-off (OEI)  $\gamma_{AP,OEI}$

The computation of aircraft designs  $S_i(\vec{V}_{free})$  was based on the aircraft scaling procedure verified in the previous section. The handling of aircraft sizing and performance constraints referred to Section 5.6.3. The generation and validation of FNN ( $\hat{Y}_i = \hat{f}(\vec{V}_{free})$ ) was conducted as described in Section 3.3. For the subsequent aircraft design optimisation,  $TOFL(\vec{V}_{free})$ ,  $LFL(\vec{V}_{free})$ ,  $\gamma_{AP,OEI}(\vec{V}_{free})$  and  $\gamma_{TO,OEI}(\vec{V}_{free})$  were considered as nonlinear constraints, in the first instance.

Additional nonlinear constraint functions may be added to the optimisation task if necessary. A classic constraint for wing sizing is the available wing tank volume  $V_{tank}(\vec{V}_{free})$  which is of particular interest for long design ranges. For the study cases presented in the following, the  $V_{tank}(\vec{V}_{free})$  was not as critical as  $LFL(\vec{V}_{free})$  for minimum wing size, and therefore, not issued in the discussion of the shown results.

As previously mentioned,  $W_{F,block}(\vec{V}_{free})$  and  $MTOW(\vec{V}_{free})$  are classic objective functions to be minimised during aircraft design optimisation. Now, Figure 6.4 shows the partial trends of  $W_{F,block,des}$  and  $MTOW$  against the design variables  $V_{free}$  listed above. The shown results are based on the FNN approximation of 1500 aircraft designs sized using the iteration scheme according to Table 5.7. The distributions represent the unconstrained SuMo responses  $\hat{Y}_i$  based on the aircraft scaling procedure. The visualisation refers to the MPD view which directly shows potential optimisation variables. It can be seen that the partial impacts of  $S_{ref}$  and  $BPR_{des}$  on both objectives are well-applicable to optimisation. The trends of  $W_{F,block,des}$

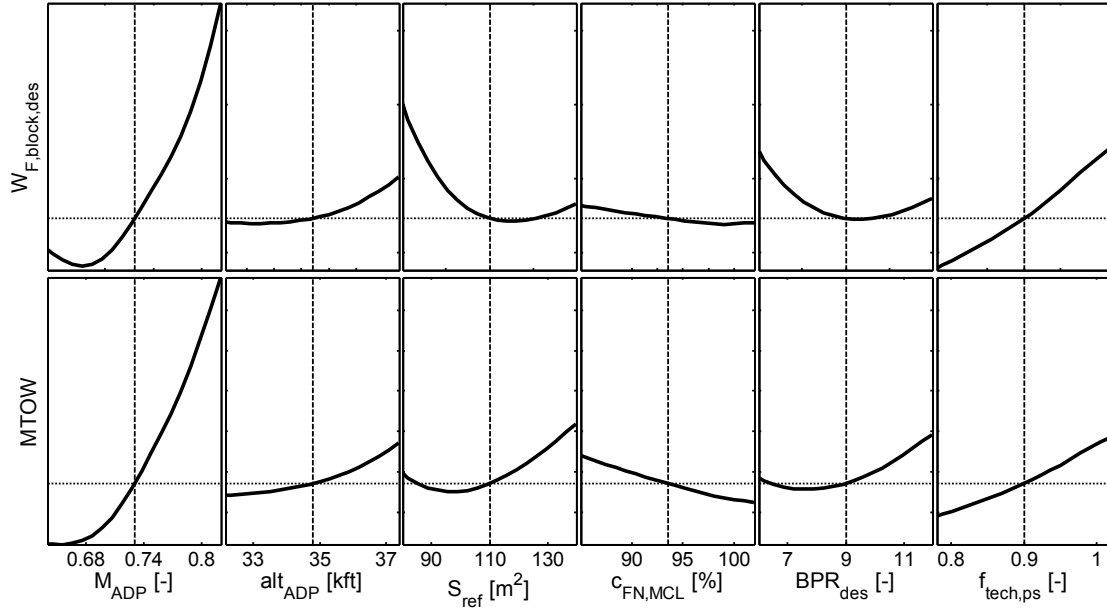


Figure 6.4.: Partial impact of exemplary system design parameters on design mission block fuel and aircraft  $MTOW$  for a typical medium range application visualised using the matrix of partial dependencies view

and  $MTOW$  against  $c_{FN,MCL}$  are monotonic, yielding minimum  $W_{F,block,des}$  and  $MTOW$  for  $c_{FN,MCL} = 100\%$ , i.e. the smallest possible engine, if only the MCL sizing constraint is considered. The consideration of  $c_{FN,MCL}$  as an optimisation variable is necessary in order to satisfy the thrust requirements during low-speed operation at all potential constraint constellations, e.g. for strict  $TOFL$  requirements.

The trends shown in the figure visualise the differing design optima for optimum fuel burn and aircraft weight. It can be seen, that minimum  $MTOW$  requires a smaller wing and a lower engine bypass ratio, i.e. a geometrically smaller engine, compared to the fuel burn (respectively  $CO_2$  emission) optimum. A significant impact on both objectives is emanating from the aircraft's aerodynamic design number  $M_{ADP}$  which exhibits a fuel burn optimum at approximately  $M_{ADP} = 0.68$  for the shown example case. The location of the relatively flat optimum of  $W_{F,block,des}$  versus  $alt_{ADP}$  is a strong function of  $S_{ref}$ . The fuel burn and  $MTOW$  trends against the engine's aerodynamic loss scaling factor  $f_{tech,ps}$  are monotonic, as expected. For the studies presented in the following,  $M_{ADP}$  and  $T_{tech,ps}$  are considered array parameters,  $alt_{ADP}$  corresponds to flight level  $FL350$ , in the first instance.

### 6.2.2. Performance Constraint Analysis

For the optimisation of aircraft design parameters, the basic sizing requirements discussed in Section 5.6.3 have to be considered as constraints to the available parametric space. The constraints acting on essential aircraft sizing parameters are typically visualised in the “performance constraint chart”, also referred to as “aircraft matching chart” [109], showing the aircraft thrust loading  $F_{NTO,tot}/MTOW$  against wing loading  $MTOW/S_{ref}$ . In Figure 6.5 (overleaf), an exemplary performance constraint chart is depicted, resulting from a wing size,

## 6. Demonstration of the Methodology

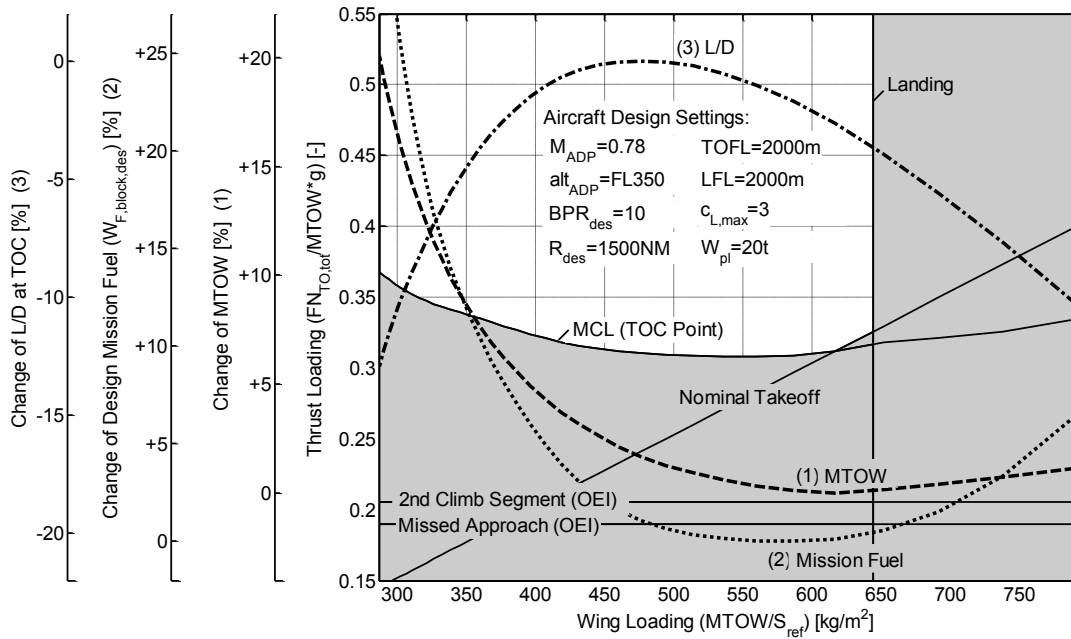


Figure 6.5.: Performance constraint chart gained from advanced medium range aircraft design study

i.e. reference area  $S_{ref}$ , study. Here, the engine thrust scaling factor  $c_{FN,MCL}$  was optimised for minimum design mission fuel burn  $W_{F,block,des}$  while meeting the previously discussed constraint functions. The figure includes all information relevant for the example case.

The criticality of the individual sizing constraints depends on a multitude of design characteristics. Low-speed operational constraints are essentially driven by the take-off and landing length requirements and the low-speed aerodynamics, i.e. the achievable lift coefficients and the additional drag share due to extended flaps, slats and landing gear. The MCL constraint for minimum thrust loading is determined by the aerodynamic efficiencies  $L/D$  at TOC conditions and the engine-specific thrust lapse rates of the investigated aircraft designs (cf. Section 5.6.3). Stronger thrust lapse due to the reduction of engine specific thrust, e.g. through an increase of turbofan design bypass ratio  $BPR_{des}$ , elevates the MCL constraint in the aircraft matching chart, while the enhancement of aerodynamic technology, i.e. an increase of  $L/D$ , lowers the MCL constraint.

For wing loadings  $MTOW/S_{ref}$  below  $620\text{kg/m}^2$  in Figure 6.5, the engine thrust scaling factor  $c_{FN,MCL}$  equals 100%. Here, the MCL constraint is significant for the optimum thrust sizing of the engines. Above wing loadings of  $620\text{kg/m}^2$ , the nominal take-off constraint is active, yielding reduced values of  $c_{FN,MCL}$  as a result of the optimisation for a given wing size  $S_{ref}$ . Here, take-off is simulated at maximum engine power settings as defined in Section 5.2.6.

The additionally shown distributions of aircraft  $MTOW$  (1), design mission fuel burn  $W_{F,block,des}$  (2) and the aerodynamic efficiency  $L/D$  at TOC conditions (3) refer to scaled aircraft designs with minimum feasible thrust loading  $FN_{TO,tot}/MTOW$  based on the discussed optimisation constraints. The reference points of the corresponding ordinate axes refer to the respective constrained optima. It can be seen that optimum wing loadings for  $W_{F,block,des}$ ,  $MTOW$  and  $L/D$  at TOC differ noticeably. While minimum  $MTOW$  occurs at a high wing

loading close to the  $LFL$  constraint, optimum wing loadings for minimum  $W_{F,block,des}$  are slightly reduced (cf. also Figure 6.4). The impact of the nominal take-off constraint on optimum fuel burn and  $MTOW$  above wing loadings of  $620\text{kg}/\text{m}^2$  is visible from the chart. The aerodynamic efficiency  $L/D$  at TOC is a strong function of  $c_L$  at TOC. For invariant Mach number and altitude at TOC,  $c_L$  directly correlates to  $S_{ref}$  and the aircraft weight at TOC, the latter of which is closely correlated to  $MTOW$ . Due to the increasing  $MTOW$  against decreasing wing loading, the  $L/D$  optimum at TOC is shifted to lower wing loadings (cf. Figure 6.5).

### 6.2.3. Investigation of Turbofan Bypass Ratio

The system-level impact of the bypass ratio of turbofan engines is analysed in References [193] and [42]. However, the technology-dependence has never been shown parametrically based on a consistent methodological setup including the parametric conceptual design of the propulsion system, the aircraft and essential mission aspects. In the following, the developed methodology is applied to the determination of optimum bypass ratios of classic 2-spool boosted turbofan engines with direct fan-drive for varying operational and technological conditions. Therefore, a conventional aircraft layout including under-wing mounting of the powerplants is considered (cf. Figure 5.10). The considered M/R air transport task, as well as essential simulation settings are summarised in Table B.8 in Appendix B.

#### 6.2.3.1. System-Level Effects of Bypass Ratio

The system-level impact of turbofan bypass ratio basically emanates from the growing fan diameter connected to increasing  $BPR$ . In Figure 6.6 (overleaf), the relative variations of important aircraft design metrics are visualised against varying design bypass ratio  $BPR_{des}$ : design mission block fuel  $W_{F,block,des}$  (1),  $MTOW$  (2), as well as specific fuel consumption  $SFC$  (3) and aerodynamic efficiency  $L/D$  (4) at ADP conditions. Here, ADP is defined by the cruise condition which corresponds to 50% fuel weight relative to  $W_{F,block,des}$ . The reference points of the shown ordinate axes refer to the respective best design case. The engine and aircraft designs involved in the depicted distributions are based on identical technology settings. The underlying technological scenario is explained in the next section. For the study, wing reference area  $S_{ref}$  and the engine design thrust scaling factor  $c_{FN_{MCL}}$  are at optimum for minimum  $W_{F,block,des}$ .

It can be seen that the isolated impact of  $BPR_{des}$  on  $W_{F,block,des}$  amounts to approximately 5% in the investigated application case, featuring minimum design mission block fuel at  $BPR_{des} = 10$ . The further increase of  $BPR_{des}$ , here, yields fuel burn penalties. The fuel burn characteristics against  $BPR_{des}$  are directly correlated with the further characteristics shown in the figure. The technology corrected  $SFC_{ADP}$ -benefit of  $BPR_{des} = 12$  relative to  $BPR_{des} = 6$  represents approximately 7%, in the shown case.<sup>6</sup> The corresponding increase of fan diameters yields 34%. The resulting impact on engine weight can be seen in Figure 5.13. Now,  $MTOW$  represents the allowable sum of the aircraft's structural and operational weights, i.e. the operating weight empty  $OEW$ , payload  $W_{pl}$  and design mission fuel consumption  $W_{F,block,des}$  plus final fuel reserves. The shown trend of  $MTOW$  against  $BPR_{des}$ , therefore,

<sup>6</sup>essential cycle characteristics including  $T_4$  and  $OPR$  unchanged.

## 6. Demonstration of the Methodology

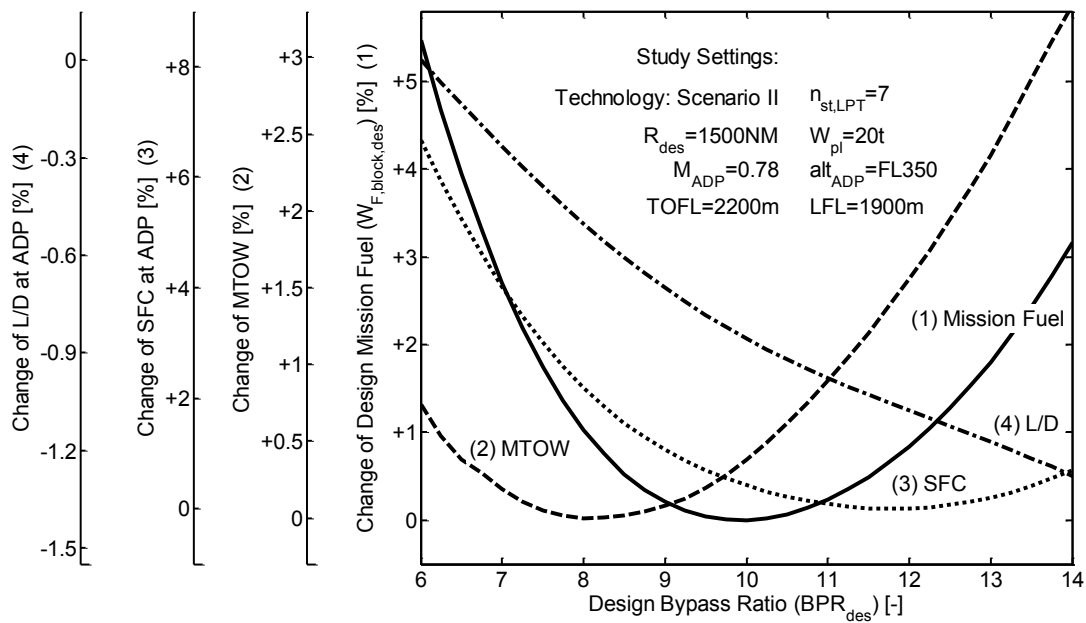


Figure 6.6.: Impact of varying turbofan bypass ratio on essential aircraft metrics

includes the variation of engine weight, as well as the fuel burn implications and cascade effects.

Increasing  $BPR_{des}$  also imposes on aircraft drag, due to the increase of nacelle wetted area emanating from the growing fan diameter and the extension of cowling length.<sup>7</sup> The increase of nacelle area, however, is mitigated by the effect of reducing fan pressure ratio  $p_{13}/p_2$  against increasing  $BPR_{des}$  (cf. Figure A.5 in Appendix A). In summary, the share of the installed nacelles wetted areas (including pylon) relative of the sum aircraft wetted areas increases from about 7% at  $BPR_{des} = 6$  to approximately 9% at  $BPR_{des} = 14$ , which translates to a change of aircraft aerodynamic efficiency  $L/D$  of 1.3% in the shown case.

Studies related to the present research have shown, that optimum  $BPR_{des}$  values are much higher if the intrinsic limitations of the direct-drive turbofan architecture are neglected [193]. The characteristics shown in Figure 6.6, however, well-correspond to the trends of block fuel and  $MTOW$  against bypass ratio identified during NASA's Ultra-Efficient Engine Technology (UEET) studies as given in Reference [42, Figure 3.16]. The UEET studies focused on large aircraft. The derived values for optimum  $BPR$ , therefore, exceed the currently identified values by approximately 15%.

### 6.2.3.2. Technology Impact on Optimum Bypass Ratio

For the further studies of engine design bypass ratio presented in the following, 4 generic technological scenarios were considered. The scenarios included engine as well as airframe-specific parameters which may be treated as technologically dependent inputs to the model. They were constructed using the technology-scaling parameters introduced in the previous

<sup>7</sup>Similar aerodynamic interference factors and transonic drag rise characteristics assumed for the calculation of nacelle drag.

chapter. A synopsis of the scenario cases is given in Table 6.3. Scenario I is considered to be representative for state-of-the-art existing M/R aircraft. Scenarios II - IV characterise elevated technology states. While Scenarios II and III consider either advanced engine or airframe technology, Scenario IV represents a combination of both enhancements.

Table 6.3.: Synopsis of technological scenarios for system level design studies

Propulsion Design	Unit	Technology Scenarios			
		I <sup>a</sup>	II	III	IV
$OPR$ at MCL	–	35	+5	<i>base</i>	+5
$T_4$ at MCL	$K$	1550	+200	<i>base</i>	+200
Loss Scaling Parameter $f_{tech,ps}$	–	1	–0.15	<i>base</i>	–0.15
<b>Structural Weight Factors <math>f_{W,tech,i}</math></b>					
Wing Group	–	1	<i>base</i>	–0.15	–0.15
Fuselage Group	–	1	<i>base</i>	–0.15	–0.15
Empennage Group	–	1	<i>base</i>	–0.15	–0.15
Landing Gear Group	–	1	<i>base</i>	–0.15	–0.15
Propulsion Group	–	1	–0.15	<i>base</i>	–0.15
OWE Residual	–	1	<i>base</i>	–0.15	–0.15
<b>Aerodynamics</b>					
Wing Flow Transition $x_{trans,wing}$	–	0.05	<i>base</i>	+0.2	+0.2
Oswald Correction $f_{OS,tech}$	–	1	<i>base</i>	+0.05	+0.05
Korn Factor $F_{Korn}$	–	0.91	<i>base</i>	+0.03	+0.03

<sup>a</sup> Scenario I is considered as a technological baseline scenario.

The representation of engine technological variation is represented by the cycle parameters burner exit temperature  $T_4$  and overall pressure ratio  $OPR$ , as well as the aerodynamic loss scaling factor  $f_{tech,ps}$ . For the scenarios featuring advanced engine technology, an increase of  $T_4$  by 200K and an enhancement of the  $OPR$  value by 5 was considered. Here, enhanced turbine cooling technology and increased allowable material temperatures were assumed, compensating the elevated compressor exit and turbine inlet temperatures. Therefore, all technology scenarios were simulated using identical turbine cooling air settings, in the first instance. Further aspects for technological scenarios, such as customer bleed and mechanical power offtakes, e.g. for more electric engine concepts, were neglected, in the first instance. Spool mechanical efficiencies were treated constant. Aerodynamic losses were assumed to be reduced by 15%.

For aircraft structural technology mapping the scaling factors  $f_{W,tech,i}$  were applied to the component weights calculated according to the methods presented in Section 5.4. For advanced technology, the calculated weights were reduced by 15%. Aerodynamic technology levels were mapped using the wing's relative flow transition coordinate  $x_{trans,wing}$ , a correction of the induced efficiency  $f_{OS,tech}$ , as well as Korn's factor  $F_{Korn}$  for the transonic drag rise characteristics of lifting surfaces. Aerodynamics were enhanced through a back-shift of  $x_{trans,wing}$  by 0.2, a increase of Oswald's efficiency by 5%, a Korn's factor increment of 0.03.

Based on these technology scenarios, the impact of turbofan bypass ratio on aircraft design

## 6. Demonstration of the Methodology

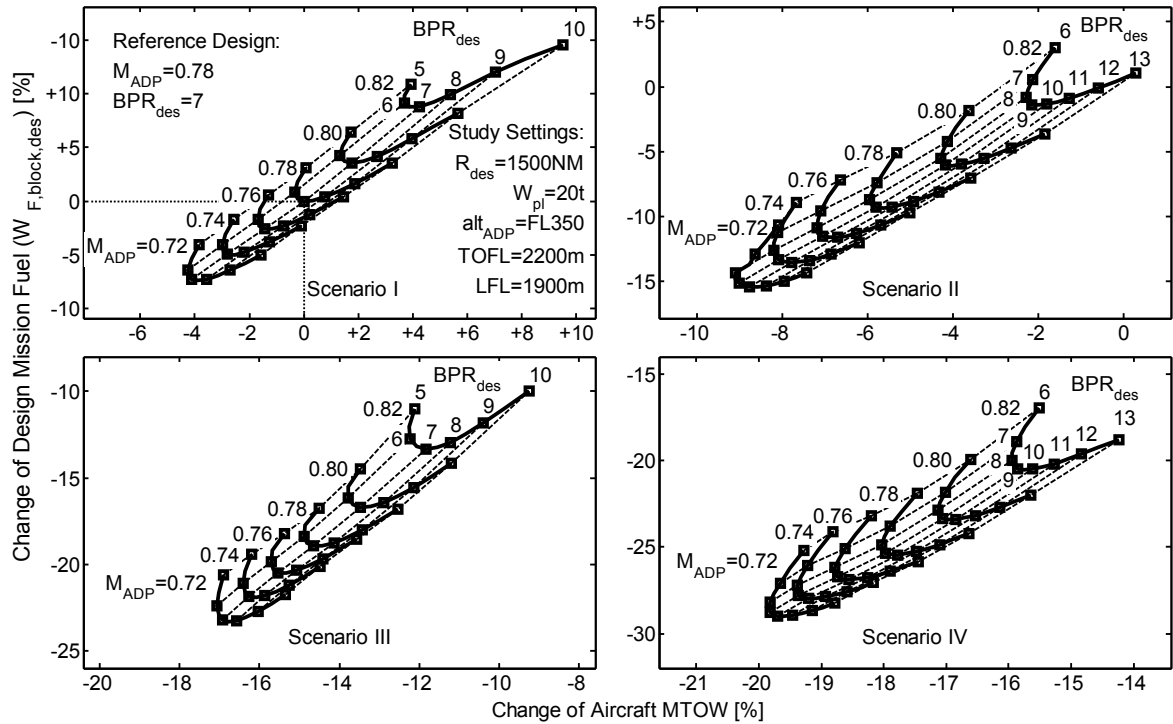


Figure 6.7.: Comparison of technology scenarios according to Table 6.3 with respect to design block fuel and  $MTOW$  as a function of turbofan bypass ratio and aircraft aerodynamic design Mach Number

mission fuel consumption  $W_{F,block,des}$  and  $MTOW$  were analysed for different aerodynamic design Mach numbers  $M_{ADP}$  ranging from 0.72 to 0.82. All investigated turbofan designs featured 2-stage HPTs and 7-stage LPTs. The numbers of booster and HPC pressure stages was iterated as functions of predefined  $OPR$  and optimum  $FPR$ . The obtained results are summarised in Figure 6.7, showing a synopsis of Scenarios I - IV. In each of the 4 charts, the resulting  $W_{F,block,des}$  characteristics are plotted against calculated  $MTOW$ . For the study, again,  $S_{ref}$  and  $c_{FN_{MCL}}$  are at optimum for minimum  $W_{F,block,des}$ . The chosen visualisation allows for the direct  $BPR_{des}$  trade-off between fuel burn and aircraft weight which is of great importance for the assessment of aircraft operational costs.

The values of  $W_{F,block,des}$  and  $MTOW$  determined for the design parametric variations are given relative to the reference design at  $M_{ADP} = 0.78$  and the corresponding optimum  $BPR_{des} = 7$ . The value is in good agreement with numbers reported in recent publications (cf. Reference [68, Figure 4]). For Scenarios I and III,  $BPR_{des}$  was varied from 5.0 to 10, for Scenarios II and IV, studied  $BPR_{des}$  range from 6.0 to 13. The charts illustrate the fuel burn and  $MTOW$  reduction potentials connected to the individual technology scenarios, as well as individual impacts of  $BPR_{des}$  and  $M_{ADP}$ . The plotted carpets illustrate the trade-off between  $W_{F,block,des}$  and  $MTOW$  against varying  $BPR_{des}$ .

The displayed reduction potentials for  $W_{F,block,des}$  and  $MTOW$  emanate from two basic effects. Firstly, the enhancement of engine and airframe technology levels, and secondly, the impact of design operational conditions which are represented by  $M_{ADP}$ . The isolated influence of technological enhancements according to assumed scenarios is summarised in

Table 6.4. Here, a comparison of  $W_{F,block,des}$  and  $MTOW$  for system designs with optimum  $BPR_{des}$  at reference  $M_{ADP}$  based on the different scenarios is given.

Table 6.4.: Comparison of technology scenarios at aerodynamic design Mach number 0.78 with respect to design mission fuel and aircraft

Scenarios	$BPR_{des,opt}$ [-]	$\Delta W_{F,block,des}$ [%]	$\Delta MTOW$ [%]
<b>I</b>	7.1	base	base
<b>II</b>	9.5	-9.6	-5.6
<b>III</b>	7.2	-19.2	-14.5
<b>IV</b>	9.8	-25.7	-17.8

For the combined technological enhancement of engine and airframe (Scenario IV), the fuel savings relative to the technological baseline ( $\Delta W_{F,block,des}$ ) amount to approximately 26%.  $MTOW$  is reduced by about 18%, simultaneously. The values given in the table suggest that optimum  $BPR_{des}$  varies insignificantly against airframe technological variation. Here, the major effects emanate from the reduced thrust requirements, which yields reduced fan diameters. However, due to constant mechanical power and bleed off-takes connected to the given transport task, and increase of optimum  $BPR_{des}$  values is counteracted. In contrast, the engine technological scenario settings impact considerably on optimum  $BPR_{des}$ . For fixed technology settings, the isolated impact of  $BPR_{des}$  on  $W_{F,block,des}$  amounts to about 5% (cf. also Figure 6.6). Including the assumed engine technological enhancement, e.g. Scenario II versus Scenario I, the block fuel impact of  $BPR_{des}$  approximately doubles.

The significant implication of aerodynamic design Mach number  $M_{ADP}$  on  $W_{F,block,des}$  and  $MTOW$  has been indicated in one of the partial dependencies shown in Figure 6.4. According to Figure 6.7, the isolated effect of  $M_{ADP}$  on fuel burn between  $M_{ADP} = 0.72$  and  $M_{ADP} = 0.82$  amounted to approximately 15%, which essentially emanated from the strong drag rise characteristics connected to the baseline Korn factor. Now, the maximum benefit in  $W_{F,block,des}$  and  $MTOW$  relative to the reference design is achieved based on technology scenario IV, choosing the minimum investigated aerodynamic design Mach number of  $M_{ADP} = 0.72$ . Here, the selection of  $BPR_{des,opt}$  yields a  $W_{F,block,des}$  reduction of approximately 29% compared to the reference design.  $MTOW$  is reduced by nearly 20%. The benefits of further reductions of  $M_{ADP}$  appear insignificant at the investigated aerodynamic design altitude as can be seen from Figures 6.4 and 6.8. Besides, the further reduction of cruise Mach number may have significant implications from an ATM point of view.

The influence of  $BPR_{des}$  on  $W_{F,block,des}$  increases with reducing  $M_{ADP}$  and the elevation of technology levels. For technology scenario IV, trends for the optimum  $BPR_{des}$  are given as a function of  $M_{ADP}$  in Figure 6.8. Additionally, the aerodynamic loss scaling factor  $f_{tech,ps}$  is varied between 0.75 and 0.95.

Figure 6.8 (overleaf) shows the relatively narrow range of optimum engine bypass ratios  $BPR_{opt}$  identified against the investigated system design Mach numbers. For Scenario IV ( $f_{tech,ps} = 0.85$ ), the values for  $BPR_{des,opt}$  range from 9.5 at  $M_{des} = 0.84$  to 11.1 at  $M_{des} = 0.64$ . For aerodynamic loss reductions ( $f_{tech,ps} = 0.75$ ), optimum  $BPR_{des}$  values are slightly increased, as a result of increasing engine thermal efficiency which, in turn, allows

## 6. Demonstration of the Methodology

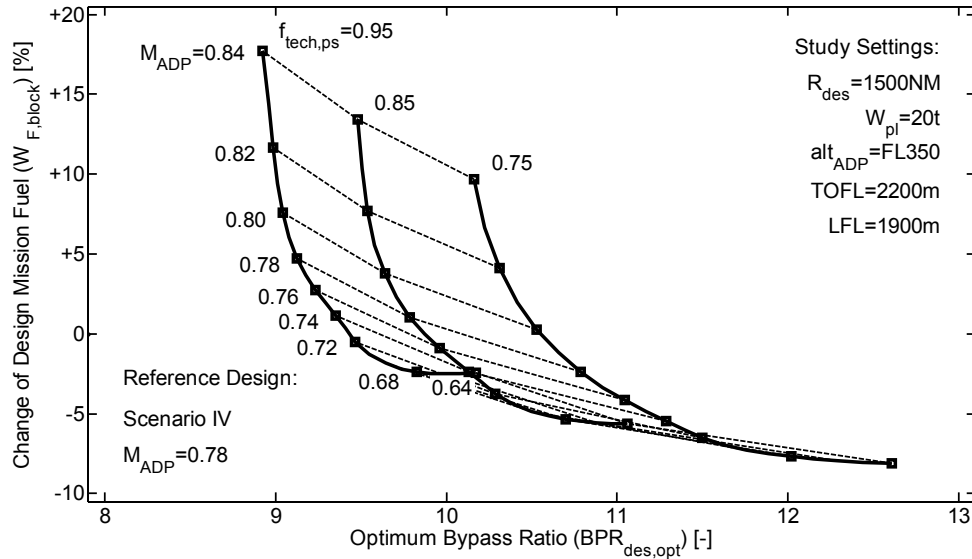


Figure 6.8.: Optimum turbofan bypass ratios against varying aircraft aerodynamic design Mach Number studies for different engine loss scaling factors based on technology scenario IV according to Table 6.3

for higher  $BPR_{des}$  at similar  $FPR$ . Now, the block fuel characteristics shown in the figure result from the superposition of the effects associated with reducing  $M_{ADP}$  and increasing  $BPR_{des}$ . At low  $M_{ADP}$ , the partial trend of  $W_{F,block,des}$  against  $M_{ADP}$  inverts (cf. also Figure 6.4) which can only be overcompensated by increasing  $BPR_{des}$  in case of strongly reduced aerodynamic losses.

### 6.2.3.3. Engine Architectural Implications

The variation of bypass ratio has significant impact on the many system components of turbofan engines. The  $SFC$  trend shown in Figure 6.6 is typical for advanced conventional turbofan engines. In particular, the turbo components connected to the low pressure (LP) spool are affected by  $BPR_{des}$  variation. Here, the growing fan diameter and simultaneous reduction of fan tip speed (cf. Reference [69, Figure 5.2.2.6a]) as a result of the reduced fan pressure ratio, but essentially driven by noise requirements, reduce LP spool speed. The correspondingly reduced blade speeds in boosters and LP turbines significantly increases the aerodynamic loadings  $\psi$  (cf. Equation 5.8) in these components, which typically results in efficiency penalties. A synopsis of empirical data and existing correlations for the prediction of stage loading impact on LP turbines is given in Reference [69, Figure 5.2.3.37]. Accordingly, for highly loaded turbines an efficiency decrement of the order of 1% per unit increase of  $\psi$  can be determined. The corresponding decrease in turbine efficiency predicted by the model introduced in Section 5.2.3 appear to be slightly overestimated (cf. also Figure 5.5).

Main limiting factors for the achievable optimum  $BPR_{des}$  and the connected fuel burn reduction potentials, hence, emanate from the investigated direct-drive turbofan architecture. In order to increase the optimum  $BPR_{des}$ , and thus, to increase optimum fuel efficiency beyond the regimes identified in the presented studies, a number of technological options are

available involving the layout of the affected turbo components, as well as the overall engine architecture. While design measures at the turbo component level, such as the increase of LPT stage count, hub/tip ratios or grid solidities, represent sensitive trade-offs between component aerodynamic operability and structural weight, significant additional potential is involved in engine architectural changes such as

- the introduction additional spools (3-spool engine configurations allow for an enhanced mechanical decoupling of high and low pressure aerodynamics),
- the introduction of new architectural components, such as a fan drive gearbox to reduce the aerodynamic mismatch of fan, booster and LPT, or
- the application of counter rotating LP spool systems.

## 6.3. Comparison of Alternative System Concepts

Even more drastic reductions in aircraft fuel consumption are expected from the application of unducted propulsor engine concepts. Essential parts of the design and analysis methods developed in Chapter 5, therefore, focus on the mapping counter rotating propeller engines, also referred to as open rotor engines. The case study presented in the following, focused on a comparative investigation of advanced conventional turbofan and counter rotating open rotor engines. Both concepts differ significantly in manifold characteristics involving aerodynamic, mechanical and aeroacoustic design as well as overall system architecture, therefore being well-suited for capability demonstration of the developed methodology.

### 6.3.1. Considered System Configurations

The preferable aircraft configuration for the installation of open rotor engines was discussed in Section 5.3.2. Accordingly, aft-fuselage engine-mounting and a T-tail arrangement were considered for open rotor powered aircraft studied in this section. The turbofan powered aircraft featured a conventional aircraft layout, i.e. conventional tail configuration and under-wing mounting of the engines. The investigated aircraft layouts can be found visualised in Figure 5.1. The considered engine configurations are outlined in the following.

The considered turbofan architectures referred to a classic 2-spool boosted turbofan featuring direct fan drive and SDSF nacelle, directly corresponding to the engine type analysed in Section 6.2. The investigated open rotor engine architecture is characterised as follows:

- 2-spool boosted turboshaft engine with booster connected to the power turbine (PT) spool,
- propulsor in tractor configuration,
- 6 + 6 bladed counter rotating propellers, and
- propellers driven by a counter rotating gear system.

The 2-spool configuration of the turboshaft engine was chosen for maximum communality with the turbofan architecture. According to Section 5.3.2, a tractor arrangement of propellers was preferred over a pusher configuration, while considering the aircraft weight balance due to the longitudinal positioning of the powerplant. For the implementation of a counter rotating propeller concept, different LP power train arrangements may be considered, involving counter rotating LPT, sequentially arranged power turbines (connected to shafts rotating in opposite

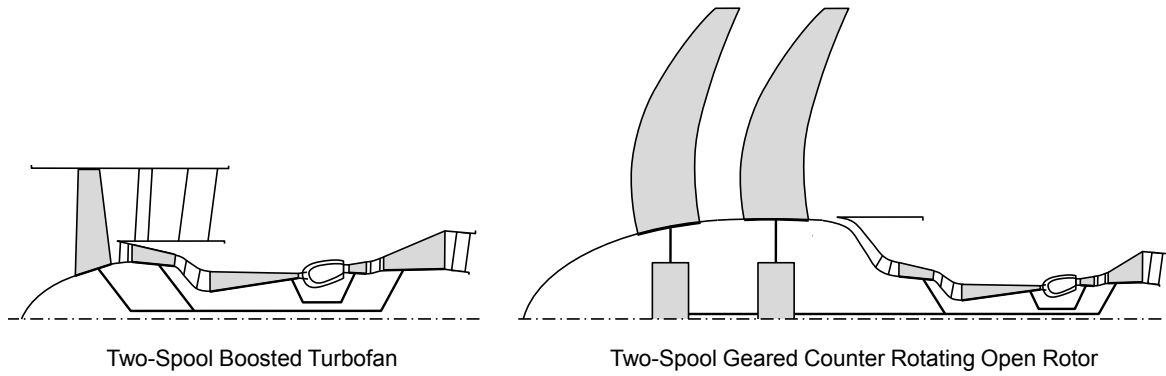


Figure 6.9.: Schematic visualisations of the comparatively investigated engine architectures

directions), as well as the application of a counter rotating gear system. Off-design behaviour of counter rotating open rotors strongly depends on power train arrangement. If driven by a counter rotating gearbox system rotational speed ratios are constant at any operational condition. For configurations driven by an integrated counter rotating LPT or via sequentially arranged free power turbines varying rotational speed ratios of the counter rotating rotors may superimpose additional challenges for the minimisation of vibrational rotor interference at potentially occurring operational condition. Hence, for the present investigation, a geared power train arrangement in tractor configuration was focused on.

In Figure 6.9 schematic visualisations of the investigated engine concepts are given. The displayed proportions illustrate the differences in engine size encountered during the present studies. All relevant aspects of engine design and integration were discussed in detail in Chapter 5.

### 6.3.2. Setup of the Study

The presented comparative design study was based on the design optimisation and performance analysis setup outlined in Sections 6.2.1 and 6.2.2. The study used the same transport task and design simulation settings as the analyses presented before (cf. Table B.8 in Appendix B). In order to ensure technological similarity of the investigated system concepts, both configurations were simulated based on technology Scenario IV according to Table 6.3. For the open rotor design investigation, propeller design power loading  $PL_{prop,des}$ <sup>8</sup> and blade tip speed  $V_{tip,prop}$  were used in correspondence to turbofan  $BPR_{des}$ . The open rotor propellers were operated at constant tip speed during mission simulation. Again, the design operational conditions were incorporated in the investigation based on the aerodynamic design Mach number  $M_{ADP}$ , while  $S_{ref}$  and  $c_{FN_{MCL}}$  were at optimum for minimum  $W_{F,block,des}$ . In the following, important aspects specific to the simulated open rotor powered aircraft designs are discussed.

The rotational speed of the PT spool was defined by booster blade tip speed. The varying propeller rotational speeds<sup>9</sup>, therefore, strongly affected the gear ratio of the drive-system.

<sup>8</sup> $PL_{prop,des} = PWSD/D_{prop}$ , where  $PWSD$  is the shaft power delivered by the power turbine, corrected for mechanical losses of the PT spool and propeller-drive gear system

<sup>9</sup>due to varying  $PL_{prop,des}$  and  $V_{tip,prop}$

The corresponding gearbox weight implications were mapped as explained in Section 5.4.2. However, the architectural implications of the gear-system were neglected, in the first instance. The power turbine was simulated using a 3-stage configuration.

Due to the higher efficiency of the propulsive device, the size of open rotor core engines is smaller than the core engine size of a turbofan powerplant delivering identical thrust. A meaningful measure for the geometric dimension of the core engine is the “core size” parameter which is defined by the HPC inlet mass flow, standard day corrected for HPC exit temperatures and pressures. For the investigated range of engine design thrust and OPR variation, the average core size of the analysed open rotor engines was approximately 20% reduced relative to the turbofan engines. The correspondingly calculated corrections of turbo component efficiencies for the open rotor engines ranged between  $-0.5\%$  and  $-0.9\%$ .

The impact of aft-fuselage mounting of the engines on aircraft fuel system weight is indicated in Reference [65, Table 2]. Accordingly, an extra charge of  $300kg$  was added to the OWE residual  $W_{res}$  of the open rotor powered aircraft investigated.

Potentially required cabin acoustic treatment for open rotor powered aircraft was not considered in the presented results. The corresponding weight penalties may be derived from References [179, Figure 21] and [38, Figure 3].

#### 6.3.3. Discussion of Simulation Results

A synopsis of the results gained from the comparative fuel burn study of open rotor and turbofan powered aircraft is presented in Figure 6.10 (overleaf). The figure contains three charts displaying the obtained trends of  $W_{F,block,des}$  against  $M_{ADP}$  (Chart I), turbofan  $BPR_{des}$  (Chart II) and open rotor  $PL_{prop,des}$  (Chart III). For the charts, a turbofan reference aircraft was chosen, featuring  $BPR_{des} = 10$  and  $M_{ADP} = 0.8$ . Chart I shows the direct comparison of the domains of turbofan and open rotor powered aircraft designs. The array parameters are  $BPR_{des}$  for turbofan domain and  $PL_{prop,des}$  for open rotor domain. Here, propeller tip speed is kept constant at  $237.7m/s$  ( $780fps$ ) in correspondence to the F7/A7 propeller design. For selected values of  $M_{ADP}$ , the characteristics of the individual aircraft domains are plotted against the corresponding array parameters (Charts II and III). The  $W_{F,block,des}$  reference point in the Figure refers to a turbofan powered aircraft designed for  $M_{ADP} = 0.8$  at optimum  $BPR_{des}$ .

The obtained fuel burn characteristics show significant benefits for the open rotor engine concept. Maximum identified advantages in  $W_{F,block,des}$  range from  $5\%$  at  $M_{ADP} = 0.84$  to approximately  $12\%$  at  $M_{ADP} = 0.64$ , due to the strong sensitivity of the open rotor concept to variations in  $M_{ADP}$ . This essentially emanates from the strong propeller design response and associated aircraft-level cascade effects due to changing  $M_{ADP}$ . Now, propeller sizing is a classic trade-off between propulsion system efficiency, installation structural weight implications, and the aerodynamic interaction of engine and airframe. As thrust requirements are elevated with increasing  $M_{ADP}$  - rooted in the rising compressibility drag - growing propeller diameters and cascaded aircraft design and performance implications strongly impact on  $W_{F,block,des}$ . An important design parameter for the identification of the best and balanced propeller diameters is  $PL_{prop,des}$  which may be optimised with regards to  $W_{F,block,des}$ .

## 6. Demonstration of the Methodology

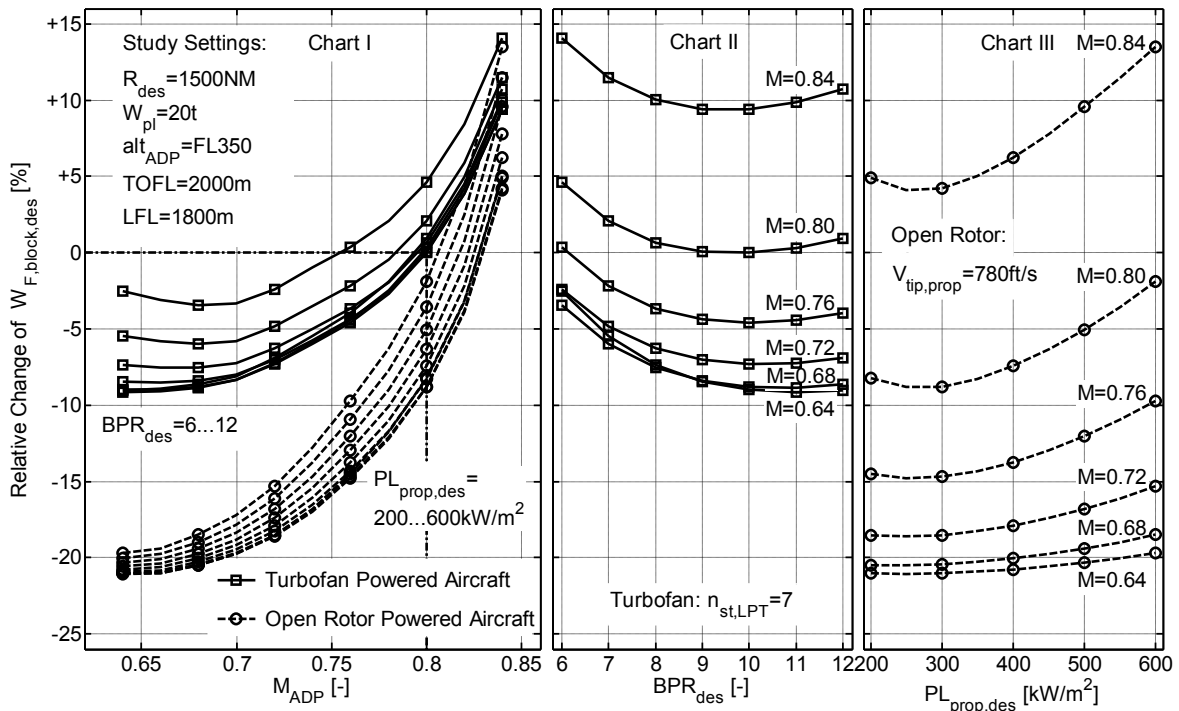


Figure 6.10.: Results of comparative study of fuelburn optimised turbofan and open rotor powered aircraft designed for different Mach numbers

In Table 6.5, a direct comparison of representative open rotor and turbofan powered aircraft is extracted from the charts in Figure 6.10, each featuring optimised  $PL_{prop,des}$  or  $BPR_{des}$ , respectively. It can be seen that the significant  $SFC$  benefits of the open rotor engine concept are compromised by the complex installation effects leading to considerable structural weight penalties of main airframe components. Therefore,  $MTOW$  of the open rotor powered aircraft is increased by approximately 5% relative to the turbofan powered aircraft, despite of reduced  $W_{F,block,des}$  and identical payload. Detailed weight breakdowns for advanced turbofan and open rotor powered aircraft are given in Reference [192, Table 1]. Beside the apparent  $MTOW$  implications,  $L/D$  of the open rotor powered aircraft during cruise is reduced relative to the turbofan powered aircraft, which mainly emanates from the additional drag due to the propeller slipstream.

The calculated relative block fuel reductions for the open rotor engine concept are considerably lower than numbers published in the past. An overview of representative open rotor fuel burn savings predicted in the past is given in Reference [192]. The reduced fuel margin results from the reduced difference in the overall efficiency of turbofan and open rotor engines as technology levels are elevated. Further penalties may be encountered for the open rotor concept, when considering the additional weights for potentially required cabin noise treatment and the propeller design trade-off between efficiency and noise.

Table 6.5.: Essential performance differences of representative Open Rotor (OR) and TurboFan (TF) powered aircraft

OR vs. TF <sup>a</sup>	Unit	$M_{ADP} = 0.70$	$M_{ADP} = 0.75$	$M_{ADP} = 0.80$
$\Delta SFC_{ADP}$	%	-18.3	-17.0	-16.4
$\Delta L/D_{ADP}$	%	-2.0	-2.7	-3.5
$\Delta MTOW$	%	+4.7	+5.2	+5.6
$\Delta W_{F,block,des}$	%	-11.4	-10.2	-8.8

<sup>a</sup> All numbers given relative to corresponding turbofan powered aircraft at identical  $M_{ADP}$ .

In order to gain more insight into the design features of the aircraft referred to in Table 6.5, a synopsis of essential design characteristics is given in Table 6.6 (overleaf). The corresponding aircraft 3-view drawings are visualised in Figure 6.11 (overleaf). The inspection of Table 6.6 instantly allows for plausibility checks for the computed aircraft designs:

- For all aircraft, the engine thrust sizing is defined by the MCL performance constraint. Hence, due to the stronger thrust lapse characteristics and the accordingly increased thrust availability the open rotor powered aircraft feature higher  $FN_{TO}/MTOW$ .
- Fuel optimum  $PL_{prop,des}$  values are below  $300kW/m^2$  for the investigated blade tip speed, however, increase for increasing  $M_{ADP}$  in response to the propeller size versus efficiency trade-off for increased design thrust requirements.
- As an optimum trade-off between the increased skin friction and wave drag shares<sup>10</sup> and the increased MTOW, the open rotor powered aircraft feature slightly higher wing loadings than the corresponding turbofan powered aircraft.
- For all aircraft,  $h_{lg}$  is constrained by the pitching freedom of the fuselage aft-contour. Moreover,  $h_{lg}$  values for the turbofan powered aircraft are not directly correlated to the trend in fan diameters, since dominated by the forward movement of aircraft center of gravity as wing sweep is reduced for the lower  $M_{ADP}$ .
- The obtained small fan diameters emanate from the low design thrust requirements of the turbofan powered aircraft.

It should be noted that the block fuel benefits of open rotor powered aircraft are essentially supported by the improved climb performance relative to the turbofan powered aircraft, therefore, enhancing the open rotor advantages for short stage lengths. The range dependency has not been analysed in depth during the present work, but should be considered during follow-up studies. Apart from that, the back-shift of aircraft center of gravity due to aft-fuselage mounting of the open rotor engines, yielded an increased size of the empennage during the studies (cf. Figure 6.11). However, the significant pylon reference area in case of aft-fuselage-mounted open rotor engines may contribute to the volume of the horizontal stabilizer. In the presented studies pylon volume was neglected during the calculation of longitudinal stability. However, in future studies, this effect should be taken into account and the fuel burn reduction potentials due to the reduced size of the empennage should be analysed.

As a second important propeller design parameter, blade tip speed  $V_{tip,prop}$  was analysed in correspondence to power loading. Beside the associated implications on  $W_{F,block,des}$ ,

<sup>10</sup>generated by the propeller slipstream and the larger empennage

## 6. Demonstration of the Methodology

Table 6.6.: Synopsis of essential design characteristics of the open rotor and turbofan powered aircraft depicted in Figure 6.11

Design Parameters	Unit	TF Aircraft			OR Aircraft		
		TF 1	TF 2	TF 3	OR 1	OR 2	OR 3
$M_{ADP}$	—	0.80	0.75	0.70	0.80	0.75	0.70
$alt_{ADP}$	$FL$	350	350	350	350	350	350
$c_{FN,MCL,opt}$	%	100	100	100	100	100	100
$S_{ref,opt}$	$m^2$	102.1	102.5	111.1	109.3	107.2	114.4
$PL_{prop,des,opt}$	$kW/m^2$	$n/a$	$n/a$	$n/a$	269.4	256.0	237.7
$BPR_{des,opt}$	—	9.6	10.0	10.5	$n/a$	$n/a$	$n/a$
$FN_{des}$	$m$	17.5	16.2	15.4	20.2	18.1	17.1
$D_{prop}$	$m$	$n/a$	$n/a$	$n/a$	4.39	4.11	4.02
$D_{fan}$	$m$	1.52	1.49	1.48	$n/a$	$n/a$	$n/a$
$h_{lg}$	$m$	2.47	2.52	2.59	1.80	1.80	1.80
$x_{CG,a/c,rel}^b$	%	0.43	0.42	0.41	0.56	0.54	0.53
$FN_{TO}/MTOW$	%	31.3	30.4	30.3	40.2	37.6	37.5
$MTOW/S_{ref}$	$kg/m^2$	580.3	563.8	509.9	581.7	567.6	521.5
<b>Performance Metrics as relative Delta to TF1<sup>a</sup></b>							
$\Delta SFC_{ADP}$	%	<i>base</i>	−3.3	−6.6	−16.4	−19.7	−23.7
$\Delta L/D_{ADP}$	%	<i>base</i>	+9.4	+15.8	−3.5	+6.4	+12.3
$\Delta MTOW$	%	<i>base</i>	−2.5	−3.9	+7.3	+2.5	+0.7
$\Delta W_{F,block,des}$	%	<i>base</i>	−5.0	−8.5	−8.8	−15.9	−19.8

<sup>a</sup> represents reference point in Figure 6.10

<sup>b</sup> relative to fuselage length

$V_{tip,prop}$  also has a major impact on propeller noise emission characteristics as can be seen in References [124, 57] and [191]. The results gained from the  $W_{F,block,des}$  study while treating  $V_{tip,prop}$  as the array parameter for the open rotor engine concept are given in Figure A.12 in Appendix A. For given F7/A7  $PL_{prop,des}$ , decreasing blade tip speed stipulated an increasing propeller power coefficient yielding a net reduction of  $\eta_{prop}$ , which reduced the open rotor block fuel benefits, particularly at high  $M_{ADP}$ . The reduction of  $V_{tip,prop}$ , however, may be an important measure for the reduction for propeller noise (cf. References [191, 192]). Thus, in order to gain a better understanding of the potential trade-off between fuel burn and noise emission characteristics of the open rotor engine concept, the influence of  $V_{tip,prop}$  on block fuel should be investigated in detailed follow-up studies.

Finally, by superimposing the identified numbers for the open rotor benefit on  $W_{F,block,des}$  and the fuel savings for the most advanced turbofan scenario relative to the technological baseline, the cumulative fuel reduction potentials of the open rotor concept may be derived. Accordingly, for  $M_{ADP} = 0.78$  open rotor block fuel is reduced by approximately 33% relative to baseline technology. By reducing  $M_{ADP}$  for the open rotor powered aircraft to a value 0.7, the overall reduction of  $W_{F,block,des}$  is increased to 38%. If related to the underlying technological scenarios, these numbers may be reflected with regards to the strategic research targets for future transport aircraft. In turn, requirements and boundary conditions for the development of new technologies may be identified.

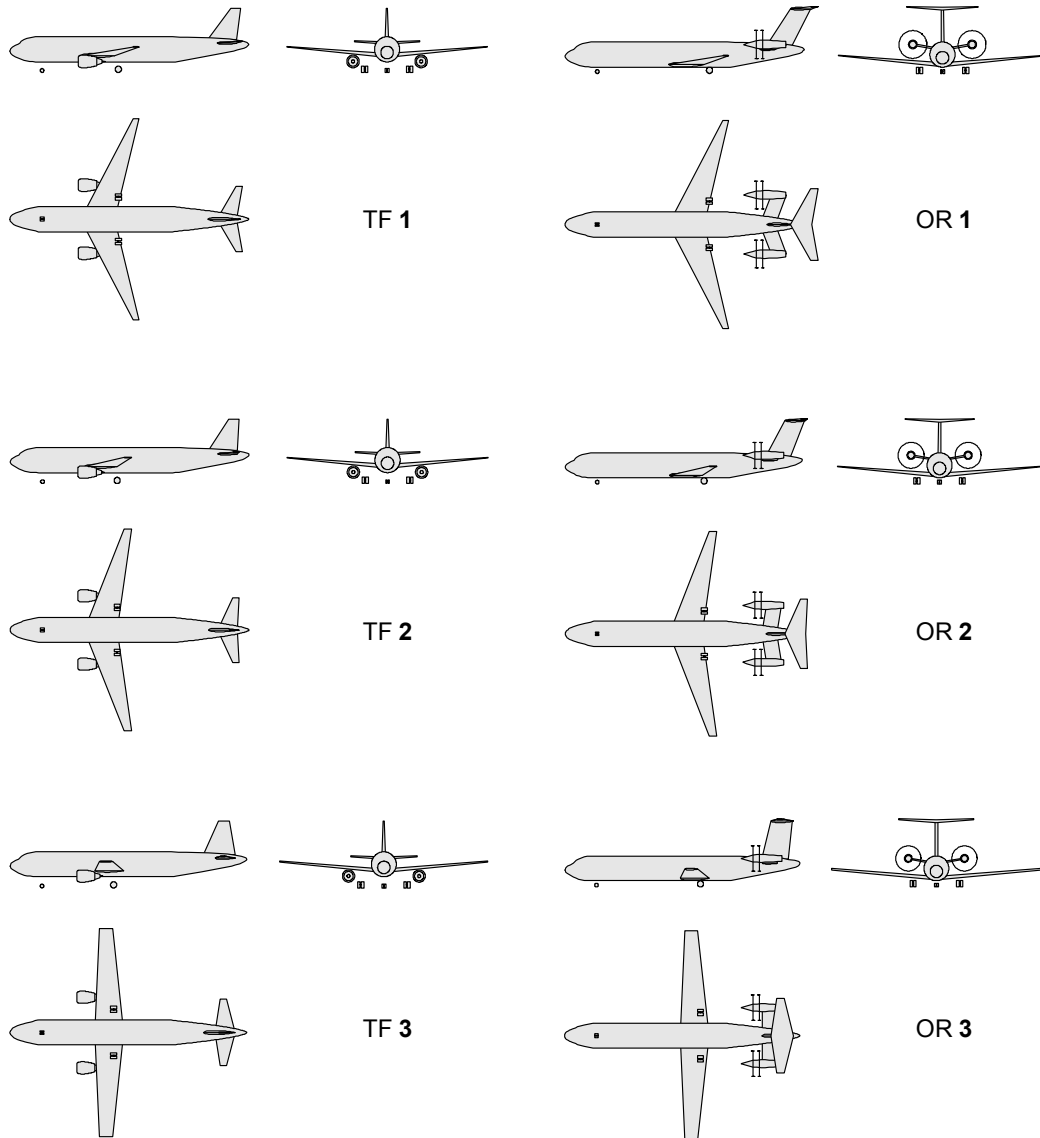


Figure 6.11.: Visualisation of open rotor and turbofan powered aircraft designs according to Table 6.6

## 6.4. Critical Assessment of Methodology

The methodological approach introduced and elaborated during the present work was tailored to meet the research demands identified as the result of a concentrated literature survey. The methodological development focused on the transparent integration of propulsion system design and performance aspects in the aircraft conceptual synthesis process. Central requirements, therefore, included the adequate mapping of the mutual couplings of the propulsion system and the airframe, comprehensive design space exploration and constrained optimisation capabilities, as well as the extensibility for refined design methods, the incorporation of new technologies, system architectures and analysis aspects. In the following, key element of the developed methodology are reviewed with regards to these aspects.

### 6.4.1. Assessment of the Discipline-Oriented Problem Decomposition

The rigorous discipline-oriented approach has proven to be a reliable way of successfully handling the complexity involved in the multidisciplinary integration of propulsion system design into the aircraft conceptual design process. The applied multi-level problem decomposition yields a straight-forward analysis structure allowing for a convenient identification and processing of feedback correlations within the aircraft synthesis procedure. The approach forms an extensible basis for the incorporation of multiple design aspects, verified through the readily implemented classic aircraft conceptual design and analysis disciplines.

Major benefits of the proposed discipline-oriented integration of propulsion system aspects are directly connected to the application of surrogate modelling techniques. Surrogate model application and the capability of evaluating propulsion system design and performance aspects at any step during the aircraft conceptual synthesis procedure, enables a high level of computational performance and flexibility for system-level analyses. Propulsion system design and performance characteristics are accessible on demand at any step within the aircraft synthesis procedure. However, the generation of mathematical surrogates for the numerous propulsion system aspects involved in multidisciplinary aircraft design requires significant “offline” effort for data sampling, SuMo regression and validation. Therefore, efficient strategies were developed during the present work featuring an enhanced role of the human expert, while ensuring reliable SuMo quality and allowing for a widely automated SuMo generation procedure at the same time. For the presented studies, feedforward neural networks were used as surrogate models at different levels of the aircraft design process, including the application within disciplinary modules as well as for system-level optimisation and design space exploration. During system design studies, surrogate-based optimisation has been identified most convenient due to the extremely rapid model response times, while smoothing the design space<sup>11</sup> and offering the direct supply of gradient information.

In fact, the availability of propulsion system surrogate models implies the consistent modelling of propulsion system design prior to the aircraft conceptual design synthesis. The selection of propulsion system aspects to be wrapped by surrogates as well as the clustering of results parameters  $y_{ps}$  in FNN (cf. Section 3.2.2) is problem-dependent and requires particular attention in order to keep SuMo generation effort small.

---

<sup>11</sup>including very large convergence radii as well as the non-existence of singularities in the validated parameter space

A particular benefit of the application of surrogate modelling within the discipline-oriented scheme is the variability of the functional correlations, i.e. the numbers of free parameters considered for the mapping of the individual aspects. If the interfaces for feedforward correlations between the disciplinary modules of the aircraft design process are well-defined, surrogate models can be replaced without impacting on the disciplinary model or on the process structure. Hence, propulsion system models can be modularly exchanged, by loading respectively unloading previously generated surrogate model packages.

The discipline-oriented approach has not yet been demonstrated for intra component MDO, such as pylon aero-elastics, which may be an important aspect during more detailed studies of particular engine installation options. Here, the optional parallelisation of disciplinary sub-tasks and the handling of the large numbers of feedbacks will require considered attention.

##### 6.4.2. On the Quality of Design Methods

The level of detail for the mapping of propulsion system physics, presented in this thesis, significantly enhances the representation of engine design aspects within the conceptual design of aircraft relative to contemporary standards. The level of modelling detail chosen for the different propulsion system design and performance aspects is correlated to the corresponding system-level impact. Therefore, heuristics for cycle design and engine sizing constraints are emphasised, as well as turbo component efficiencies, ducting losses and turbine cooling air demands.

For the demonstration of the methodological approach, most of the methods used for the mapping of aircraft characteristics referred to semi-empirical models taken from established handbooks. The choice of models was tailored to map first order design implications connected to the investigated propulsion system architectures and installation options. A multitude of aircraft conceptual design aspects including the mapping of aircraft systems and cabin layout were treated invariant in the overall model. While landing gear sizing implications due to propulsion system design and installation were accurately evaluated during the presented studies, the impact of engine type and associated performance on aircraft trim and stability characteristics was neglected, in the first instance. For an appropriate sizing of horizontal and vertical tail planes, these aspects should be considered, in the future.

In order to detach from the evolutionary advancement of existing system configurations and to further opening up the system design space, the paradigm shift to a consistent set of physics-based methods for the integrated multidisciplinary design and analysis of aircraft concepts will be required. Here, major challenges will be connected to the assurance of model validity in absence of sufficiently detailed empirical information, as well as the compliance with model response times required during aircraft conceptual design.

In the present work, system physics mostly remained within the envelope of well-understood topological arrangements, allowing for the application of semi-empirical correlations. However, for a number of system design aspects featuring small empirical database, simple physic-based methods had to be developed. In particular, the small empirical database for aircraft powered by high-speed counter-rotating propellers necessitated the introduction and validation of new methods for the efficiency mapping of counter-rotating swept propellers, as well as the estimation of engine primary and secondary installation weights. The achieved quality of propeller size and efficiency mapping appears adequate for aircraft conceptual design studies.

Therefore, the results obtained from the studies presented in this chapter may add to the definition of requirements for future research and concept development. However, the current analytical resolution of the problem is yet insufficient in order to derive direct geometric implications for system designs. The aero-acoustic design and structural integration of counter rotating open rotor remain a key challenge for appropriate aircraft conceptual design.

### **6.4.3. Extensibility of the Methodology**

As part of this chapter, the discipline-oriented approach to propulsion system integration has been demonstrated for a limited number of essential application cases. Therefore, an initial set of aircraft and engine conceptual methods was compiled and implemented. However, based on the discipline-oriented decomposition of the aircraft conceptual design process, the developed methodological framework features high flexibility towards the integration of additional system analysis aspect, the multidisciplinary design of new system concepts, as well as the sophistication of methods within the readily implemented disciplinary modules.

By decomposing the aircraft conceptual design problem according to the involved engineering disciplines, the followed approach intrinsically facilitates the application of classic disciplinary expert modules, including CAD for the geometry description, as well as discretised methods for the aerodynamic and structural design evaluation. Here, surrogate-based model integration may facilitate acceptable computational effort during system-level design studies, despite of more sophisticated disciplinary analyses.

Moreover, the implemented methodology is well-suited for the conduct of probabilistic design and technology assessment. In a recent enhancement of the methodology, the quasi-random LHS scheme was extended to incorporate non-deterministic system analysis. Therefore, the uniform space stratification of standard LHS was adapted to allow for arbitrary probability density distributions for the individual variables  $V_i$  constituting the input space  $F$  (cf. Section 3.3.1), while maintaining the LHS-intrinsic space-filling qualities.

Additional methodological extensibility is associated to the enhanced utilisation of the software GasTurb and its computer engine decks. The software offers a direct connection to NASA's CEA program, and thus, allows for the investigation of alternative fuel types during aircraft-level studies. Beyond that, the computer engine decks represent a convenient means of interfacing GasTurb with external codes, such as for the aerodynamic and mechanical design and analysis of engine components, in order to further increase the level of detail in the aircraft-level representation of engine design and technology.

## 7. Conclusion and Future Work

In this thesis, a unified and comprehensively validated methodological approach to incorporating the design of advanced propulsion system concepts in the aircraft conceptual process was presented. The challenges connected to this multidisciplinary design problem were tackled by a rigorous discipline-oriented procedure for the aircraft conceptual design synthesis. Engine conceptual design and performance mapping was based on the software GasTurb 11, and subsequently integrated in the aircraft disciplinary analysis tasks via neural network based surrogate models. The developed methodology was demonstrated for representative analysis applications including the technology-dependent optimisation of engine design parameters as well as the comparison of alternative, advanced propulsion system architectures at the aircraft system level.

### 7.1. Important Results and Findings

In order to demonstrate the applicability of the proposed methodological setup to integrated system-level design tasks, parametric studies were presented, focusing on two different propulsion system architectures: a two-spool boosted turbofan featuring direct fan drive and a short duct separate flow nacelle, and, a two-spool boosted geared counter rotating open rotor. For both propulsion concepts, twin-engine aircraft layouts based on cylindrical pressurised fuselages and low-set cantilever wings were assumed, while featuring under-wing turbofan mounting or aft-fuselage open rotor mounting, respectively. The underlying design operational scenario referred to a typical medium range transport application.

As a meaningful subject for aircraft-level investigation, turbofan design bypass ratio  $BPR_{des}$  was investigated with regards to its impact on aircraft design and performance characteristics. Based on four technological scenarios, covering engine as well as aircraft-specific technology parameters, aircraft were sized and optimised for minimum design block fuel  $W_{F,block,des}$ . For technology standards of contemporary aircraft, fuel burn optimum  $BPR_{des}$  values of approximately 7 were identified. Advanced engine technology settings increased optimum  $BPR_{des}$  to the order of 10. However, optimum values of  $BPR_{des}$  were found rather insensitive to airframe technological enhancement. In an additional sensitivity study involving even further reduced aerodynamic losses in the engine, optimum values of  $BPR_{des}$  did not increase significantly further. It could be concluded that  $BPR_{des}$  is not only limited by powerplant weight and aircraft geometric integration, but essentially by propulsion system internal limitations, intrinsic to the investigated direct-drive turbofan architecture. Here, the challenge of matching the aerodynamic loadings of the low-spool turbo components while maintaining reasonable stage counts was aggravated significantly, when  $BPR_{des}$  was pushed clearly beyond 10. The identified  $W_{F,block,des}$  reduction of the considered most advanced turbofan powered aircraft yielded approximately 26% relative to contemporary technology. Here, the partial contribution of the enhanced engine technology was approximately 10%.

## 7. Conclusion and Future Work

The corresponding reduction in aircraft Maximum Take-Off Weight (MTOW) yielded 18%. The further enhancement of optimum  $BPR_{des}$ , and thus, the utilisation of further fuel burn reduction potentials may be expected from more elaborate low-spool architectures including geared and counter rotating arrangements.

As an additional system design parameter impacting on aircraft and engine design as well as Air Traffic Management aspects, design cruise Mach number  $M_{ADP}$  and the connected trends in  $W_{F,block,des}$  and aircraft  $MTOW$  were investigated. Accordingly, a reduction in  $M_{ADP}$  from the reference value of 0.78 down to 0.72 resulted in additional  $W_{F,block,des}$  savings of 4% while  $MTOW$  was concurrently reduced by 2% and increased  $BPR_{des}$  was tolerated for minimum fuel burn.

The additional fuel reduction potentials associated with the open rotor engine concept were investigated in a comparative study of open rotor and turbofan powered aircraft. For both system concepts, the most advanced of the considered technology scenarios was employed.  $W_{F,block,des}$  of both system concepts was systematically analysed for a wide range of  $M_{ADP}$ . As expected, the open rotor concept benefited more from reduced  $M_{ADP}$  than the turbofan engine concept. However, it was found that the significant benefits of the investigated open rotor architecture in terms of Specific Fuel Consumption (SFC) were compromised by the complex installation effects leading to considerable structural weight penalties of main airframe components. Despite of reduced  $W_{F,block,des}$  and identical payload the  $MTOW$  values of the investigated open rotor aircraft exceeded those of the turbofan aircraft by approximately 5%. Beside the apparent  $MTOW$  implications, the aerodynamic efficiency of the open rotor aircraft during cruise was degraded due to the additional nacelle and pylon drag caused by the propeller slipstream. For optimised open rotor aircraft,  $W_{F,block,des}$  reduction potentials between 8.8% and 11.4% were computed relative to the turbofan concept. These fuel savings were reduced in comparison to the numbers predicted for open rotor engines in the past. Further fuel penalties for this concept may be encountered when considering the additional weights for potentially required cabin noise treatment, as well as the propeller design trade-off between efficiency and noise.

The cumulative block fuel reduction potential identified for the studied open rotor powered aircraft yielded 33% relative to the turbofan powered aircraft featuring baseline technology settings when assuming  $M_{ADP} = 0.78$ . By reducing  $M_{ADP}$  for the open rotor powered aircraft to a value 0.7, the overall block fuel reduction potential was increased to 38%. Related to the underlying technological scenarios, the obtained numbers on fuel burn reduction may be reflected with regards to the strategic research targets for future transport aircraft. In turn, requirements and boundary conditions for the development of new technologies may be identified.

### 7.2. Reflection of Motivation and Research Goals

The research demands identified at the beginning of the presented research, stipulated the elaboration of a flexible methodological approach to propulsion system integration in aircraft conceptual design allowing for fast-responding, full-parametric analyses of advanced and unconventional system architectures. Therefore, a standardised concept for the handling of propulsion system design and operational characteristics within the aircraft conceptual design process was required. In order to adequately map the physics of advanced propulsion

system design and integration aspects, the methodological requirements also included the formulation of a consistent set of system design methods, aiming at enhancing the level of detail of engine design representation in aircraft conceptual design.

In order to tackle these research demands the propulsion system was identified as a contributor to the aircraft conceptual design disciplines. Therefore, engine design and performance aspects were included in a rigorous discipline-oriented decomposition scheme applied to the aircraft conceptual design process. Here, the application of surrogate modelling techniques proved to be a key enabler for the discipline-oriented integration of propulsion system characteristics. Moreover, the fast responding behaviour of the employed neural network based approximations allowed for parametric “optimisation-in-the-loop” studies, thereby enabling efficient design space exploration and a quick gain of knowledge on system behaviour. In order to reduce the additional “offline” effort required for the creation of engine surrogate models efficient strategies were developed, utilising GasTurb 11 computer engine decks for efficient sampling of surrogate model regression and validation data.

The results gained from the performed case studies demonstrated both, the capabilities of the elaborated approach, as well as the importance of considering the system-level impact of new propulsion system concepts, in order to assess the true efficiency potentials relative to advanced conventional technology. Here, the formulated system design methods revealed adequate accuracy for the addressed conceptual design tasks. Therefore, the developed methodology may contribute to a more synergistic technology development, by incorporating the analysis of the technology implications on aircraft design and operational characteristics at very early stages of technology evaluation.

### 7.3. Perspectives for Further Methodological Development

Essential applied parts of the methodological approach presented in this thesis explicitly focus on gas turbine engine concepts. The discipline-oriented approach to integrating propulsion system aspects in the aircraft conceptual design synthesis procedure, however, also allows for the investigation of more radical flight propulsion concepts and the corresponding integration options, in the future. Three basic starting points are considered for further developing the methodology presented in this thesis:

1. the development of methods for the mapping of further advanced propulsion system design and integration concepts,
2. the incorporation of further system design and analysis disciplines in the aircraft synthesis procedure, and
3. the sophistication of disciplinary analysis models including the paradigm shift to physics-based methods for the mapping of aerodynamics and structures, representing an essential premise for the reliable conceptual synthesis of revolutionary design solutions in the long term.

Follow-on studies based on the presented methodological approach should consider the aircraft-level analysis of novel engine architectures and further advanced technology standards. Potential technological candidates involve radical thermodynamics such as intercooled, recuperative and topping cycles, as well as innovative solutions for the propulsive device such as geared or counter rotating ducted fans, and distributed propulsion featuring boundary

## 7. Conclusion and Future Work

layer ingestion. Further methodological extension should particularly focus on analysing the potentials of alternative energy sources including the option of fully electric-powered aircraft. Investigations should also emphasise on identifying aerodynamic, structural and performance synergy effects between propulsion system integration and novel airframe architectures, e.g. joint-wing or box-wing concepts.

The benefits in evaluating advanced propulsion system technologies, gained from the developed methodological framework, may be significantly enhanced through the incorporation of additional system design and analysis aspects, such as engine and aircraft noise modelling; climate impact assessment; life cycle cost evaluation; product family and airline fleet design; as well as, airport and operations planning.

The sophistication of existing disciplinary analysis models may offer additional insight to targeted system physics. This involves both, propulsion system as well as aircraft design and performance mapping. Important degrees of freedom for the enhancement of the existing design and analysis methods include

- the system geometric description using Computer Aided Design (CAD) software,
- the discretised mapping of aircraft structures and aerodynamics, e.g. through high-end low-fidelity numerical methods based on a more detailed handling of actual load scenarios, e.g. landing shock and gust loads,
- the more detailed capturing of the aerodynamic interactions of airframe and propulsion system,
- improved loss models for turbo component aerodynamics, e.g. including transonic loss mapping,
- the direct geometry-based estimation of aircraft and engine component weights,
- more realistic operational simulation including aircraft trim conditions, head, back and cross wind effects, gust load implications, 3-dimensional flight paths, the evaluation of transient operational conditions and the detailed mapping of LTO cycles, as well as
- the supplementation of aircraft design analyses, such as payload/range, load and balance, and gust load charts.

The sophistication of disciplinary models should also consider potential applications of stronger interdisciplinary couplings such as linearised aero-elastic analyses of powerplant installation structures. In particular, the process-incorporation of appropriate aero-acoustic methods is necessary for the identification of best and balanced designs of unducted engine concepts with regards to the trade-off between fuel burn and noise emission characteristics.

# Bibliography

- [1] Energy consumption characteristics of transports using the prop-fan concept. NASA Contractor Report, Boeing Commercial Airplane Company, Seattle, Washington, October 1976. NASA-CR-137937.
- [2] DC-9 Airplane Characteristics for Airport Planning. Douglas Aircraft Company, published on [www.boeing.com](http://www.boeing.com), June 1984.
- [3] Full scale technology demonstration of a modern counterrotating unducted fan engine concept - component test. Technical report, GE Aircraft Engines, Cincinnati, Ohio, prepared for NASA-Lewis Research Center under Contract NAS3-24210, December 1987. NASA-CR-180868.
- [4] Full scale technology demonstration of a modern counterrotating unducted fan engine concept - design report. Technical report, GE Aircraft Engines, Cincinnati, Ohio, prepared for NASA-Lewis Research Center under Contract NAS3-24210, December 1987. NASA-CR-180867.
- [5] Full scale technology demonstration of a modern counterrotating unducted fan engine concept - engine test. Technical report, GE Aircraft Engines, Cincinnati, Ohio, prepared for NASA-Lewis Research Center under Contract NAS3-24210, December 1987. NASA-CR-180869.
- [6] MD-80 Series Airplane Characteristics for Airport Planning. Douglas Aircraft Company, published on [www.boeing.com](http://www.boeing.com), June 1990. Revision 12/1989.
- [7] *Jane's Aero-Engines*. Jane's Information Group Limited, 1995.
- [8] A320 - Airplane Characteristics for Airport Planning. Airbus S.A.S., 31707 Blagnac Cedex, France, August 2003. Revision No.20.
- [9] JMP - Statistical Discovery, Release 6.0.3. SAS Institute, Inc., 2006.
- [10] Luftfahrttechnisches Handbuch. [www.lth-online.de](http://www.lth-online.de), 2006.
- [11] Performance prediction and simulation of gas turbine engine operation for aircraft, marine, vehicular, and power generation. Final Report of the RTO Applied Vehicle Technology Panel (AVT) Task Group AVT-036, North Atlantic Treaty Organisation (NATO), February 2007. TR-AVT-036.
- [12] V2500 turbofan engine The innovative power. MTU Aero Engines GmbH, Dachauer Straße 665, 80995 Munich, Germany, May 2007.
- [13] Pacelab APD Release 1.1.2. PACE Aerospace Engineering and Information Technology GmbH, 2 September 2009.

## Bibliography

- [14] Pacelab Suite Release 4.0.3. PACE Aerospace Engineering and Information Technology GmbH, 17 August 2009.
- [15] Advisory Council for Aeronautics Research in Europe. Strategic Research Agenda Volume I, October 2002.
- [16] Airbus Customer Services, Flight Operations Support & Line Assistance, Blagnac, France. *Getting to Grips With Fuel Economy*, November 2001.
- [17] Airbus Customer Services, Flight Operations Support & Line Assistance, Blagnac, France. *Getting to Grips With Aircraft Performance*, January 2002.
- [18] N. Alexandrov and R. Lewis. Comparative properties of collaborative optimization and other approaches to mdo. In *First ASMO UK /ISSMO Conference on Engineering Design Optimization, 8-9 July*. MCB Press, 1999.
- [19] N. Alexandrov and R. Lewis. Analytical and computational properties of distributed approaches to mdo. In *8th AIAA/NASA/ISSMO Symposium on Multidisciplinary Analysis and Optimization, 6-8 September, Long Beach, California, 2000*. AIAA-2000-4718.
- [20] J. Allison, B. Roth, M. Kokkolaras, I. Kroo, and P. Papalambros. Aircraft family design using decomposition-based methods. In *11th AIAA/ISSMO Multidisciplinary Analysis and Optimization Conference, Portsmouth, Virginia, 6 - 8 September, 2006*. AIAA 2006-6950.
- [21] R. Anderson. Advanced Propfan Engine Technology (APET) Definition Study, Single-And Counter-Rotation Gearbox / Pitch Change Mechanism Design, Final Report. Technical report, Allison Gas Turbine Division, General Motors Corporation, 1985. NASA-CR-168115.
- [22] N. Antoine. *Aircraft Optimization for Minimal Environmental Impact*. PhD thesis, Stanford University, Department of Aeronautics and Astronautics, August 2004.
- [23] S. Azarm and J. Sobieszczanski-Sobieski. Reduction method with system analysis for multiobjective optimization-based design. Technical report, NASA Langley Research Center, Hampton, Virginia, April 1993. NASA-CR-191456, ICASE Report No. 93-22.
- [24] R. Bellman. *Adaptive Control Processes: A Guided Tour*. Princeton University Press, 1961.
- [25] A. Betz. Schraubenpropeller mit geringstem Energieverlust. *Nachrichten der Gesellschaft der Wissenschaften zu Göttingen*, 1919. With an Appendix by L. Prandtl.
- [26] A. Betz. The theory of contra vanes applied to the propeller. *Ingenieur-Archiv*, 9(6), 1938. NACA-TM-909.
- [27] S. Boggia and K. Rüd. Intercooled recuperated aero engine. In *Deutscher Luft- und Raumfahrt Kongress, Dresden, Germany, 20-23 September, 2004*.
- [28] A. Bradley. An aero-engine vision for 2020. Presentation at 8th ASC-CEAS Workshop, "Aeroacoustics of New Aircraft & Engine Configurations", 11-12 November, Budapest, Hungary, 2004.

- [29] S. Bretschneider, O. Arago, and S. Staudacher. Architecture of a techno and environmental risk assessment tool using a multi-modular build approach. In *18th International Symposium on Air-Breathing Engines, 2-7 September, Beijing, China, 2007*. ISABE-2007-1103.
- [30] S. Briceno and D. Mavris. Quiet supersonic jet engine performance tradeoff analysis using a response surface methodology approach. In *SAE World Aviation Congress, Phoenix, Arizona, November 5-7, 2002*.
- [31] S. Briceno and D. Mavris. Implementation of a physics-based decision-making framework for evaluation of the multi-disciplinary aircraft uncertainty. In *SAE World Aviation Congress, Montreal, Canada, September 9-12*. SAE International, 2003. SAE 2003-01-3055.
- [32] CFS Engineering CEASIOM application. CEASIOM website. <http://www.ceasiom.com>, 2010.
- [33] S. Chai and W. Mason. Landing gear integration in aircraft conceptual design. Technical report, Virginia Polytechnic Institute and State University supported by NASA Ames Research Center under Grant NAG-2-919, September 1996.
- [34] M. Chambers, M. Ardema, A. Patron, A. Hahn, H. Miura, and M. Moore. Analytical fuselage and wing weight estimation of transport aircraft. Technical report, NASA Ames Research Center, Moffet Field, California, 1996. NASA-TM-110392.
- [35] W. Chen, J. Allen, D. Mavris, and F. Mistree. A concept exploration method for determining robust top-level specifications. *Journal of Engineering Optimization*, 26:137–158, 1996.
- [36] E. Commission. Flightpath 2050: Europe’s vision for aviation, report of the high level group on aviation research. Publications Office of the European Union, Luxembourg, 2011.
- [37] Conceptual Research Corporation, Playa del Rey, California. Website of RDS Software. <http://www.aircraftdesign.com/rds.shtml>, January 2010.
- [38] J. Conlon and J. Bowles. Application of advanced high speed turboprop technology for future civil short-haul transport design. In *AIAA Aircraft System And Technology Conference, 21-23 August, Los Angeles, California, 1978*. AIAA-78-1487.
- [39] J. Crigler. Application of theodorsen’s theory to propeller design. Technical report, National Advisory Committee for Aeronautical (NACA), 1944. NACA Report 924.
- [40] D. Daberkow. *A Formulation of Metamodel Implementation Processes for Complex Systems Design*. Dissertation, Georgia Institute of Technology, 2002.
- [41] D. Daggett. Ultra efficient engine technology systems integration and environmental assessment. Technical report, Boeing Commercial Airplane Group, Seattle, Washington, July 2002. NASA/CR-2002-211754.
- [42] D. Daggett, S. Brown, and R. Kawai. Ultra-efficient engine diameter study. Technical report, Boeing Commercial Airplane Group, Seattle, Washington, August 2003. NASA/CR-2003-212309.
- [43] Dassault Systèmes. Simulia website. <http://www.simulia.com>, July 2010.

## Bibliography

- [44] R. Davidson. Optimization and performance calculation of dual-rotation propellers. Technical report, NASA Langley Research Center, Hampton, Virginia, 1981. NASA TP-1948.
- [45] D. Davis and E. Stearns. Energy efficient engine - flight propulsion system, final design and analysis. Technical report, General Electric Company, 1985. NASA-CR-168219.
- [46] Design, Analysis and Research Corporation. *Advanced Aircraft Analysis User's Manual Version 3.2*, June 2009.
- [47] S. Dixon. *Fluid Mechanics, Thermodynamics of Turbomachinery*. Reed Educational and Professional Publishing Ltd, 4 edition, 1998.
- [48] F. Donus. Ermittlung der Genauigkeit und Erarbeitung von Verbesserungsvorschlägen bei der Gewichtsabschätzung mit Gasturb 11. Master's thesis, Institut für Luftfahrtantriebe, Universität Stuttgart, June 2008.
- [49] G. Doulgeris. *Modelling & Integration of Advanced Propulsion Systems*. PhD thesis, School of Engineering, Cranfield University, March 2008.
- [50] D. Rumelhart, G. Hinton, and R. Williams. *Learning Internal Representations by Error Propagation*, volume Parallel Data Processing, Vol.1. The M.I.T. Press, Cambridge, Massachusetts, 1986.
- [51] R. Egelhofer. *Aircraft Design Driven by Climate Change*. PhD thesis, Technische Universität München, Institut für Luft- und Raumfahrt, 2009.
- [52] Embarcadero Technologies, Inc. Delphi website. <http://www.embarcadero.com/products/delphi>, July 2010.
- [53] P. Fantini. *Effective Multiobjective MDO for Conceptual Design, An Aircraft Design Perspective*. PhD thesis, Cranfield University, School of Engineering, 2007.
- [54] Federal Aviation Administration. Electronic Code of Federal Regulation. U.S. Government Printing Office, Washington DC, <http://ecfr.gpoaccess.gov>, November 2010.
- [55] A. Forrester, A. Sóbester, and A. Keane. *Engineering Design via Surrogate Modelling: A Practical Guide*. John Wiley & Sons, Ltd., 2008.
- [56] J. Frota. NACRE - An Overview: Towards a Silent-by-Design Aircraft? In *Presentation held at 15th AIAA/CEAS Aeroacoustics Conference, 12 May, Miami, Florida, 2009*.
- [57] G. Hoff et al. Experimental performance and acoustic investigation of modern, counter-rotating blade concepts. Technical report, GE Aircraft Engines, Advanced Technology Operations, Cincinnati, Ohio, prepared for NASA Lewis Research Center unter Contract NAS3-24080, January 1990. NASA-CR-185158.
- [58] N. Gasparovic. Das Zweistromtriebwerk bei optimaler und nicht-optimaler Auslegung. *Forschung im Ingenieurwesen*, 42(5):157–168, 1976.
- [59] J. Gauntner. Algorithm for calculating turbine cooling flow and the resulting decrease in turbine efficiency. NASA Technical Memorandum, Lewis Research Center, Cleveland, Ohio, February 1980. NASA-TM-81453.

- [60] K. Geiselhart. A technique for integration engine cycle and aircraft configuration optimization. Technical report, Lockheed Engineering & Sciences Company, Hampton, Virginia, February 1994. NASA-CR-191602.
- [61] J. Giesing and J.-F. Barthelemy. A summary of industry mdo applications and needs. In *7th AIAA/USAF/NASA/ISSMO Symposium on Multidisciplinary Analysis and Optimization, September 2-4, St. Louis, MO*, 1998. AIAA 98-4737.
- [62] A. Glassman. Computer program for preliminary design analysis of axial flow turbines. NASA Technical Note, Lewis Research Center, Cleveland, Ohio, March 1972. NASA TN D-6702.
- [63] A. Glassman. Users manual for updated computer code for axial-flow compressor conceptual design. Technical report, NASA Lewis Research Center, Cleveland, Ohio, July 1992. NASA Contractor Report 189171.
- [64] J. Godston and C. Reynolds. Propulsion system integration configurations for future prop-fan powered aircraft. *Journal of Aircraft*, 22(12):1027–1033, 1985.
- [65] M. Goldsmith and J. Bowles. Potential benefits for propfan technology on derivatives of future short-to-medium-range transport aircraft. In *AIAA/SAE/ASME 16th Joint Propulsion Conference, 30 June-2 July, Hartford, Connecticut*, 1980. AIAA-80-1090.
- [66] S. Goldstein. On the vortex theory of screw propellers. *Proc. R. Soc. of London*, pages pp. 440–65, 1929.
- [67] S. Gordon. Thermodynamic and transport combustion properties of hydrocarbons with air. Part 1: Properties in SI units. Technical report, NASA Lewis Research Center, Cleveland, Ohio, July 1982. NASA-TP-1906.
- [68] J. Green. Laminar Flow Control – Back to the Future? In *38th Fluid Dynamics Conference and Exhibit, 23-26 June, Seattle, Washington*, 2008. AIAA-2008-3738.
- [69] H. Grieb. *Projektierung von Turboflugtriebwerken*. Birkhäuser Verlag, Basel-Boston-Berlin, 2004.
- [70] H. Grieb and D. Eckardt. Turbofan and propfan as basis for future economic propulsion concepts. In *AIAA/ASME/SAE/ASEE 22nd Joint Propulsion Conference, Huntsville, Alabama, June 16-18*, 1986. AIAA-86-1474.
- [71] J. Guptill, R. Coroneos, S. Patnaik, D. Hopkins, and L. Berke. Cometboards users manual, release 1.0. NASA Technical Memorandum, Lewis Research Center, Cleveland, Ohio, October 1996. NASA-TM-4537.
- [72] O. Gur, W. Mason, and J. Schetz. Full configuration drag estimation. In *27th AIAA Applied Aerodynamics Conference, San Antonio, Texas, 22 - 25 June*. American Institute of Aeronautics and Astronautics, Inc., 2009. AIAA 2009-4109.
- [73] M. Guynn, J. Berton, K. Fisher, W. Haller, M. Tong, and D. Thurman. Analysis of turbofan design options for an advanced single-aisle transport aircraft. In *9th AIAA Aviation Technology, Integration, and Operations Conference (ATIO), 21-23 September, Hilton Head, South Carolina*, 2009. AIAA-2009-6942.

## Bibliography

- [74] M. Guynn, J. Berton, K. Fisher, W. Haller, M. Tong, and D. Thurman. Engine concept study for an advanced single-aisle transport. NASA Technical Memorandum, Langley Research Center, Hampton, Virginia, August 2009. NASA/TM-2009-215784.
- [75] H. Borst et. al. Summary of Propeller Design Procedures and Data, Volumes I-III. Technical report, US Army Air Mobility Research and Development Laboratory, 1973. USAAMRDL Technical Reports 73-34A, 73-34B, 73-34C.
- [76] R. Hager and D. Vrabel. Advanced turboprop project. NASA Special Publication, 1988. NASA-SP-495.
- [77] M. Healy, J. Kowalikt, and J. Ramsay. Airplane engine selection by optimization on surface fit approximations. *Journal of Aircraft*, 12(7):593–599, July 1975.
- [78] W. Heinze, C. Österheld, and P. Horst. Multidisziplinäres Flugzeugentwurfsverfahren PrADOProgrammentwurf und Anwendung im Rahmen von Flugzeug-Konzeptstudien. In *DGLR-Jahrestagung, 17-20 September, Hamburg, Germany*, 2001.
- [79] D. Howe. The prediction of aircraft wing mass. *Journal of Aerospace Engineering*, 210:135–145, 1996. Proceedings of the Instituting of Mechanical Engineers, Part G.
- [80] D. Howe. *Aircraft Conceptual Design Synthesis*. Professional Engineering Publishing, 2000.
- [81] International Aero Engines. V2500 The Power Of Choice. Advertising brochure, USA, 1996.
- [82] International Aero Engines. Type Certificate Sheet E40NE. U.S. Department of Transportation, Federal Aviation Administration, June 1999.
- [83] International Aero Engines. V2500 - The Engine Of Choice for Airbus A319, A320, and A321, Boeing MD-90 twinjet, Airbus Corporate Jetliner. <http://www.i-a-e.com>, 2010.
- [84] P. Jackson, K. Munson, and L. Peacock, editors. *Jane's All The World's Aircraft*. Jane's Information Group Limited, ninety-first year of issue edition, 2000-2001.
- [85] L. Jenkinson, P. Simpkin, and D. Rhodes. *Civil Jet Aircraft Design*. Butterworth-Heinemann Publications, 1999.
- [86] D. Jones. A taxonomy of global optimization methods based on response surfaces. *Journal of Global Optimization*, 21:345–383, 2001.
- [87] D. Jones, M. Schonlau, and W. Welch. Efficient global optimization of expensive black-box functions. *Journal of Global Optimization*, 13:455–492, 1998.
- [88] E. Kessler. Advancing the state-of-the-art in the civil aircraft design: A knowledge-based multidisciplinary engineering approach. In *European Conference on Computational Fluid Dynamics, ECCOMAS CFD, September 5-8, Egmond aan Zee, The Netherlands*, 2006.
- [89] H. Kim, S. Ragon, G. Soremekun, B. Malone, and J. Sobieszczanski-Sobieski. Flexible approximation model approach for bi-level integrated system synthesis. In *10th AIAA/ISSMO Multidisciplinary Analysis and Optimization Conference, Albany, New York, 30 August - 1 September*. American Institute of Aeronautics and Astronautics, Inc., 2004. AIAA-2004-4545.

- [90] M. Kirby. *A Methodology for Technology Identification, Evaluation, and Selection in Conceptual and Preliminary Aircraft Design*. PhD thesis, Georgia Institute of Technology, March 2001.
- [91] P. Koch. *Hierarchical Modeling and Robust Synthesis for the Preliminary Design of Large Scale Complex Systems*. PhD thesis, Georgia Institute of Technology, December 1997.
- [92] J.-J. Korsia and G. D. Spiegeleer. VITAL, An European Program For Greener Aero-Engines. In *25th International Congress of the Aeronautical Sciences, 3-8 September 2004, Hamburg, Germany*, 2006.
- [93] I. Kroo. An interactive system for aircraft design and optimization. In *1992 Aerospace Design Conference, 3-6 February, Irvine, California*, 1992. AIAA-92-1190.
- [94] I. Kroo. Distributed multidisciplinary design and collaborative optimization. In *VKI lecture series on Optimization Methods & Tools for Multicriteria/Multidisciplinary Design, 15-19 November*, 2004.
- [95] I. Kroo, S. A. R. Braun, P. Gage, and I. Sobieski. Multidisciplinary optimization methods for aircraft preliminary design. In *5th AIAA/USAF/NASA/ISSMO Symposium on Multidisciplinary Analysis and Optimization, 7-9 September, Panama City, Florida*, 1994. AIAA 94-4325.
- [96] I. Kroo and V. Manning. Collaborative optimization: Status and directions. In *8th AIAA/NASA/ISSMO Symposium on Multidisciplinary Analysis and Optimization, 6-8 September, Long Beach, California*, 2000. AIAA-2000-4721.
- [97] J. Kurzke. Calculation of installation effects within performance computer programs. In *AGARD Lecture Series 183: "Steady and Transient Performance Prediction of Gas Turbine Engines"*, 1992. AGARD-LS-183.
- [98] J. Kurzke. Performance modeling methodology: Efficiency definitions for cooled single and multistage turbines. In *Proceeding of ASME Turbo Expo Land, Sea & Air, Amsterdam, The Netherlands, 3-6 June*, 2002. 2002-GT-30497.
- [99] J. Kurzke. Gas turbine cycle design – off-design behavior. In *Short Course Gas Turbine Performance, Stuttgart, Germany, 24 - 28 September*. Deutsche Gesellschaft für Luft- und Raumfahrt DGLR e.V., 2007.
- [100] J. Kurzke. *GasTurb 11 – Design and Off-Design Performance of Gas Turbines*, 2007.
- [101] J. Kurzke. Gasturb details 5, build 5.0.0.31, compile date 02.04.2007, 2007.
- [102] J. Kurzke. *Generic Turbojet Deck – Steady State and Transient Performance*, 2007.
- [103] J. Kurzke. *Geared Turbofan Deck - Steady State and Transient Performance*, 2008.
- [104] J. Kurzke. GasTurb website. <http://www.gasturb.de>, March 2010.
- [105] J. Kurzke. Gasturb11, compiled with delphi 2007 on 27 january, 2010.
- [106] J. Kurzke and C. Riegler. A new compressor map scaling procedure for preliminary conceptual design of gas turbines. In *Proceedings of ASME IGTI Turbo Expo, Munich, Germany, 8-11 May*, 2000.

## Bibliography

- [107] K. Kyprianidis, B. Lehmayr, A. Alexiou, and L. Xu. TERA2020 – Rationale, Objectives and Design Algorithm. In *European Workshop on New Aero Engine Concepts Munich, 30 June – 1 July, 2010*.
- [108] A. Kyser. An elementary analysis of the effect of sweep, mach number, and lift coefficient on wing-structure weight. Technical report, NASA Langley Research Center, Hampton, Virginia, September 1977. NASA-TM-74072.
- [109] L. Loftin Jr. Subsonic aircraft: Evolution and the matching of size to performance. Technical report, NASA Langley Research Center, Hampton, Virginia, August 1980. NASA Reference Publication 1060.
- [110] T. Lavelle, R. Plencner, and J. Seidel. Concurrent optimization of airframe and engine design parameters. In *4th Symposium on Multidisciplinary Analysis and Optimization cosponsored by the AIAA, USAF, NASA, and OAI, 21-23 September, Cleveland, Ohio, 1992*. AIAA-92-4713.
- [111] B. Lehmayr, K. Kyprianidis, A. Alexiou, and L. Xu. Tera2020 optimisation of newac configurations. In *European Workshop on New Aero Engine Concepts Munich, 30 June – 1 July, 2010*.
- [112] S. Lehner and W. Crossley. Combinatorial optimization to include greener technologies in a short- to medium-range commercial aircraft. In *26th Congress of International Council of the Aeronautical Sciences including the 8th AIAA Aviation, Technology Integration, and Operations Conference, 14-19 September, Anchorage, Alaska, 2008*. AIAA-2008-8963.
- [113] S. Lehner and W. Crossley. Hybrid optimization for a combinatorial aircraft design problem. In *9th AIAA Aviation Technology, Integration, and Operations Conference (ATIO), 21 - 23 September, Hilton Head, South Carolina, 2009*. AIAA 2009-7116.
- [114] S. Lehner, L. Lurati, G. Bower, E. Cramer, W. Crossley, F. Engelsens, I. Kroo, S. Smith, and K. Willcox. Advanced multidisciplinary optimization techniques for efficient subsonic aircraft design. In *48th AIAA Aerospace Sciences Meeting Including the New Horizons Forum and Aerospace Exposition, 4 - 7 January 2010, Orlando, Florida, 2010*. AIAA 2010-1321.
- [115] K. Levenberg. A method for the solution of certain problems in least squares. *Quarterly of Applied Mathematics*, 2:164–168, 1944.
- [116] J.-H. Lewe. *An Integrated Decision-Making Framework for Transportation Architectures: Application to Aviation Systems Design*. PhD thesis, School of Aerospace Engineering, Georgia Institute of Technology, April 2005.
- [117] R. Lewis. *Turbomachinery Performance Analysis*. Elsevier Science & Technology Books, May 1996.
- [118] S. Lieblein. Experimental flow in two-dimensional cascades. In *ITS Aerodynamic Design of Axial Flow Compressors*, pages 183–226, 1965. NASA-SP-36.
- [119] S. Lieblein, F. Schwenk, and R. Broderick. Diffusion factor for estimating losses and limiting blades loadings in axial-flow-compressors blade elements. NACA Research Memorandum, Lewis Flight Propulsion Laboratory, Cleveland, Ohio, June 1953. NACA RM E53D01.

- [120] C. Liersch and M. Hepperle. A unified approach for multidisciplinary preliminary aircraft design. In *2nd CEAS European Air and Space Conference, 26-29 October, Manchester, UK, 2009*.
- [121] U. Lindemann, M. Maurer, and T. Braun. *Structural Complexity Management - An Approach for the Field of Product Design*. Springer-Verlag Berlin Heidelberg, 2009.
- [122] Lissys Limited. Piano website. Copyright Lissys Limited / D. Simos, <http://www.piano.aero>, 2009.
- [123] C. Lock. Interference velocity for a close pair of contra-rotating airscrews. Technical report, National Physical Laboratory, Aerodynamics Division, July 1941. Reports and Memoranda No. 2084.
- [124] B. Magliozzi, P. Brown, and D. Parzych. Acoustic test and analysis of a counterrotating prop-fan model. Technical report, Hamilton Standard, United Technologies Corporation, prepared for NASA-Lewis Research Center, Cleveland, Ohio, 1987. NASA-CR-179590.
- [125] D. Marquardt. An algorithm for least-squares estimation of nonlinear parameters. marquardt. *SIAM Journal on Applied Mathematics*, 11:431–441, 1963.
- [126] D. Mavris and D. DeLaurentis. An integrated approach to military aircraft selection and concept evaluation. In *1st AIAA Aircraft Engineering Technology, and Operations Congress, Los Angeles, California, 19-21 September*. American Institute of Aeronautics and Astronautics, Inc., 1995. AIAA-95-3921.
- [127] D. Mavris, D. DeLaurentis, O. Bandte, and M. Hale. A stochastic approach to multidisciplinary aircraft analysis and design. In *36th AIAA Aerospace Sciences Meeting and Exhibit, 12-15 January, Reno, Nevada, 1998*. AIAA-98-0912.
- [128] B. McBride and S. Gordon. Computer program for calculation of complex chemical equilibrium compositions and applications ii. users manual and program description. Technical report, Lewis Research Center, Cleveland, Ohio, June 1996. NASA Reference Publication 1311.
- [129] E. McClure. *An Evolving-Requirements Technology Assessment Process For Advanced Propulsion Concepts*. PhD thesis, School of Aerospace Engineering, Georgia Institute of Technology, August 2006.
- [130] B. McCormick. *Aerodynamics Aeronautics and Flight Mechanics*. John Wiley & Sons, 2 edition, 1995.
- [131] L. McCullers. Aircraft configuration optimization including optimized flight profiles. In *Recent Experiences in Multidisciplinary Analysis and Optimization, Proceedings of a symposium held at NASA Langley Research Center, Hampton, Virginia April 24-26*, pages 395–412, 1984. NASA Conference Publication 2327, Part 1.
- [132] B. McKay. Ideal optimization of counterrotating propellers. In *AIAA/ASME/SAE/ASEE 24th Joint Propulsion Conference, Boston, Massachusetts, July 11-13, 1988*.
- [133] M. McKay, R. Beckman, and W. Conover. A comparison of three methods for selecting values of input variables in the analysis of output from a computer code. *Technometrics*, 21(2):239–245, May 1979.

## Bibliography

- [134] Microsoft Corporation. Microsoft Developers Network website. <http://msdn.microsoft.com>, July 2010.
- [135] Microsoft Corporation. Microsoft Office website. <http://office.microsoft.com>, July 2010.
- [136] Microsoft Corporation. Microsoft Windows website. <http://windows.microsoft.com>, July 2010.
- [137] D. Mikkelson, G. Mitchell, and L. Bober. Summary of recent nasa propeller research. In *AGARD Fluid Dynamics Panel Meeting on Aerodynamics and Acoustics of Propellers, Toronto, Canada, October 1-4, 1984*. NASA-TM-83733.
- [138] A. Misra. Fundamental aeronautics program. NASA Seal/Secondary Air System Research Symposium, 18 November, 2008. NASA/CP-2009-215677.
- [139] H.-G. Münzberg and J. Kurzke. *Gasturbinen – Betriebsverhalten und Optimierung*. Springer-Verlag New York Heidelberg Berlin, 1977.
- [140] I. Moir and A. Seabridge. *Aircraft Systems: Mechanical, Electrical, and Avionics Subsystems Integration*. AIAA Educational Series. John Wiley & Sons Ltd, in the UK, American Institute of Aeronautics and Astronautics, Inc., in the United States, 3 edition, 2008.
- [141] MTU Aero Engines GmbH. GEnx turbofan engine - The next generation turbofan. Advertising brochure, Germany, May 2009.
- [142] MTU Aero Engines GmbH. GP7000 turbofan engine - The innovative power. Advertising brochure, Germany, May 2010.
- [143] J. Muehlbauer, J. H. Jr., S. Lindenbaum, C. Randall, N. Searle, and R. S. Jr. Advanced turboprop cargo aircraft systems study. Technical report, Lockheed-Georgia Company, Marietta, Georgia, November 1981. NASA-CR-165813.
- [144] J. Muehlbauer and S. Morris. Advanced turboprop cargo aircraft systems study. *Journal of Aircraft*, 20(6):523–529, June 1983.
- [145] G. Niemann, H. Winter, and B.-R. Höhn. *Maschinenelemente, Band I: Konstruktion and Berechnung von Verbindungen, Lagern, Wellen*. Springer-Verlag Berlin Heidelberg New York, 3 edition, 2001.
- [146] S. Ogaji, P. Pilidis, and R. Hales. TERA – A Tool for Aero-engine Modelling and Management. In *2nd World Congress on Engineering Asset Management and the 4th International Conference on Condition Monitoring, 11-14 June, Harrogate, UK*, 2007.
- [147] E. Onat and G. Klees. A method to estimate weight and dimensions of large and small gas turbine engines. Technical report, Boeing Military Airplane Development, Seattle, Washington, January 1979. NASA-CR-199481.
- [148] T. Otten, H. Hemmer, M. Plohr, A. Döpelheuer, R. Schaber, and K.-P. Rüd. Konzeptstudie zu zukünftigen hochbypass-triebwerken mit gegenläufigem fan. In *Deutscher Luft- und Raumfahrtkongress (DLRK), 8-10 September, Aachen, Germany*, 2009.
- [149] PACE Aerospace Engineering and Information Technology GmbH. *Pacelab APD Release 1.1 – User Guide*, 24 April 2009.

- [150] J. Palmer. The turbomatch scheme for aero/industrial gas turbine engine design point/off design performance calculation. SME, Thermal Power Group, Cranfield University, 1990.
- [151] Y. Panchenko, H. Moustapha, S. Mah, K. Patel, M. Dowhan, and D. Hall. Preliminary multi-disciplinary optimization in turbomachinery design. In *RTO AVT Symposium on "Reduction of Military Vehicle Acquisition Time and Cost through Advanced Modelling and Virtual Simulation"*, 22-25 April, Paris, France, 2002.
- [152] T. Pardessus. Concurrent engineering development and practices for aircraft design at airbus. In *24th International Congress of the Aeronautical Sciences, 29 August - 3 September, Yokohama, Japan, 2004*.
- [153] D. Pascovici. *Thermo Economic and Risk Analysis for Advanced Long Range Aero Engines*. PhD thesis, School of Engineering, Cranfield University, December 2008.
- [154] S. Patnaik, R. Coroneos, J. Guptill, and D. Hopkins. Subsonic aircraft design optimization with neural network and regression approximators. *Journal of Aircraft*, 42(5):1347–1349, September-October 2005.
- [155] S. Patnaik, R. Coroneos, J. Guptill, D. Hopkins, and W. Haller. A subsonic aircraft design optimization with neural network and regression approximators. In *10th Multidisciplinary Analysis and Optimization Conference cosponsored by the American Institute of Aeronautics and Astronautics and the International Society for Structural and Multidisciplinary Optimization, 30 August - 1 September, Albany, New York, 2004*. AIAA-2004-4606.
- [156] S. Patnaik, J. Guptill, D. Hopkins, and T. Lavelle. Neural network and regression approximations in high-speed civil aircraft design optimization. *Journal of Aircraft*, 35(6):839–850, November-December 1998.
- [157] S. Patnaik, J. Guptill, D. Hopkins, and T. Lavelle. Neural network and regression approximations in high speed civil transport aircraft design optimization. NASA Technical Memorandum, Lewis Research Center, Cleveland, Ohio, April 1998. NASA/TM-1998-206316.
- [158] S. Patnaik, J. Guptill, D. Hopkins, and T. Lavelle. Cascade optimization for aircraft engines with regression and neural network analysis-approximators. NASA Technical Memorandum, Glenn Research Center, Cleveland, Ohio, July 2000. NASA/TM-2000-209177.
- [159] S. Patnaik, J. Guptill, D. Hopkins, and T. Lavelle. Optimization for aircraft engines with regression and neural-network analysis approximators. *Journal of Propulsion and Power*, 17(1):85–92, January-February 2001.
- [160] S. Patnaik, D. Hopkins, and L. Berke. A general-purpose optimization engine for multi-disciplinary design applications. In *6th Multidisciplinary Analysis and Optimization Symposium cosponsored by AIAA, NASA, and USAF, 4-6 September, Bellevue, Washington, 1996*. AIAA-96-4163.
- [161] S. Patnaik, T. Lavelle, D. Hopkins, and R. Coroneos. Cascade optimization strategy for aircraft and air-breathing propulsion system concepts. *Journal of Aircraft*, 34(1):136–139, 1997.

## Bibliography

- [162] S. Patnaik, T. Lavelle, D. Hopkins, and R. Coronets. Cascade optimization strategy for aircraft air-breathing propulsion system concepts. In *6th Symposium on Multidisciplinary Analysis and Optimization cosponsored by AIAA, USAS, NASA, and ISSO, 4-6 September, Bellevue, Washington, 1996*. AIAA-96-4145.
- [163] C. Peddie and R. Shaw. NASA Ultra Efficient Engine Technology Project Overview. 2003 NASA Seal/Secondary Air System Workshop, Volume 1, pp. 43-90, September 2004. NASA/CP-2004-212963/Vol1.
- [164] Phoenix integration, Inc. Phoenix integration, Inc. website. <http://www.phoenix-int.com>, July 2010.
- [165] R. Plencner, P. Senty, and T. Wickenheiser. Propeller performance and weight predictions appended to the navy/nasa engine program. NASA Technical Memorandum, Lewis Research Center, Cleveland, Ohio, August 1983. NASA-TM-83458.
- [166] R. Plencner and C. Snyder. The Navy / Nasa Engine Program (NEPP) - A User's Manual. NASA Technical Memorandum, Lewis Research Center, Cleveland, Ohio, August 1991. NASA-TM-105186.
- [167] L. Prandtl. Theory of Lifting Surfaces - Part I. NACA Technical Note 9, July 1920.
- [168] W. Press, S. Teukolsky, W. Vetterling, and B. Flannery. *Numerical Recipes 3rd Edition: The Art of Scientific Computing*. Cambridge University Press, 3 edition, September 2007.
- [169] N. Queipo, R. Haftka, W. Shyy, T. Goeland, R. Vaidyanathan, and P. K. Tucker. Surrogate-based analysis and optimization. Technical report, Marshall Space Flight Center, Huntsville, Alabama, 2005. Report under NAG8-1791.
- [170] R. C. Quintero. *Techno-Economic and Environmental Risk Assessment of Innovative Propulsion Systems for Short-Range Civil Aircraft*. PhD thesis, School of Engineering, Cranfield University, April 2009.
- [171] D. Raymer. RDS: A PC-Based Aircraft Design Sizing, and Performance System. In *AIAA Aircraft Design Systems Meeting, 24-26 August, Hilton Head, South Carolina, 1992*. AIAA-92-4226.
- [172] D. Raymer. *Enhanced Aircraft Conceptual Design Using Multidisciplinary Optimization*. PhD thesis, Department of Aeronautics, Royal Institute of Technology, Stockholm, Sweden, 2002. ISBN 91-7283-259-2.
- [173] D. Raymer. *Aircraft Design: A Conceptual Approach*. AIAA Education Series. American Institute of Aeronautics and Astronautics, Inc., New York, NY, 4 edition, 2006.
- [174] S. Remy. The airbus / engine & nacelle manufacturers relationship: Towards a more integrated, environmentally friendly engineering design. In *24th International Congress of the Aeronautical Sciences, 29 August - 3 September 2004, Yokohama, Japan, 2004*.
- [175] B. Rey. Ceasiom tutorial. CFS Engineering, <http://www.ceasiom.com>, March 2010.
- [176] C. Reynolds. Advanced Propfan Engine Technology (APET) Single- and Counterrotation Gearbox / Pitch Change Mechanism, Final Report. Technical report, Pratt & Whitney United Technologies Corporation, 1985. NASA-CR-168114, Vol. 1 & 2.

- [177] J. Robinson and J. Martin. An overview of nasa's integrated design and engineering analysis (idea) environment. In *Joint Army-Navy-NASA-Air Force (JANNAF) 6th Modeling and Simulation / 4th Liquid Propulsion / 3rd Spacecraft Propulsion Joint Subcommittee Meeting Orlando, Florida, December 8-12, 2008*.
- [178] J. L. Rogers. Demaid: A design manager's aide for intelligent decomposition user's guide. Technical report, Langley Research Center, Hampton, Virginia, March 1989. NASA-TM-101575.
- [179] C. Rohrbach and F. Metzger. The prop-fan – a new look in propulsors. In *AIAA/SAE 11th Propulsion Conference, Anaheim, California, September 29 – October 1, 1975*. AIAA-75-1208.
- [180] D. Roskam. *Airplane Design, Part I: Preliminary Sizing of Airplanes*. Roskam Aviation and Engineering Corporation, Ottawa, Kansas, second printing edition, 1985.
- [181] D. Roskam. *Airplane Design, Part V: Component Weight Estimation*. Design, Analysis and Research Corporation (DARcorporation), Lawrence, Kansas, second printing edition, 2003.
- [182] D. Roskam. *Airplane Design, Part VIII: Airplane Cost Estimation: Design, Development, Manufacturing and Operating*. Design, Analysis and Research Corporation (DARcorporation), Lawrence, Kansas, second printing edition, 2003.
- [183] D. Roskam. *Airplane Design, Part VI: Preliminary Calculation of Aerodynamic, Thrust and Power Characteristics*. Design, Analysis and Research Corporation (DARcorporation), Lawrence, Kansas, second printing edition, 2004.
- [184] B. Roth. *A Theoretical Treatment of Technical Risk in Modern Propulsion System Design*. Dissertation, Georgia Institute of Technology, March 2000.
- [185] D. Sargisson. Advanced Propfan Engine Technology (APET) and Single-Rotation Gearbox / Pitch Change Mechanism, Final Report. Technical report, General Electric Company, 1985. NASA-CR-168113.
- [186] R. Schaber. *Numerische Auslegung und Simulation von Gasturbinen*. PhD thesis, Lehrstuhl für Flugantriebe, Technische Universität München, December 2000.
- [187] K. Schmidt. Some aspects on gas turbine steady state performance. In *Short Course Gas Turbine Performance, Stuttgart, Germany, 24 - 28 September*. Deutsche Gesellschaft für Luft- und Raumfahrt DGLR e.V., 2007.
- [188] A. Seitz. Missionsabhängigkeit von Optimalkonfiguration für Triebwerke in konventioneller Anordnung. Master's thesis, Lehrstuhl für Flugantriebe, Technische Universität München, April 2007.
- [189] A. Seitz, S. Donnerhack, K. Broichhausen, and J. Seifert. An integrated parametric model for engine and aircraft design and performance optimization. In *44th AIAA/ASME/SAE/ASEE Joint Propulsion Conference & Exhibit, Hartford, Connecticut, July 21-23, 2008*. AIAA 2008-4671.

- [190] A. Seitz, S. Donnerhack, K. Broichhausen, and J. Seifert. A new approach for CO2 emission reduction applying state-of-the-art engine and airframe technology. In *ICAS 2008 Congress including the 8th AIAA 2008 ATIO Conference, Anchorage, Alaska, September 14 –19, 2008*. AIAA-2008-8974.
- [191] A. Seitz, S. Donnerhack, and D. Schmitt. Emission comparison of turbofan and open rotor engines under special consideration of aircraft and mission design aspects. In *2nd CEAS European Air and Space Conference, Manchester, GB, October 26 –29, 2009*.
- [192] A. Seitz, S. Donnerhack, and D. Schmitt. Emission comparison of turbofan and open rotor engines under special consideration of aircraft and mission design aspects. *The Aeronautical Journal*, 115(1168), June 2011.
- [193] A. Seitz, S. Donnerhack, and J. Seifert. Implication of ultra high bypass engines on aircraft design features and mission. In *1st CEAS European Air and Space Conference, 10-13 September, Berlin, Germany, 2007*. CEAS-2007-297.
- [194] D. Simos. Piano Online User Guide. Copyright Lissys Limited / D. Simos, <http://www.piano.aero>, 2009.
- [195] T. Simpson, A. Booker, D. Ghosh, A. Giunta, P. Koch, and R.-J. Yang. Approximation methods in multidisciplinary analysis and optimization: A panel discussion. In *9th AIAA/ISSMO Symposium on Multidisciplinary Analysis & Optimization, Atlanta, Georgia, September 2-4, 2002*.
- [196] T. Simpson, J. Peplinski, P. Koch, and J. Allen. On the use of statistics in design and the implications for deterministic computer experiments. In *ASME Design Engineering Technical Conferences, September 14-17, 1997, Sacramento, California, 1997*. DETC97DTM3881.
- [197] S. Smith. A simple correlation of turbine efficiency. *Journal of the Royal Aeronautical Society*, 69:467–470, 1965.
- [198] I. Sobieski, V. Manning, and I. Kroo. Response surface estimation and refinement in collaborative optimization. In *7th AIAA/USAF/NASA/ISSMO Symposium on Multidisciplinary Analysis and Optimization, 2-4 September, St Louis, MO, 1998*. AIAA-98-4753.
- [199] J. Sobieski. Multidisciplinary system optimization by linear decomposition. In *Recent Experiences in Multidisciplinary Analysis and Optimization, Symposium held at NASA Langley Research Center, Hampton, Virginia April 24-26*, pages 343–366, 1984. NASA-CP-2327, Part I.
- [200] J. Sobieszczanski-Sobieski. A linear decomposition method for large optimization problems - blueprint for development. NASA Technical Memorandum, Langley Research Center, Hampton, Virginia, February 1982. NASA-TM-83248.
- [201] J. Sobieszczanski-Sobieski. Optimization by decomposition: A step from hierarchic to non-hierarchic systems. In *Recent Advances in Multidisciplinary Analysis and Optimization, Part 1*, pages 51–78. NASA Langley Research Center, Hampton, Virginia, April 1989.
- [202] J. Sobieszczanski-Sobieski. Sensitivity of complex, internally coupled systems. *AIAA Journal*, 28(1):153–160, 1990.

- [203] J. Sobieszczanski-Sobieski. A system approach to aircraft optimization. Technical report, NASA Langley Research Center, Hampton, Virginia, March 1991. NASA-TM-104074.
- [204] J. Sobieszczanski-Sobieski. Two alternative ways for solving the coordination problem in multilevel optimization. NASA Technical Memorandum, Langley Research Center, Hampton, Virginia, August 1991. NASA-TM-104036.
- [205] J. Sobieszczanski-Sobieski, J. Agte, and R. S. Jr. Bi-level integrated system synthesis (bliss). NASA Technical Memorandum, Langley Research Center, Hampton, Virginia, August 1998. NASA-TM-1998-208715.
- [206] J. Sobieszczanski-Sobieski, M. Emiley, J. Agte, and R. S. Jr. Advancement of bi-level integrated system synthesis (bliss). NASA Technical Memorandum, Langley Research Center, Hampton, Virginia, December 2000. NASA/TM-2000-210305.
- [207] J. Sobieszczanski-Sobieski and R. T. Haftka. Multidisciplinary aerospace design optimization: survey of recent developments, structural and multidisciplinary optimization. In *AIAA 34th Aerospace Sciences Meeting and Exhibit, Reno, NV, January 15-18, 1996*. AIAA-9149-407.
- [208] I. Sommerville. *Software Engineering*. Addison-Wesley Publishers Ltd. / Pearson Education Ltd., 7 edition, 2004.
- [209] C. Österheld, W. Heinze, and P. Horst. Preliminary design of a blended wing body configuration using the design tool prado. In *CEAS Conference on Multidisciplinary Aircraft Design and Optimisation, 25-26 June, Cologne, Germany, 2001*.
- [210] W. Stewart. A study of axial-flow turbine efficiency characteristics in terms of velocity diagram parameters. In *ASME Winter Annual Meeting, New York City, 26 November - 1 December, 1961*. ASME 61-WA-37.
- [211] K. Swift and J. Booker. *Process Selection - From Design to Manufacture*. Butterworth-Heinemann Publications, 2 edition, 2003.
- [212] H. Syamsudin and J. P. Fielding. An approach to improve airframe conceptual design process. In *24th International Congress of the Aeronautical Sciences, 29 August - 3 September 2004, Yokohama, Japan, 2004*. Note.
- [213] The Mathworks, Inc. Matlab neural network toolbox, version 6.0.2, February 2009.
- [214] The Mathworks, Inc. Matlab statistics toolbox, version 7.1, February 2009.
- [215] The Mathworks, Inc. Matlab, version 7.8 (r2009a), February 2009.
- [216] The MathWorks, Inc. Matlab website. Copyright 1994-2010, <http://www.mathworks.com>, 2010.
- [217] T. Theodorsen. The Theory of Propellers, Volumes I-IV. Technical report, National Advisory Committee for Aeronautical (NACA), 1944. NACA Reports 775-778.
- [218] M. Tong, I. Halliwell, and L. Ghosn. A computer code for gas turbine engine weight and disk life estimation. *ASME Journal of Engineering for Gas Turbines and Power*, 126(2):265–270, April 2004.

## Bibliography

- [219] M. Tong, S. Jones, W. Haller, and R. Handschuh. Engine conceptual design studies for a hybrid wing body aircraft. In *American Society of Mechanical Engineers Turbo Expo 2009, Orlando, Florida, June 8–12, 2009*. GT2009–59568.
- [220] M. Tong and B. Naylor. An object-oriented computer code for aircraft engine weight estimation. In *American Society of Mechanical Engineers Gas Turbine Technical Congress and Exposition (Turbo Expo 2008), Berlin, Germany, June 9–13, 2008*. GT2008–50062, NASA/TM–2009-215656.
- [221] E. Torenbeek. *Synthesis of Subsonic Airplane Design*. Kluwer Academic Publishers, Dordrecht / Boston / London, 1982.
- [222] A. Trout and E. Hall. Method for determining optimum division of power between jet and propeller for maximum thrust power of a turbine-propeller engine. NACA Technical Note, Lewis Flight Propulsion Laboratory Cleveland, Ohio, September 1950. NACA-TN-2178.
- [223] J. W. Foss. A computer program for detailed analysis of the takeoff and approach performance capabilities of transport category aircraft. Technical report, NASA Langley Research Center, Hampton, Virginia, June 1979. NASA-TM-80120.
- [224] H. Wainauski, C. Rohrbach, and T. Wynosky. Prop-Fan Performance Terminology. In *Aerospace Technology Conference and Exposition, Long Beach, California, October 5-8, 1987*. SAE Paper 871838.
- [225] P. Walsh and P. Fletcher. *Gas Turbine Performance*. Blackwell Science Ltd, 2 edition, 2004.
- [226] C. Werner-Westphal, W. Heinze, and P. Horst. Multidisciplinary integrated preliminary design applied to unconventional aircraft configurations. *Journal of Aircraft*, 45(2):581–590, March-April 2008.
- [227] G. Wilfert, J. Sieber, A. Rolt, N. Baker, A. Touyeras, and S. Colantouni. New environmental friendly aero engine core concepts. In *18th International Symposium on Air-Breathing Engines, 2-7 September, Beijing, China, 2007*. ISABE-2007-1120.
- [228] G. Wrenn. An indirect method for numerical optimization using the kreisselmeiersteinhauser function. Technical report, Planning Research Corporation, Aerospace Technologie Division, Hampton, Virginia, March 1989. NASA-CR-4220.
- [229] S. Xie, J. Milthorpe, and W. Smith. A contribution-based decomposition method for multidisciplinary engineering optimization. In *10th AIAA/ISSMO Multidisciplinary Analysis and Optimization Conference, Albany, New York, Aug 30 - Sep 1, 2004*.
- [230] S. Yaros, M. Sexstone, L. Huebner, J. Lamar, R. M. Jr., A. Torres, C. Burley, R. Scott, and W. Small. Synergistic airframe-propulsion interactions and integrations. NASA Technical Memorandum, Langley Research Center, Hampton, Virginia, March 1998. NASA/TM-1998-207644.
- [231] J. Zentner. *A Design Space Exploration Process for Large Scale, Multi-objective Computer Simulations*. PhD thesis, School of Aerospace Engineering, Georgia Institute of Technology, August 2006.

# A. Additional Figures

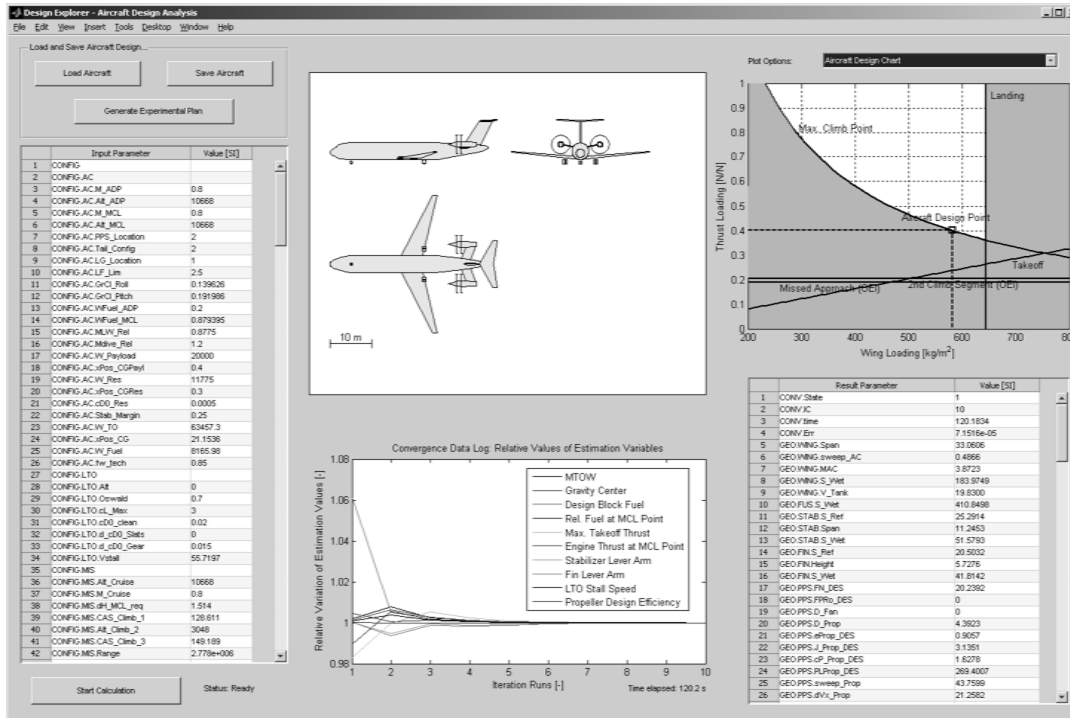


Figure A.1.: Graphical user interface of the implemented software

### A. Additional Figures

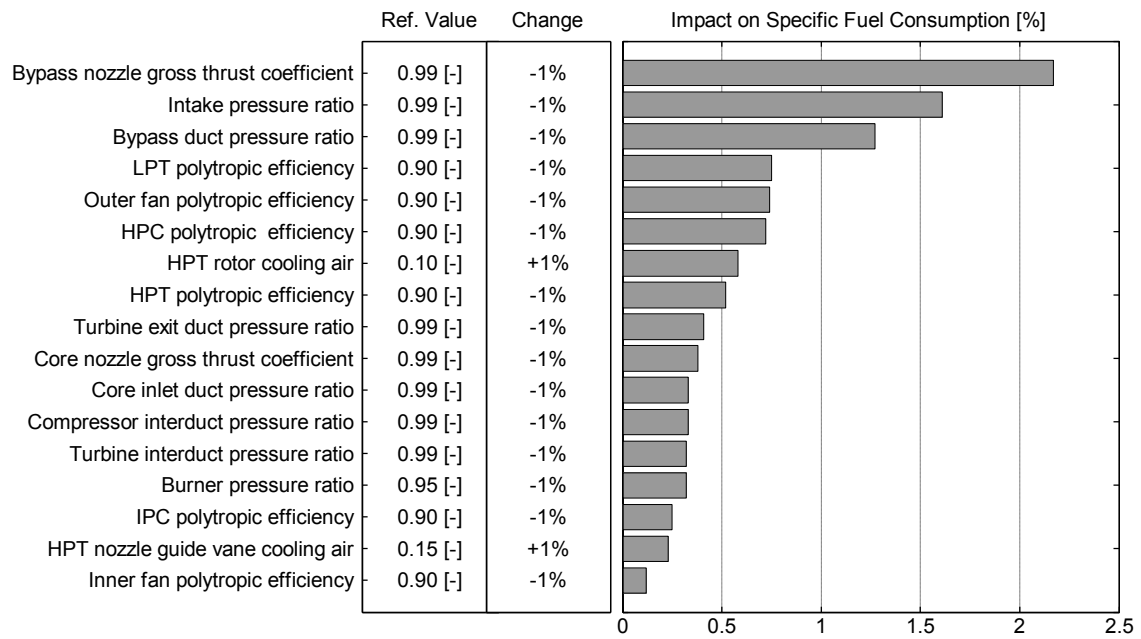


Figure A.2.: Impact of conceptual engine design parameters on design point specific fuel consumption according to sensitivity analysis for generic 2-spool boosted turbofan engine performed in GasTurb11

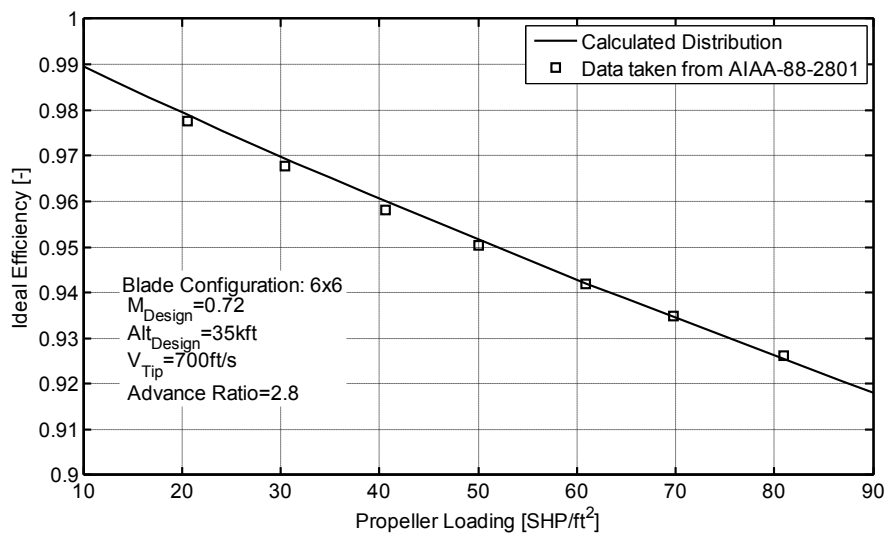


Figure A.3.: Validation of propeller design code: Ideal induced efficiency (Validation data taken from Reference [132, Figure 2])

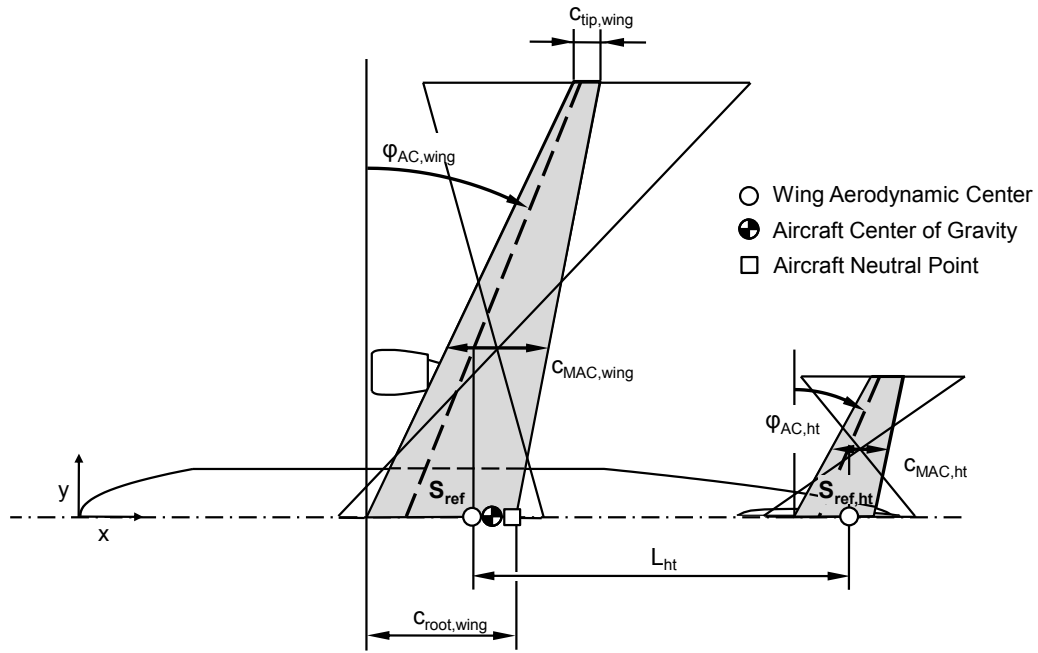


Figure A.4.: Parameterisation of Wing Planform

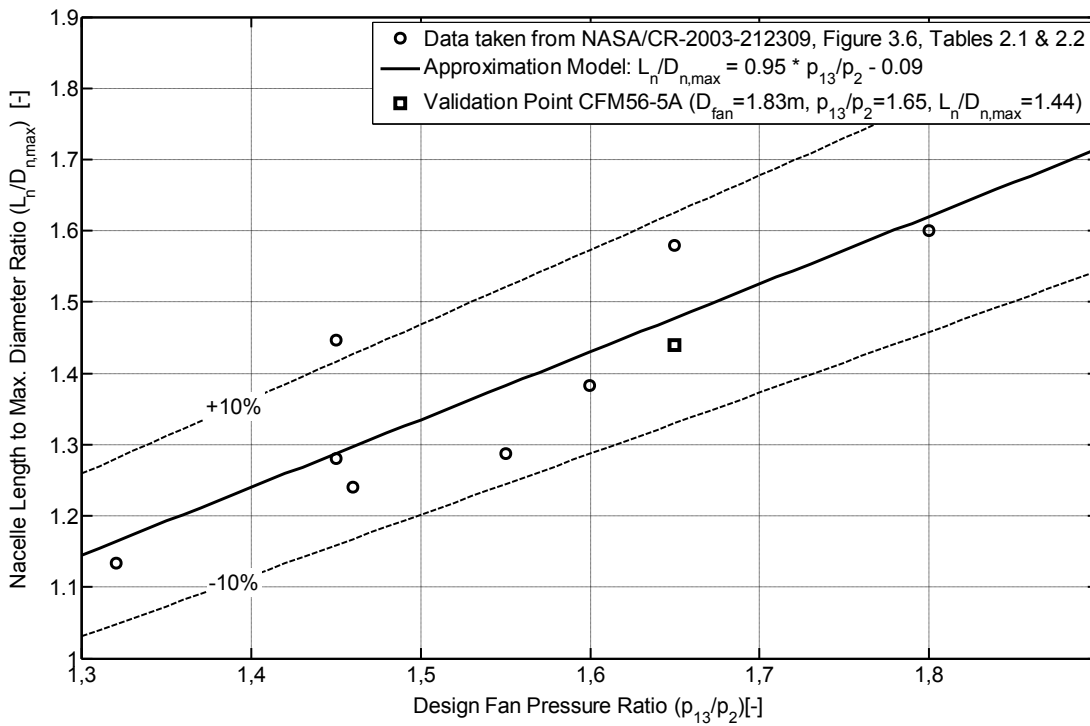


Figure A.5.: Validation of nacelle shape model for short duct separate flow turbofan engines

A. Additional Figures

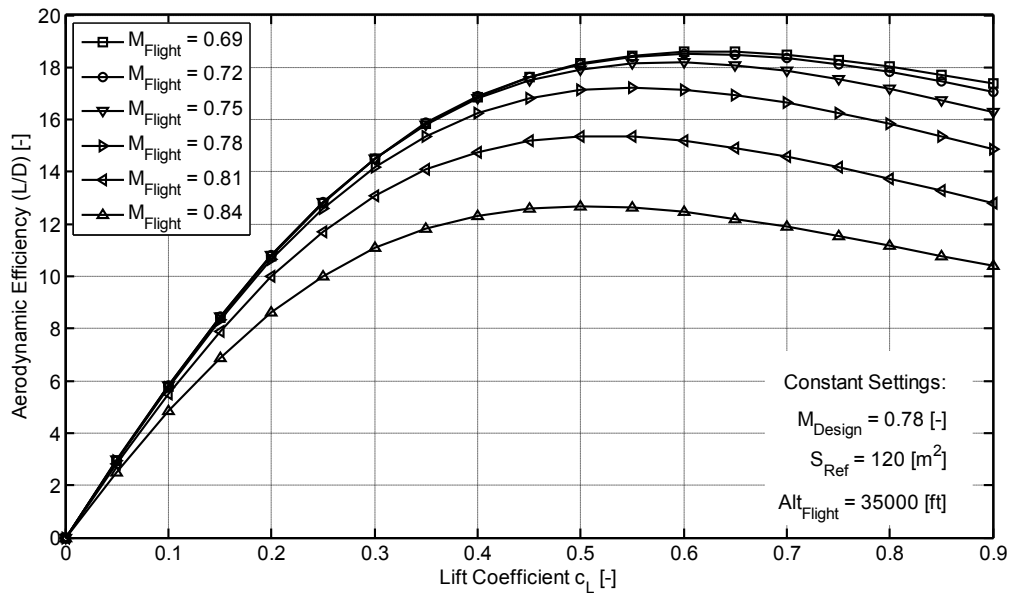


Figure A.6.: Exemplary high-speed polar plot for a typical medium range aircraft configuration

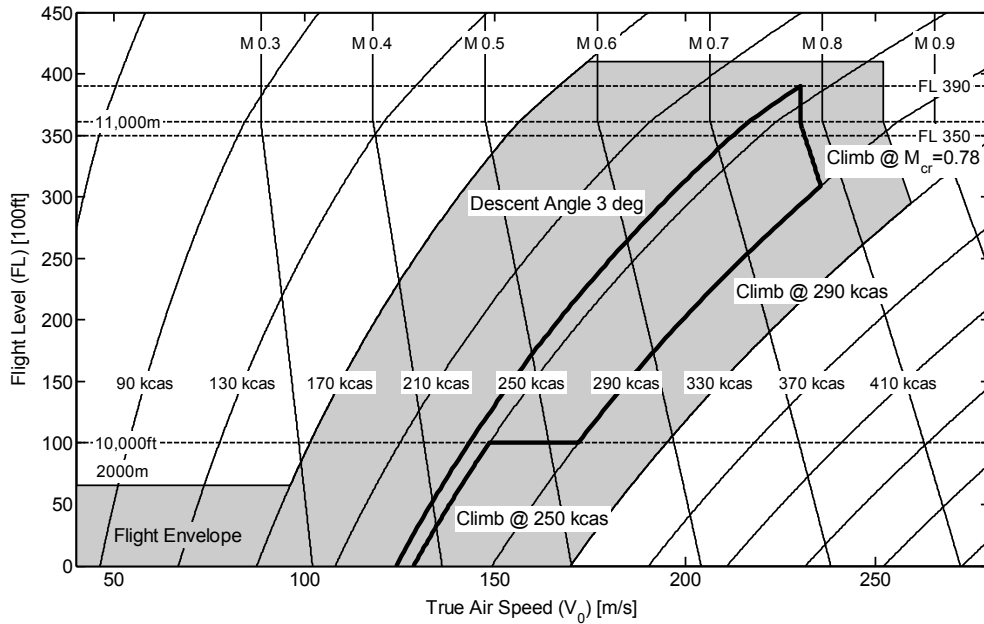


Figure A.7.: Visualisation of typical flight mission profile simulated

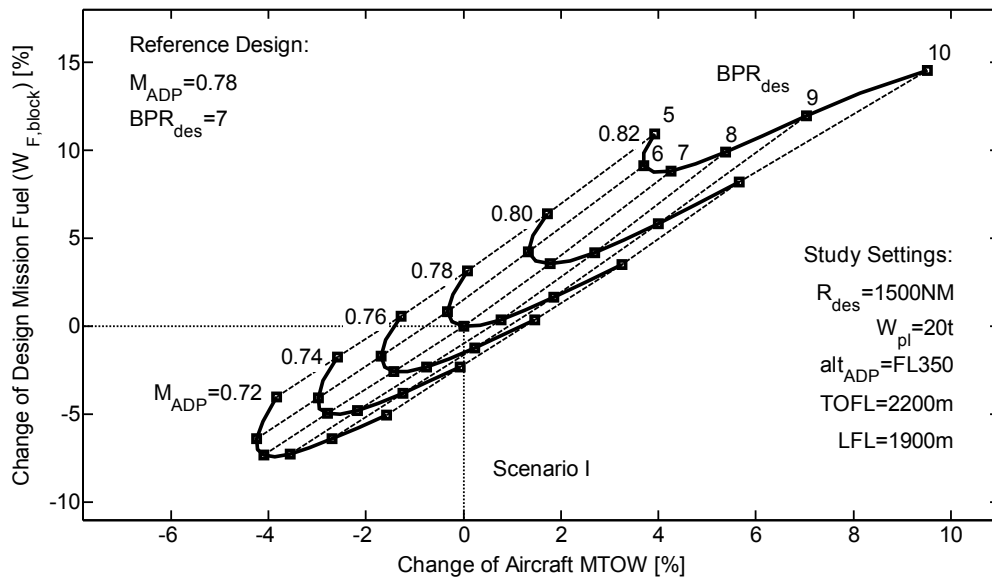


Figure A.8.: Characteristics of technology scenario I according to Table 6.3 with respect to design block fuel and  $MTOW$  as a function of turbofan bypass ratio and aircraft aerodynamic design Mach Number

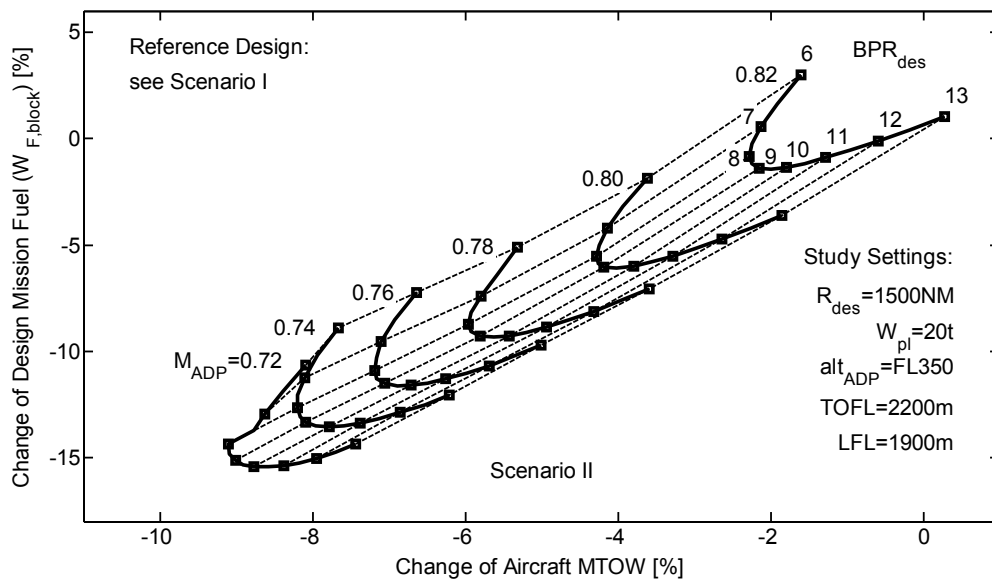


Figure A.9.: Characteristics of technology scenario II according to Table 6.3 with respect to design block fuel and  $MTOW$  as a function of turbofan bypass ratio and aircraft aerodynamic design Mach Number

A. Additional Figures

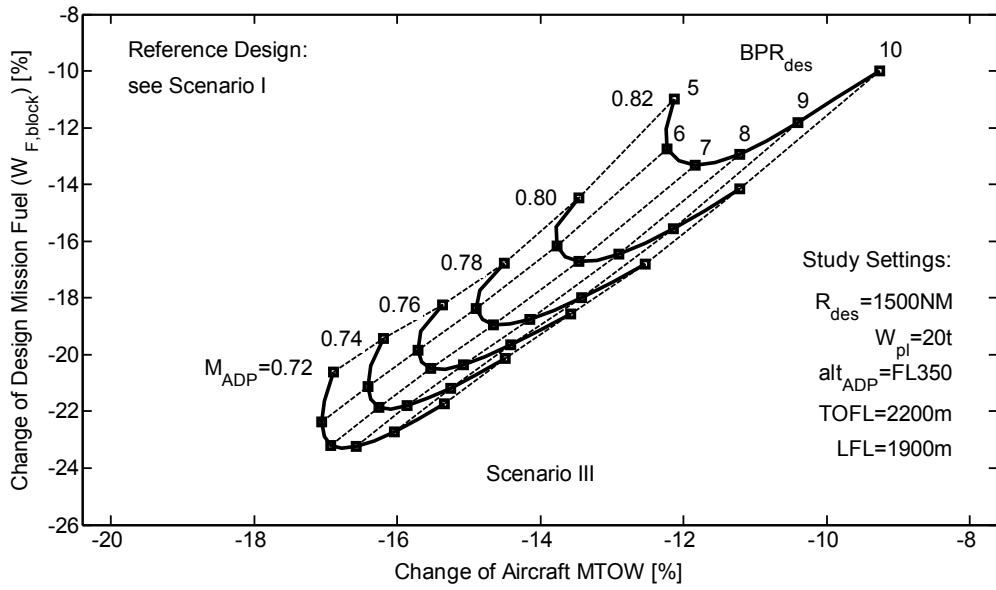


Figure A.10.: Characteristics of technology scenario III according to Table 6.3 with respect to design block fuel and *MTOW* as a function of turbofan bypass ratio and aircraft aerodynamic design Mach Number

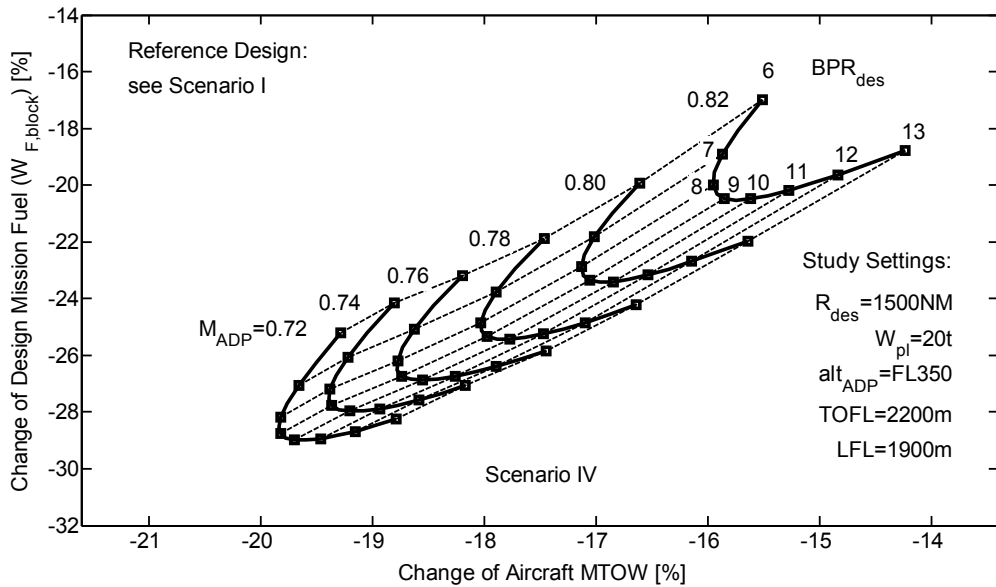


Figure A.11.: Characteristics of technology scenario IV according to Table 6.3 with respect to design block fuel and *MTOW* as a function of turbofan bypass ratio and aircraft aerodynamic design Mach Number

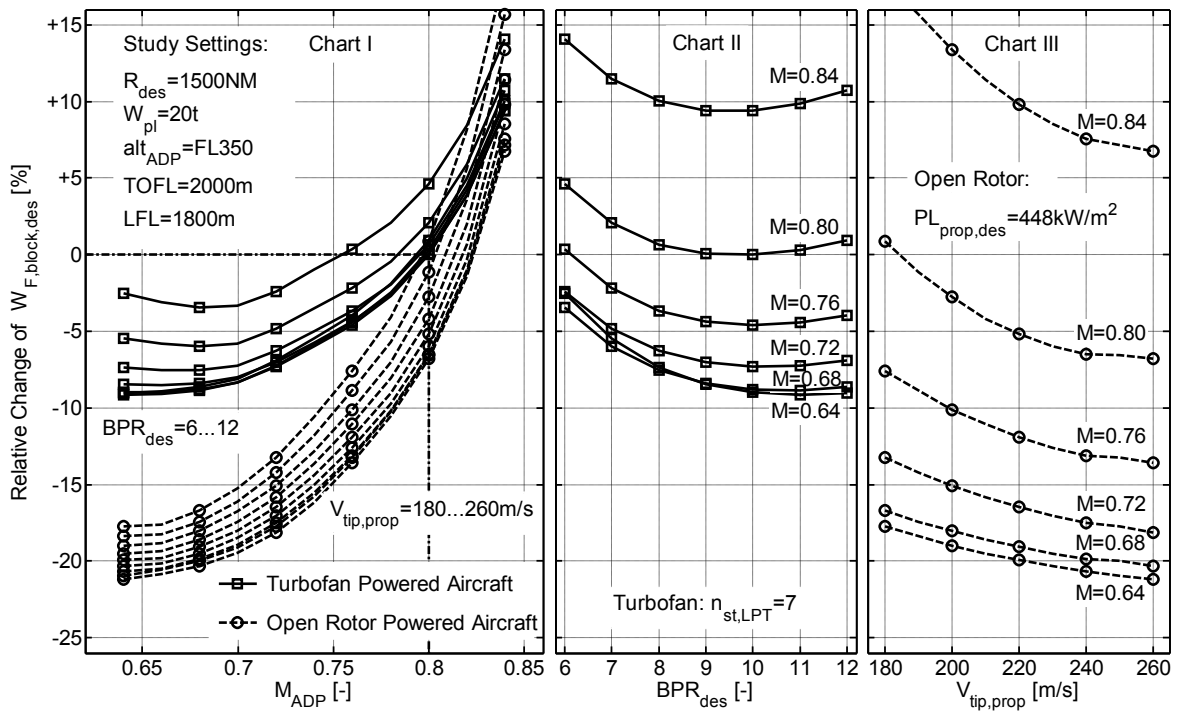


Figure A.12.: Results of comparative study of fuelburn optimised turbofan and open rotor powered aircraft designed for different Mach numbers ( $M_{ADP}$ ): Study of propeller tip speed  $V_{tip,prop}$



## B. Additional Tables

Table B.1.: Characterisation of simple example case for the demonstration and validation of the implemented approach to surrogate model creation

<b>Problem Description</b>	<i>Value</i>	<i>Unit</i>
<i>Problem type</i>	<i>turbofan engine deck</i>	–
<i>Simulation model</i>	<i>GasTurb11</i>	–
Input parameters ( $V_i$ ):		
<i>Design net thrust</i>	{18...34}	<i>kN</i>
<i>Flight altitude</i>	{9,500...12,500}	<i>m</i>
<i>Flight Mach number</i>	{0.65...0.85}	–
<i>Power lever setting</i>	{0...100}	%
Response parameters ( $f_k(\vec{V})$ ):		
<i>Net thrust</i>	$f(\vec{V})$	<i>kN</i>
<i>Specific fuel consumption</i>	$f(\vec{V})$	<i>g/kN·s</i>
<b>Surrogate Model Architecture</b>		
<i>Type</i>	<i>feedforward neural network</i>	–
<i>Hidden layers</i>	1	–
<i>Neuron configuration<sup>a</sup></i>	[4,15,2]	–
<i>Transfer function</i>	<i>tangent sigmoid</i>	–
<b>Training Setup</b>		
<i>Sampling plan</i>	<i>latin hypercube</i>	–
<i>Training data sets</i>	1000	–
<i>Training algorithm</i>	<i>Levenberg – Marquardt</i>	–
<i>Training epochs</i>	1500	–
<i>Performance (<math>f_{pf}</math>)</i>	$5.1 \times 10^{-6}$	–
<b>Validation Results</b>		
<i>Sampling plan</i>	<i>latin hypercube</i>	–
<i>Validation data sets</i>	100	–
Maximum relative errors:		
<i>Net thrust</i>	1.15	%
<i>Specific fuel consumption</i>	0.49	%
Mean relative errors:		
<i>Net thrust</i>	0.27	%
<i>Specific fuel consumption</i>	0.12	%

<sup>a</sup> [input layer, hidden layer(s), output layer]

Table B.2.: Book keeping scheme for the assignment of cooling air work potentials for single and multi-stage cooled turbines

Cooling Air Share	Work Potentials [%]		
	1-stage Turbine	2-stage Turbine	3-stage Turbine
NGV	100	100	100
Blade 1	0	50	67
Vane 2	–	50	67
Blade 2	–	0	33
Vane 3	–	–	33
Blade 3	–	–	0

Table B.3.: Validation of counter-rotating propeller design code using the F7 / A7 blade configuration

Configuration: <b>F7/A7</b>	Ref.	Validation Results		
		Value <sup>a</sup>	Unit	Error <sup>b</sup> [%]
Flight Mach number	[4, Table 5-2]	0.72	–	<i>n/a</i>
Flight altitude	[4, Table 5-1]	10,668	<i>m</i>	<i>n/a</i>
Propeller tip speed	[4, Table 5-2]	237.7	<i>m/s</i>	<i>n/a</i>
Power coefficient	[4, Table 5-2]	2.66	–	<i>n/a</i>
Blade tip sweep <sup>c</sup>	[4, Table 5-2]	31/31	<i>deg</i>	<i>n/a</i>
Propeller hub/tip ratio	[4, Table 5-2]	0.425	–	<i>n/a</i>
Net thrust	[4, Table 5-1]	22.65	<i>kN</i>	<i>n/a</i>
Geometric advance ratio	[4, Table 5-2]	2.8	–	±0
Power coefficient (annulus)	[4, Table 5-2]	4.14	–	–1.43
Power loading	[4, Table 5-2]	437.4	<i>kW/m<sup>2</sup></i>	–1.86
Power loading (annulus)	[4, Table 5-2]	679.6	<i>kW/m<sup>2</sup></i>	–0.96
Propeller diameter	[4, Table 5-1]	3.58	<i>m</i>	+0.56
Propeller efficiency	[4, Table 5-2]	0.865	–	+1.88

<sup>a</sup> Calculated values are based on propeller design code described in Section 5.2.5.

<sup>b</sup> errors of calculated values relative to reference values, errors of input parameters are marked as *n/a*

<sup>c</sup> front blade row / aft blade row (F7 / A7 reference values: 33 / 29)

Table B.4.: Outline of start value setting cases used for the verification of the proposed iteration strategy

$\mathbf{V}_{it,est,i}$	Cases of Start Value Settings ( $S_{SV,i}$ )									
	1	2	3	4	5	6	7	8	9	10
$MTOW$	75	69	63	67	71	73	77	61	65	79
$x_{GC,a/c}$	17.6	17.9	16.1	15.5	15.2	17.3	15.8	17.0	16.7	16.35
$W_{F,Block}$	12.3	11.7	12.6	12.0	11.4	11.1	10.5	10.2	10.8	12850
$FN_{req,TOC}$	29.4	22.2	27.0	25.8	18.6	23.4	28.2	21.0	19.8	24.6
$FN_{TO}$	118.5	125.5	104.5	90.5	83.5	132.5	146.5	139.5	111.5	97.5
$L_{HT}$	19.3	17.5	16.9	21.7	21.1	20.5	18.7	19.9	16.3	18.1
$L_{VT}$	18.1	21.7	19.9	19.3	21.1	17.5	20.5	18.7	16.9	16.3
$V_{stall}$	41.5	44.5	59.5	53.5	47.5	62.5	56.5	68.5	50.5	65.5

$MTOW$  [t]: maximum take-off weight  
 $x_{GC,a/c}$  [m]: aircraft longitudinal c.g. position  
 $W_{F,Block}$  [t]: design mission block fuel  
 $FN_{req,TOC}$  [kN]: engine thrust requirement at TOC conditions  
 $FN_{TO}$  [kN]: engine take-off thrust  
 $L_{HT}$  [m]: lever arm of horizontal tail plane  
 $L_{VT}$  [m]: lever arm of vertical tail plane  
 $V_{stall}$  [m/s]: minimum stall speed

## B. Additional Tables

Table B.5.: Synopsis of aircraft design settings used for the verification of the proposed aircraft design scaling procedure

$V_{free,i}$	Aircraft Design Cases ( $S_{AD,i}$ )									
	<b>1</b>	<b>2</b>	<b>3</b>	<b>4</b>	<b>5</b>	<b>6</b>	<b>7</b>	<b>8</b>	<b>9</b>	<b>10</b>
$M_{ADP}$	0.81	0.69	0.64	0.67	0.83	0.71	0.76	0.79	0.74	0.86
$alt_{ADP}$	11.9	11.7	11.3	11.5	10.5	10.3	10.7	10.9	10.1	11.1
$PS_{loc}$	w	w	w	f	w	f	f	w	w	w
$Tail_{con}$	1	c	t	t	c	t	t	t	c	c
$f_{tech,W}$	0.95	0.97	0.93	0.99	0.89	0.85	0.91	0.87	0.81	0.83
$R_{des}$	1,775	1,675	1,625	1,475	1,575	1,375	1,425	1,725	1,525	1,325
$W_{pl}$	18.2	20.6	19.4	21.0	21.4	20.2	18.6	19.8	21.8	19.0
$S_{ref}$	102.5	122.5	137.5	132.5	112.5	107.5	117.5	147.5	142.5	127.5
$AR_{wing}$	9	10.2	10.6	9.8	9.4	11	8.2	8.6	11.4	11.8
$L_{fus}$	38.8	39.3	35.8	38.3	37.3	37.8	39.8	36.8	35.3	36.3
$c_{FN,MCL}$	100	95.5	98.8	97.7	96.6	90.0	94.4	92.2	93.3	91.1
$BPR_{des}$	7.3	5.8	6.3	8.3	7.8	6.8	5.3	10.3	9.8	9.3

<sup>a</sup>  $M_{ADP}$  [-]: Mach number at aerodynamic design point

<sup>b</sup>  $alt_{ADP}$  [km]: altitude at aerodynamic design point

<sup>c</sup>  $PS_{loc}$  [-]: propulsion system installation location (w = under-wing, f = aft-fuselage)

<sup>d</sup>  $Tail_{con}$  [-]: tail plane configuration (c = conventional, t = t-tail)

<sup>e</sup>  $f_{tech,W}$  [-]: technology scaling factor for aircraft structural weights

<sup>f</sup>  $R_{des}$  [NM]: aircraft design range at maximum structural payload

<sup>g</sup>  $W_{pl}$  [t]: maximum structural payload

<sup>h</sup>  $S_{ref}$  [m<sup>2</sup>]: wing reference area

<sup>i</sup>  $AR_{wing}$  [-]: wing aspect ratio

<sup>j</sup>  $L_{fus}$  [m]: fuselage length

<sup>k</sup>  $c_{FN,MCL}$  [%]: thrust scaling parameter for maximum climb point (TOC) evaluation

<sup>l</sup>  $BPR_{des}$  [-]: engine design bypass ratio

Table B.6.: Model validation results: Overview of Airbus A320-200 geometry description

<b>Wing</b>	Ref.	Validation		
		Value <sup>a</sup>	Unit	Error <sup>b</sup> [%]
Reference area	[8]	122.4	<i>m</i>	<i>n/a</i>
Aspect ratio	-	9.5	-	<i>n/a</i>
Sweep at 25% MAC	[10]	24.96	<i>deg</i>	<i>n/a</i>
Dihedral <sup>c</sup>	[8]	5	<i>deg</i>	<i>n/a</i>
Span	[8]	34.1	<i>m</i>	±0
Tip ground clearance <sup>d</sup>	[8]	3.9	<i>m</i>	+0.13
Tank volume <sup>e</sup>	[10]	24.01	<i>m</i> <sup>3</sup>	+0.6
Taper	[10]	0.183	-	-23.8
<b>Fuselage</b>				
Width	[8]	3.95	<i>m</i>	<i>n/a</i>
Length	[8]	37.57	<i>m</i>	<i>n/a</i>
Wetted area	[10]	402.4	<i>m</i> <sup>2</sup>	-1.1
<b>Horizontal Stabilizer</b>				
Reference area	[8]	31	<i>m</i> <sup>2</sup>	<i>n/a</i>
Aspect ratio	-	5	<i>m</i>	<i>n/a</i>
Sweep at 25% MAC	[8]	28	<i>deg</i>	<i>n/a</i>
Dihedral <sup>c</sup>	[8]	6	<i>deg</i>	<i>n/a</i>
Span	[8]	12.45	<i>m</i>	±0
Lever arm	[8]	18.08	<i>m</i>	+2.8
<b>Vertical Fin</b>				
Reference area <sup>c</sup>	[8]	21.5	<i>m</i> <sup>2</sup>	<i>n/a</i>
Aspect ratio	-	1.6	-	<i>n/a</i>
Sweep at 25% MAC <sup>c</sup>	[8]	35	<i>deg</i>	<i>n/a</i>
Height	[8]	5.87	<i>m</i>	±0
Lever arm <sup>c</sup>	[8]	16.89	<i>m</i>	+1.0
<b>Landing Gear</b>				
NLG longitudinal position	[8]	5.07	<i>m</i>	<i>n/a</i>
MLG track width	[8]	7.59	<i>m</i>	<i>n/a</i>
MLG Longitudinal position	[8]	17.98	<i>m</i>	+1.5
<b>Engine Position</b>				
Relative spanwise	[10]	0.339	-	<i>n/a</i>
Gully height <sup>c</sup>	[8]	0.58	<i>m</i>	<i>n/a</i>
Nacelle / wing tangent angle <sup>c</sup>	[8]	9	<i>deg</i>	<i>n/a</i>
Nacelle ground clearance	[8]	0.55	<i>m</i>	-20.9

<sup>a</sup> calculated values are based on full aircraft design and sizing procedure

<sup>b</sup> errors of calculated values relative to reference values, errors of input parameters are marked as *n/a*

<sup>c</sup> reference values measured from 2D aircraft projection

<sup>d</sup> maximum ramp weight, mean longitudinal center of gravity position

<sup>e</sup> including outer wing and center wing tank

Table B.7.: Model validation: Overview of weight prediction results for Airbus A320-200

Standard Weight Terms	Ref.	Validation		Calibration	
		Value <sup>a</sup> [kg]	Error <sup>b</sup> [%]	Value <sup>a</sup> [kg]	Error <sup>b</sup> [%]
MTOW	[10]	70,665	-3.9	73,565	+0.1
MLW	[10]	64,500	<i>n/a</i>	64,500	<i>n/a</i>
MZFW	[10]	60,500	<i>n/a</i>	60,500	<i>n/a</i>
Fuel <sup>c</sup>	[8]	12,415	-2.9	12,857	+0.5
Payload <sup>d</sup>	[8]	20,279	<i>n/a</i>	20,279	<i>n/a</i>
OWE	[8]	37,971	-6.1	40429	$\pm 0.0^i$
<b>Wing Group</b>	[10]	8,340	-15.8	8574	-13.5
Structure	[10]	7,581	-17.1	7815	-14.6
Slats	[10]	292	<i>n/a</i>	292	<i>n/a</i>
Inner flaps	[10]	227	<i>n/a</i>	227	<i>n/a</i>
Outer flaps	[10]	240	<i>n/a</i>	240	<i>n/a</i>
<b>Fuselage Group</b>	[10]	17,263	-8.6	17,318	-8.3
Structure	[10]	7,332	-18.1	7,387	-17.5
Systems	[10]	4,379	<i>n/a</i>	4,379	<i>n/a</i>
Furnishings	[10]	2,439	<i>n/a</i>	2,439	<i>n/a</i>
Operator items	[10]	3,113	<i>n/a</i>	3,113	<i>n/a</i>
<b>Empennage Group</b>		1,612	+55.7	1,612	+55.7
Horizontal stabilizer	[10]	994	+61.6	994	+61.6
Vertical fin	[10]	618	+47.1	618	+47.1
<b>Landing Gear Group</b>		2,845	+27.1	3,057	+32.9
Nose landing gear	[10]	366	+14.4	380	+18.8
Main landing gear	[10]	2,557	+29.1	2,677	+35.2
<b>Propulsion Group</b>		6,540	-6.7	6,792	-3.1
Powerplant system <sup>e</sup>	[7]	3,165	-7.0	3,290	-3.3
Mounting structure <sup>f</sup>	-	105	+5.0	106	+6.0
<b>OWE Residual<sup>g</sup></b>	-	1,293 <sup>h</sup>	<i>n/a</i>	3,076 <sup>i</sup>	<i>n/a</i>

<sup>a</sup> calculated values are based on full aircraft design and sizing procedure

<sup>b</sup> errors of calculated values relative to reference values, errors of input parameters are marked as *n/a*

<sup>c</sup> take-off fuel required for 1550NM design mission at maximum structural payload including 200NM diversion flight, 30min hold and 10% final fuel reserves

<sup>d</sup> maximum structural payload

<sup>e</sup> includes engine weight (dry) [82], nacelle group, exhaust and thrust reverser system

<sup>f</sup> value per engine, based on the author's assessment

<sup>g</sup> includes systems and aircraft components not explicitly modelled

<sup>h</sup> Value results from OWE value acc. to Reference [8], reduced by all OWE items listed above.

<sup>i</sup> OWE is calibrated using OWE residual value.

Table B.8.: Outline of considered transport task scenario and synopsis of common analysis settings

<b>Transport Task</b>	<b>Settings</b>	
	Value	Unit
Design payload <sup>a</sup>	20,000	<i>kg</i>
Design range <sup>b</sup>	1500	<i>NM</i>
Takeoff field length	2200	<i>m</i>
Landing field length	2000	<i>m</i>
<b>Operational Simulation Conditions</b>		
Atmospheric Conditions	<i>ISA</i>	–
Airport field altitude	<i>SeaLevel</i>	<i>m</i>
CAS of 1st climb segment	250	<i>kts</i>
Altitude of 2nd climb segment	10,000	<i>ft</i>
CAS of 3rd climb segment	290	<i>kts</i>
Mach number of 4th climb segment	$M_{cruise}$	–
Climb rate at top of climb point	300	<i>ft/s</i>
Descent angle <sup>c</sup>	3	<i>deg</i>
Diversion distance	200	<i>NM</i>
Holding time	30	<i>min</i>
Final fuel reserve <sup>d</sup>	10	%
Fuel heating value <sup>e</sup>	43.124	<i>MJ/kg</i>
<b>Aircraft Design Settings</b>		
Wing aspect ratio	10	–
Relative thickness at MAC	12	%
Fuselage length	38	<i>m</i>
Fuselage diameter	4	<i>m</i>
Horizontal tail volume coefficient	1.1	–
Vertical tail volume coefficient	0.09	–
Pitch angle <sup>f</sup>	11	<i>deg</i>
Roll angle <sup>f</sup>	8	<i>deg</i>
Nose landing gear relative load	8	%
Static stability margin	25	% <i>MAC</i>
Cabin bleed air <sup>g</sup>	1	<i>lb</i>
Mechanical power offtake <sup>h</sup>	70	<i>kW</i>

<sup>a</sup> maximum structural payload

<sup>b</sup> at maximum structural payload

<sup>c</sup> CDA assumed.

<sup>d</sup> relative to mission block fuel consumption

<sup>e</sup> lower caloric value

<sup>f</sup> required during takeoff and landing manoeuvres

<sup>g</sup> per engine, taken at HPC exit

<sup>h</sup> per engine, taken from HP spool